143

# NATIONAL ADVISORY COMMITTEE FOR AERONAUTICS

# WARTIME REPORT

### ORIGINALLY ISSUED

June 1945 as
Advance ▮▮▮▮▮▮ Report L5E21

COMPLETED TABULATION IN THE UNITED STATES

OF TESTS OF 24 AIRFOILS AT HIGH MACH NUMBERS

(Derived from Interrupted Work at Guidonia, Italy

in the 1.31- by 1.74-Foot High-Speed Tunnel)

By Antonio Ferri

Langley Memorial Aeronautical Laboratory
Langley Field, Va.

# NACA

### WASHINGTON

NATIONAL ADVISORY COMMITTEE FOR AERONAUTICS

ADVANCE ███████ REPORT

COMPLETED TABULATION IN THE UNITED STATES

OF TESTS OF 24 AIRFOILS AT HIGH MACH NUMBERS

(Derived from Interrupted Work at Guidonia, Italy

in the 1.31- by 1.74-Foot High-Speed Tunnel)

By Antonio Ferri

SUMMARY

Two-dimensional data for 24 airfoil sections tested in the 1.31- by 1.74-foot high-speed tunnel at Guidonia, Italy, are presented. The test Mach numbers ranged from 0.40 to 0.94 and the test Reynolds numbers from 340,000 to 420,000. The results indicate that thickness ratio is the dominating shape parameter at very high Mach numbers and that important aerodynamic advantages are to be gained by using the thinnest possible sections.

The results of preliminary tests made to investigate the effects of jet boundaries, Reynolds number, and humidity at very high speeds are also presented. It was found that the jet-boundary effects became very large at high Mach numbers when models large with respect to the tunnel height were used. In the absence of suitable correction factors for large models it was considered essential to use models small enough to make the jet-boundary effects negligible. It was indicated that the data presented for the 24 airfoils tested are essentially free from jet-boundary and humidity effects.

INTRODUCTION

The rapid increase in airplane speeds during the past 5 years has greatly accentuated the need for experimental data in the subsonic Mach number range above 0.7. Experimental aerodynamic data in this speed range, however, are still very scarce. There are two principal reasons for the lack of data. First, the experimental equipment required to obtain data at high

speeds on models of significant size is extremely costly
to construct and operate.   Second, the problems of tech-
nique involved in obta██████████ these speeds are very
complex and are not yet fully understood.   The tunnel-
wall-effect phenomena occurring at very high Mach numbers
with the presence of shock waves become so complex that
there seems little hope at present of obtaining correc-
tions for these effects by analytical methods.

The principal purpose of this report is to present
aerodynamic data for 19 related airfoils and for 5
miscellaneous airfoils at Mach numbers in the range 0.40
to 0.94.   The data were obtained on models of 1.575-inch
and 1.965-inch chord in the 1.31- by 1.74-foot high-speed
tunnel at Guidonia, Italy.   Before the presentation of
the test results, a description is given of the equipment
used and the findings of preliminary tests made in an
attempt to develop a suitable testing technique and to
determine the isolated effects of such experimental varia-
bles as Reynolds number, ratio of the size of the model
to the size of the tunnel, and humidity.

The results presented herein represent the completed
part of a broad high-speed research program at Guidonia,
which was interrupted by the war.


## I. EFFECTS OF REYNOLDS NUMBER, JET BOUNDARIES, AND

## HUMIDITY IN TESTS OF AIRFOILS AT HIGH SPEEDS


A systematic study of the effects of Reynolds number,
air-stream boundaries, and humidity at high speeds was
made prior to the main part of the present investigation.
It is not certain, of course, that these are the only
factors affecting the results, but they are considered
the most important.


### WIND TUNNEL


All the tests were made in the high-speed tunnel at
Guidonia (reference 1), a single-return tunnel that could
function at a pressure below atmospheric.   The pressure
in the test section of the tunnel could be varied
from 1.0 atmosphere to 0.1 atmosphere.   The tunnel had a

system of refrigeration by which the temperature at low speeds could be held constant at as low a value as 15° Centigrade. The temperature of the air as it left the compressor was very variable, depending on the velocity and the pressure of the jet.

The tunnel was powered by a 3000-horsepower fourteen-stage axial-flow compressor, which could produce a velocity ranging from 0.4 to 2.9 times the speed of sound when one minimum retangular section of the jet 1.31 by 1.74 feet in size was used. In tests at subsonic speeds the test section of the jet was kept constant at these dimensions.

The jet was enclosed between two straight, parallel side walls, which were perpendicular to the axis of the model. The jet was not restrained by top and bottom walls. (See fig. 1.) The effuser A-A was shaped in such a way as to give a uniform flow at the plane a-a. This uniform flow was attained in a series of preliminary tests by increasing the length of the parallel-sided effuser until satisfactory flow distribution was obtained. The diffuser B-B was placed in a position to give uniform flow and to eliminate the vibrations that tended to occur. With the diffuser shape and location finally determined, the velocity was constant along the plane b-b in the test section of the tunnel even at the highest speeds. By varying the position and the dimensions of the diffuser a stable and uniform flow could be obtained even in the Mach number range approaching and exceeding the speed of sound (Mach numbers of 0.9 to 1.2). The present test program included measurements made at Mach numbers up to 0.94. Information on the shape and location of the diffuser has been lost; therefore, the exact dimensions of this setup are not available.

The velocity and the Mach number were determined from a tunnel calibration based on measurements of the total pressure in the large section of the tunnel ahead of the entrance cone and on measurements of the static pressure at the wall near the exit of the entrance cone. In order to check the velocity measured in this manner, pitot-static tubes were installed at the top and bottom of the jet just downstream of the exit of the entrance cone. These tubes gave a qualitative indication of the jet-boundary interference effects. When the velocities measured by these tubes were appreciably different from the velocity indicated by the entrance-cone pressure

calibration, it was usually found that the interference effects were so large that they appreciably altered the aerodynamic characteristics of the test models. No data were taken when this condition existed.

## EFFECT OF REYNOLDS NUMBER AND AIR-STREAM BOUNDARIES

Experimental methods.- In the study of Reynolds number effects at high speed, preliminary tests were made first on cylinders and spheres of various dimensions (reference 2). An analogous series of preliminary tests was then made for airfoils. Models of airfoils of constant profile but of varying chord were tested.

For the study of the effect of the air-stream boundaries, tests were made with varying ratio of model chord to tunnel height over a range of Mach numbers. The ratios used were: 0.0755, 0.0942, 0.113, and 0.151. The Reynolds number at each Mach number was held approximately constant by varying the density.

Test models.- A profile was chosen having an arc for the upper surface and a straight line for the lower surface because this profile could be exactly reproduced in various sizes. The upper surface could be made by use of a lathe and the lower surface could be formed by use of a shaper. The leading edge and the trailing edge were sharp. The maximum thickness chosen was 8 percent, and the profile was designated C-8 (fig. 2). Four models were constructed with such a profile; three with chords of 1.575, 1.969, and 2.362 inches (4, 5, and 6 cm) for force tests and one with a chord of 3.15 inches (8 cm) for determining the pressure distribution along the profile.

Tests and results.- At Mach numbers of 0.4, 0.5, 0.6, 0.7, 0.8, and 0.9, the lift coefficient, the drag coefficient, and the pitching-moment coefficient about the quarter-chord point of the airfoil were determined for the three profiles having chords of 1.575, 1.969, and 2.362 inches. All the models were tested at two Reynolds numbers: approximately 250,000 and 480,000. The model with the 1.575-inch chord was also tested at a Reynolds number of 150,000. For the profile having a chord of 3.15 inches, pressure readings were made at angles of attack between $-3.5^\circ$ and $4.5^\circ$ for Mach numbers

of approximately 0.7, 0.8, and 0.9. Values of lift and
of pitching moment were obtained from the pressure distri-
butions. Force-test results are shown in figures 3 to 8.
In figures 9 to 11 the results of pressure measurements
are presented. Figure 12 shows the results obtained from
integration of the pressure diagrams compared with the
results obtained by use of the balance.

Reynolds number effects.- The results of the pre-
liminary tests of cylinders and spheres showed that for
the range of Reynolds numbers covered in the tests the
effect of Reynolds number decreased as the velocity
increased. At Mach numbers close to 1.0 there was vir-
tually no Reynolds number effect. In the airfoil tests
the importance of Reynolds number was considerable at
low Mach numbers and the effect of Reynolds number was
noted up to the critical Mach numbers at which the phe-
nomenon of shock began to appear (figs. 3 to 6). For
supercritical Mach numbers, the effect of Reynolds number
became less until it virtually disappeared for Mach num-
bers very near 1.0. In this range the formation of shock
waves seems to control the aerodynamic phenomena and the
development of the boundary layer. The boundary-layer
thickness probably depends to a large extent on the angle
of deviation of the air as it passes through the shock
wave. The friction drag is a reduced part of the total
drag and, therefore, the Reynolds number effect is small.
The Reynolds number, however, could have an effect on
the characteristics of the shock wave itself through its
action on the boundary layer, but such an effect is not
indicated. In general, these airfoil test results con-
firmed the results of the sphere tests. Large-scale
tunnel tests made at the Deutsche Versuchsanstalt für
Luftfahrt (the DVL) in Germany and flight tests made at
various times showed similar results.

Effect of air-stream boundaries.- The jet-boundary
effects for the ratios of chord to jet height of 0.0755
to 0.113 covered in these tests appear to be negligible.
Essentially equivalent results were obtained at a given
Reynolds number for all values of the ratios employed
in the tests. For a larger jet-boundary effect, a test
was made of the model with a chord of 3.15 inches for
which the ratio of the chord of the model to the height
of the air stream (0.151) is twice that normally used in
the tests. From the results of integration (fig. 12)
the values obtained for $C_L$ and $C_{m_{c/4}}$ are seen to

coincide at high Mach numbers with the values found by
the force tests.  This agreement indicates that the
boundaries of the air stream probably did not interfere
appreciably with the distribution of the pressures.  For
a Mach number of 0.94 the effect of the air-stream
boundaries is important for the model of 3.15-inch chord
but is not important for the models of 1.575- and
1.969-inch chord.  For higher Mach numbers the boundaries
also affected the results obtained with the two smaller
models.

It is interesting to note that the phenomenon of
choking of the air stream, which occurs in closed-throat
wind tunnels at high speeds (reference 3), did not occur
in the tunnel in which the present tests were made.  For
example, for model C-8, which had a chord of 3.15 inches,
it is estimated that choking in a closed-throat tunnel
would occur at a Mach number of 0.88 or lower.  The
choking Mach number for the 2.352-inch-chord model is
estimated to be 0.90 or lower.  These choking Mach num-
bers were calculated from one-dimensional theory for the
zero-lift condition.  They are therefore somewhat higher
than the choking Mach numbers that would actually be
obtained, especially for angles of attack other than that
for zero lift.  In the present tests it was possible to
obtain data for these models at Mach numbers as high
as 0.94, and the results of the jet-boundary-effect tests
indicate that the data are essentially free from tunnel-
wall effects at this Mach number.

## EFFECT OF HUMIDITY AND CONDENSATION

The air becomes very cold in the expansion that
occurs in the tunnel at high speeds.  (The process is
very nearly adiabatic.)  Total condensation may occur in
the whole jet at high speeds if the dew point is passed.
Even if condensation does not occur in the jet, there is
a possibility of its occurring in the low pressure
regions over the test model where an additional expansion
and temperature drop occur.  Very low local temperatures,
which are usually smaller than the local dew point, are
found at high subsonic speeds; local condensation there-
fore could occur and could produce a "condensation shock"
or a localized region in which condensation occurs.

Condensation complicates and modifies the flow over the body because it alters the values of the temperature, the pressure, and the speed in the air stream and, hence, modifies the values of the resultant aerodynamic forces. A complete examination of the effects of the phenomenon of condensation shock is very complicated. The variables involved include the value of the local humidity, the speed of the condensation, the possibility of the existence of supersaturated air, and the scale of the model.

The condensation process is not instantaneous but requires a finite time and its beginning may depend on such factors as the nuclei of condensation. (The supersaturated air may sometimes exist for a time at a temperature much lower than the critical.) If the tests are made at small scale, the air can pass through the low temperature region in so short a time that appreciable condensation does not occur. Condensation is therefore less likely to occur in small-scale tests than in large-scale tests. In flight, for example, when appreciable relative humidity is present, condensation normally occurs and is easily seen on propellers and wings in high-speed dives. Since the characteristics of the condensation vary with scale, it would appear to be practically impossible to simulate full-scale conditions in tests in which small models are employed. The problem is further complicated because the degrees of supersaturation existing in the tests in a wind tunnel may be different from in flight and the beginning of the condensation depends on certain variable conditions of the air. The condensation characteristics of different wind tunnels, even with the same setup, have in several instances been noted to be widely different. In the subsonic tunnel of the Aerodynamische Versuchsanstalt (the AVA) at Göttingen, for example, it is normally necessary to dry the air before it converges in the test section to prevent condensation; however, in the Langley 24-inch high-speed tunnel, which has a comparable entrance-cone shape and which operates under similar conditions, it is not necessary to dry the air, and complete condensation seldom occurs for relative humidities below 60 percent.

All the test data obtained up to the present time tend to indicate that even for large-scale models the effects of humidity are of secondary importance provided that the percentage of humidity is low. In the Guidonia high-speed tunnel previously described, it was very difficult to study humidity effects because of an automatic

drying up of the air which took place.  A small quantity
of water was removed from the tunnel air by the pump which
was used to evacuate the tunnel to the low initial pres-
sure.  The condensation that occurred when the tunnel was
started was believed to cause water to collect behind the
test section and to adhere to the tunnel walls.  As a
result of this automatic water removal, fog did not occur
in the test section even at supersonic velocities and no
air-drying equipment was necessary.  Because the humidity
became less during the progress of a test in this tunnel,
it was impossible to give precise results as to the effect
of humidity, but the general indication of the data that
have been obtained was that the humidity effects were not
appreciable, at least not for the small-scale models
tested.

    Tests to study the effects of humidity have been
conducted in the 8.86-foot high-speed tunnel of the DVL
in Germany using an NACA 0015-64 airfoil section with
a 1.64-foot chord.  In this wind tunnel the amount of
condensation existing in the test section can be con-
trolled by varying the cooling of the tunnel and thus
regulating the temperature of the air in the test section.
For very high values of relative humidity, it is necessary
to eliminate the cooling entirely in order to raise the
temperature enough to avoid condensation.  The results of
the humidity-effect investigation in the DVL tunnel dem-
onstrated that, even for the relatively large-scale model
employed, the humidity effects were of secondary impor-
tance when the relative humidity was small.

    In order to indicate the conditions under which con-
densation might occur in flight, figure 13 is presented
showing the local Mach number as a function of the flight
Mach number for which the conditions required for satura-
tion are reached.  (Adiabatic expansion of the air from
its static condition to the conditions corresponding to
local Mach number is assumed.)  Also shown in figure 13
are the values of maximum local Mach number that are
attained locally on two typical airfoils.  The data cal-
culated for the NACA 23015 airfoil (unpublished) were
obtained from tests made in the Langley 24-inch high-
speed tunnel.  The data for the NACA 0015-64 airfoil were
obtained from the DVL tests mentioned previously.  Fig-
ure 13 indicates that, even for very low values of the
relative humidity, local Mach numbers are obtained at
which condensation is possible when the flight Mach num-
ber is 0.6 or greater.

The discussion in the preceding paragraphs has shown that humidity effects are likely to be most pronounced under large-scale conditions. Systematic tests to determine humidity effects could best be made in a large-scale wind tunnel in which the temperature of the circulating air could be varied by regulating the cooling. The tests in such a wind tunnel could be made at various periods in order to cover a wide range of relative humidities. Figure 14 has been prepared to indicate the conditions for saturation in the test section of a wind tunnel for three values of relative humidity and for various temperatures of the air in the entrance cone of the wind tunnel where the airspeed is low. Also shown in figure 14 is a comparison of the maximum local Mach numbers of the NACA 23015 and 0015-64 airfoils as functions of the stream Mach number to determine at what Mach number the conditions for saturation are locally reached. The figure shows that, for high relative humidity, it is necessary to have a high temperature of the tunnel air stream in order to eliminate condensation in the test section. It is also shown that, even if condensation is eliminated in the test section, the necessary conditions for the formation of local condensation over the test model will normally be attained.

## COMPARISON OF TEST RESULTS FROM VARIOUS

## WIND TUNNELS AND FROM FLIGHT

Airfoil tests.- For a thorough examination of the accuracy and significance of the test results obtained in a given wind tunnel, it is essential that the results be compared with those obtained in other wind tunnels and in free flight on models of similar profile. As a step in this direction, tests were conducted on the NACA 0015-64 airfoil in both the Guidonia 1.31- by 1.74-foot rectangular high-speed tunnel and in the DVL 8.86-foot-diameter high-speed tunnel, which has closed circular walls. The model used had a rectangular plan form enclosed between two end plates. The chord of the model was 1.638 feet (50 cm), the span was 4.5 feet, and the end plates were 23.6 by 43.2 inches. The ratio of the model chord to the tunnel diameter was 0.185. With this setup, the choking Mach number was about 0.86, which is considerably higher than the choking Mach number that would have been obtained with the model completely

spanning the tunnel jet.  The data obtained in these
tests consisted of pressure distributions and wake sur-
veys.

The test conditions were adjusted to produce an
equivalent relative humidity of the air of 20 percent at
sea level.  The Reynolds number varied with the Mach num-
ber from about 5,800,000 to 6,400,000 in the high-speed
range of the tests.

The model tested at Guidonia had the same profile
but was of much smaller scale, the model chord being
1.575 inches (4 cm) and the ratio of model chord to tun-
nel depth being 0.0755.  The relative humidity in the
Guidonia tests was always very low.  The Reynolds num-
bers were, of course, very much lower than those of the
DVL tests and varied around a value of about 500,000.
Force measurements of lift, drag, and moment were made
in the Guidonia tests; pressure-distribution and wake-
drag measurements were made in the DVL tests.  The
results obtained are compared in figures 15 to 17.
Figure 18 shows pressure-distribution measurements made
at the DVL for one angle of attack, $\alpha = -0.25°$.  It may
be noted that the results from the two tunnels are at
variance, especially at high speeds.  This lack of agree-
ment indicates that the testing technique and the pro-
portions of the testing system are of great importance
in high-speed wind-tunnel work.

The differences in the drag-coefficient values at
low Mach numbers are probably due to the difference in
Reynolds numbers.  The largest differences between the
results from the two tunnels are in the drag and pitching-
moment coefficients at high Mach numbers.  The abrupt
changes in the coefficients from the DVL tests at Mach
numbers in the vicinity of 0.8 are probably associated
with the phenomenon of choking, and the results obtained
in this range are therefore considered extremely ques-
tionable.  Because of the much smaller relative size of
the model in the Guidonia tests and also because of the
fact that the jet was not restrained by top and bottom
walls, similar effects did not occur.  Further tests were
made at the DVL tunnel of a smaller model of the same
profile having a chord of 1.148 feet, the model-chord to
tunnel-diameter ratio being 0.13.  The results obtained
with the smaller model are shown in figure 16.  It will
be noted that the rate of drag rise past the critical
speed is appreciably less than with the larger model and

thus is in better agreement with the results of the
Guidonia tests.

Free-flight tests were in the general research pro-
gram at Guidonia, but they were interrupted by the war.
The few flight tests made, however, indicated that the
drag-coefficient curves had about the same slopes at
supercritical speeds as were obtained in the Guidonia
wind-tunnel tests.

Bomb tests.- Additional comparisons between high-
speed wind-tunnel and flight data were obtained in tests
of an airplane bomb of conventional shape. The approxi-
mate shape of the bomb is indicated in figures 19 and 20,
which show the results of the tests. The bomb was
launched in flight at an altitude of 39,300 feet, and
its trajectory as a function of time was recorded with a
phototheodolite. The speed, the Mach number, the accel-
eration, and the drag coefficient were obtained from the
trajectory data. A one-third scale model of this bomb
was tested in the DVL 8.86-foot-diameter high-speed tun-
nel (the ratio of bomb diameter to tunnel diameter
was 0.0455, much lower than that normally used). A one-
tenth scale model of the same bomb was tested in the
Guidonia 1.31- by 1.74-foot rectangular high-speed tun-
nel using a ratio of model diameter to air-stream height
of about 0.0714. Similar tests were made in a wind tun-
nel at the AVA in Göttingen, which has a partly free air
stream similar to that at Guidonia but 47 inches high.
The size of the model used in these tests is not known,
but it is believed that the ratio of model diameter to
tunnel air-stream height was considerably higher than
that used in the tests in the other wind tunnels. The
results shown in figure 19 indicate reasonably good
agreement in the form of the drag curves obtained. As
might be expected, however, the drag-coefficient values
obtained at very high Mach numbers in the closed DVL tun-
nel are higher than those found at Guidonia in the
relatively unrestricted jet. The results obtained in a
subsequent launching of the bomb, with reinforcements to
the tail structure, in flight tests at the DVL are shown
in figure 20.

## CONCLUSIONS

The following conclusions were drawn from the investigation of the effects of Reynolds number, air-stream boundaries, and humidity in tests of airfoils at high speeds:

1. It has been shown that the ratio of tunnel height to model size, the form of the test section, and the testing technique have a very great bearing on the results obtained at subsonic Mach numbers above 0.7.

2. Reynolds number effects were of secondary importance at very high Mach numbers for the range investigated.

3. In the absence of suitable correction factors, the only safe experimental technique consists in keeping the scale of the model small enough so that the corrections required are negligible.

4. In a closed air stream, the model must be small enough that the highest desired test Mach number is below the choking Mach number of the tunnel, at which the effects of the tunnel walls on the flow over the model become extremely large.

5. By use of a jet which is not restrained by top and bottom walls the maximum Mach number that can be used for a given value of the ratio of jet height to model chord is appreciably higher than the value that can be obtained in a closed jet.

6. The considerations of condensation phenomena that have been discussed have brought out the fact that the conditions under which condensation occurs depend on many variables and that only with great difficulty could flight conditions be simulated in wind-tunnel tests in which small-scale models are used. Wind-tunnel tests should be conducted with low values of the relative humidity, because under such conditions the effects of condensation are known to be negligibly small.

II. TEST RESULTS FOR 24 AIRFOILS IN THE MACH

NUMBER RANGE OF 0.40 TO 0.94

APPARATUS AND METHODS

Twenty-four profiles were tested in the 1.31 by
1.74-foot high-speed tunnel at Guidonia with the partly
free test section previously described. For every pro-
file the lift, the drag, and the pitching moment at the
quarter-chord point were measured by use of the three-
component semiautomatic balance described in reference 4.
The extremities of the models were fixed at the balance
supports, and the models were checked during the tests to
verify that the aerodynamic loads did not bend them
appreciably. All the tests were repeated with the model
inverted. For some models, the tests were repeated later
when the static atmospheric conditions were completely
different and with different humidities in the test sec-
tion. (The values of the relative humidity were always
low.) The differences in the results obtained were not
appreciable.

All the models were made of well-polished steel and
had chords of 1.575 inches for thickness ratios of 3 per-
cent or greater. In order to prevent excessive bending,
the models with thickness ratios of less than 3 percent
had chords of 1.969 inches.

The profiles of small models seldom correspond
exactly with the profile desired. For purposes of accu-
racy, therefore, an optical device was constructed that
permitted photographing with extreme precision the true
section of each model on a greatly increased scale. For
each model two end sections were photographed and the
true profile was projected on the photograph to provide
the desired comparison. Because the airfoils were con-
structed by machine, the profile shape did not vary across
the model span. This fact was confirmed by superimposing
drawings of the two end sections. It was verified that
the surface was adequately smooth by observing the tan-
gential illuminated surface under great magnification.

Figure 21 shows the specified shapes of the profiles
tested. In figure 22 the actual shapes of the profiles
tested are compared with the specified shapes. In order

that the difference between the actual and the specified profiles may be clearly seen, the ordinate scale used in figure 22 has been enlarged.  Table I shows the ordinates of the profiles tested.

All the tests were performed at an approximately constant Reynolds number varying in the range from 340,000 to 420,000.  The density, and consequently the Reynolds number, had to be kept low for the thinner airfoils in order to prevent excessive loads.

## AIRFOILS TESTED

The profiles listed in the following table were tested:

| Airfoil | Reference | Airfoil | Reference |
|---------|-----------|---------|-----------|
| NACA 0006-64 | 5 | NACA 2315 | 6 |
| NACA 0009-64 | 5 | NACA 2406 | 6 |
| NACA 0012-64 | 5 | NACA 2409 | 6 |
| NACA 0015-64 | 5 | NACA 2412 | 6 |
| NACA 0006-34 | 5 | U.S.N.P.S. 1 (4 percent thick) | 7 |
| NACA 0008-34 | 5 | U.S.N.P.S. 2 (8 percent thick) | 7 |
| NACA 0012-34 | 5 | U.S.N.P.S. 3 (10 percent thick) | 7 |
| NACA 0006-63 | 5 | NACA M1 (6 percent thick) | 7 |
| NACA 0009-63 | 5 | NACA 0006T | 6 |
| NACA 2306 | 6 | NACA 2509 | 6 |
| NACA 2309 | 6 | Davis (9 percent thick) | -------- |
| NACA 2312 | 6 | ETH309 | (a) |

[a]Developed at Zurich University.

RESULTS

In figures 23 to 46 the results of the tests of the 24 airfoils are shown in the form of the usual coefficients: $C_L$ and $C_D$ are plotted against the test Mach number at the same angles of attack, and $C_{m_c/4}$ is plotted against the Mach number at values of $C_L$ corresponding to the given angles of attack. Figures 47 to 70 show $a$, $C_D$, and $C_{m_c/4}$ plotted against the corresponding $C_L$ for each airfoil at the same Mach numbers. In figure 71 the angle of zero lift is plotted against Mach number for representative airfoils of the group. Figure 72 gives the maximum lift-drag ratio $(L/D)_{max}$, $a$ for $(L/D)_{max}$, and $C_L$ for $(L/D)_{max}$ as functions of Mach number for all the airfoils tested. Figures 73 and 74 present $C_{D_{min}}$ and $(L/D)_{max}$ as functions of the maximum percentage thickness for all the airfoils at various Mach numbers, and figures 75 and 76 show $C_{D_{min}}$ and $(L/D)_{max}$ plotted against Mach number for several groups of airfoils having the same maximum thickness.

It can be observed from the test results that:

The lift-coefficient curve as a function of Mach number presents a maximum and later a minimum value. The Mach numbers at these values can be defined as the first and the second critical Mach numbers for the lift. The Mach number at which the drag-coefficient curve abruptly bends upward is defined herein as the critical Mach number for the drag. It will be noted that the critical Mach numbers as defined herein are different for the lift and for the drag data. The critical Mach numbers used, furthermore, do not necessarily correspond to the stream Mach number at which local sonic velocity is reached.

The rate of drag rise past the critical Mach number increases as the lift coefficient, the angle of attack, and the thickness ratio are increased.

The first critical Mach number for $C_L$ and the critical Mach number for $C_D$ for each airfoil is lowered with the increase in angle of attack.

For each series of airfoils at the same angles of attack, these critical Mach numbers decrease as the thickness increases.

The critical Mach numbers at the same thickness and the same angle of attack are much lower for the cambered profiles than for the symmetrical profiles tested at the same angle of attack. At equal thickness and equal camber, the critical Mach numbers are higher where the maximum thickness was at the 40-percent-chord station than where it was at the 30-percent-chord station.

Above the critical Mach numbers, the drag increases and the lift decreases very rapidly; for a profile with a larger thickness and sharper curvature, the increase in drag and the decrease in lift is sharper.

These general phenomena agree with results of other laboratories. (See, for example, reference 4.)

Lift.- At subsonic Mach numbers the increase in lift coefficient with Mach number follows approximately the theoretical relation $\dfrac{1}{\sqrt{1 - M^2}}$, especially for the low thickness ratios. After the first critical Mach number is reached, the lift coefficient decreases very rapidly until it reaches a minimum at the second critical Mach number when it again starts to increase. This second critical Mach number is lowered with the decrease in the first critical Mach number. Airfoils with larger camber had greater decreases in lift. For these airfoils, generally, the angle of attack for zero lift changed greatly and tended toward positive values (fig. 71). At the highest test Mach numbers all the wings functioned in a manner very similar to symmetrical profiles. This phenomenon agrees with the fact that the value of the angle of zero lift for an unsymmetrical profile changes sign and becomes considerably reduced in magnitude in passing from a subsonic to a supersonic velocity.

The lift-curve slope $dC_L/d\alpha$ increases up to the first critical Mach number after which there is a considerable decrease up to the second critical Mach number. (See figs. 47 to 70.) The second critical Mach number is greatly affected by the value of the maximum percentage thickness. For the lower thicknesses tested,

the second critical Mach number was reached only at the
maximum speed of the test.

Moment.- The curve of pitching-moment coefficient
against Mach number has a fairly regular form (figs. 33
to 46). Generally, the value of $C_{m_{c/4}}$ remains constant
up to the first critical Mach number and then tends to
decrease. For the larger thickness ratios there is an
increase in $C_{m_{c/4}}$ at the first critical Mach number,
and it appears that the center of pressure moves forward.
When the Mach number is increased beyond the critical
value, $C_{m_{c/4}}$ decreases until it reaches a minimum and
then tends to increase.

The center of pressure moves appreciably at low
values of $C_L$ for profiles of large camber. For sym-
metrical profiles the variations of $C_{m_{c/4}}$ at low values
of $C_L$ are small, especially if the maximum thickness
is about 40 percent of the chord.

Drag and lift-drag ratio.- The value of $(L/D)_{max}$
decreased rapidly beyond the first critical Mach number
for the lift and continued to decrease until the second
critical Mach number was reached. It then varied very
slowly with further increase in Mach number (fig. 72).
The larger thicknesses suffer more pronounced relative
changes in $(L/D)_{max}$. The angle of attack and the lift
coefficient corresponding to the $(L/D)_{max}$ (fig. 72)
decrease as far as the second critical point and then
begin to increase rapidly. The variations are appreciably
influenced by the value of maximum thickness ratio and
by the mean camber.

In order to emphasize the importance of maximum per-
centage thickness on the values of $C_{D_{min}}$ and $(L/D)_{max}$,
figures 73 and 74 were prepared to show the values of
these factors as a function of maximum percentage thickness
at constant Mach number for each series considered. These
figures show that the effect of the maximum percentage
thickness becomes greater as the Mach number increases
for all profiles tested. For Mach numbers around 0.8,
the effects of thickness ratio are very large. At low
test speeds, for example, when the maximum thickness is

varied from 6 to 12 percent, $c_{D_{min}}$ increases about
30 percent; at Mach numbers around 0.8 or greater, the
increase becomes 200 to 400 percent. The ratio
of the values of $(L/D)_{max}$ for the NACA 0006-34 airfoil
to those for the NACA 0012-34 airfoil changes from
about 1.18 at a Mach number of 0.65 to 4.5 at a Mach
number of 0.85 and to 2.2 at a Mach number of 0.94. It
is also interesting to compare the aerodynamic character-
istics of various profiles at equal maximum percentage
thicknesses. (See figs. 75 and 76.)

The larger increments in $c_{D_{min}}$ occur for the pro-
files with larger camber, for which the critical Mach
number is lower. With increase in the value of the maxi-
mum percentage thickness, the value of $dc_{D_{min}}/dM$
increases and even at very high Mach numbers this differ-
ence between various profiles is considerable.

The profile shape has considerable effect on $(L/D)_{max}$
(fig. 76); the unsymmetrical profiles have larger $(L/D)_{max}$
values at low Mach numbers. At higher speeds, the symmet-
rical profiles with the maximum thickness at about 40 per-
cent of the chord had higher efficiencies than those with
the maximum thickness at 30 percent of the chord. The
difference between the various profile types is consid-
erable for low Mach numbers; however, it decreases with
increase in Mach number and is small for Mach numbers
around 0.94.

## CONCLUSIONS

The following conclusions may be drawn from the
results obtained from tests of 24 small-scale airfoils
in the Guidonia high-speed tunnel:

1. At subsonic Mach numbers both the profile shape
and the thickness ratio had a large effect on the minimum
drag coefficient.

2. Reducing the thickness ratio, moving the point
of maximum thickness from 30 to 40 percent of the chord,
and reducing the camber all tended to increase the
critical Mach number.

3. Airfoils of large percentage thickness should not
be used at high Mach numbers because of the radical
adverse changes in their characteristics at supercritical
speeds.

4. When the critical speed was exceeded, the drag
coefficients increased rapidly. Abrupt decreases in lift
and changes in moment occurred at somewhat higher critical
Mach numbers.

5. The lift coefficient continued to decrease as the
speed was advanced beyond the first critical Mach number
until a second critical Mach number was reached, beyond
which the lift coefficient increased in value.

6. At very high supercritical Mach numbers the
thickness ratio is the dominating variable, the drag
coefficient being almost directly proportional to the
thickness at a Mach number of 0.94.


National Advisory Committee for Aeronautics
        Langley Memorial Aeronautical Laboratory
              Langley Field, Va.

# REFERENCES

1. Ferri, Antonio:  La galleria ultrasonora di Guidonia.
      Atti di Guidonia  No. 15, 1939.  (Available in Air-
      craft Engineering, vol. XII, no. 140, Oct. 1940,
      pp. 302-305.)

2. Ferri, Antonio:  Influenza del numero di Reynolds ai
      grandi numeri di Mach.  Atti di Guidonia
      No. 67-68-69, 1942.  (Available as R.T.P. Tr. No. 1933,
      British Ministry of Aircraft Production.)

3. Byrne, Robert W.:  Experimental Constriction Effects
      in High-Speed Wind Tunnels.  NACA ACR No. L4L07a,
      1944.

4. Ferri, Antonio:  Investigations and Experiments in
      the Guidonia Supersonic Wind Tunnel.  NACA TM
      No. 901, 1939.

5. Stack, John, and von Doenhoff, Albert E.:  Tests of
      16 Related Airfoils at High Speeds.  NACA Rep.
      No. 492, 1934.

6. Jacobs, Eastman N., Ward, Kenneth E., and Pinkerton,
      Robert M.:  The Characteristics of 78 Related Air-
      foil Sections from Tests in the Variable-Density
      Wind Tunnel.  NACA Rep. No. 460, 1933.

7. Jacobs, Eastman N., and Anderson, Raymond F.:  Large-
      Scale Aerodynamic Characteristics of Airfoils as
      Tested in the Variable Density Wind Tunnel.  NACA
      Rep. No. 352, 1930.

TABLE I

ORDINATES OF ACTUAL AIRFOILS

[All stations and ordinates in percent chord]

**First table block**

| Station | NACA 0006-64 Upper surface | NACA 0006-64 Lower surface | NACA 0009-64 Upper surface | NACA 0009-64 Lower surface | NACA 0012-64 Upper surface | NACA 0012-64 Lower surface | NACA 0015-64 Upper surface | NACA 0015-64 Lower surface | NACA 0006-34 Upper surface | NACA 0006-34 Lower surface | NACA 0008-34 Upper surface | NACA 0008-34 Lower surface | NACA 0012-34 Upper surface | NACA 0012-34 Lower surface | NACA 0006-63 Upper surface | NACA 0006-63 Lower surface | NACA 0009-63 Upper surface | NACA 0009-63 Lower surface | NACA 2306 Upper surface | NACA 2306 Lower surface | NACA 2309 Upper surface | NACA 2309 Lower surface | NACA 2312 Upper surface | NACA 2312 Lower surface |
|---|---|---|---|---|---|---|---|---|---|---|---|---|---|---|---|---|---|---|---|---|---|---|---|---|
| 0 | 0 | 0 | 0 | 0 | 0 | 0 | 0 | 0 | 0 | 0 | 0 | 0 | 0 | 0 | 0 | 0 | 0 | 0 | 0 | 0 | 0 | 0 | 0 | 0 |
| 1.25 | .80 | .85 | 1.19 | 1.21 | 1.50 | 1.52 | 2.00 | 1.90 | .50 | .49 | .86 | .90 | .98 | 1.11 | .95 | .94 | 1.40 | 1.34 | 1.35 | .069 | 1.40 | 1.08 | 2.30 | 1.67 |
| 2.50 | 1.15 | 1.19 | 1.69 | 1.74 | 1.50 | 1.25 | 2.89 | 2.75 | .72 | .74 | 1.25 | 1.25 | 1.30 | 1.59 | 1.85 | 1.26 | 1.98 | 1.85 | 1.97 | .095 | 2.10 | 1.38 | 3.25 | 2.24 |
| 5.00 | 1.64 | 1.61 | 2.39 | 2.42 | 3.01 | 3.00 | 3.95 | 3.81 | 1.10 | 1.11 | 1.80 | 1.79 | 2.31 | 2.55 | 1.85 | 1.84 | 2.69 | 2.50 | 2.69 | 1.19 | 3.10 | 1.78 | 5.38 | 2.91 |
| 7.50 | 1.95 | 1.95 | 2.85 | 2.89 | 3.58 | 3.58 | 4.63 | 4.16 | 1.40 | 1.42 | 2.23 | 2.22 | 3.01 | 3.00 | 2.14 | 2.15 | 3.18 | 2.96 | 3.21 | 1.23 | 3.85 | 2.04 | 5.95 | 3.34 |
| 10 | 2.20 | 2.20 | 3.21 | 3.25 | 3.98 | 3.99 | 5.14 | 5.00 | 1.68 | 1.70 | 2.55 | 2.56 | 3.55 | 3.40 | 2.39 | 2.40 | 3.55 | 3.05 | 3.65 | 1.30 | 4.38 | 2.04 | 5.95 | 3.64 |
| 15 | 2.51 | 2.50 | 3.67 | 3.71 | 4.63 | 4.60 | 5.94 | 6.00 | 2.11 | 2.10 | 3.09 | 3.09 | 4.40 | 4.40 | 2.79 | 2.80 | 4.34 | 4.05 | 4.28 | 1.30 | 5.17 | 2.45 | 7.06 | 3.98 |
| 20 | 2.67 | 2.69 | 4.04 | 4.40 | 5.09 | 5.07 | 6.55 | 6.59 | 2.44 | 2.41 | 3.43 | 3.45 | 5.00 | 5.04 | 2.97 | 2.86 | 4.54 | 4.39 | 4.68 | 1.21 | 5.66 | 2.45 | 7.52 | 4.10 |
| 25 | 2.91 | 2.91 | 4.40 | 4.46 | 5.64 | 5.69 | 7.50 | 7.29 | 2.86 | 2.85 | 3.79 | 3.91 | 5.71 | 5.90 | 2.97 | 2.96 | 4.37 | 4.39 | 6.20 | 1.21 | 6.20 | 2.65 | 8.00 | 4.10 |
| 30 | 3.00 | 3.00 | 4.46 | 4.50 | 5.70 | 5.71 | 7.28 | 7.50 | 3.00 | 3.00 | 3.80 | 4.10 | 5.90 | 5.69 | 2.96 | 2.86 | 4.00 | 4.39 | 4.88 | 1.04 | 5.90 | 2.57 | 7.81 | 4.08 |
| 40 | 2.86 | 2.83 | 4.50 | 4.50 | 5.19 | 5.20 | 6.55 | 6.65 | 2.80 | 2.94 | 3.55 | 3.58 | 5.09 | 5.09 | 2.80 | 2.80 | 4.57 | 3.90 | 4.86 | .89 | 5.28 | 2.13 | 7.17 | 3.89 |
| 50 | 2.55 | 2.56 | 3.47 | 3.90 | 4.35 | 3.24 | 5.55 | 5.59 | 2.53 | 2.70 | 3.02 | 3.00 | 4.23 | 4.29 | 2.57 | 2.55 | 4.00 | 3.38 | 4.39 | .79 | 5.28 | 2.13 | 6.17 | 3.50 |
| 60 | 2.13 | 2.10 | 2.61 | 3.25 | 3.84 | 3.21 | 5.55 | 5.59 | 1.89 | 2.20 | 2.27 | 2.26 | 3.25 | 3.20 | 1.54 | 2.16 | 2.75 | 2.73 | 2.32 | .69 | 5.21 | 1.80 | 4.92 | 3.09 |
| 70 | 1.57 | 1.59 | 1.61 | 2.40 | 1.84 | 1.90 | 2.30 | 2.08 | .89 | 1.56 | 1.71 | 2.24 | 3.25 | 1.79 | 1.54 | 1.99 | 1.02 | 2.16 | 1.29 | .41 | 3.65 | 1.35 | 4.21 | 2.86 |
| 80 | .93 | .90 | 1.81 | 1.77 | 1.60 | 1.90 | 2.30 | 1.51 | .51 | .49 | .71 | .71 | 1.80 | 1.79 | .54 | .99 | 1.02 | .99 | 1.90 | .35 | 1.27 | .81 | 3.19 | 1.85 |
| 90 | .53 | .51 | .51 | .75 | 1.23 | .34 | 1.23 | 1.08 | .10 | .10 | .08 | .08 | .95 | .93 | .05 | .60 | .54 | .55 | 1.00 | .25 | .60 | .48 | 1.80 | 1.02 |
| 95 | .33 | .33 | | | | | | | | | | | | | | | | | | | | | | |
| 100 | .09 | .15 | .12 | .09 | .12 | .06 | .03 | .03 | .10 | .10 | .08 | .08 | 0 | 0 | .05 | .08 | 0 | 0 | .012 | 0 | .03 | 0 | 1.02 | .61 |

**Second table block**

| Station | NACA 2315 Upper surface | NACA 2315 Lower surface | NACA 2406 Upper surface | NACA 2406 Lower surface | NACA 2409 Upper surface | NACA 2409 Lower surface | NACA 2412 Upper surface | NACA 2412 Lower surface | U.S.N.P.S.1 Upper surface | U.S.N.P.S.1 Lower surface | U.S.N.P.S.2 Upper surface | U.S.N.P.S.2 Lower surface | U.S.N.P.S.3 Upper surface | U.S.N.P.S.3 Lower surface | M1 Upper surface | M1 Lower surface | NACA 0006T Upper surface | NACA 0006T Lower surface | NACA 2509 Upper surface | NACA 2509 Lower surface | Davis 9 percent Upper surface | Davis 9 percent Lower surface | ETH609 Upper surface | ETH609 Lower surface |
|---|---|---|---|---|---|---|---|---|---|---|---|---|---|---|---|---|---|---|---|---|---|---|---|---|
| 0 | 0 | 0 | 0 | 0 | 0 | 0 | 0 | 0 | 0.30 | 0.30 | 0.72 | 0.72 | 0.60 | 0.60 | 0 | 0 | 0 | 0 | 0 | 0 | 0 | 0 | 0 | 0 |
| 1.25 | 2.50 | .11 | .94 | .65 | .60 | 1.20 | 1.85 | 1.74 | 1.07 | 0 | 2.45 | .20 | 3.10 | .18 | .82 | .90 | .55 | .68 | 1.70 | 1.16 | 1.25 | .76 | 1.50 | .52 |
| 2.50 | 3.39 | 2.70 | 1.43 | .89 | 2.35 | 1.65 | 2.72 | 2.20 | 1.50 | 0 | 3.30 | .07 | 5.15 | .03 | 1.23 | 1.25 | .95 | 1.00 | 2.25 | 1.39 | 1.76 | 1.08 | 2.15 | .81 |
| 5.00 | 5.34 | 3.59 | 2.48 | 1.20 | 3.26 | 2.13 | 3.96 | 2.99 | 1.50 | 0 | 4.50 | 0 | 5.90 | 0 | 1.78 | 1.76 | 1.45 | 1.50 | 3.05 | 1.78 | 2.50 | 1.61 | 3.08 | 1.25 |
| 7.50 | 6.61 | 4.25 | 3.05 | 1.35 | 3.97 | 2.50 | 4.97 | 3.52 | 2.65 | 0 | 5.58 | 0 | 6.60 | 0 | 2.10 | 2.10 | 1.88 | 1.88 | 3.45 | 2.01 | 3.15 | 2.00 | 3.75 | 1.70 |
| 10 | 8.00 | 4.48 | 3.85 | 1.45 | 4.55 | 2.87 | 5.75 | 3.87 | 3.00 | 0 | 6.85 | 0 | 7.60 | 0 | 2.69 | 2.30 | 2.15 | 2.17 | 4.10 | 2.80 | 3.45 | 2.61 | 5.35 | 1.77 |
| 15 | 9.21 | 4.48 | 4.35 | 1.38 | 5.25 | 2.91 | 6.74 | 4.29 | 4.00 | 0 | 7.44 | 0 | 8.73 | 0 | 2.87 | 2.61 | 2.74 | 2.55 | 5.29 | 3.50 | 4.10 | 3.13 | 5.75 | 2.40 |
| 20 | 9.32 | 4.26 | 4.90 | 1.20 | 5.25 | 2.46 | 7.29 | 4.38 | 4.80 | 0 | 7.80 | 0 | 9.97 | 0 | 3.00 | 2.95 | 2.89 | 2.60 | 5.95 | 3.50 | 5.21 | 3.22 | 5.75 | 2.40 |
| 25 | 9.21 | 4.15 | 5.09 | 1.20 | 6.37 | 2.16 | 7.13 | 3.78 | 3.97 | 0 | 7.40 | 0 | 8.08 | 0 | 3.00 | 2.70 | 2.89 | 2.60 | 5.07 | 3.22 | 5.49 | 2.63 | 6.50 | 2.15 |
| 30 | 8.32 | 3.50 | 5.31 | 1.00 | 5.31 | 1.80 | 6.25 | 3.30 | 3.57 | 0 | 7.40 | 0 | 8.08 | 0 | 2.83 | 2.70 | 2.65 | 2.35 | 5.99 | 2.03 | 4.60 | 1.85 | 5.87 | 2.00 |
| 40 | 7.60 | 3.20 | 3.12 | .77 | 4.12 | 1.37 | 5.31 | 2.78 | 3.37 | 0 | 5.40 | 0 | 7.16 | 0 | 2.10 | 1.90 | 2.25 | 1.79 | 5.49 | 1.69 | 3.65 | 1.47 | 4.92 | 1.47 |
| 50 | 5.34 | 2.30 | 2.43 | .52 | 3.12 | 1.00 | 3.67 | 1.96 | 2.10 | 0 | 2.43 | 0 | 1.88 | 0 | 1.56 | 1.30 | 1.77 | 1.60 | 3.42 | 1.30 | 3.42 | 1.01 | 3.49 | 1.01 |
| 60 | 4.30 | 1.30 | 1.60 | .20 | 1.60 | .56 | 1.96 | 1.31 | 1.72 | 0 | 1.42 | 0 | 1.50 | .50 | .54 | .90 | 1.20 | .60 | 1.90 | .51 | 1.27 | .40 | 1.80 | .64 |
| 70 | 2.31 | 1.21 | .67 | .10 | .75 | .34 | 1.03 | .85 | .15 | .15 | .20 | .20 | 0 | 0 | .42 | .35 | .68 | .30 | 1.00 | .31 | .60 | .19 | .95 | .30 |
| 80 | 1.21 | .62 | | | -.08 | .05 | 0 | .42 | | | | | | | 0 | | .40 | | 0 | | | | | .17 |
| 90 | 0 | 0 | 0 | 0 | 0 | 0 | 0 | 0 | 0 | 0 | 0 | 0 | 0 | 0 | 0 | 0 | 0 | 0 | 0 | 0 | 0 | 0 | 0 | 0 |

Figure 1.- Sketch of the test section of the Guidonia high-speed tunnel showing model location.

Figure 2.- Profile of C-8 airfoil section.

Figure 3.— Lift-, drag-, and moment-coefficient characteristics of a C-8 airfoil section at M = 0.50.

Figure 4. — Lift-, drag-, and moment-coefficient characteristics of a C-8 airfoil section at M = 0.60.

Figure 5. — Lift-, drag-, and moment-coefficient characteristics of a C-8 airfoil section at M = 0.70.
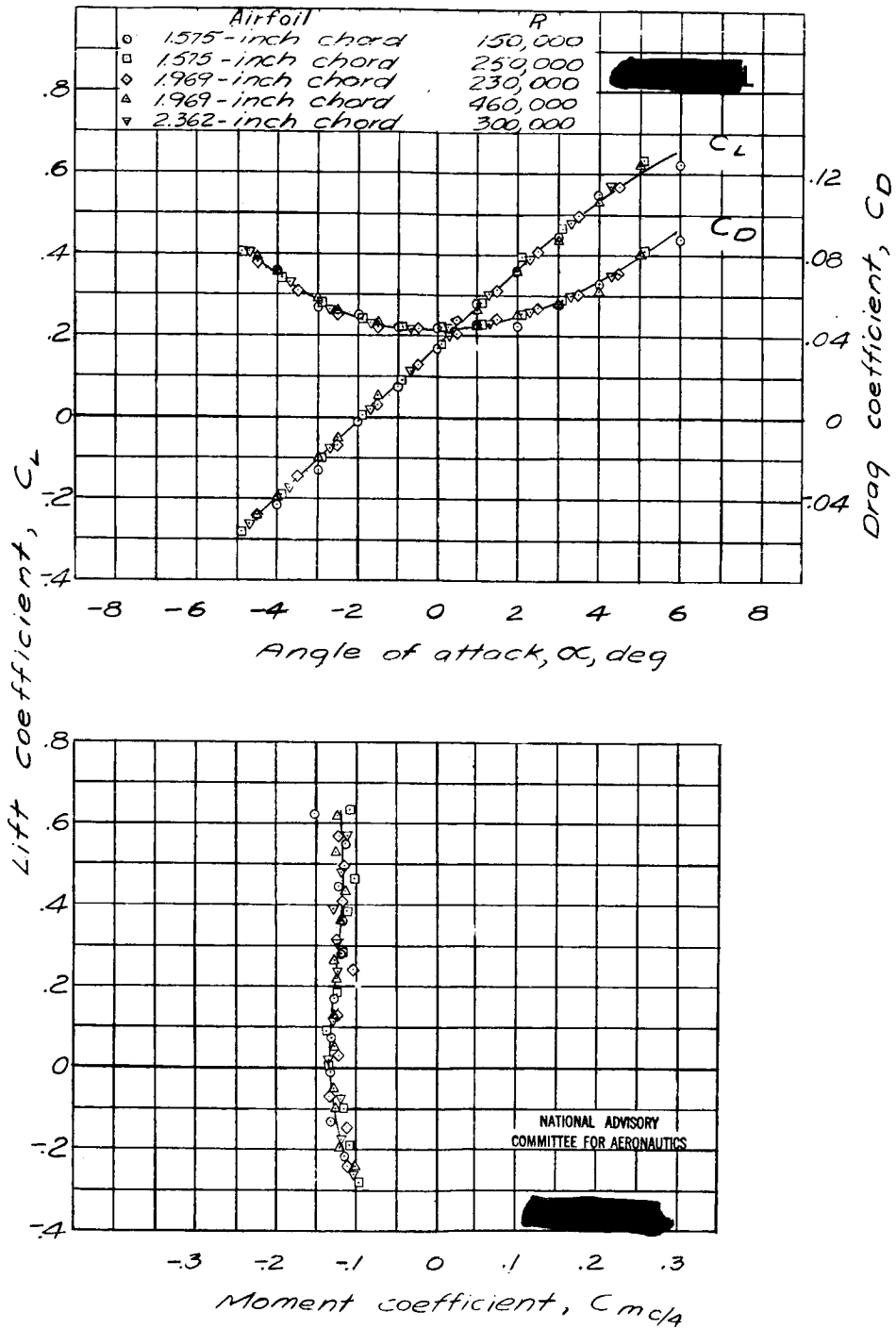
Figure 6 .— Lift-, drag-, and moment-coefficient characteristics of a C-8 airfoil section at M = 0.80.
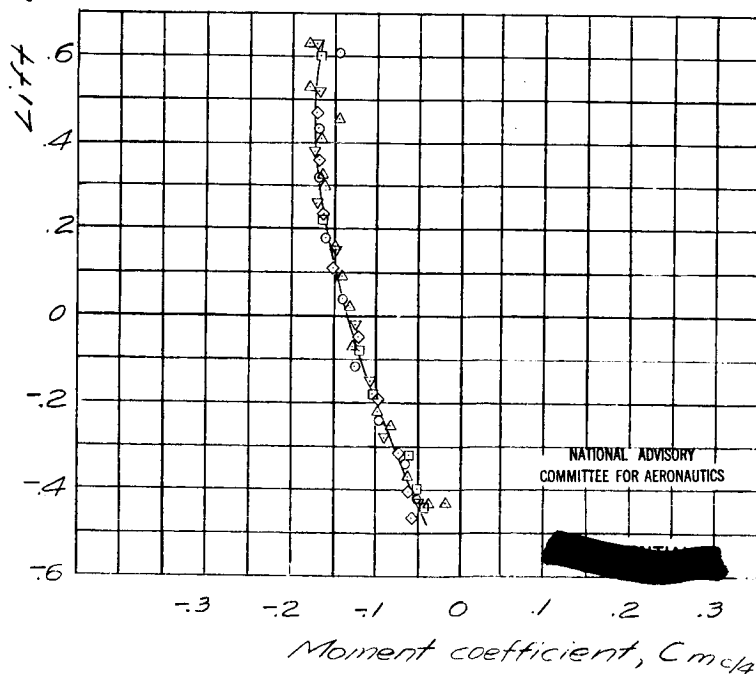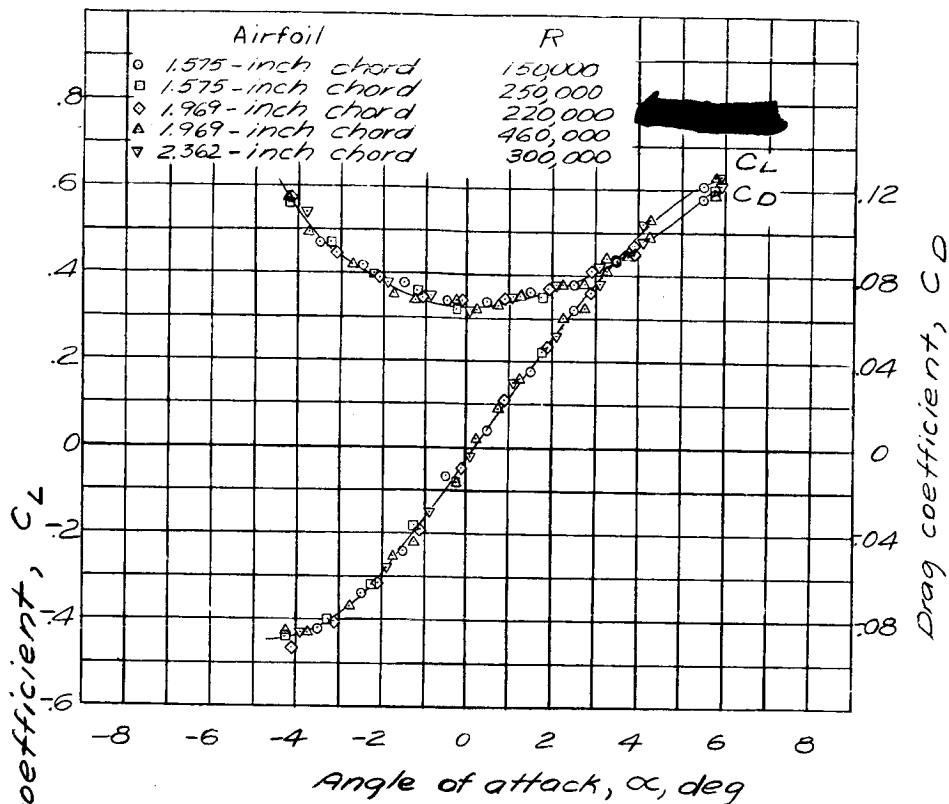
Figure 7.— Lift-, drag-, and moment-coefficient
        characteristics of a C-8 airfoil section at
        M=0.90.
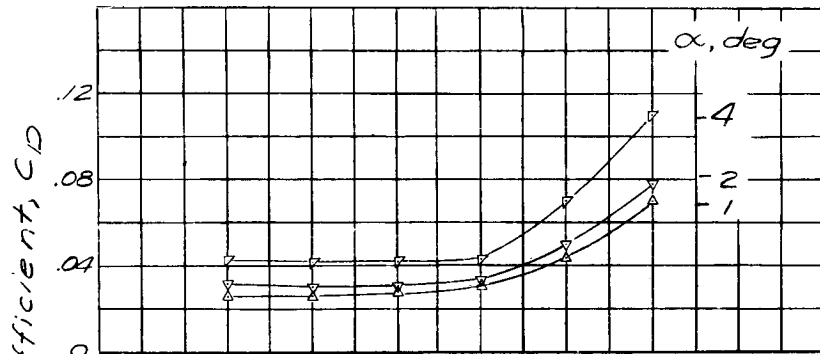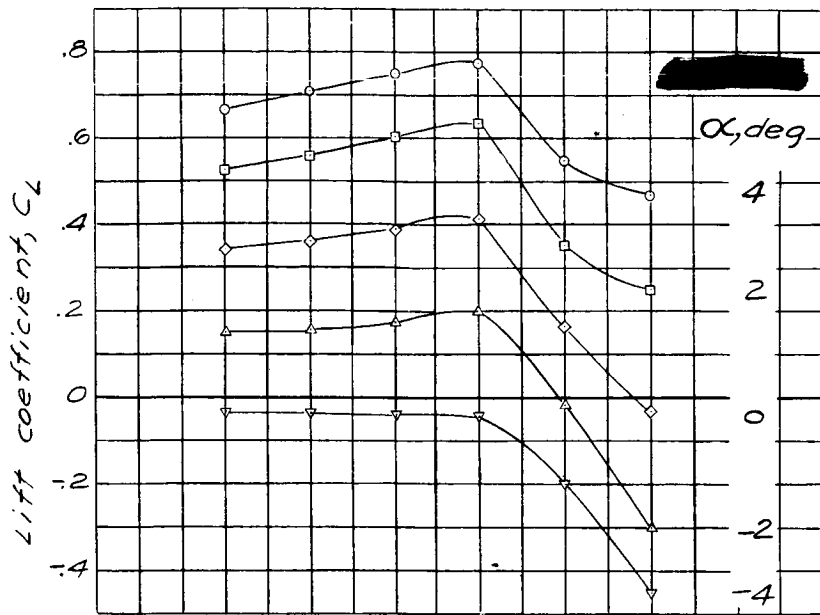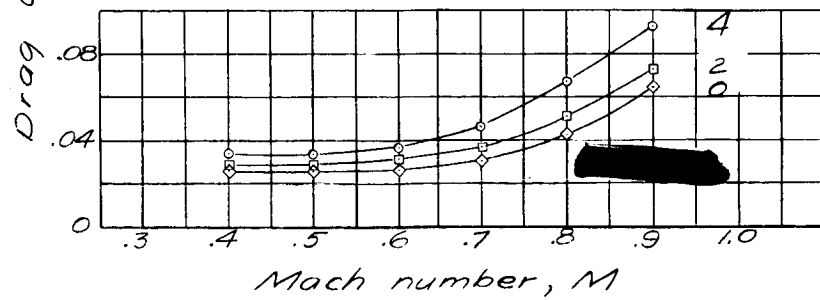
(a) At various angles of attack.

Figure 8. – Variation of lift and drag coefficients with Mach number for a C-8 airfoil section.
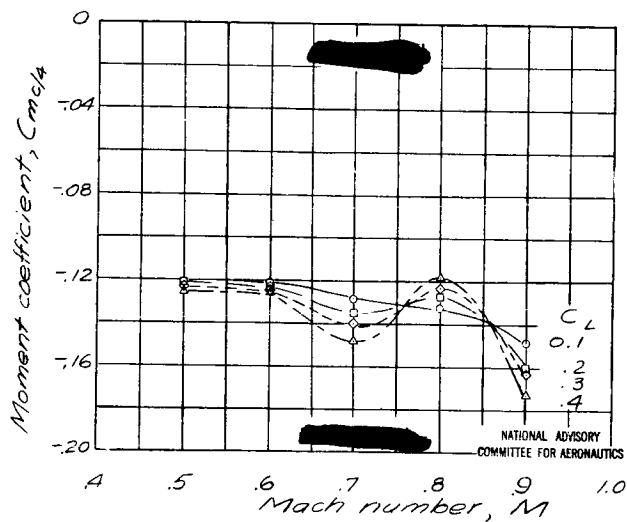
(b) At various values of lift coefficient.

Figure 8. - Concluded.
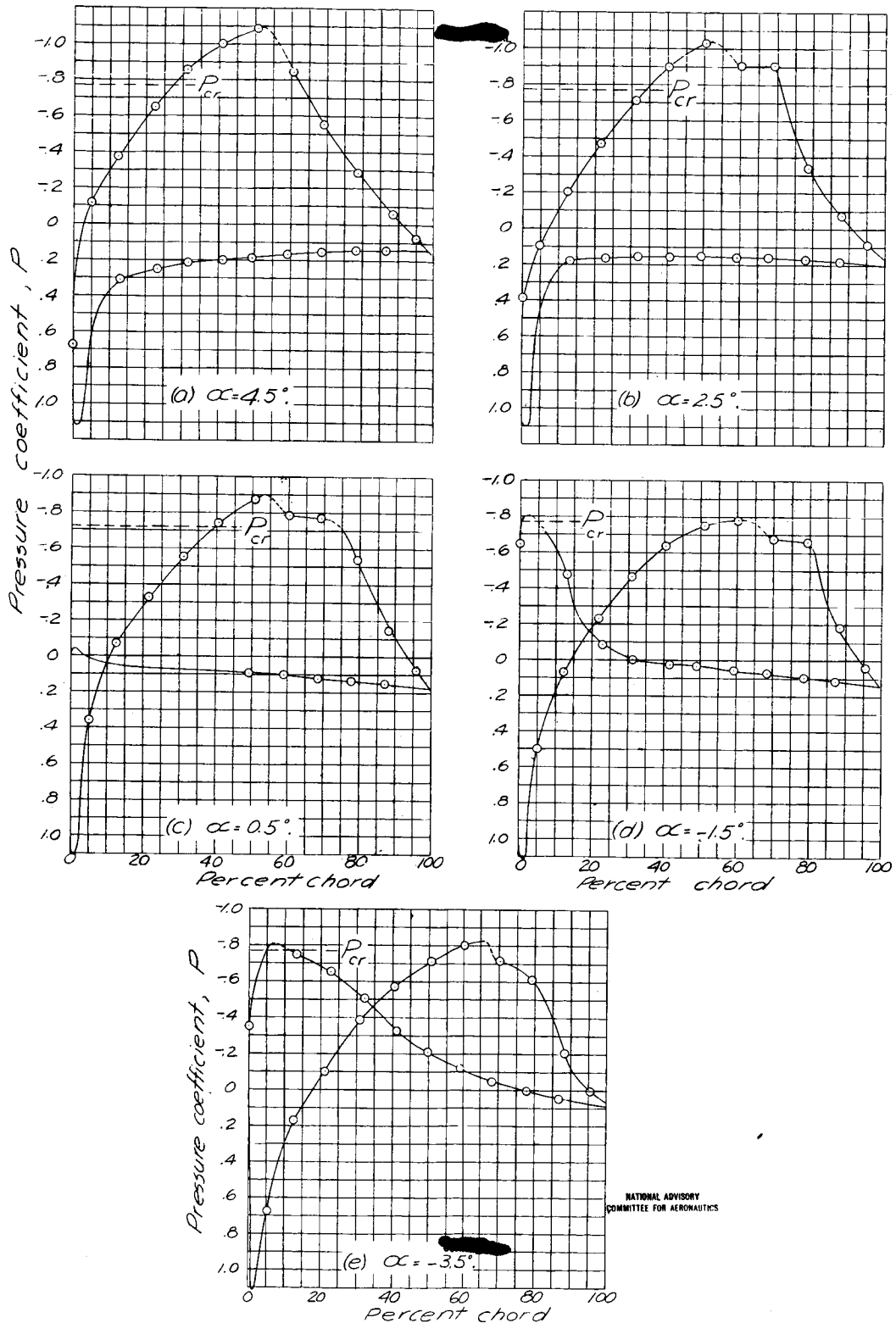
Figure 9.— Pressure-distribution measurements
for a G-8 airfoil section. M = 0.70; airfoil chord, 3.15 inches.
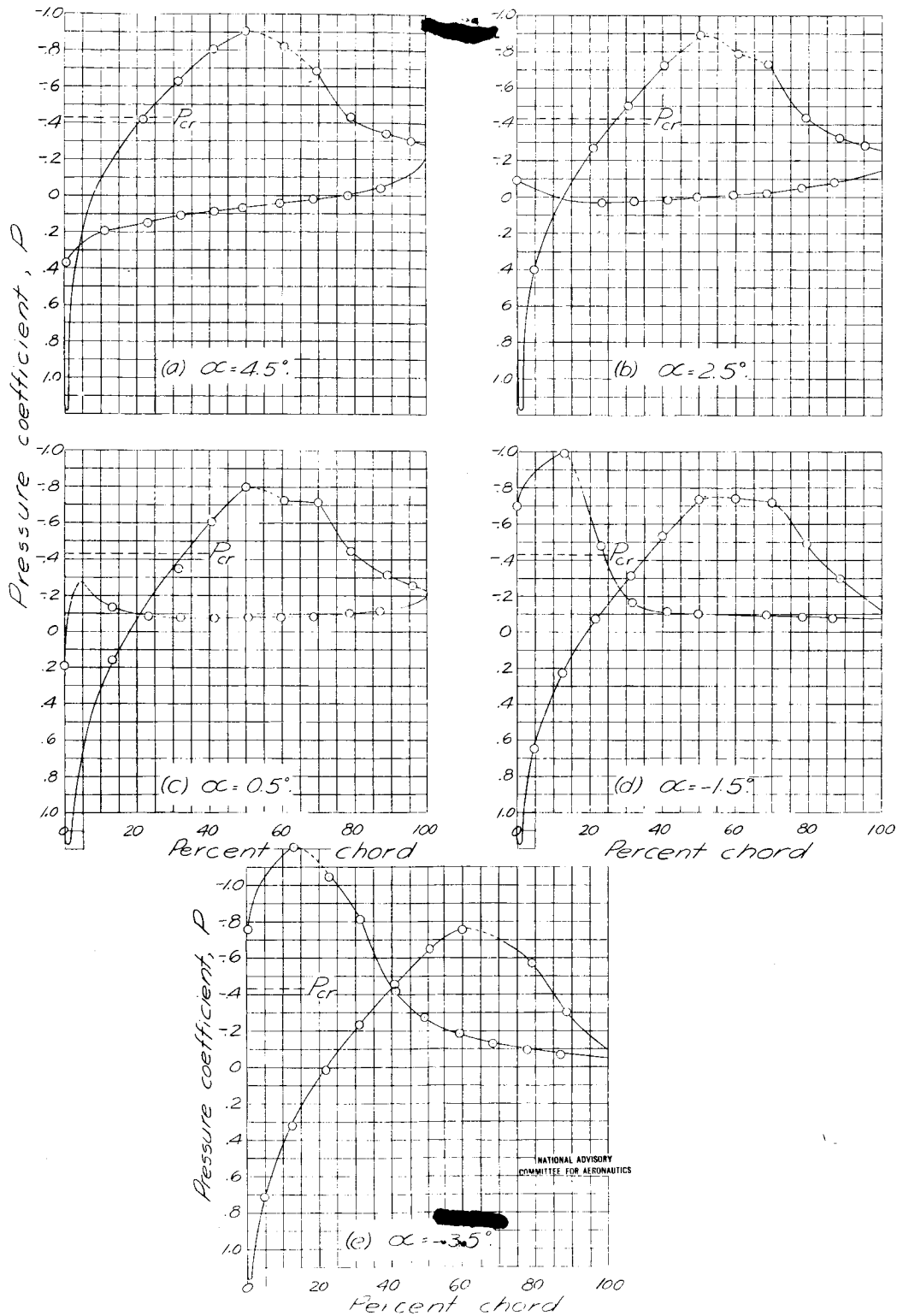
Figure 10. — Pressure distribution measurements for a C-8 airfoil section. M = 0.80; airfoil chord, 3.15 inches.
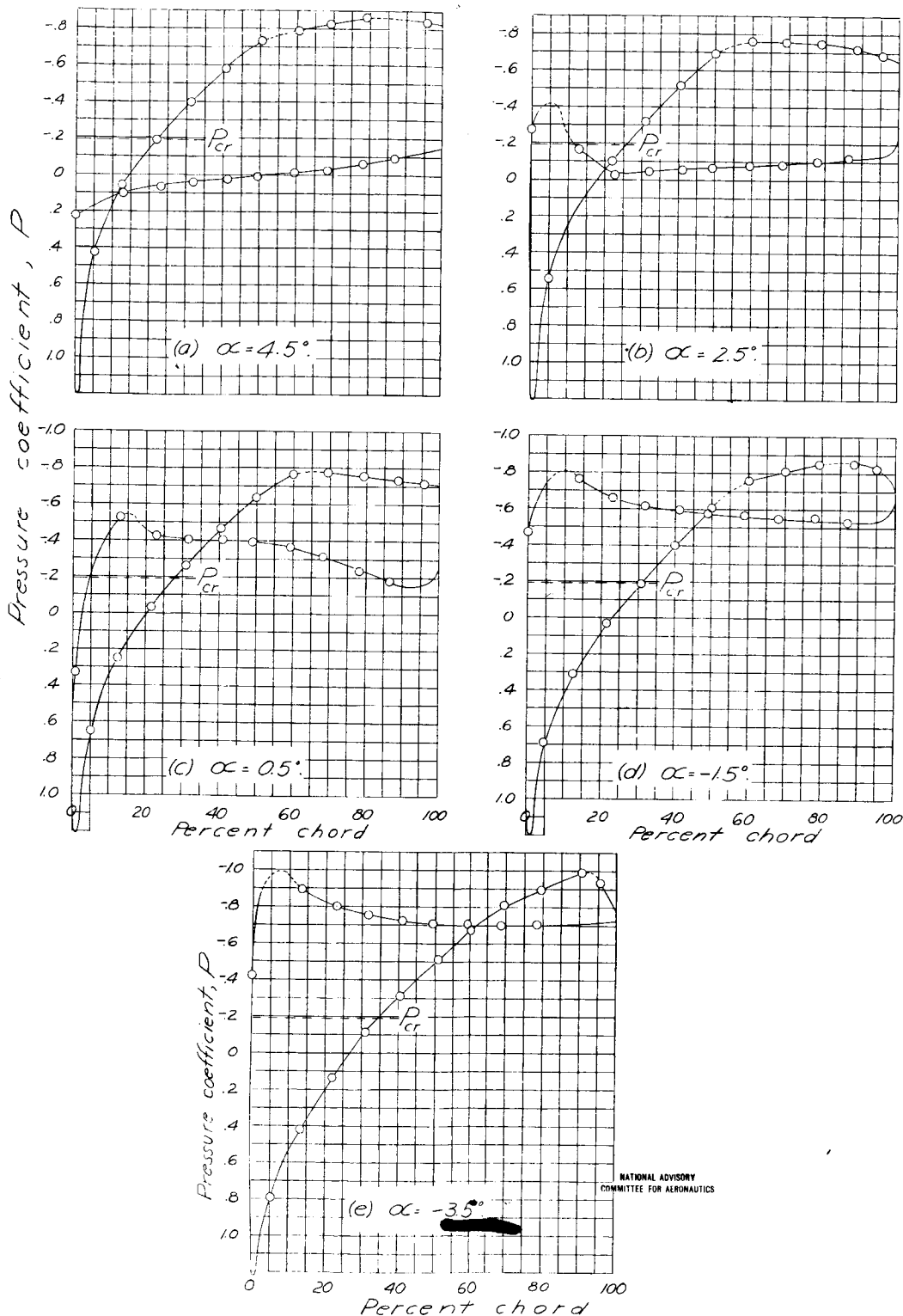
Figure 11.— Pressure-distribution measurements for a C-8 airfoil section, M = 0.90; airfoil chord, 3.15 inches.

——— 1.969-inch chord, R=500,000
○   3.150-inch chord, R=800,000

Angle of attack, α, deg

NATIONAL ADVISORY
COMMITTEE FOR AERONAUTICS

Moment coefficient, $Cm_{c/4}$

(a) M = 0.70.
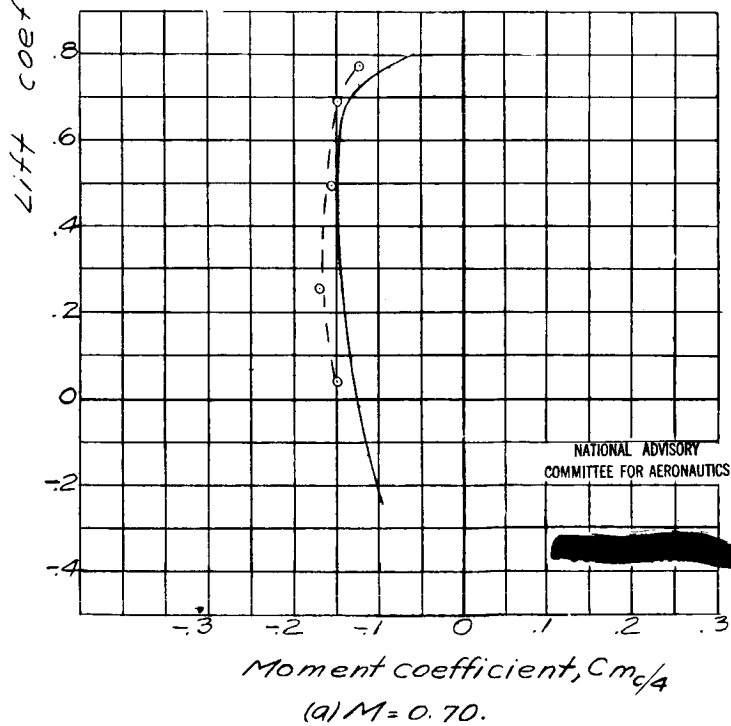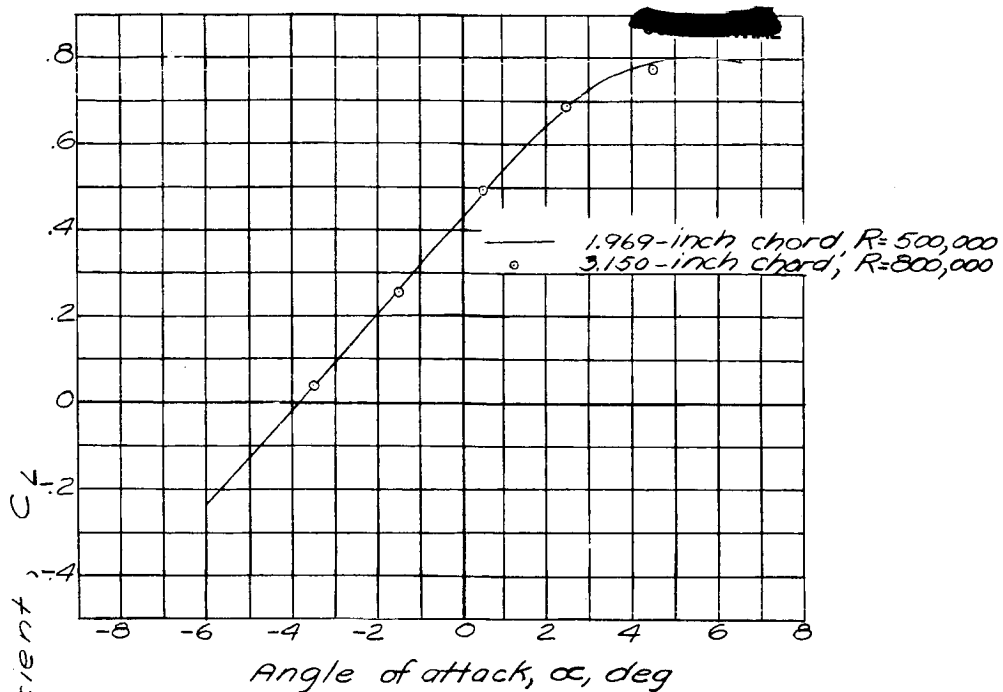
Figure 12.— Comparison of results obtained on
C-8 airfoil section for models of two sizes
at high Mach numbers.

(b) $M = 0.80$.
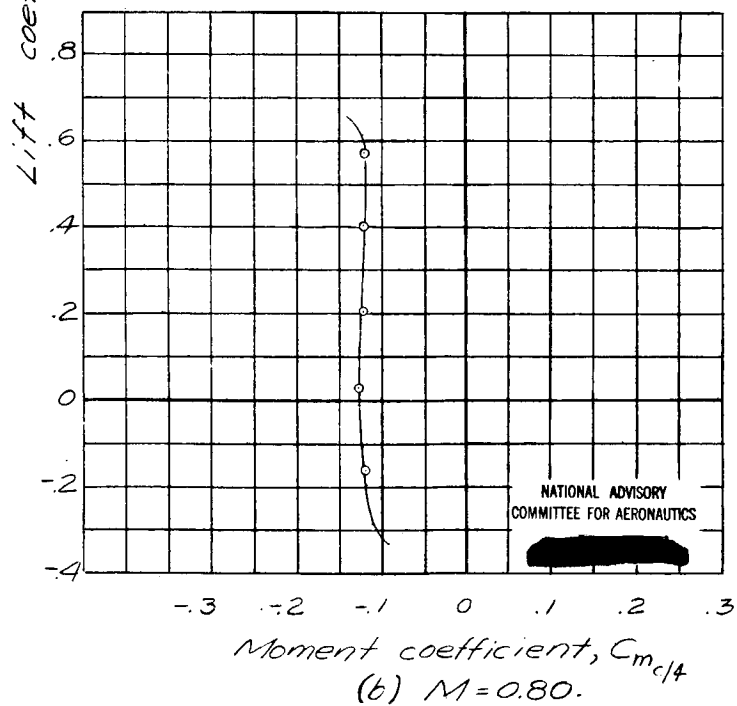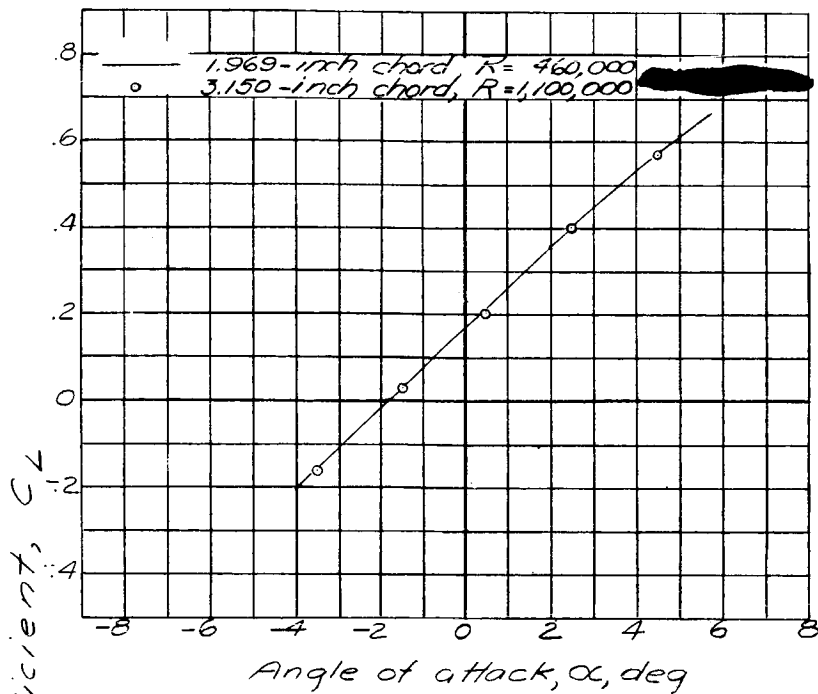
Figure 12. — Continued.
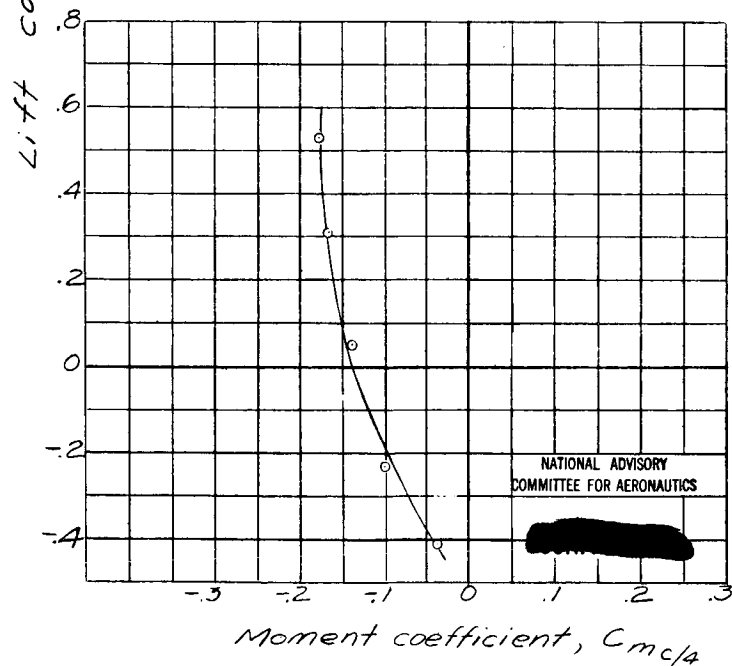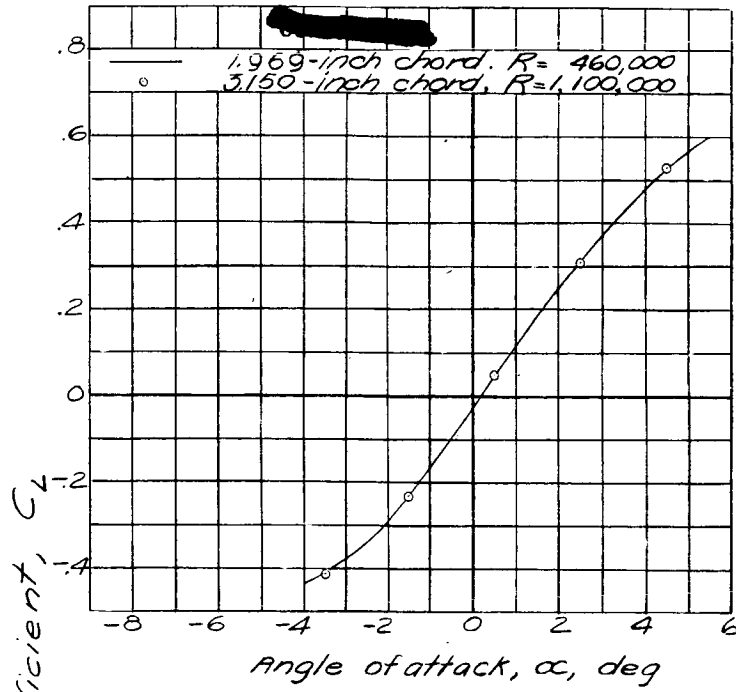
(C) M = 0.90.

Figure 12 .— Concluded.
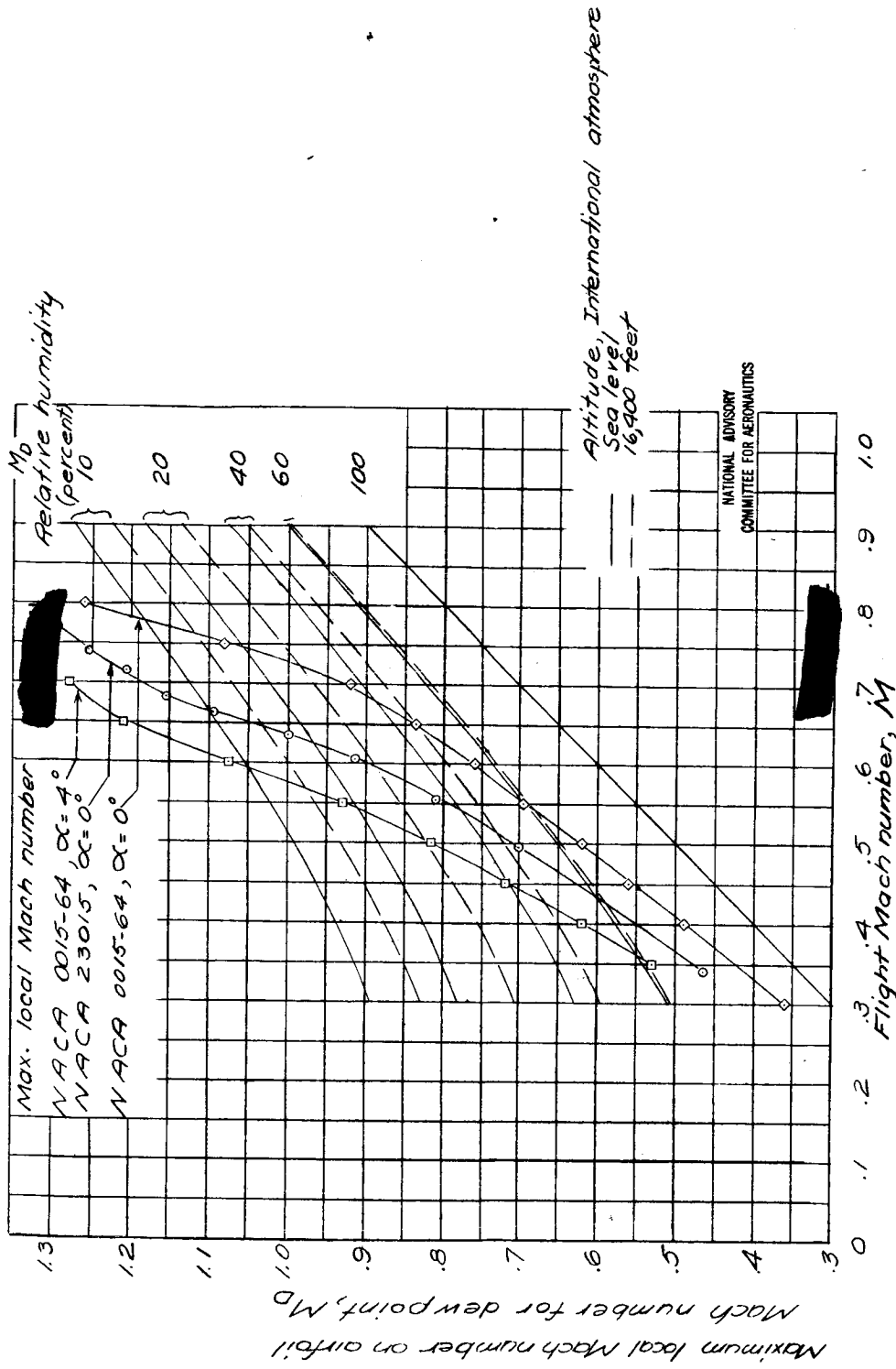
Figure 13.— Diagram for determining the dew point at various Mach numbers for several values of the relative humidity at sea level and at altitude.
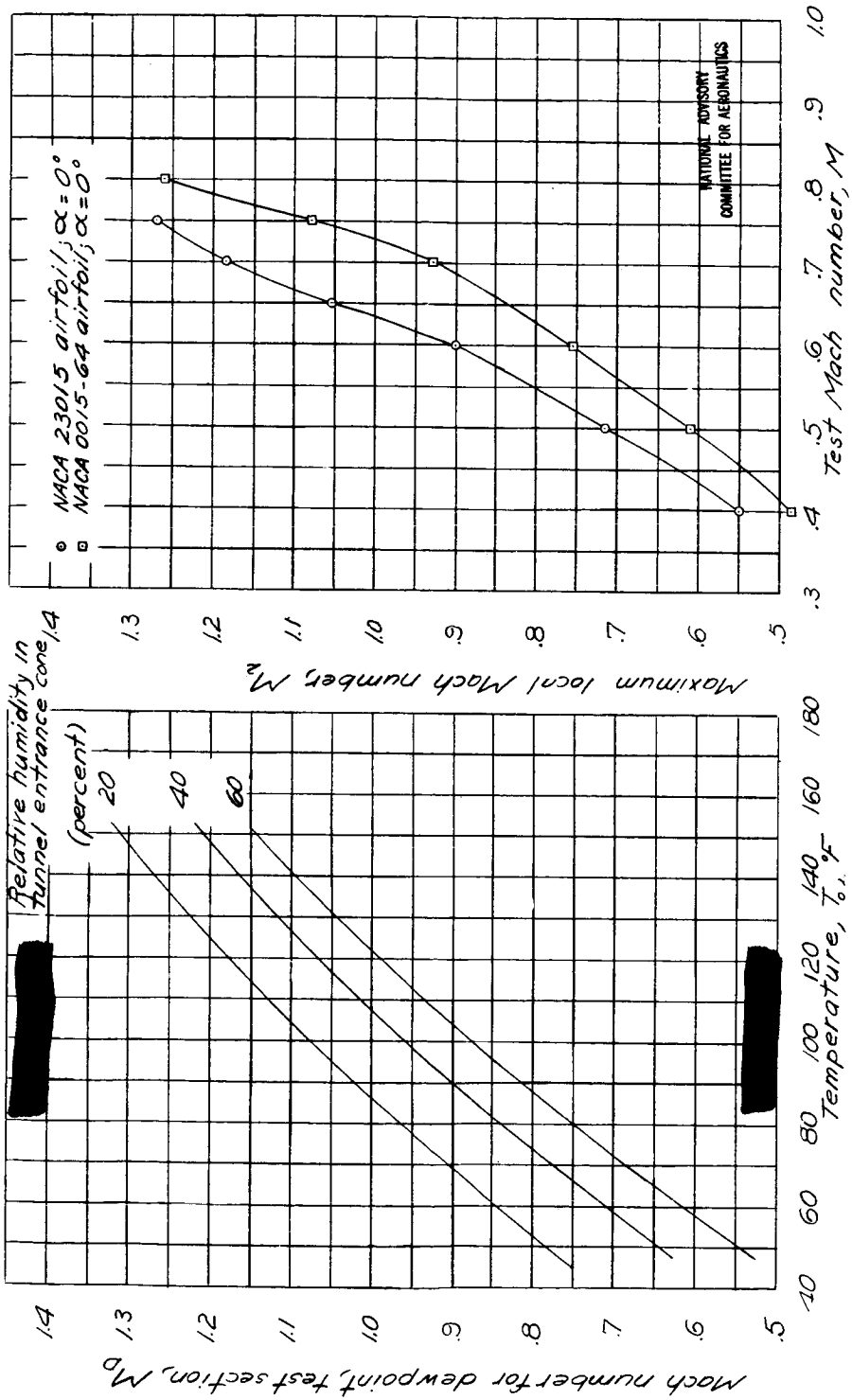
Figure 14.- Diagram for determining the Mach number for which saturation throughout the test section ($M_D$) or locally on the profile ($M_L$) occurs as a function of the temperature in the tunnel entrance cone.
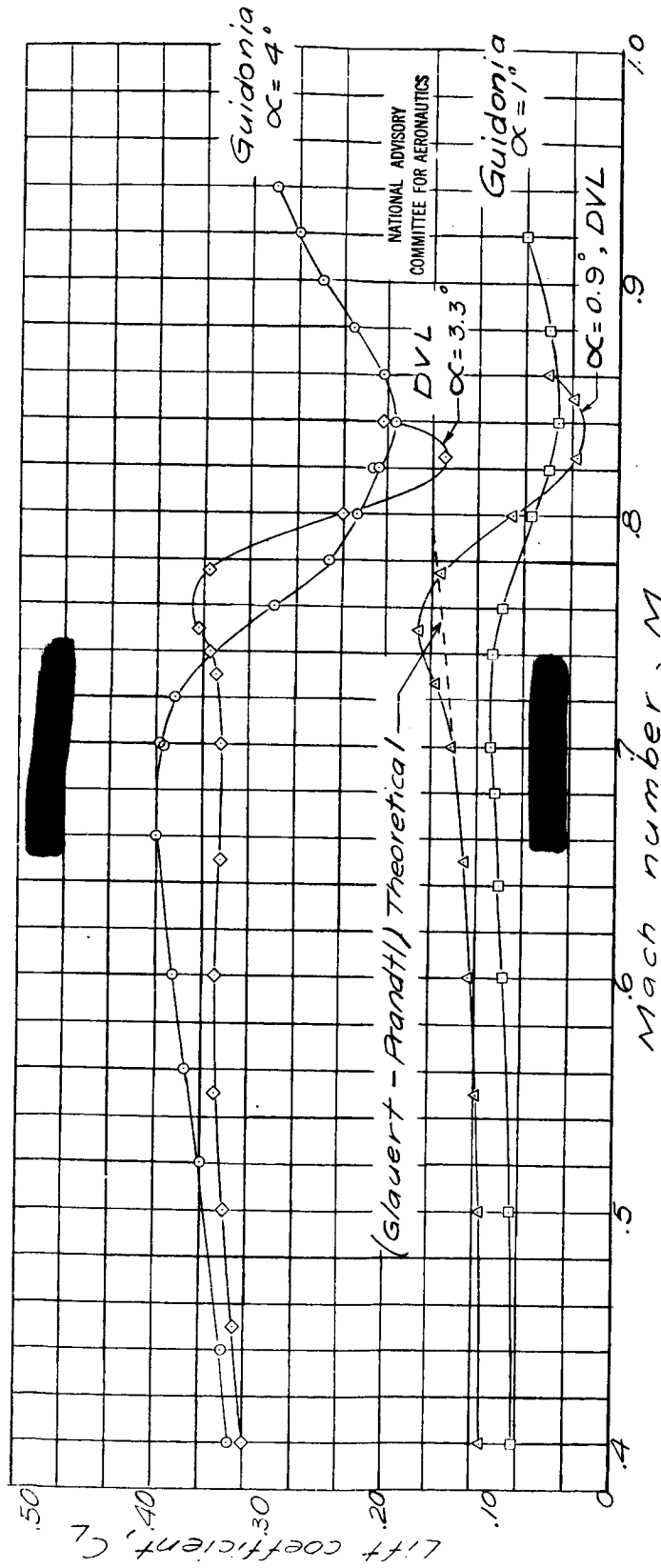
Figure 15.– Comparison of variation of lift coefficient with Mach number for an NACA 0015-64 airfoil with results of tests made in the German DVL tunnel.

Fig. 16
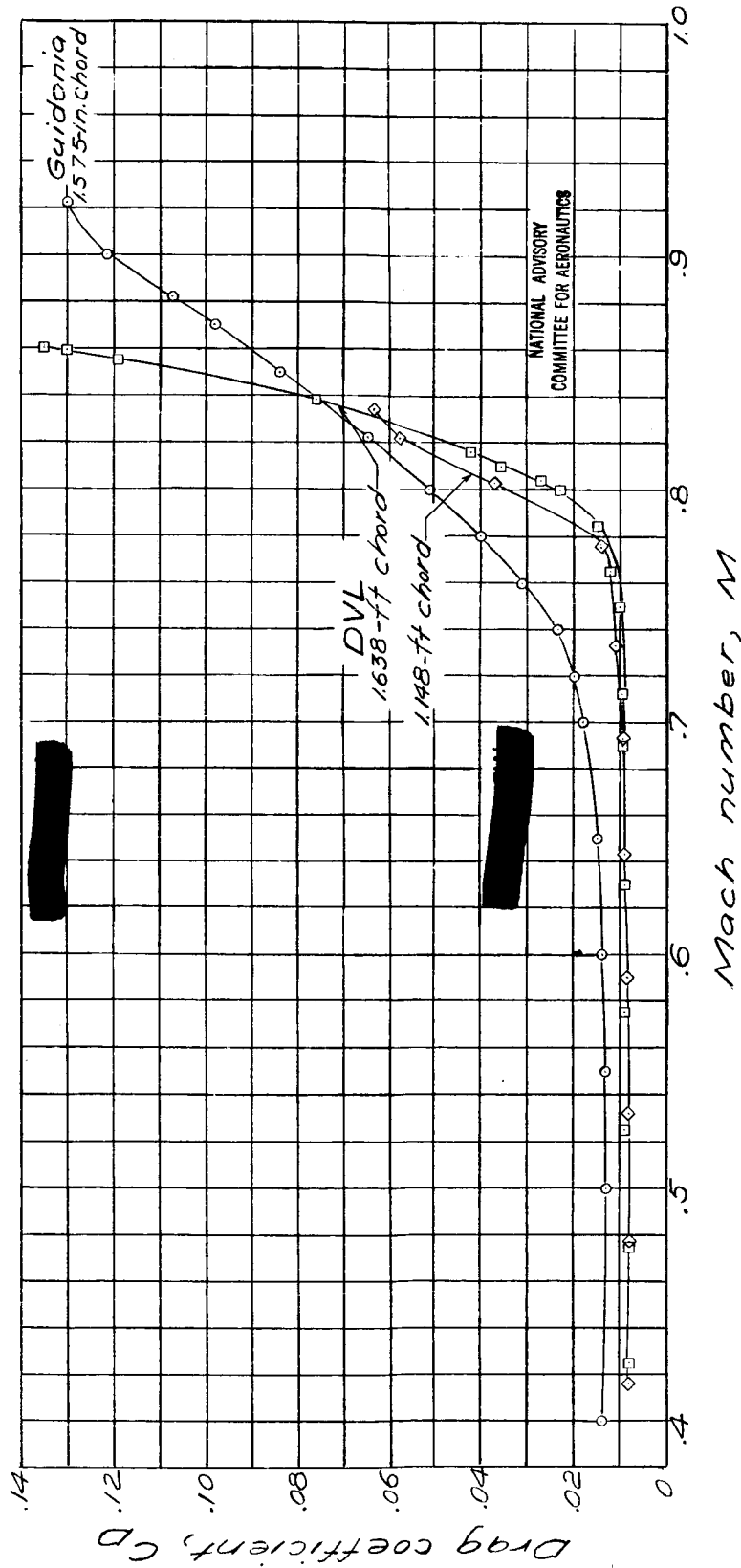


Figure 16.— Comparison of variation of drag coefficient with Mach number for an NACA 0015-64 airfoil with results of tests made in the German DVL tunnel. $\alpha = 0°$.
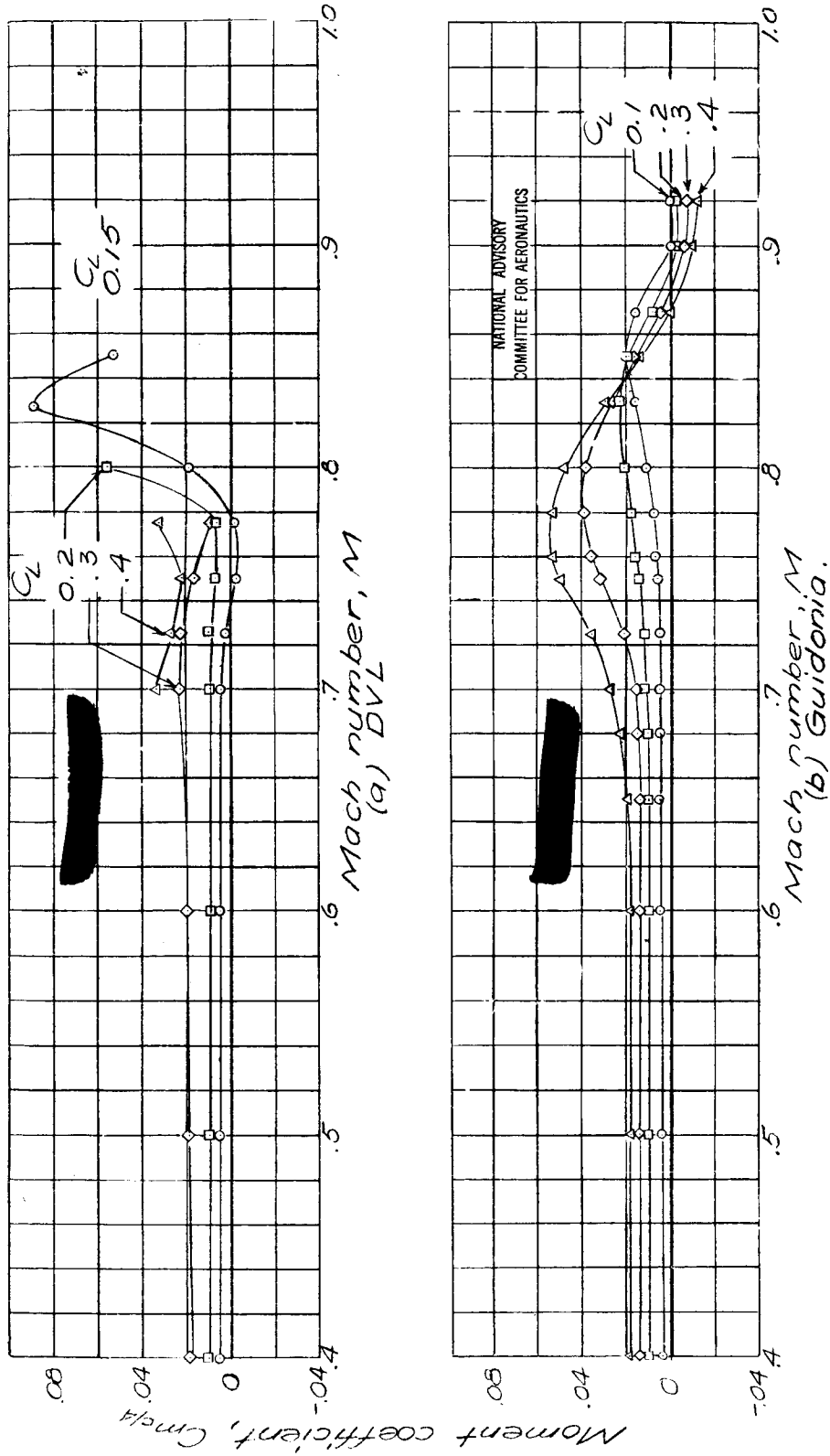
Figure 17.— Comparison of variation of moment coefficient with Mach number for an NACA 0015-64 airfoil with results of tests made in the German DVL tunnel.
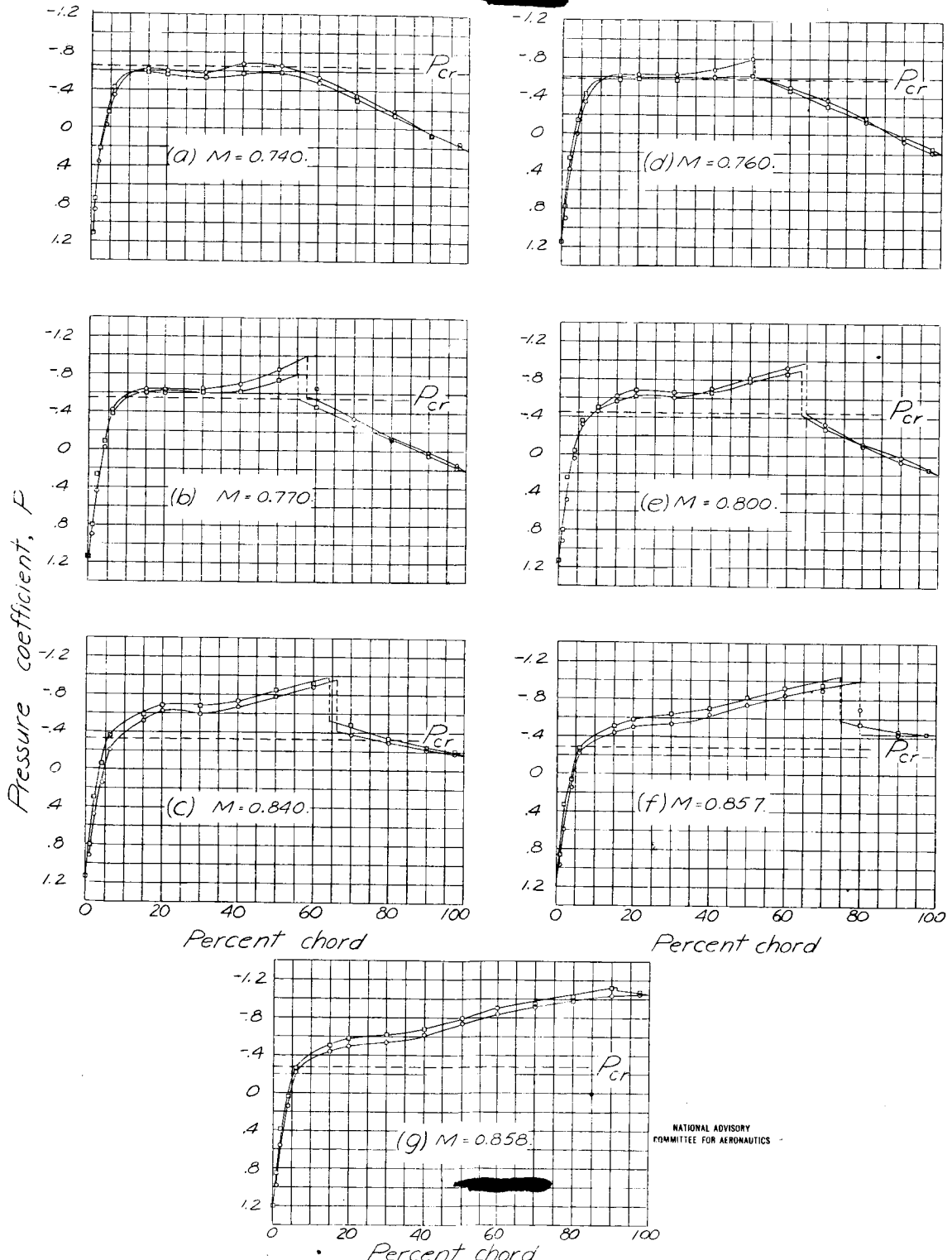
Figure 18.— Pressure-distribution measurements for an NACA 0015-64 airfoil, $\alpha = -0.25°$, from the German DVL wind tunnel.
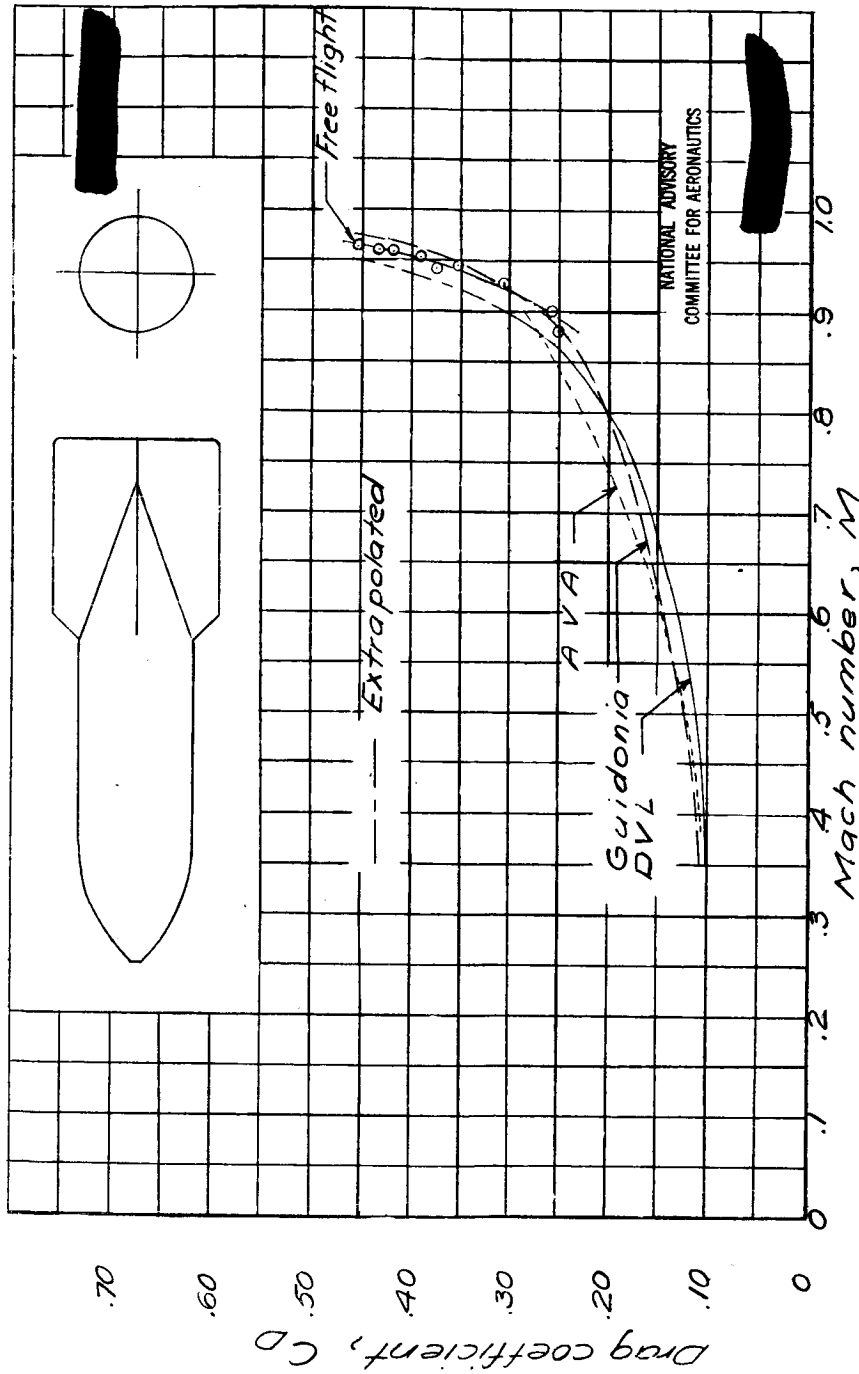
Figure 19.— Variation of drag coefficient with Mach number for a 550-pound bomb (without reinforcement) as tested in the German DVL tunnel, the German AVA tunnel, the Guidonia high-speed tunnel, and in free flight.
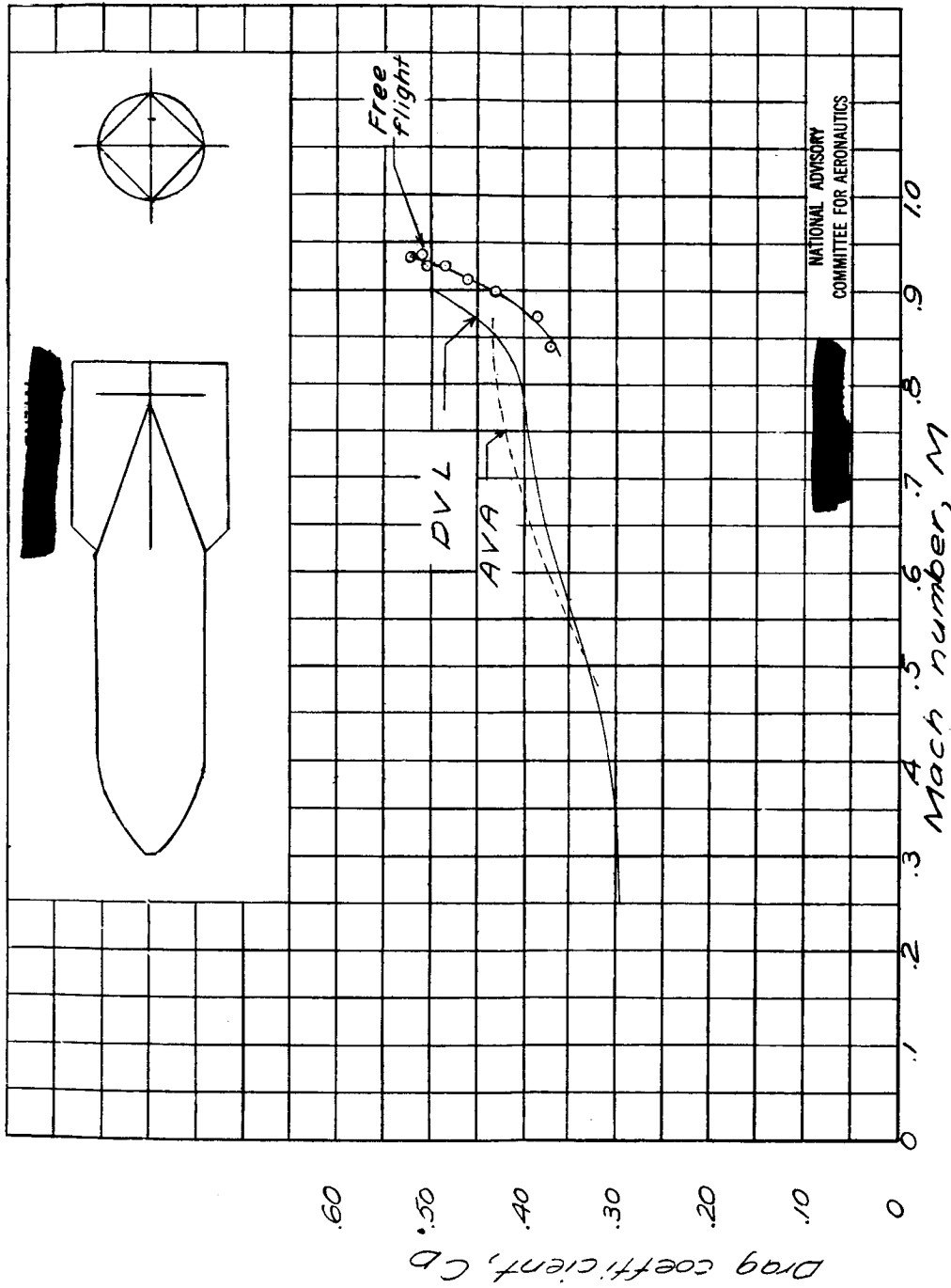
Figure 20. — Variation of drag coefficient with Mach number for a 550-pound bomb with reinforcement rods 0.63 inch in diameter as tested in the German DVL tunnel, the German AVA tunnel, and in free flight.

NATIONAL ADVISORY
COMMITTEE FOR AERONAUTICS

Mach number, M

Drag coefficient, $C_D$
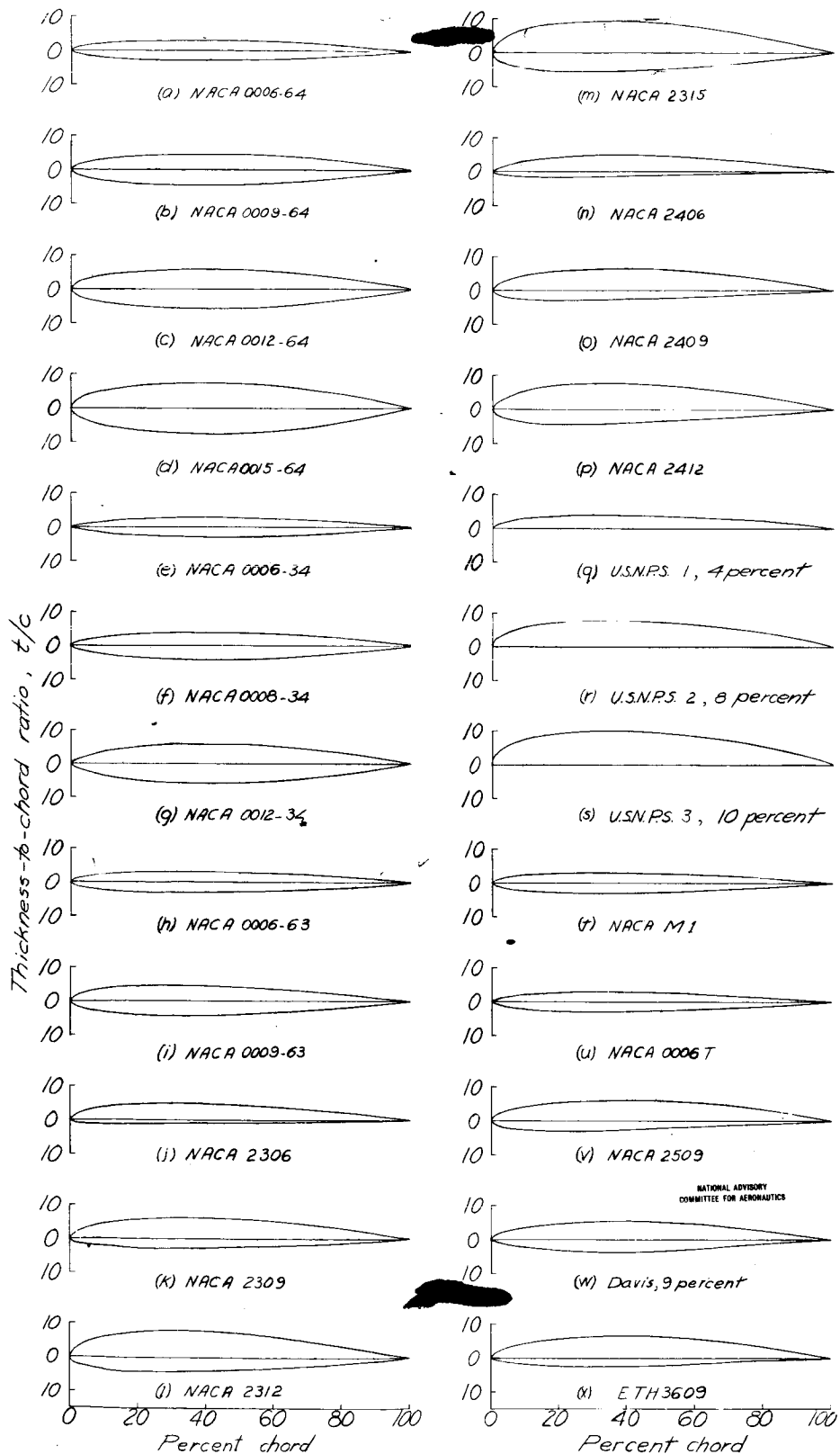
Figure 21.— Specified shapes of the airfoils.
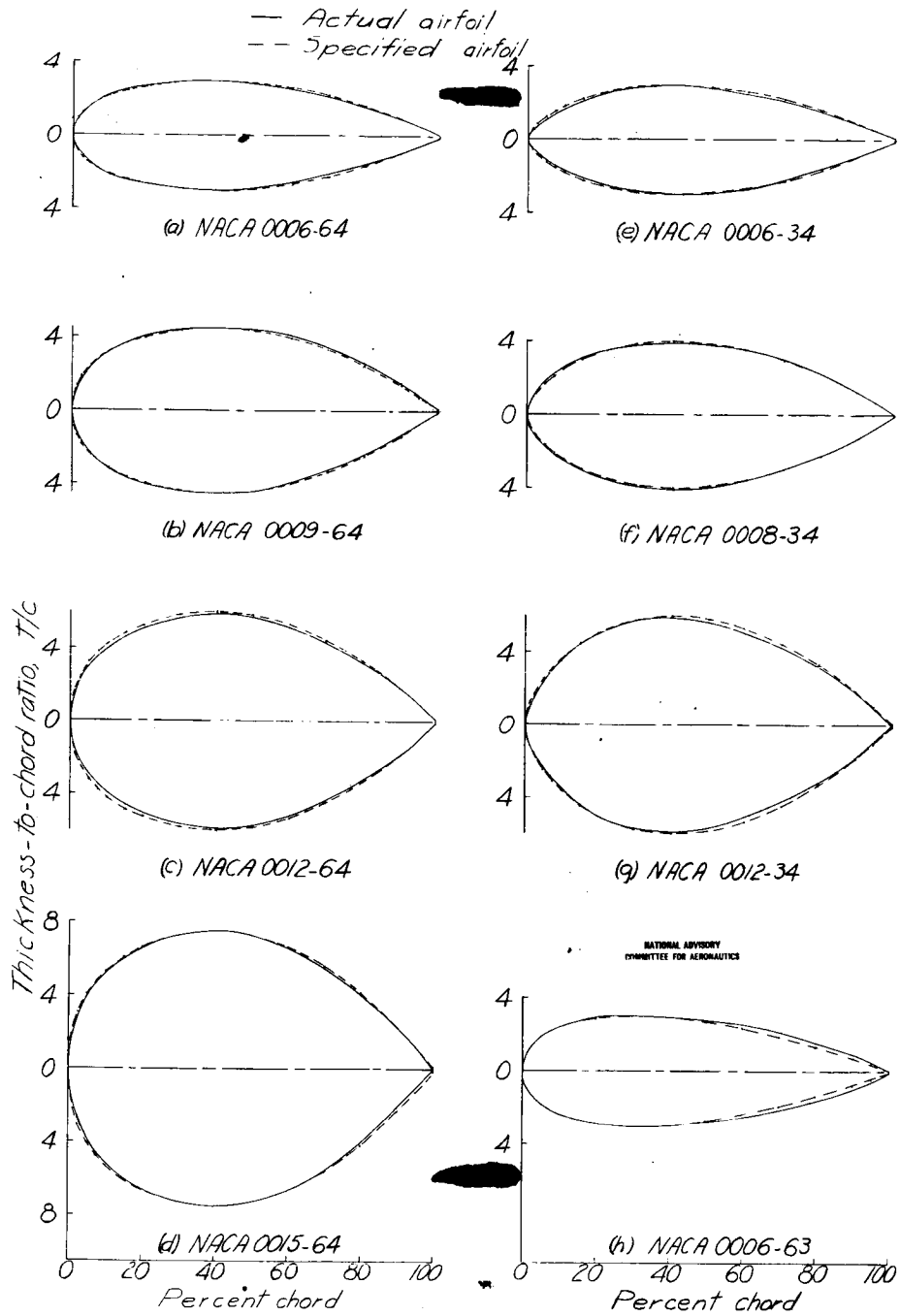
Figure 22.— Actual airfoils tested as
compared with specified airfoil shapes.
Ordinate scale five times chord scale.

— Actual airfoil
-- Specified airfoil

(i) NACA 0009-63

(m) NACA 2315

(j) NACA 2306

(n) NACA 2406

(k) NACA 2309

(o) NACA 2409

Thickness-to-chord ratio, T/c

(l) NACA 2312

NATIONAL ADVISORY
COMMITTEE FOR AERONAUTICS

(p) NACA 2412

Percent chord

Percent chord

Figure 22.— Continued.

— Actual airfoil
- Specified airfoil

(q) U.S.N.P.S. 1,
4 percent thick

(u) NACA 0006 T

(r) U.S.N.P.S. 2,
8 percent thick

(v) NACA 2509

*Thickness-to-chord ratio, t/c*

(s) U.S.N.P.S. 3,
10 percent thick

(w) Davis, 9 percent

(t) NACA M 1

NATIONAL ADVISORY
COMMITTEE FOR AERONAUTICS

(x) ETH 3609

Percent chord

Percent chord

Figure 22.— Concluded.

Figure 23 .— Effect of compressibility on the aerodynamic characteristics of the NACA 0006-64 airfoil.
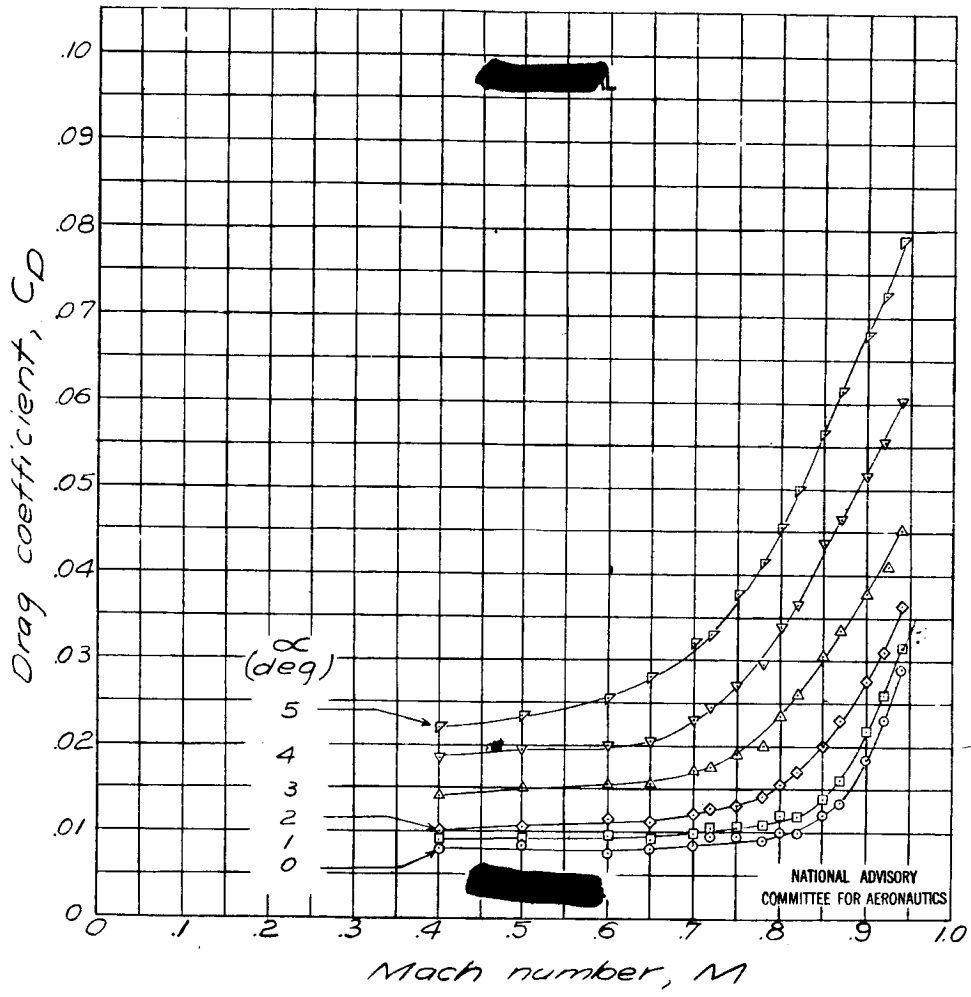
Figure 23 . — Continued.
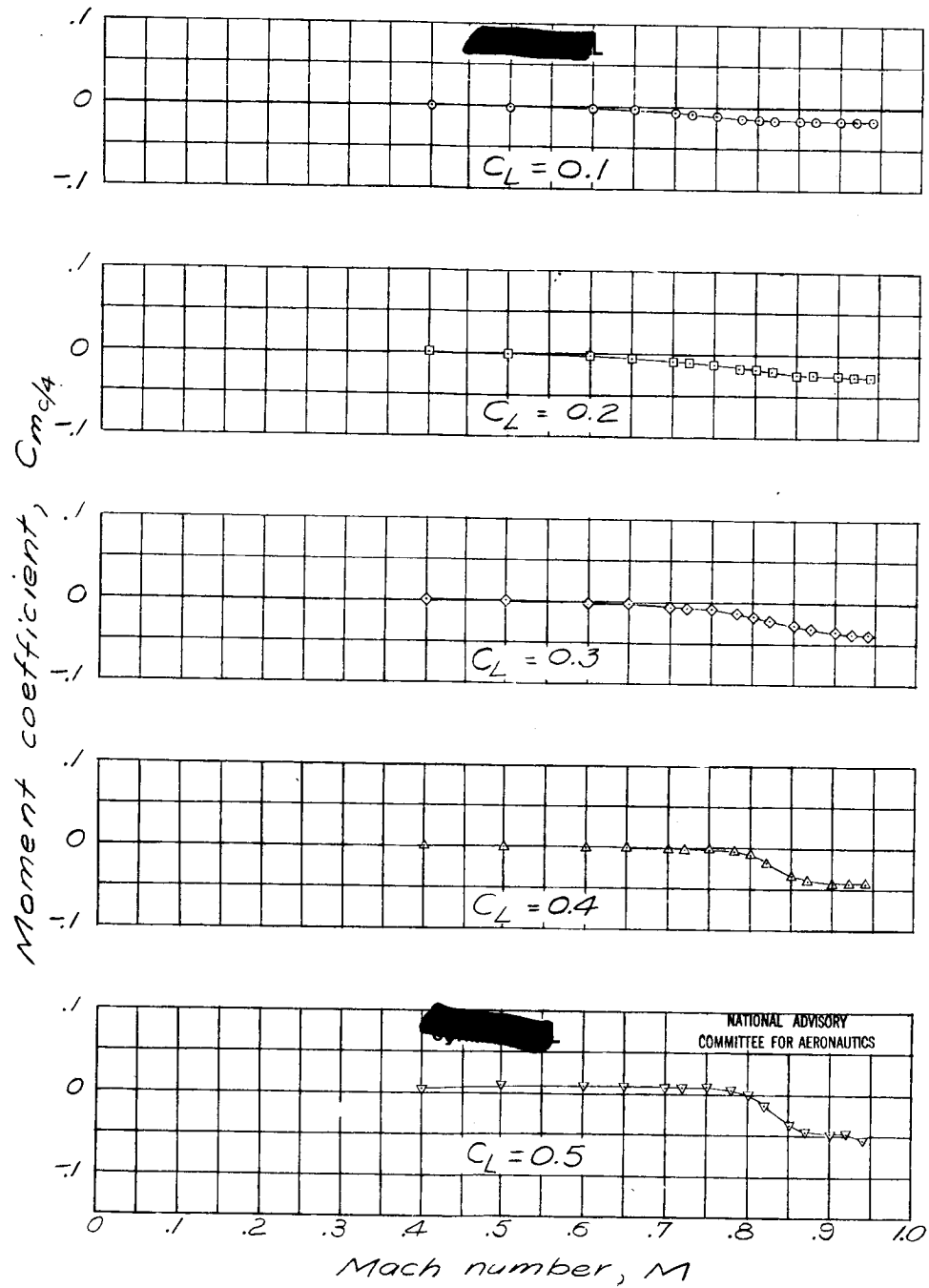
Figure 23 .— Concluded.

Fig. 24
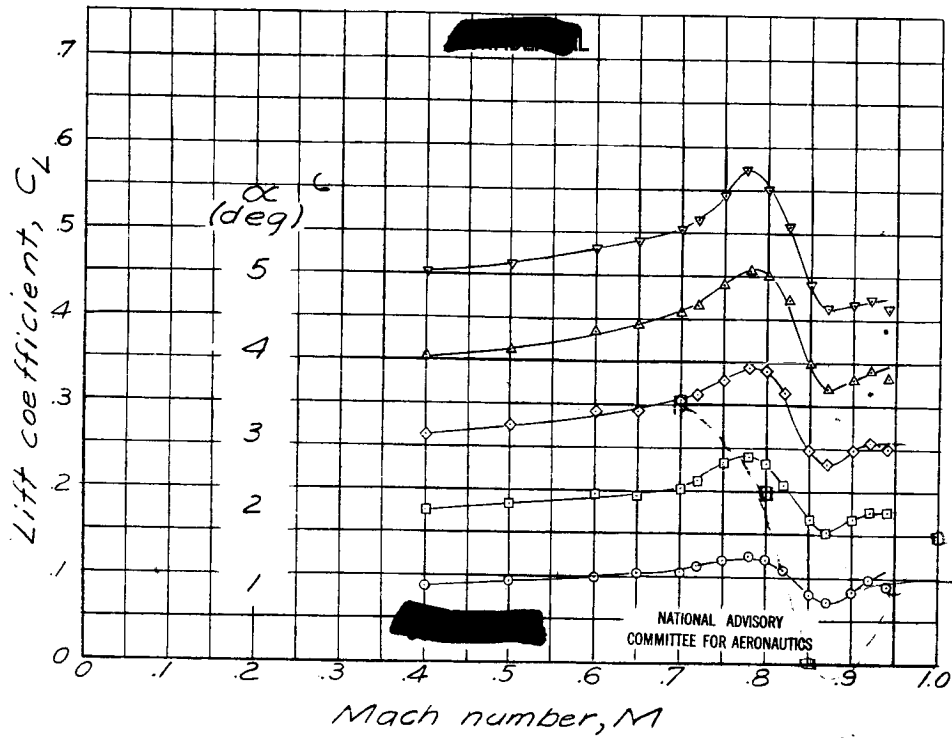


Figure 24 .— Effect of compressibility on the aerodynamic characteristics of the NACA 0009-64 airfoil.
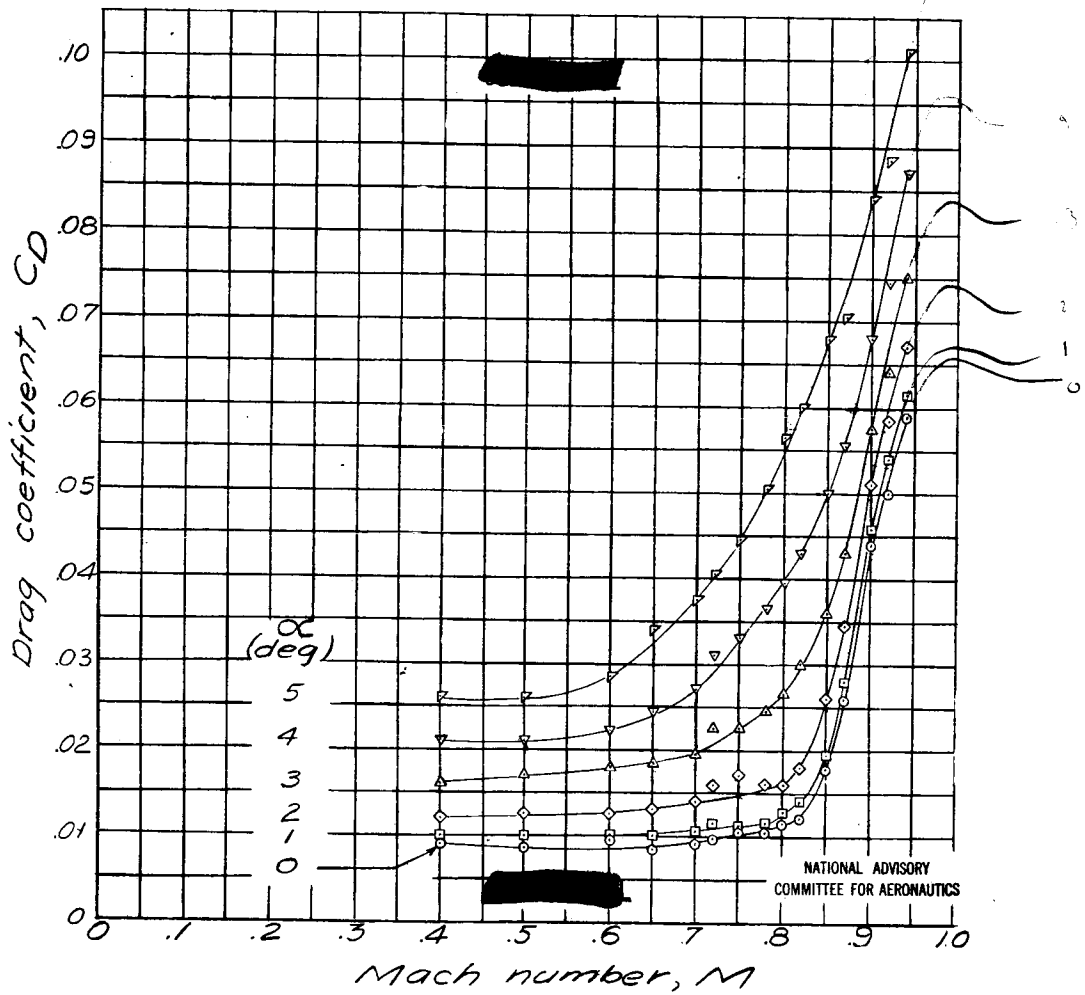
Figure 24 .— Continued.
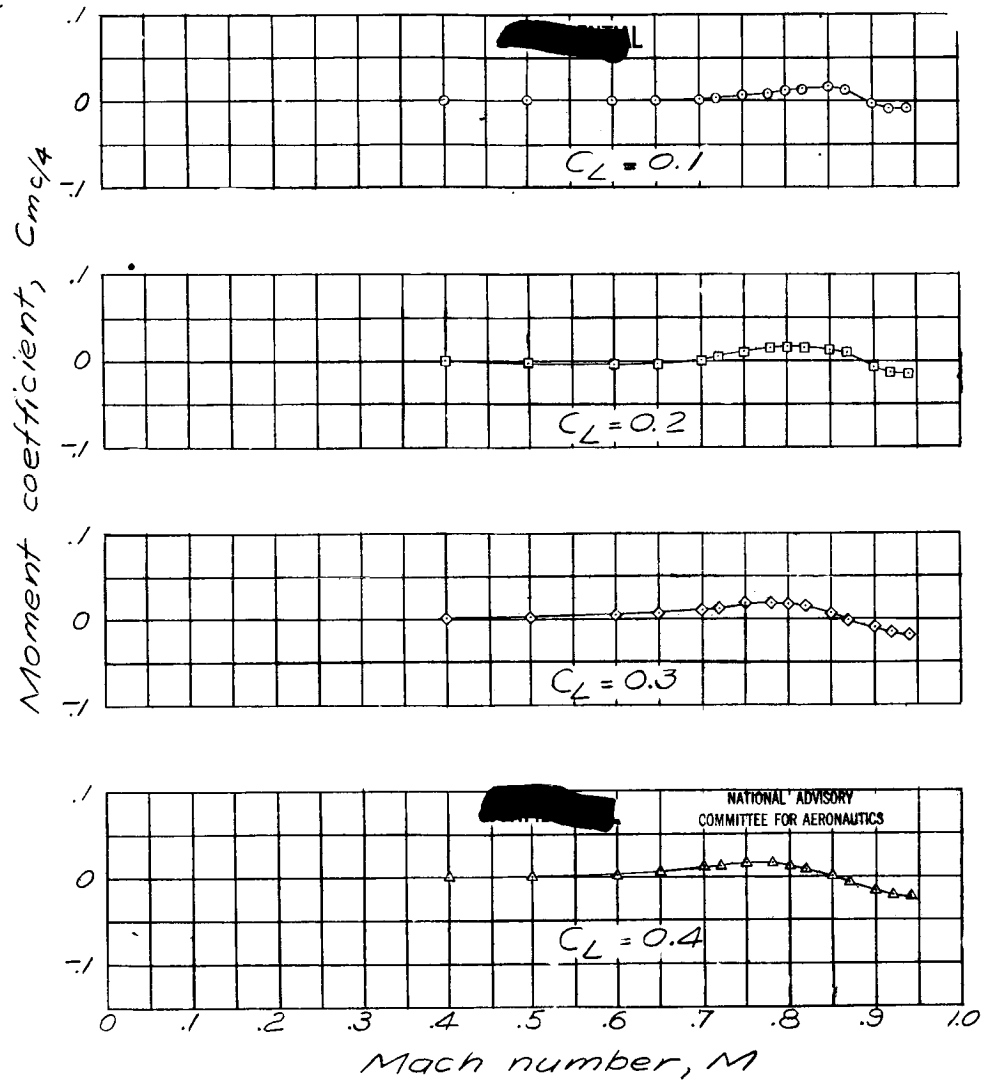
Figure 24.— Concluded.
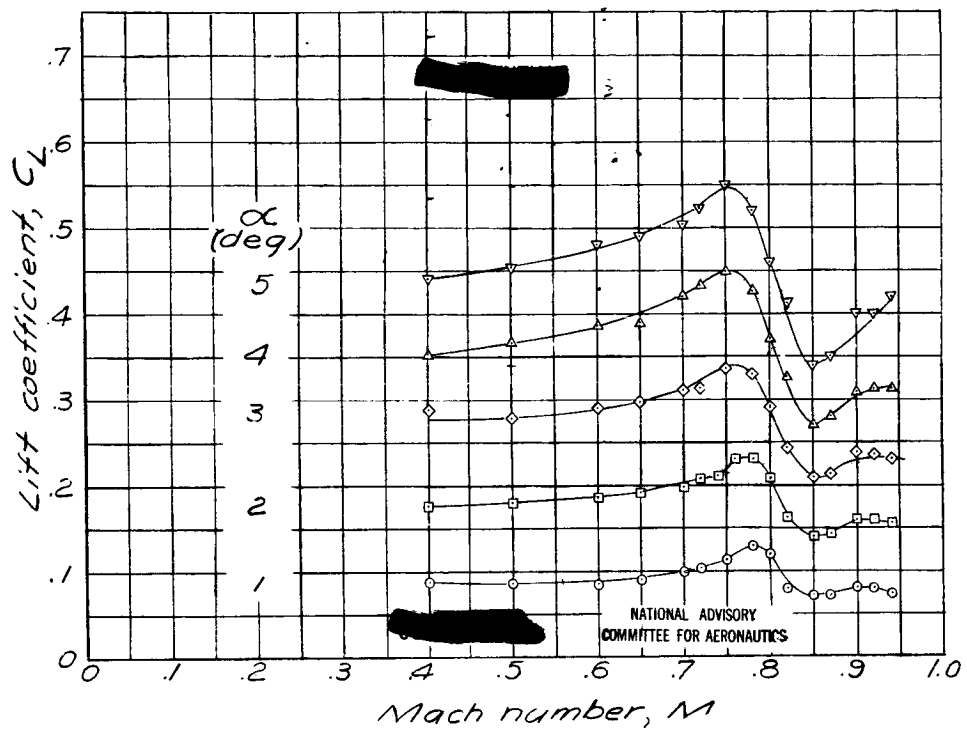
Figure 25 .— Effect of compressibility on the aerodynamic characteristics of the NACA 0012-64 airfoil.
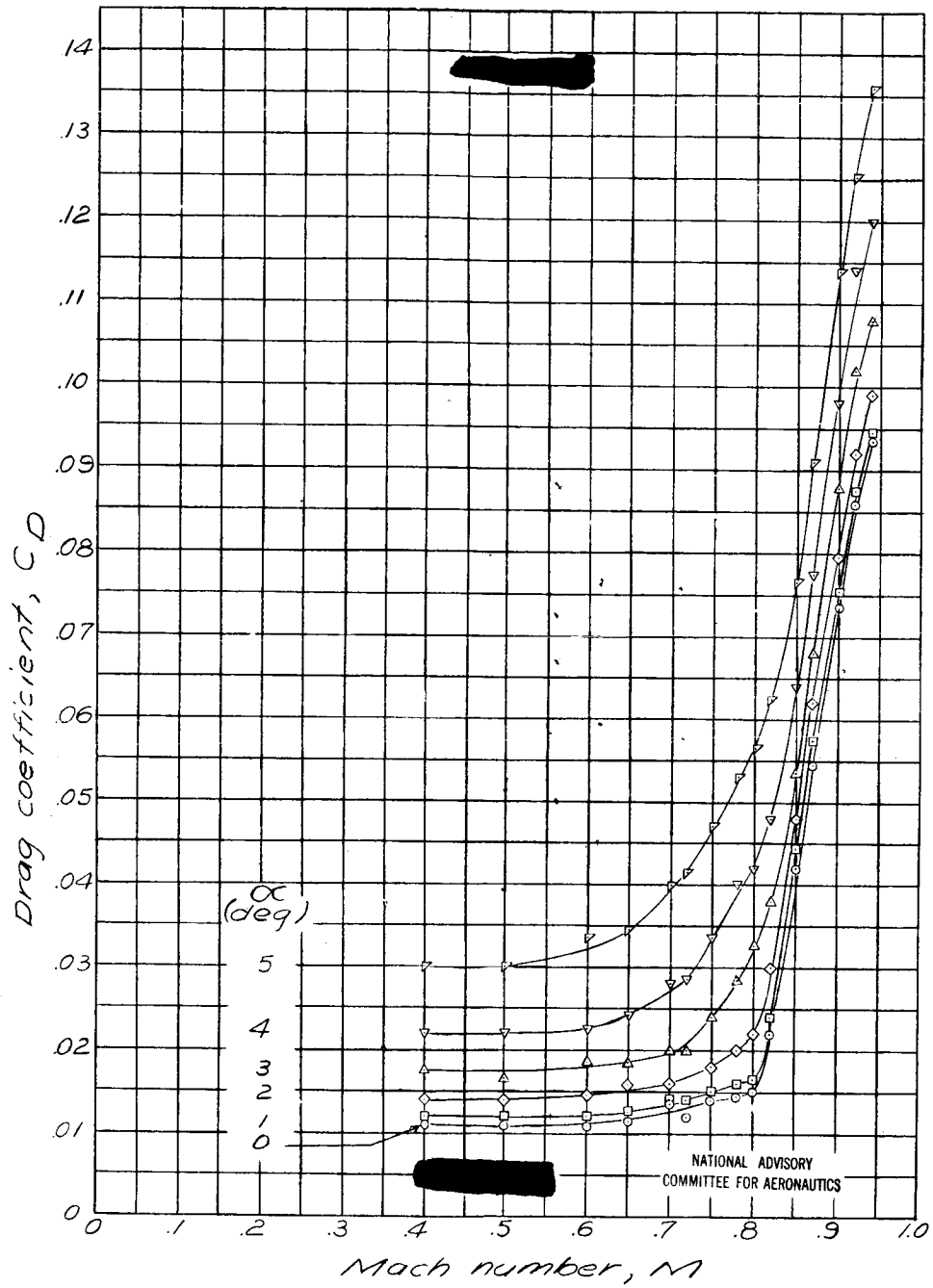
Figure 25 .— Continued.
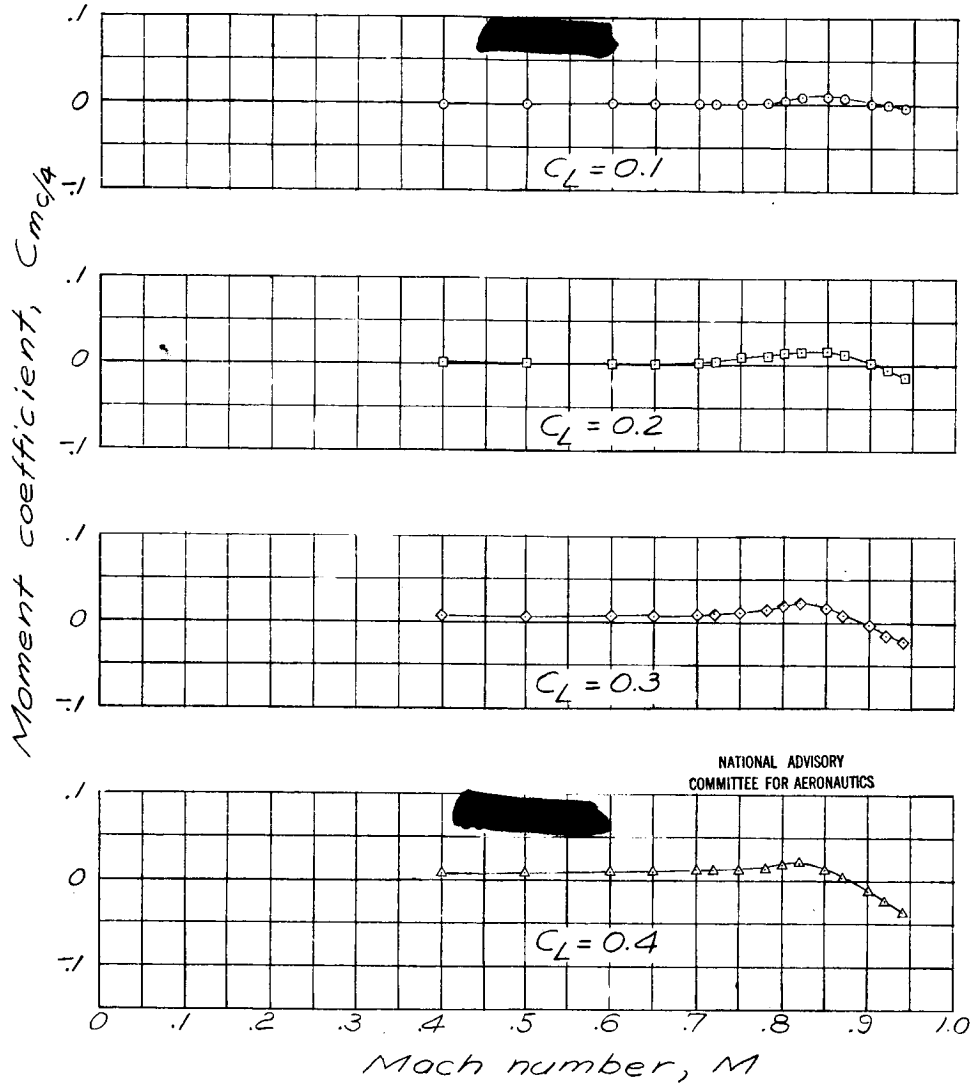
Figure 25.— Concluded.
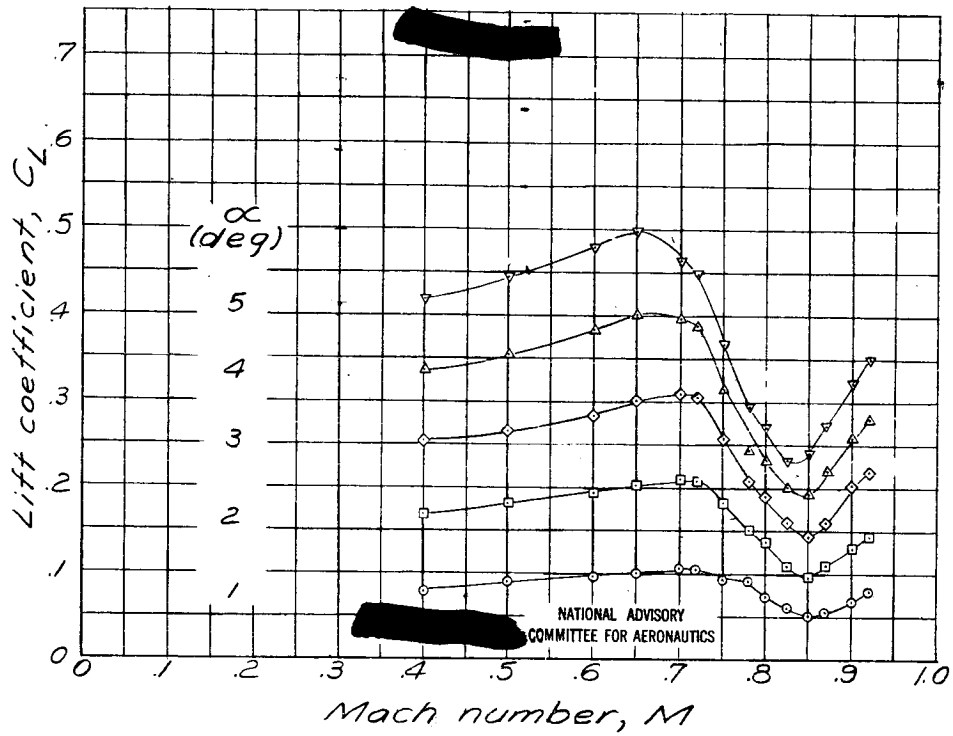
Figure 26 .— Effect of compressibility on the aerodynamic characteristics of the NACA 0015-64 airfoil.
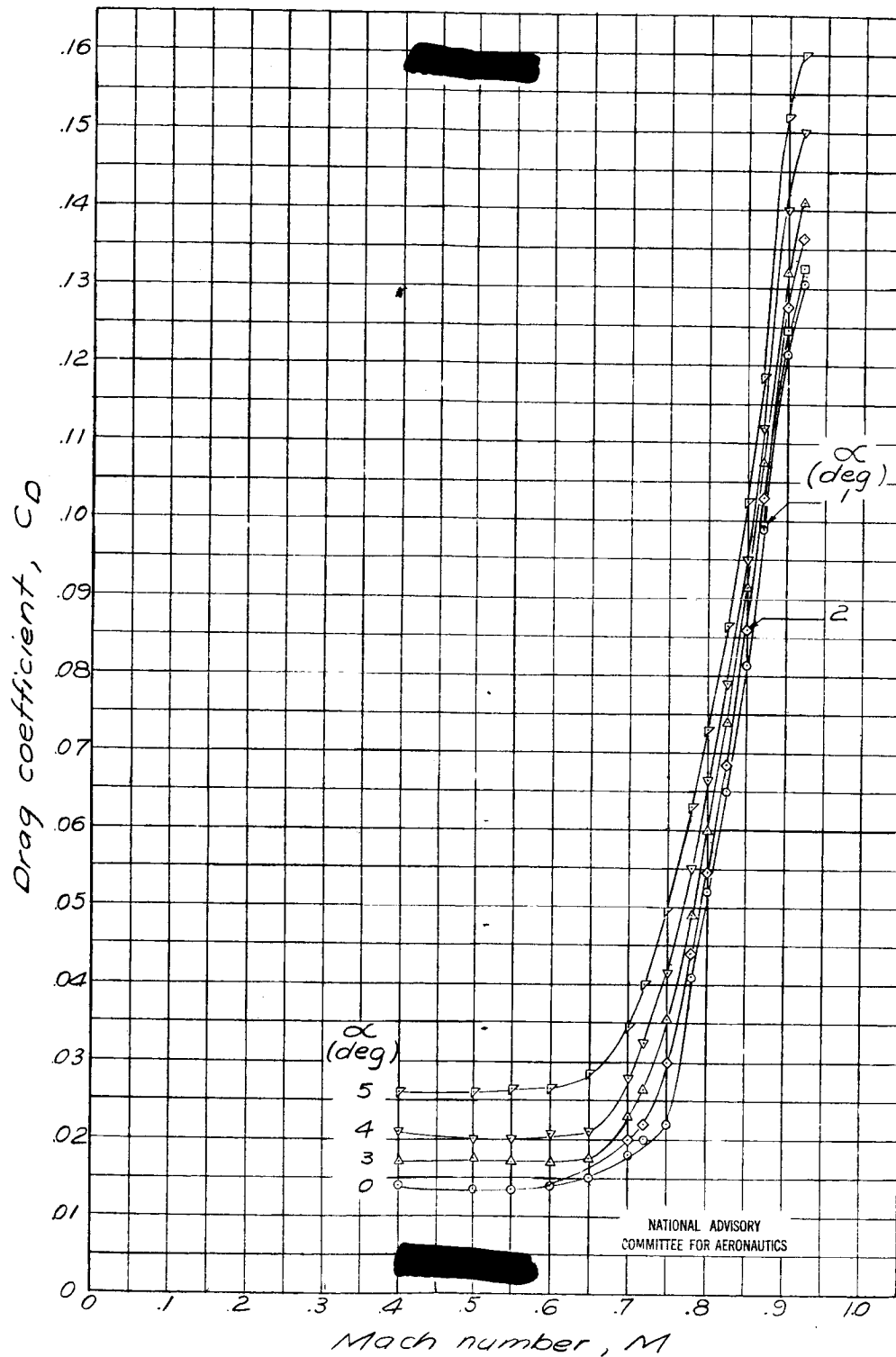
Figure 26.— Continued.
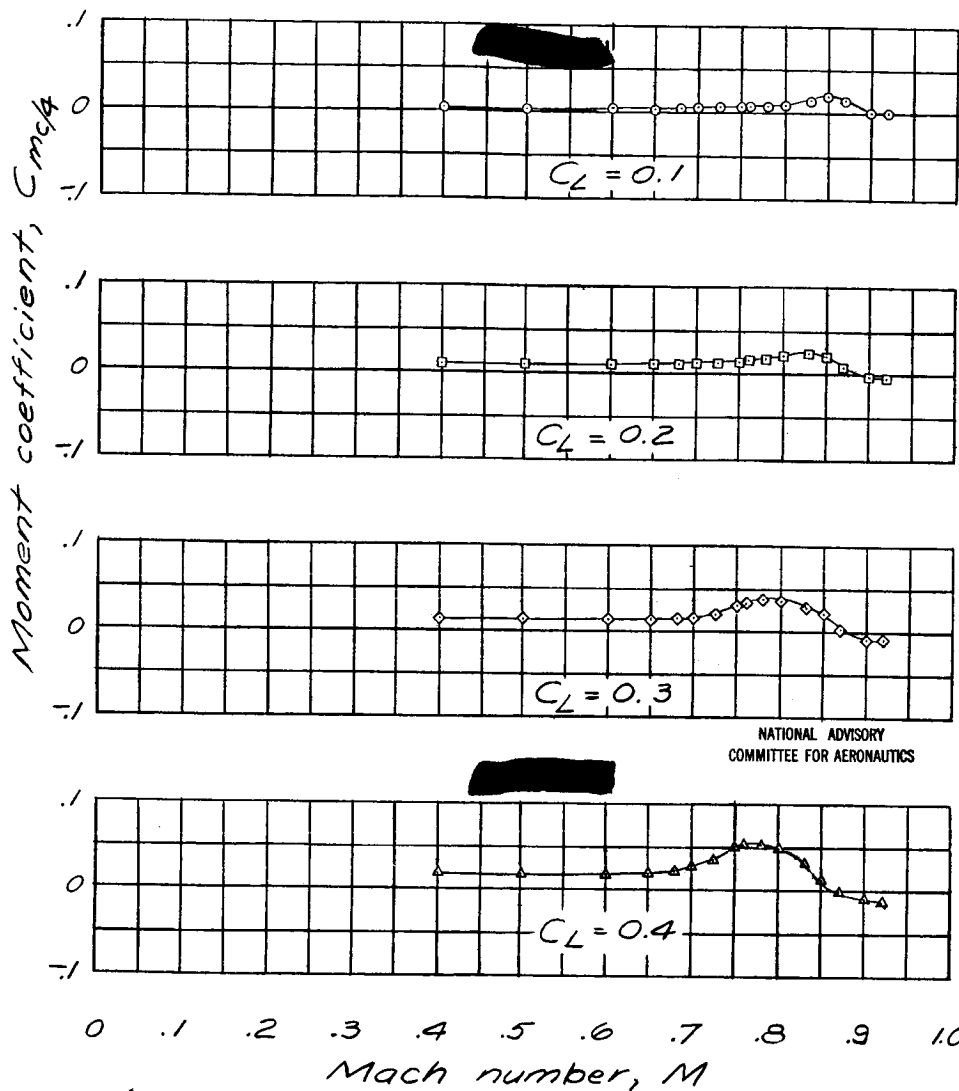
Figure 26 .— Concluded.
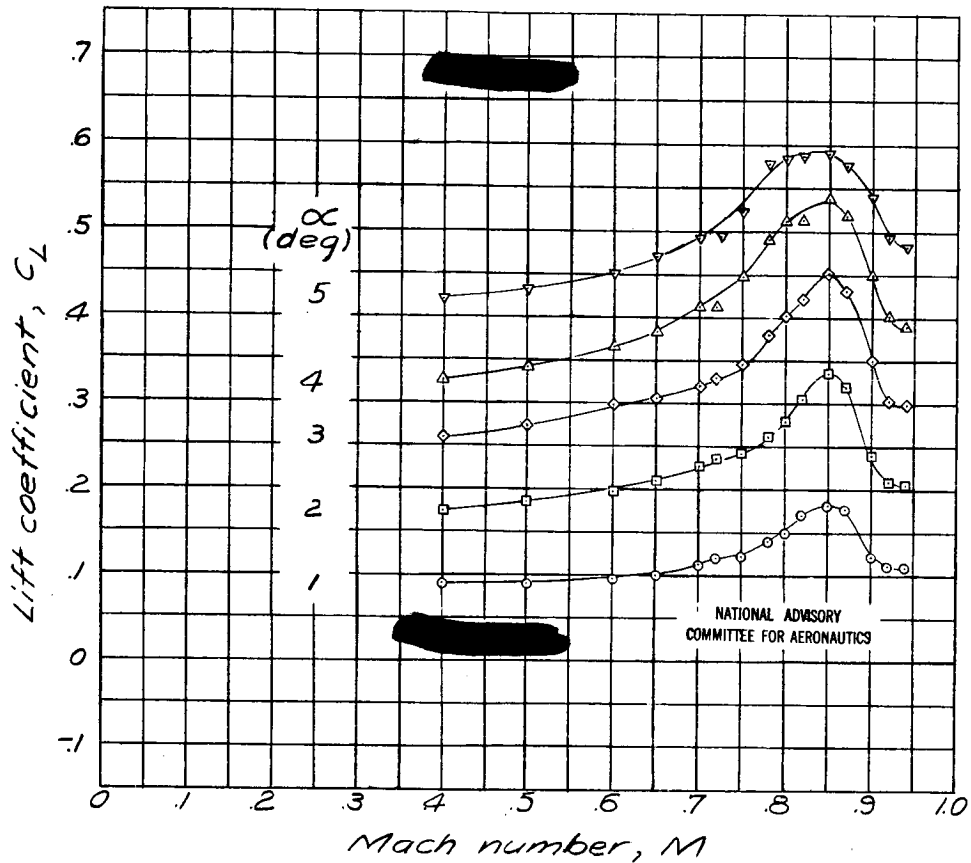
Figure 27 .— Effect of compressibility on the aerodynamic characteristics of the NACA 0006-34 airfoil.
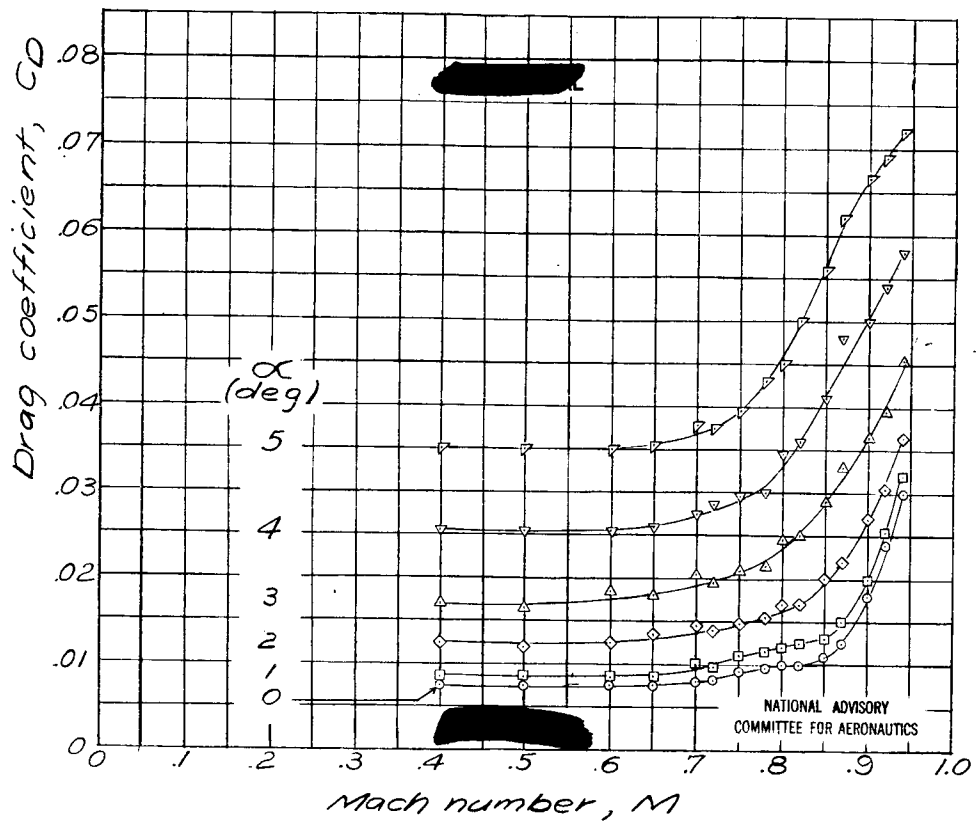
Figure 27 .— Continued.
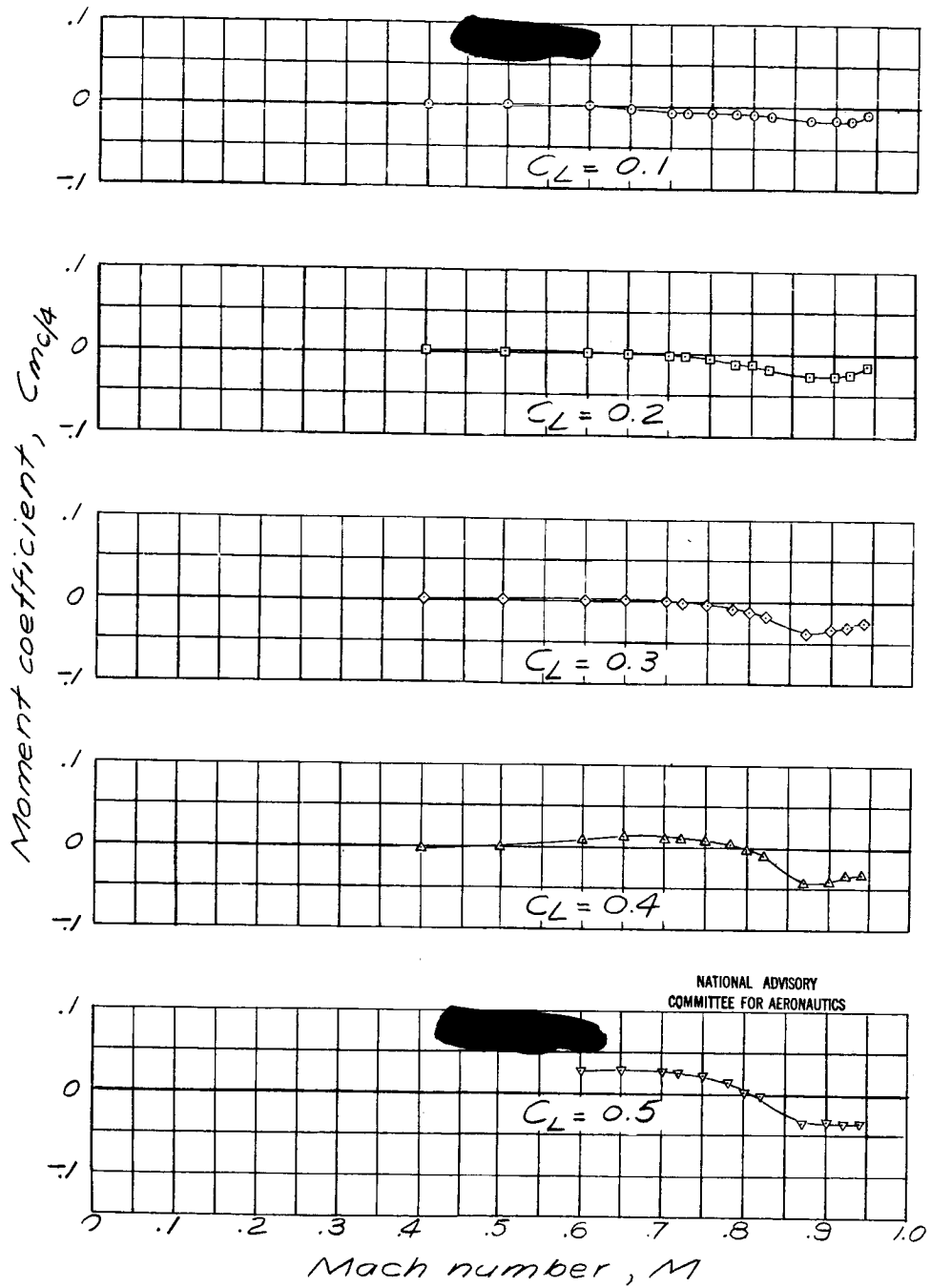
Figure 27. — Concluded.
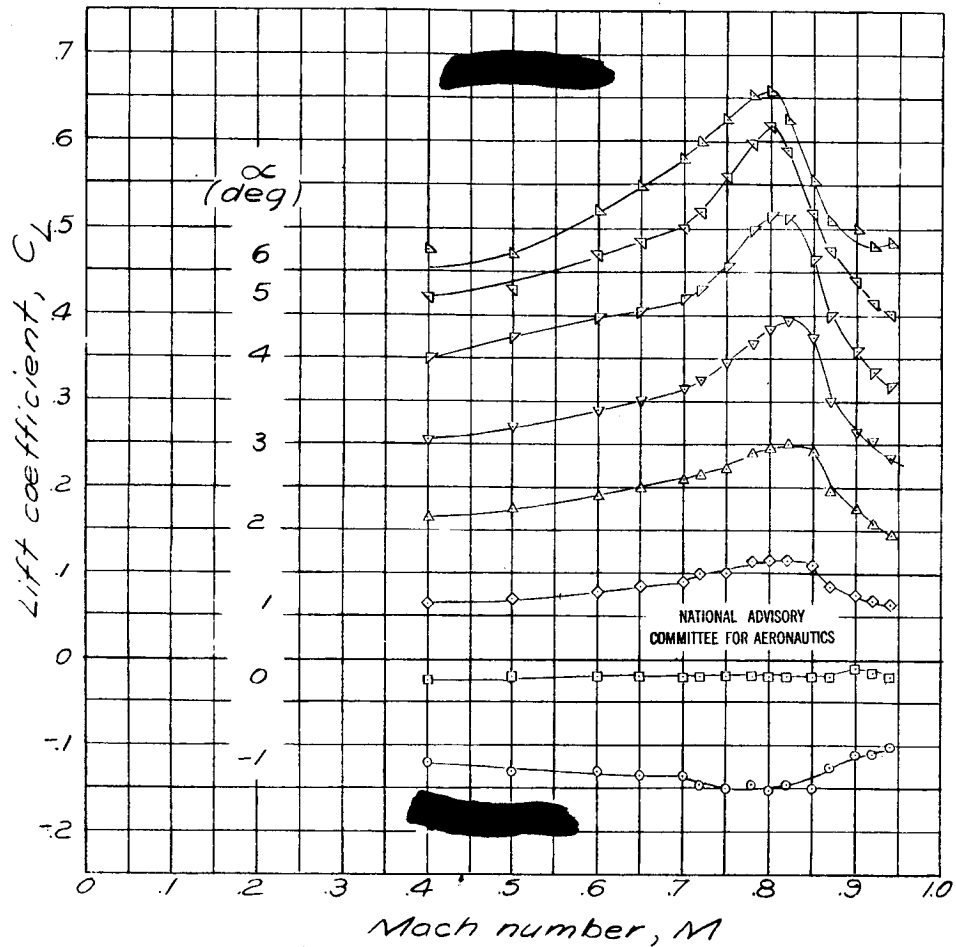
Figure 28.— Effect of compressibility on the
aerodynamic characteristics of the
NACA 0008-34 airfoil.
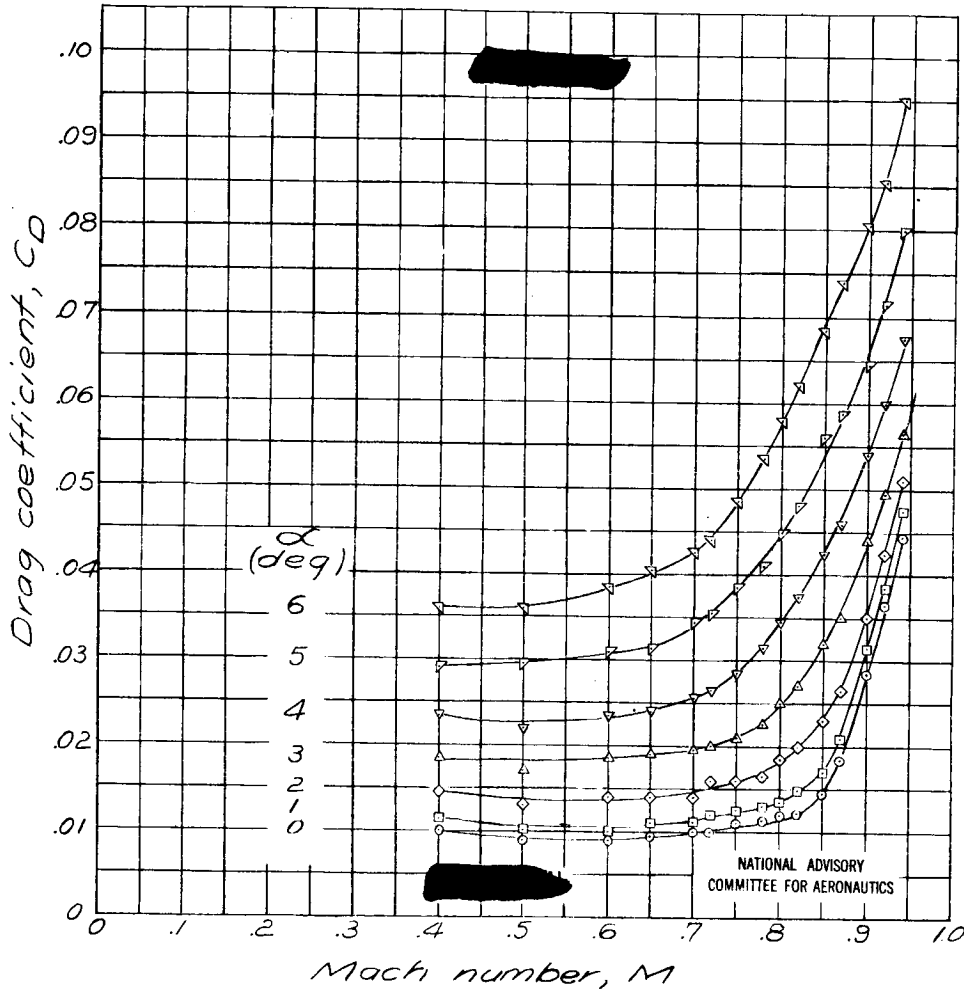
Figure 28 .— Continued.
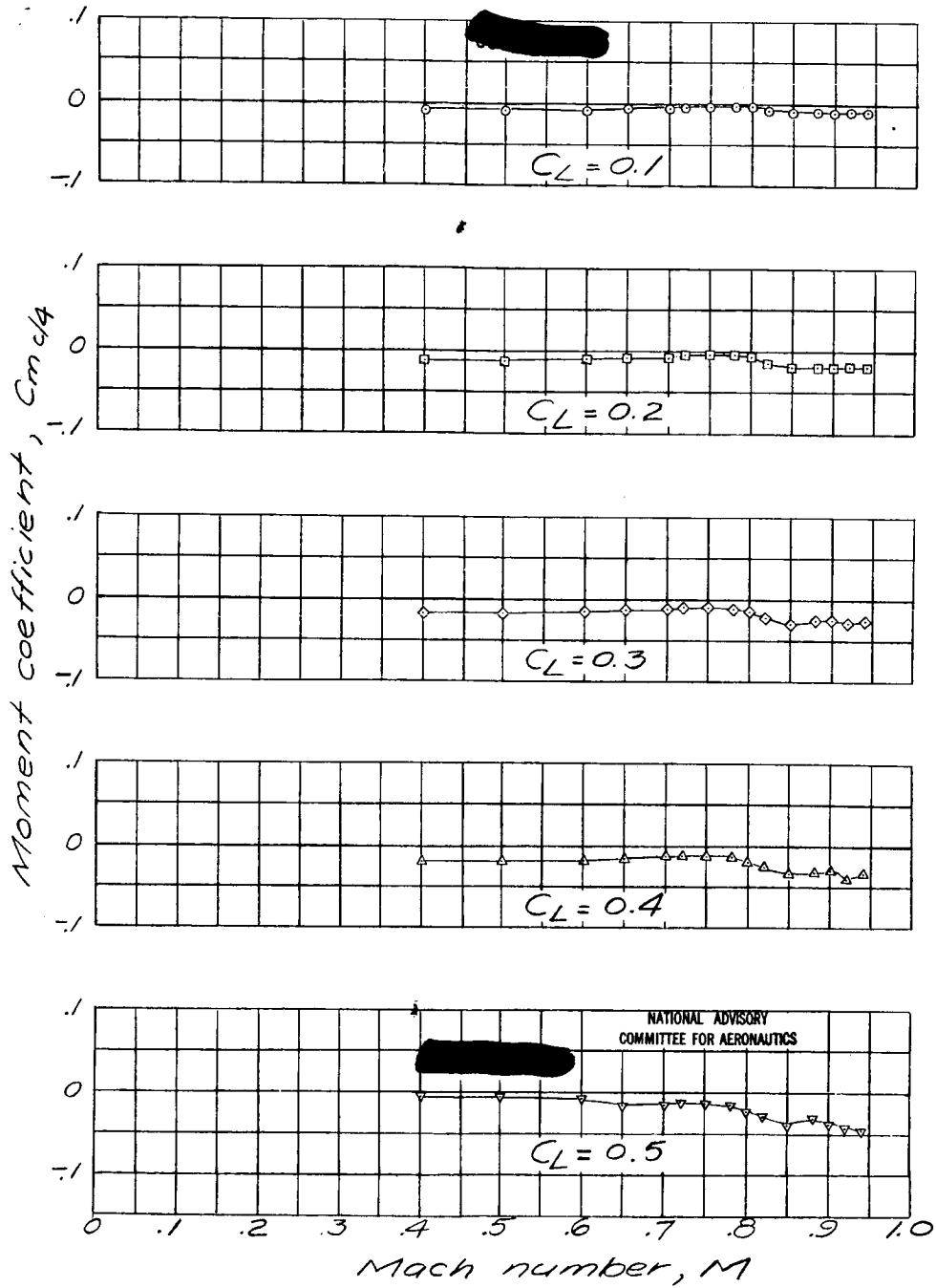
Figure 28 .— Concluded.
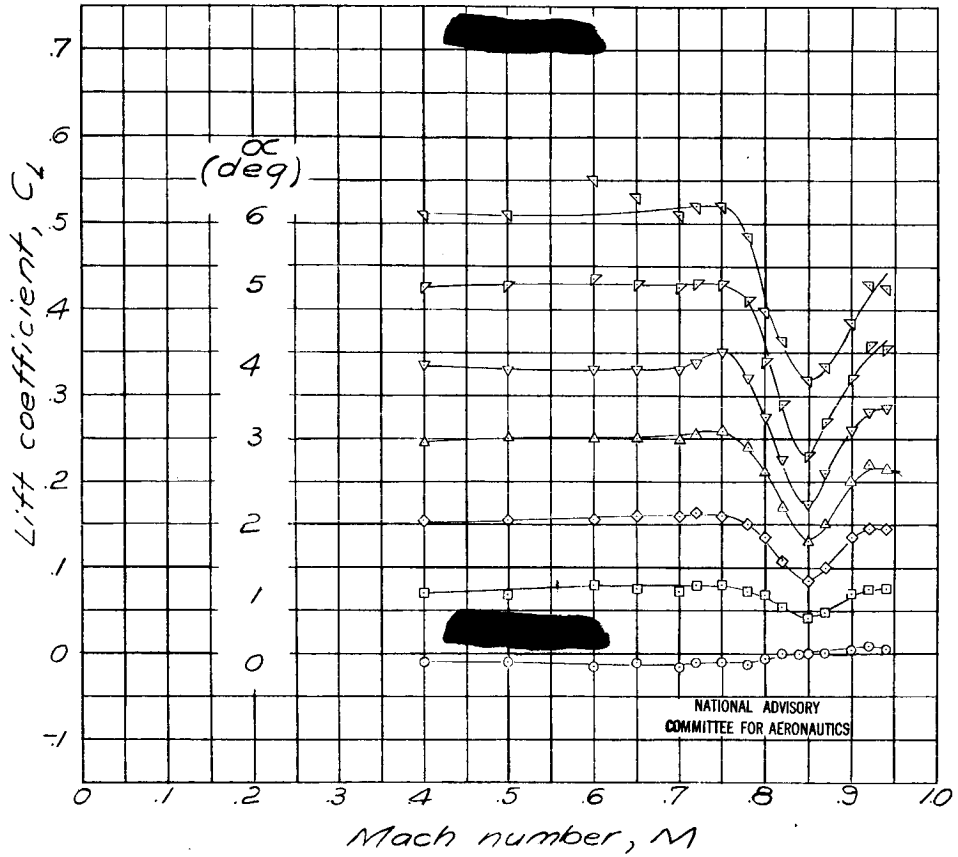
Figure 29.— Effect of compressibility on the aerodynamic characteristics of the NACA 0012-34 airfoil.
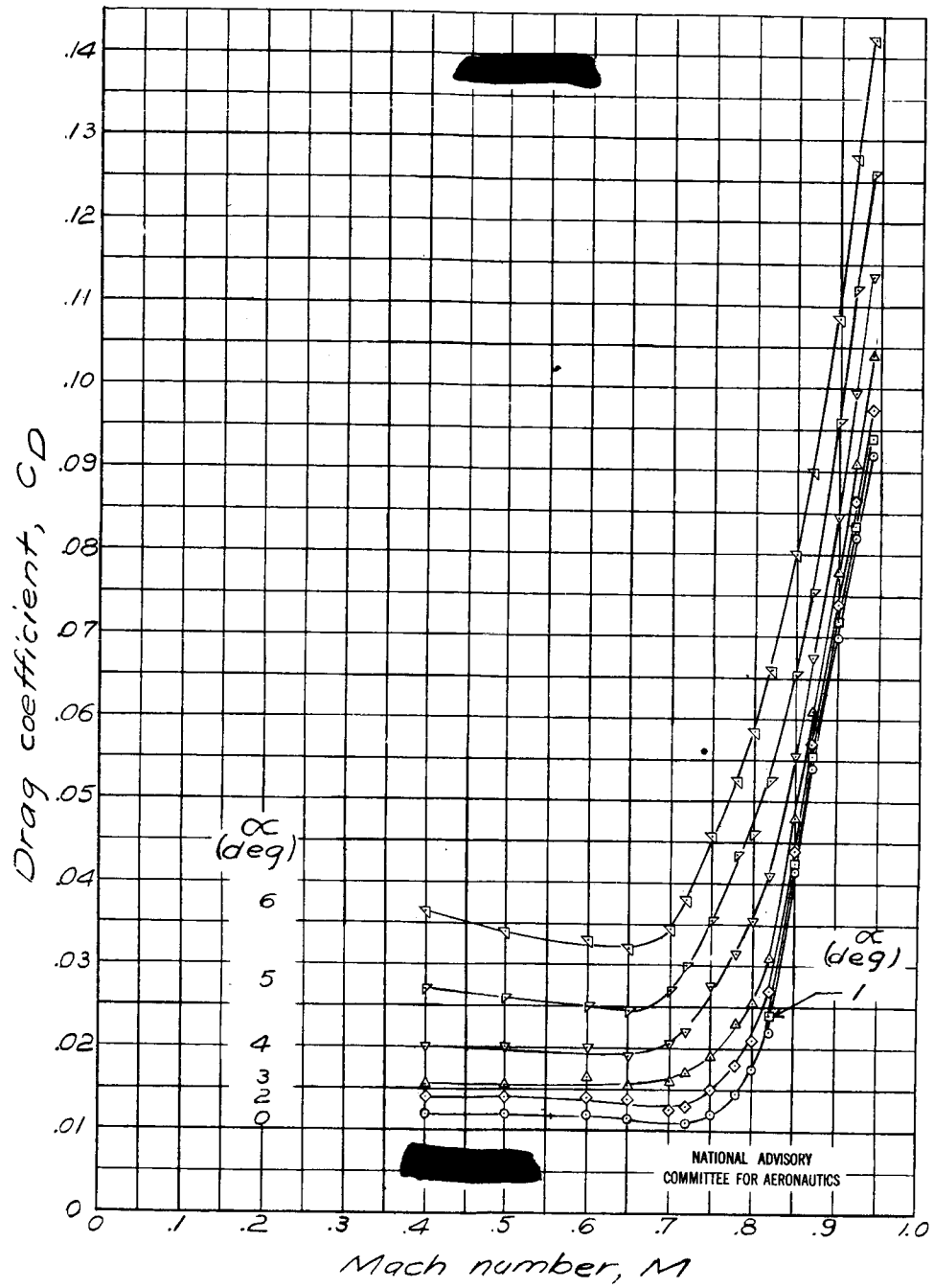
Figure 29 .— Continued.
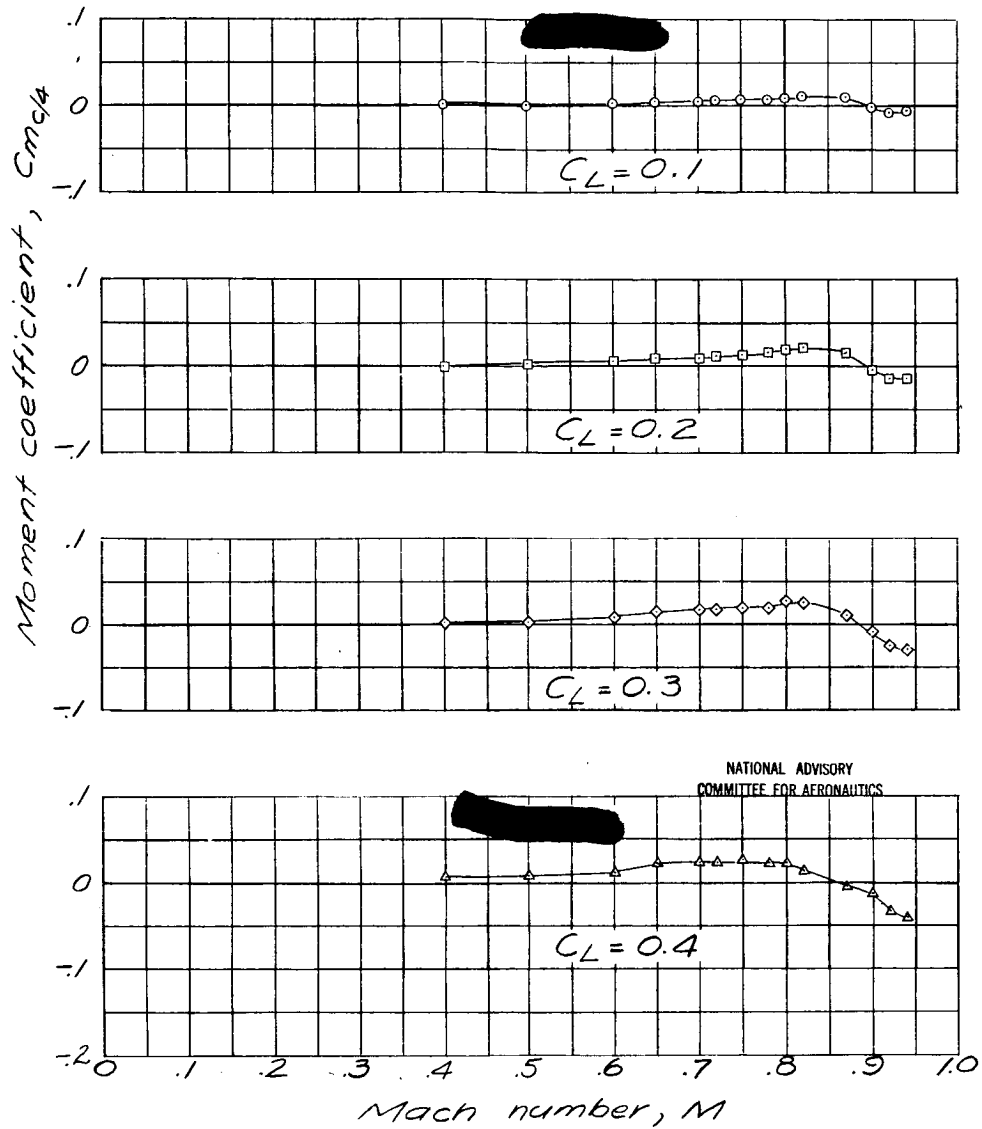
Figure 29.— Concluded.
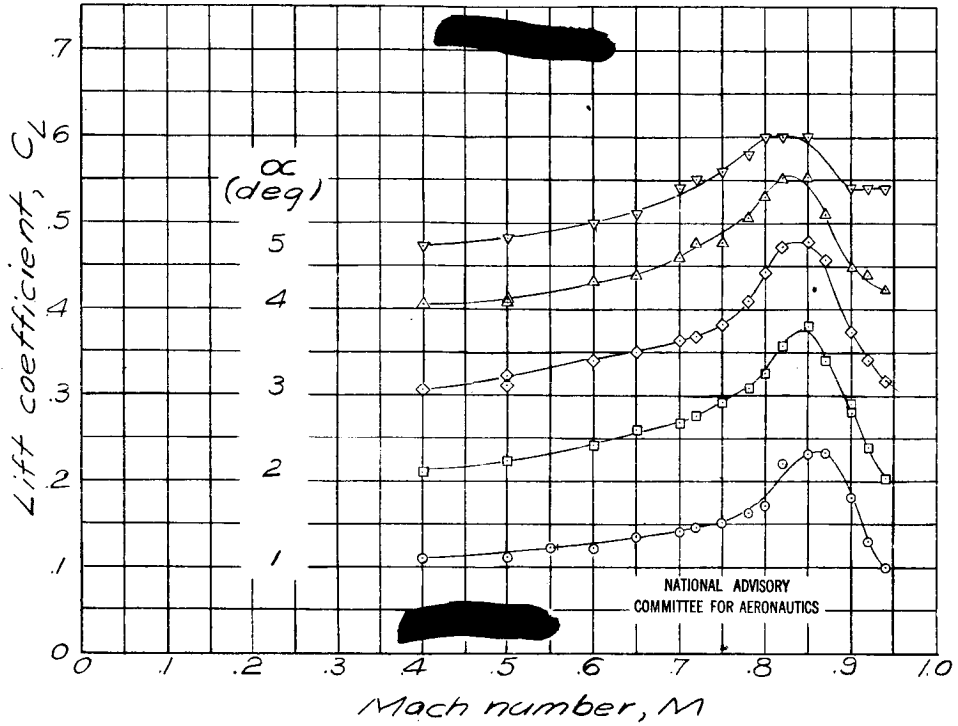
Figure 30 .— Effect of compressibility on the aerodynamic characteristics of the NACA 0006-63 airfoil.
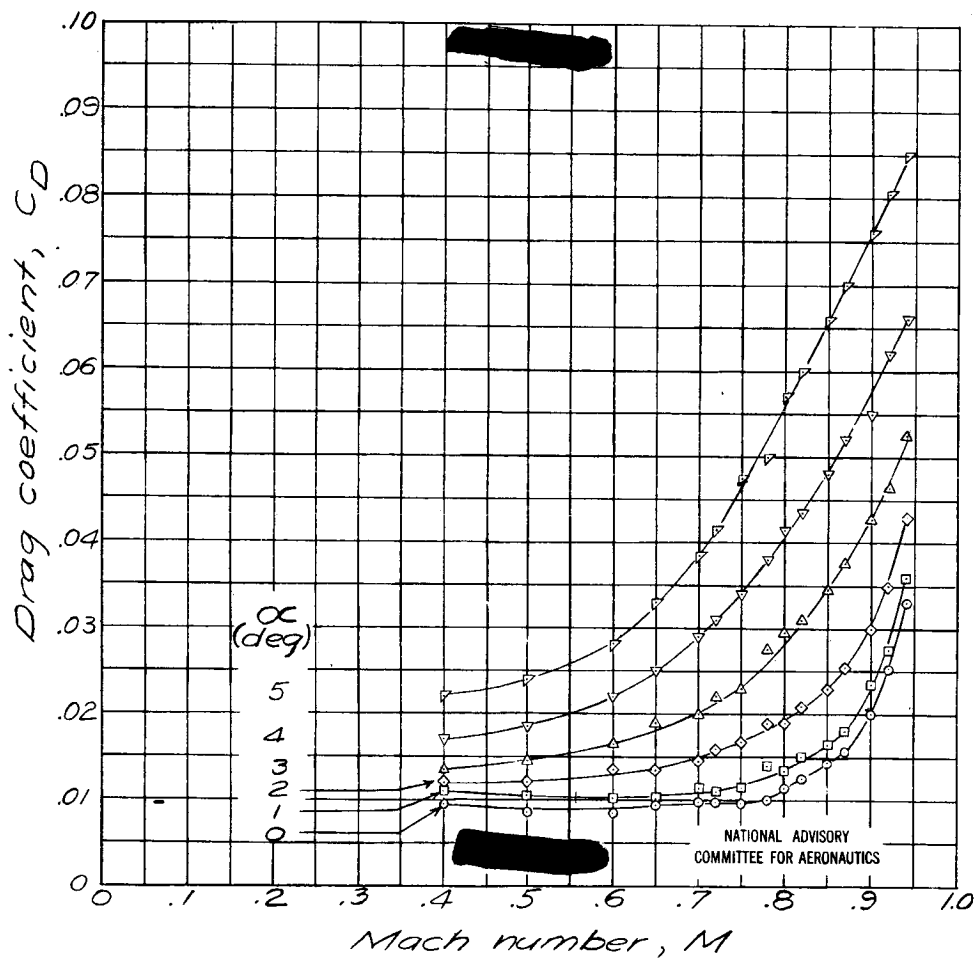
Figure 30 .— Continued.
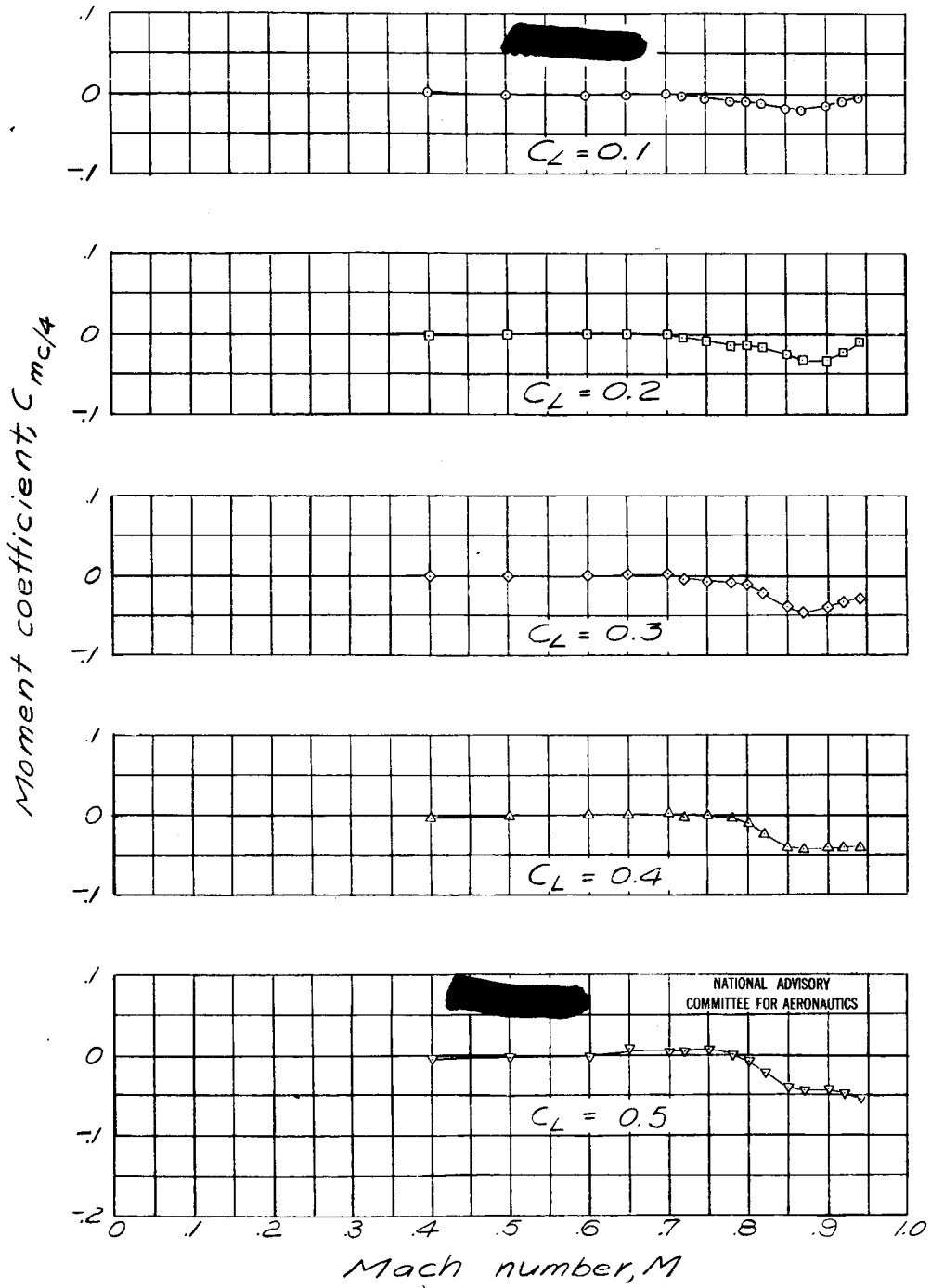
Figure 30 .— Concluded.
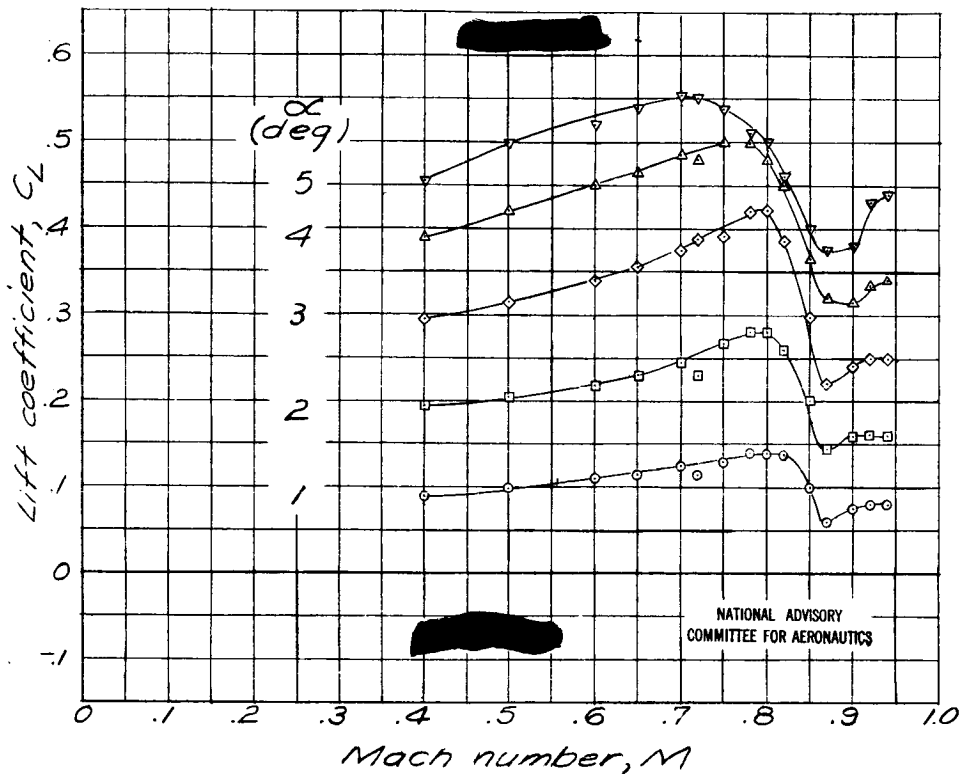
Figure 31. — Effect of compressibility on the aerodynamic characteristics of the NACA 0009-63 airfoil.
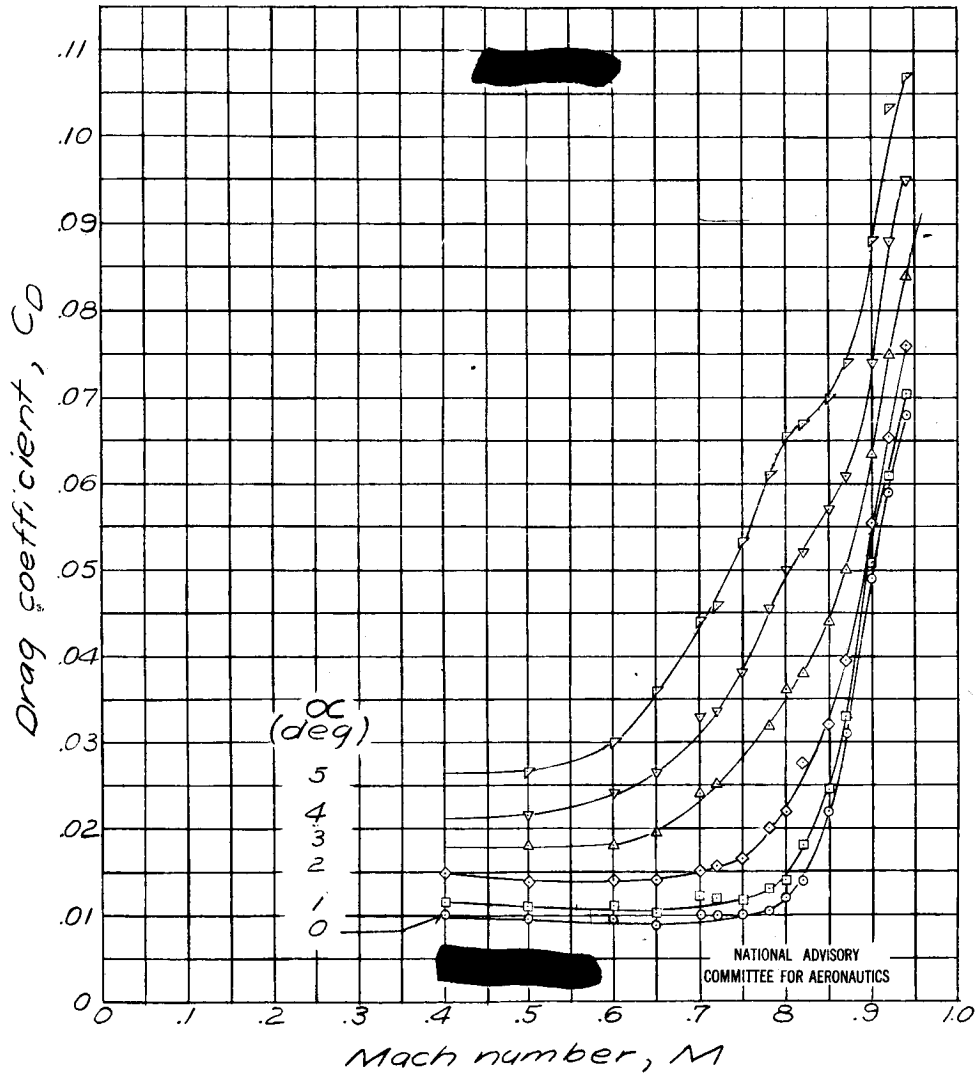
Figure 31 .— Continued.
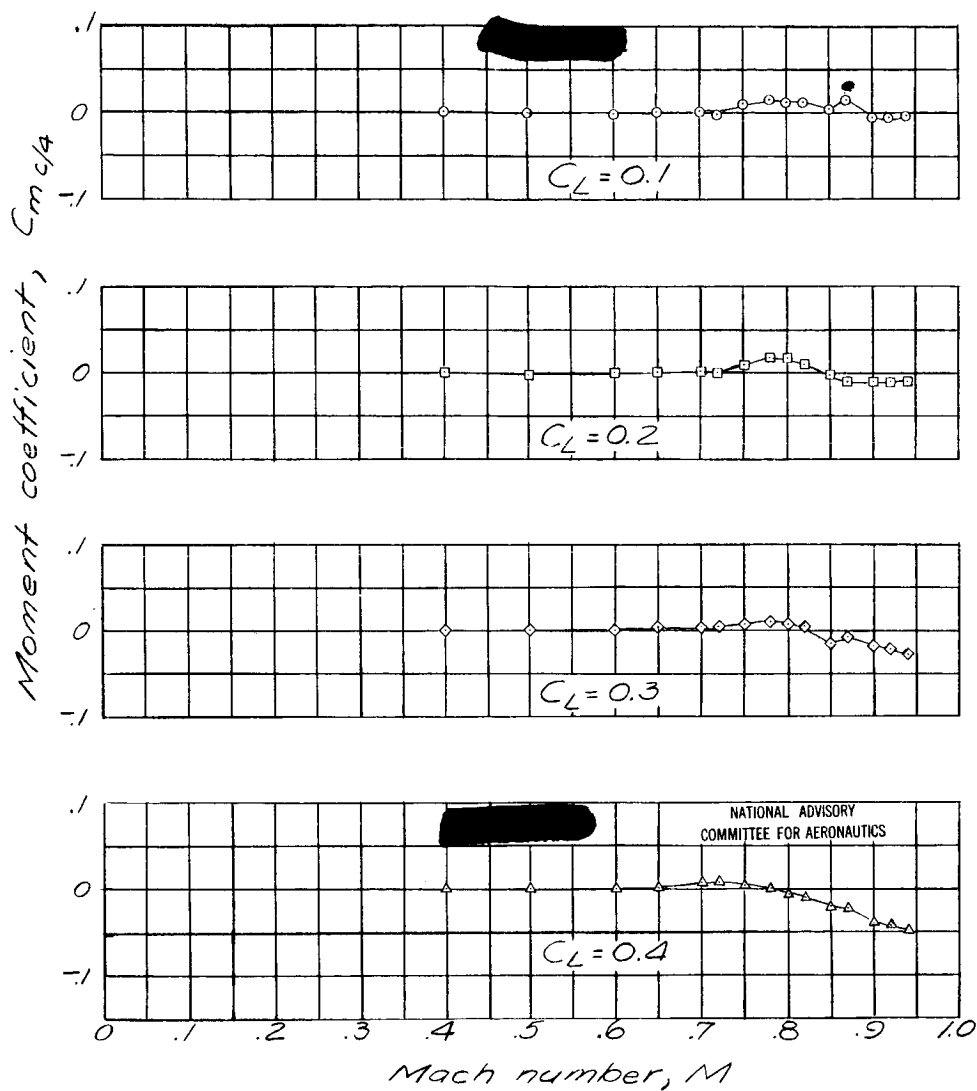
Figure 31. — Concluded.
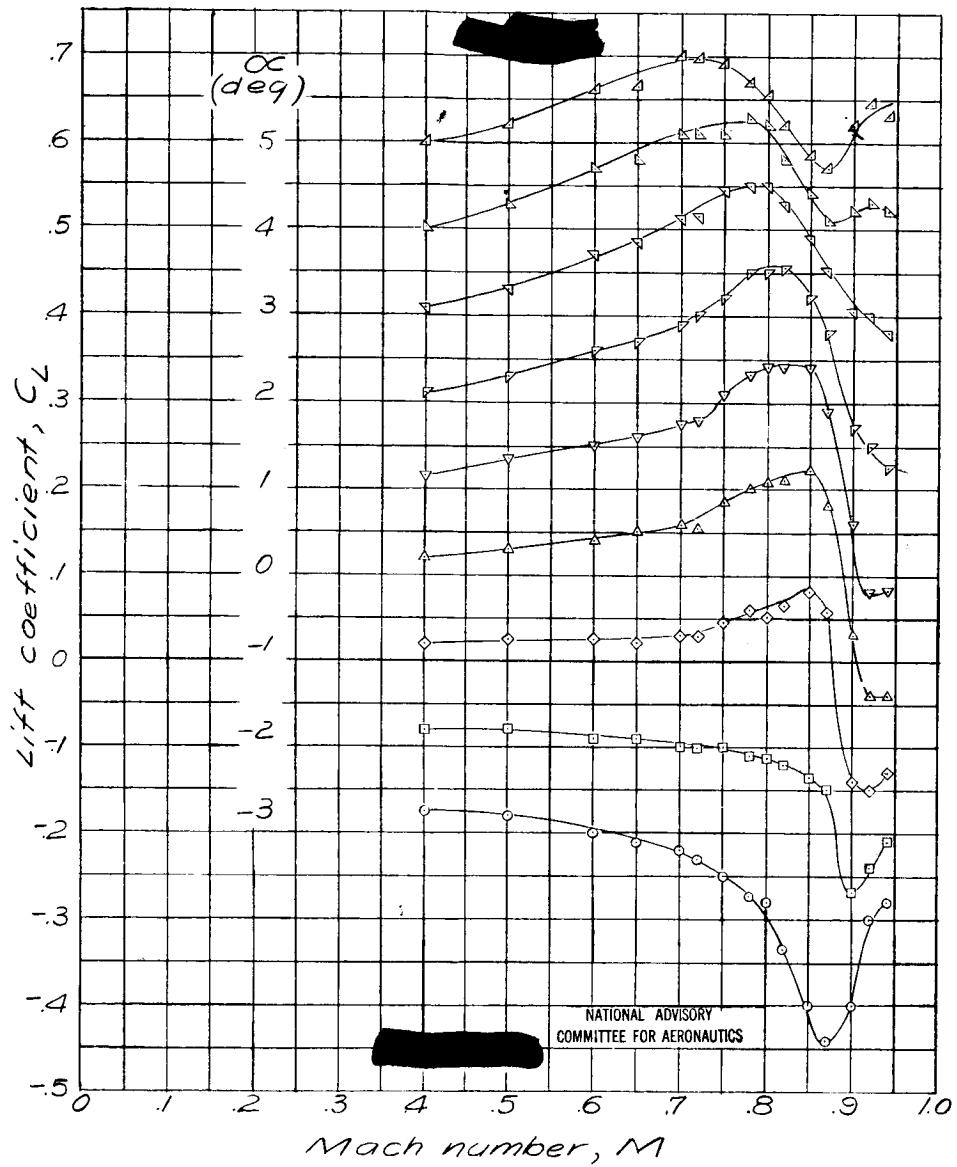
Figure 32.— Effect of compressibility on the aerodynamic characteristics of the NACA 2306 airfoil.
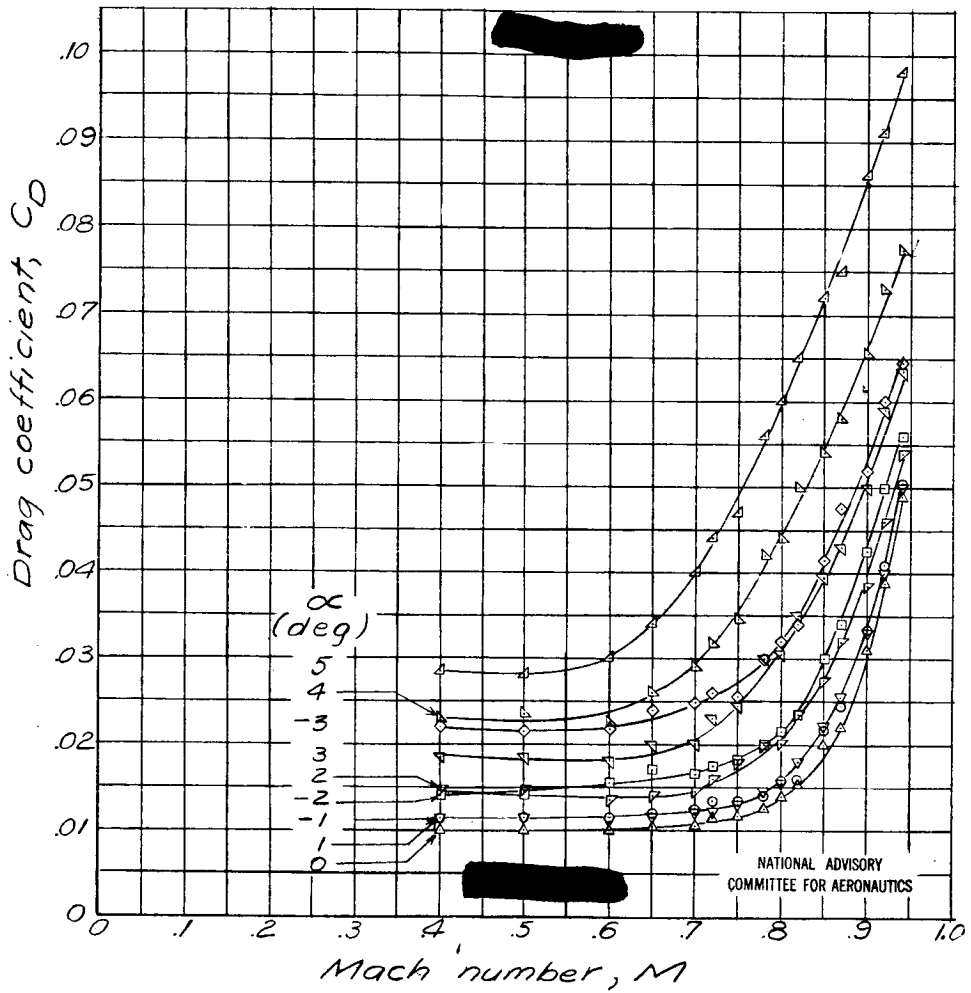
Figure 32.— Continued.
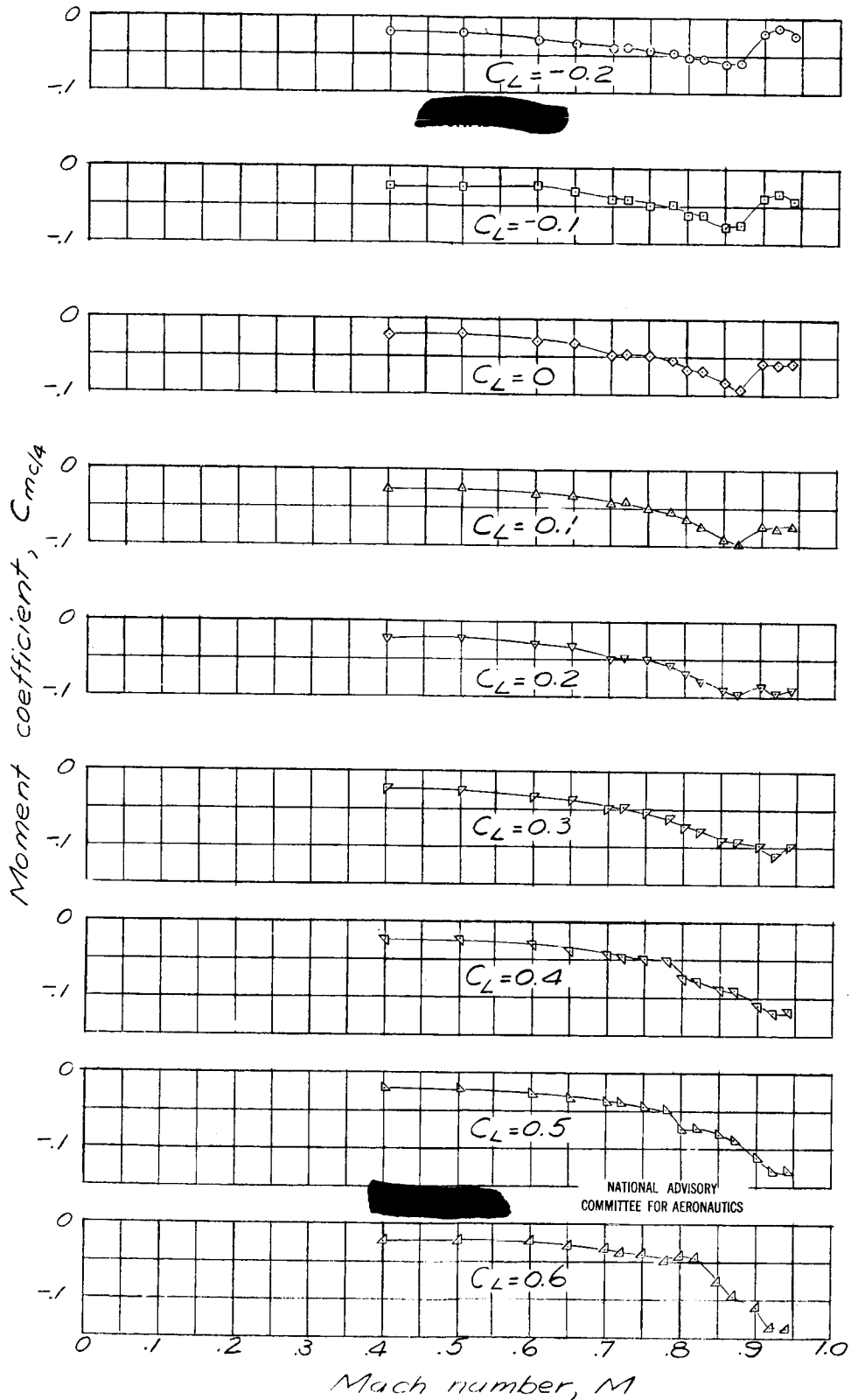
Figure 32. — Concluded.
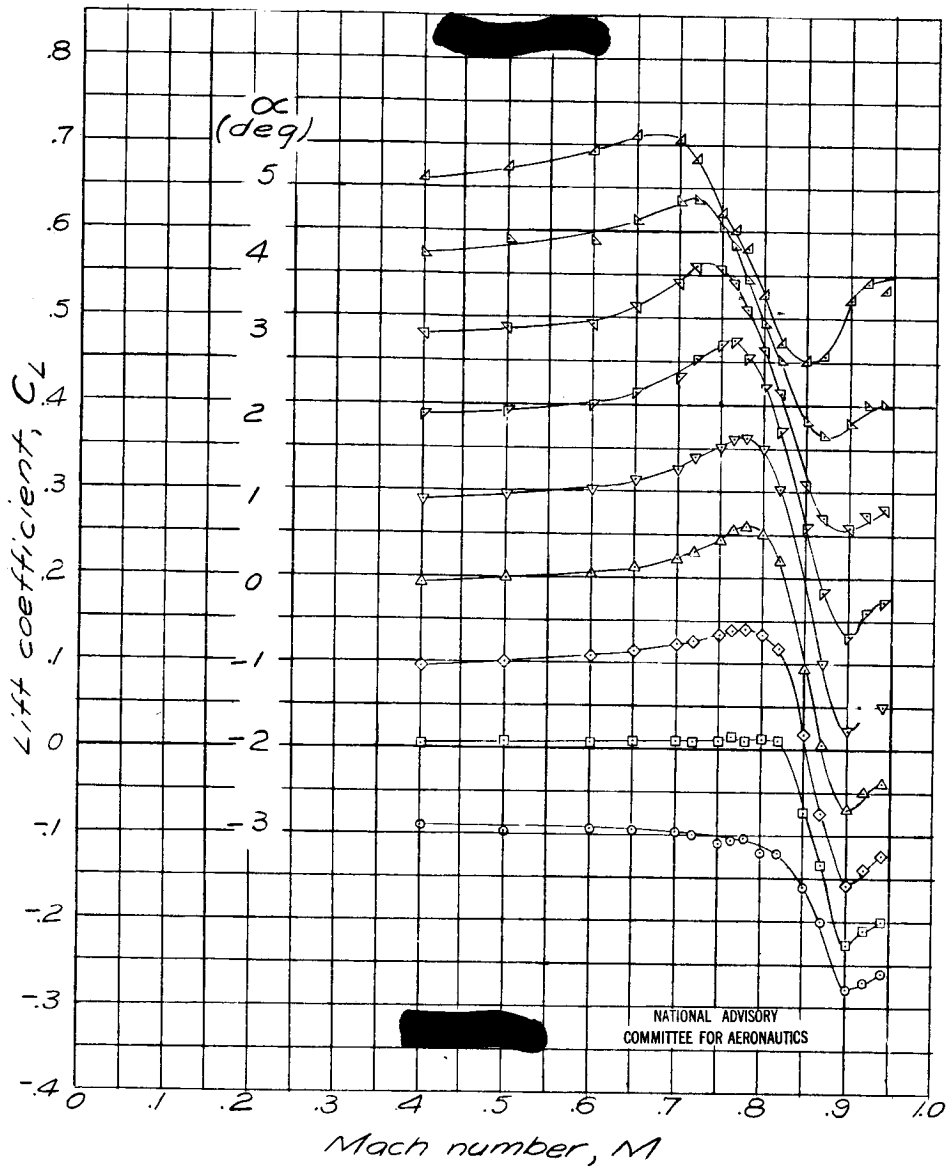
Figure 33 .— Effect of compressibility on the aerodynamic characteristics of the NACA 2309 airfoil.
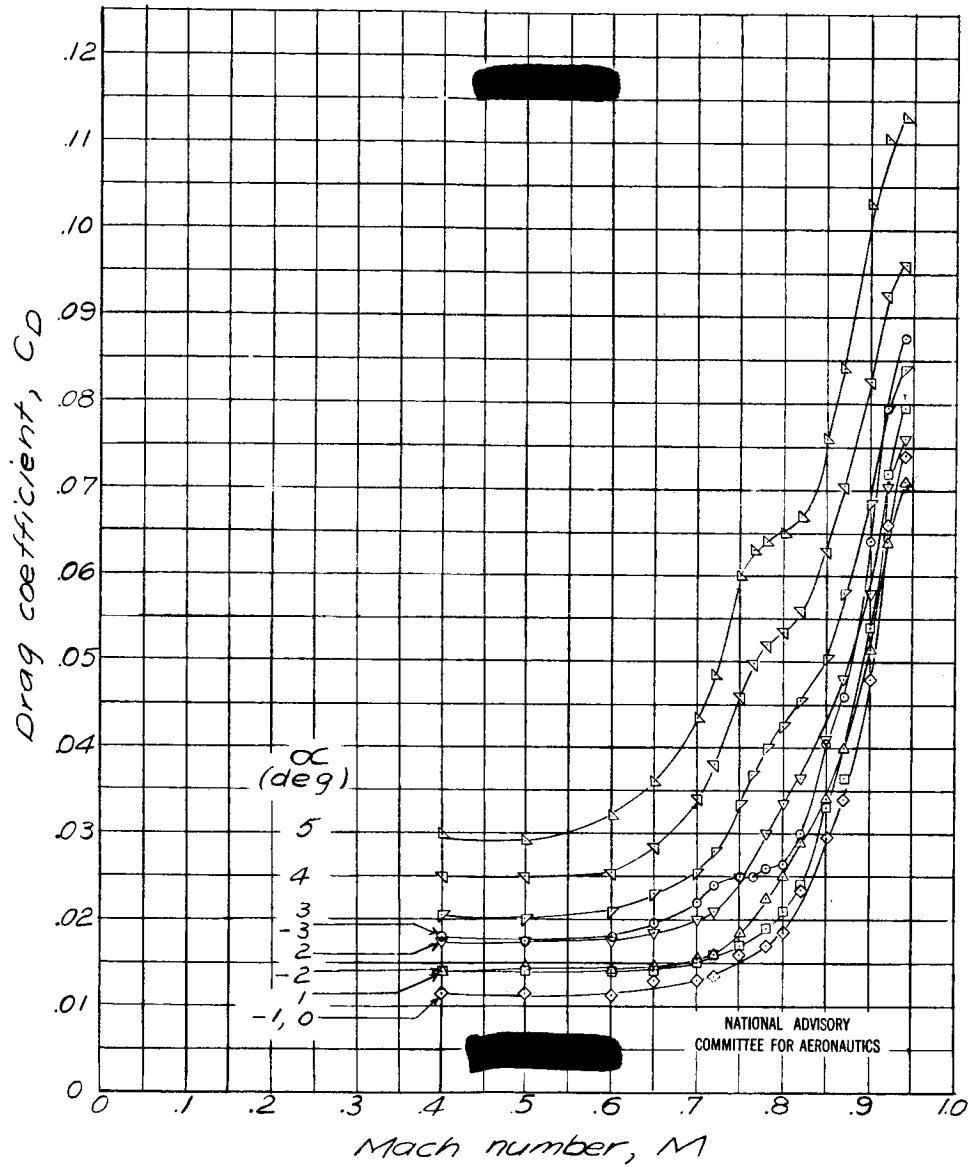
Figure 33.— Continued.
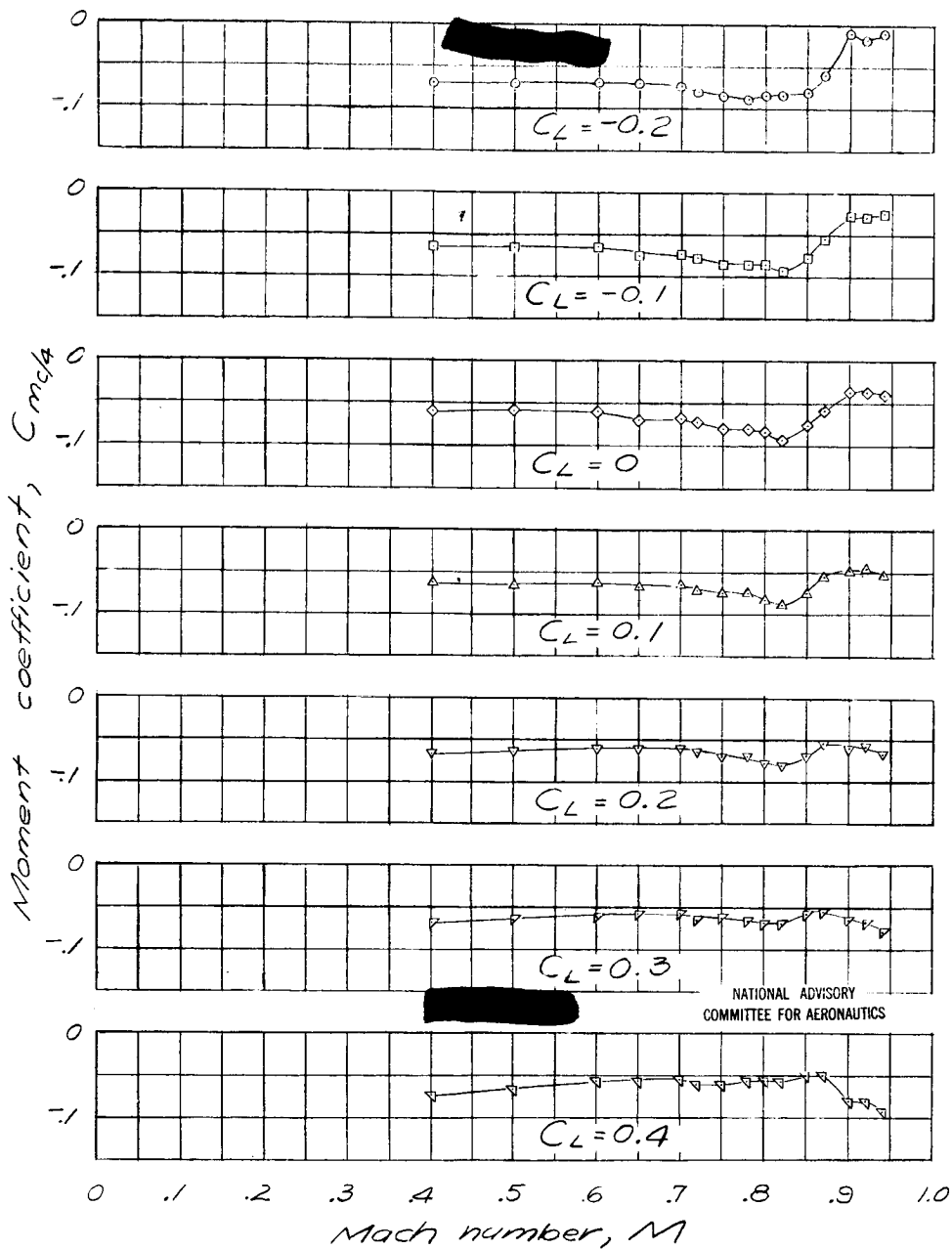
Figure 33 .— Concluded.
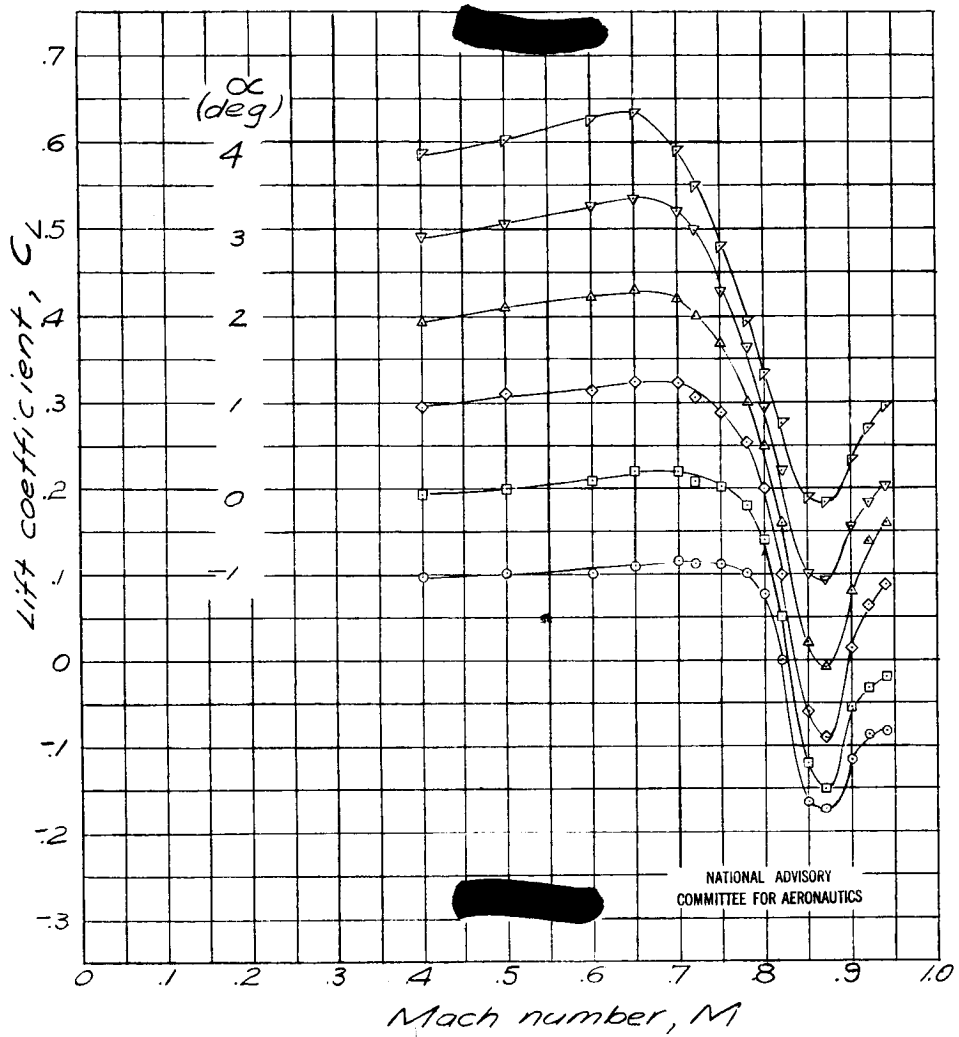
Figure 34.— Effect of compressibility on the aerodynamic characteristics of the NACA 2312 airfoil
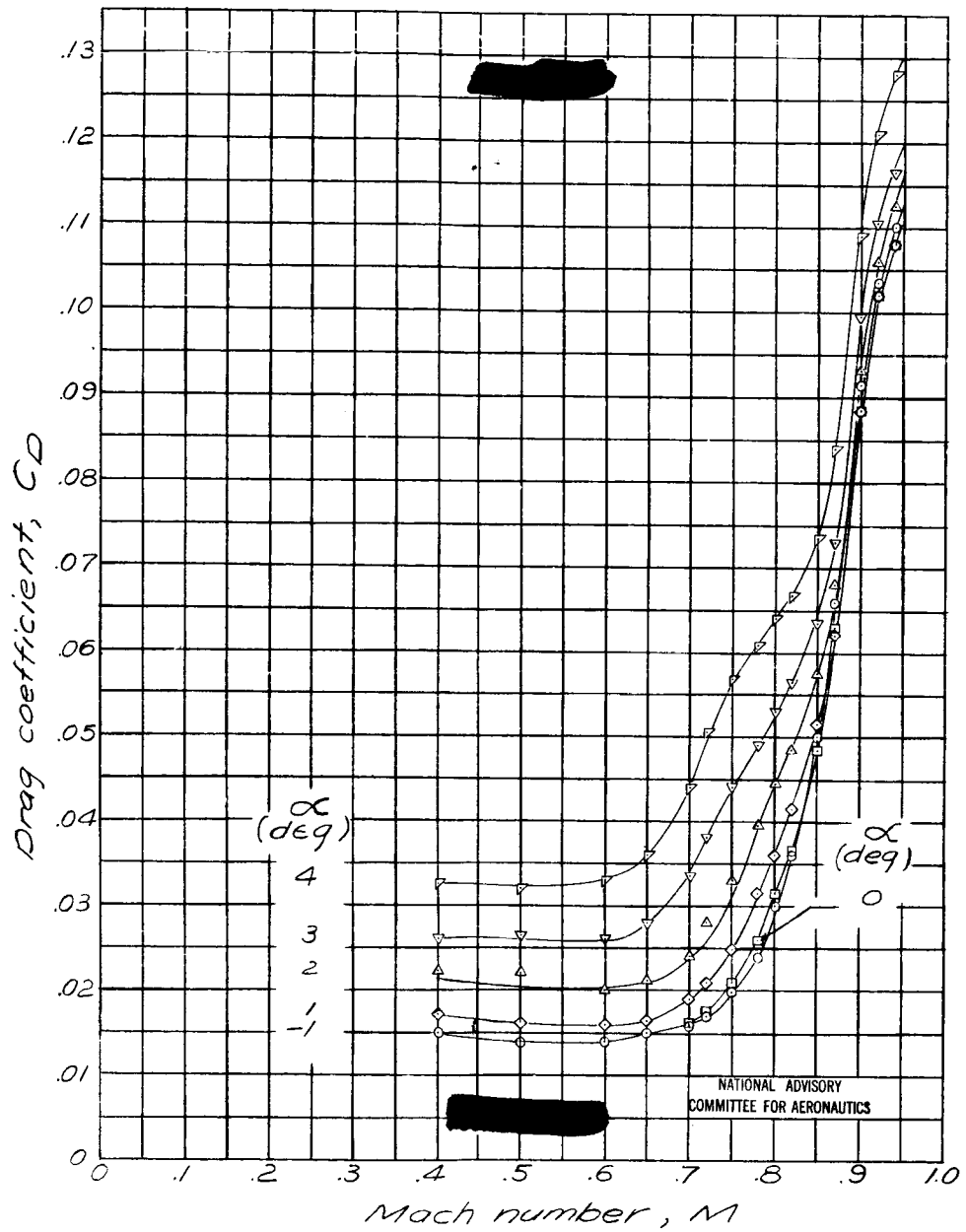
Figure 34.— Continued.
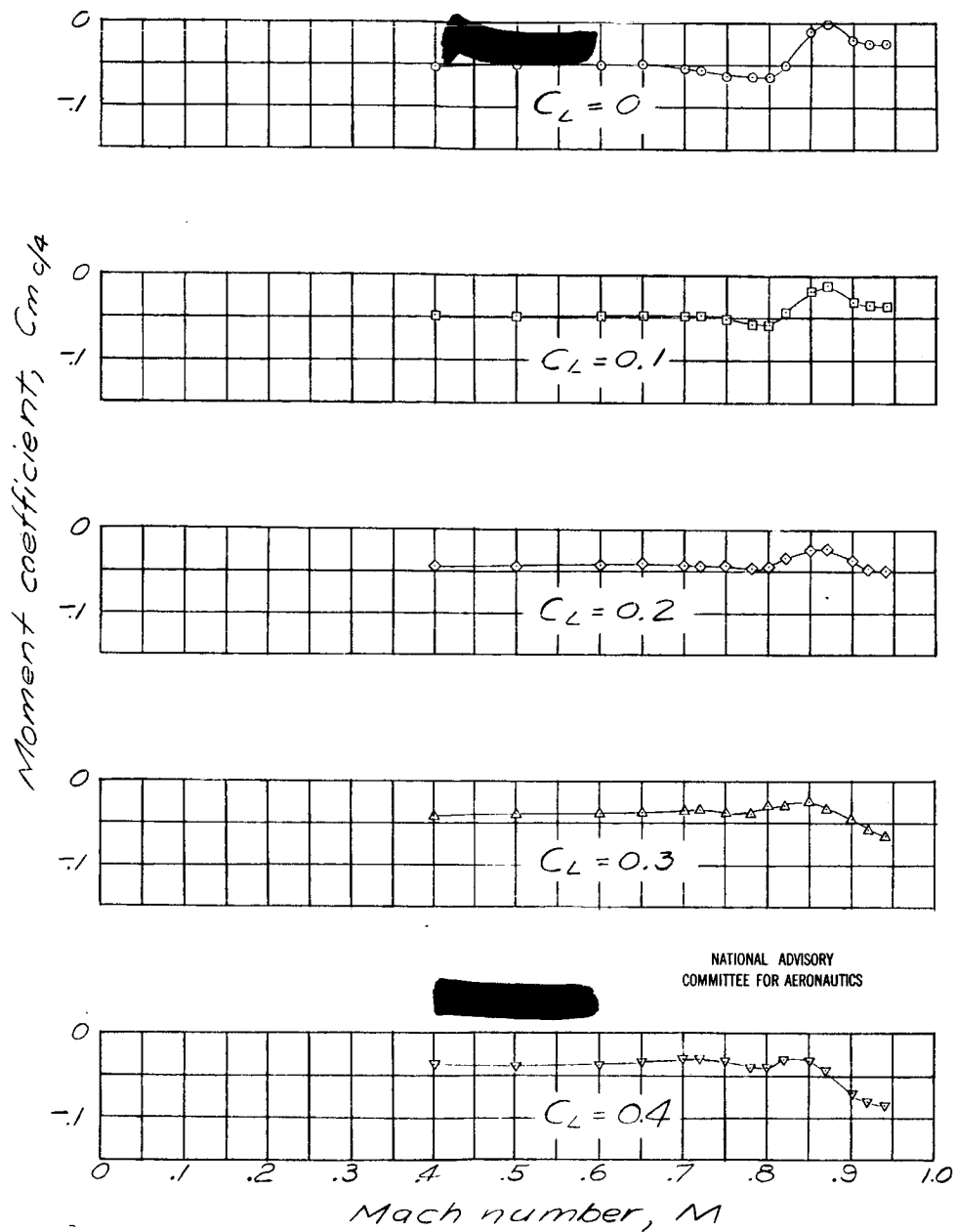
Figure 34.— Concluded.
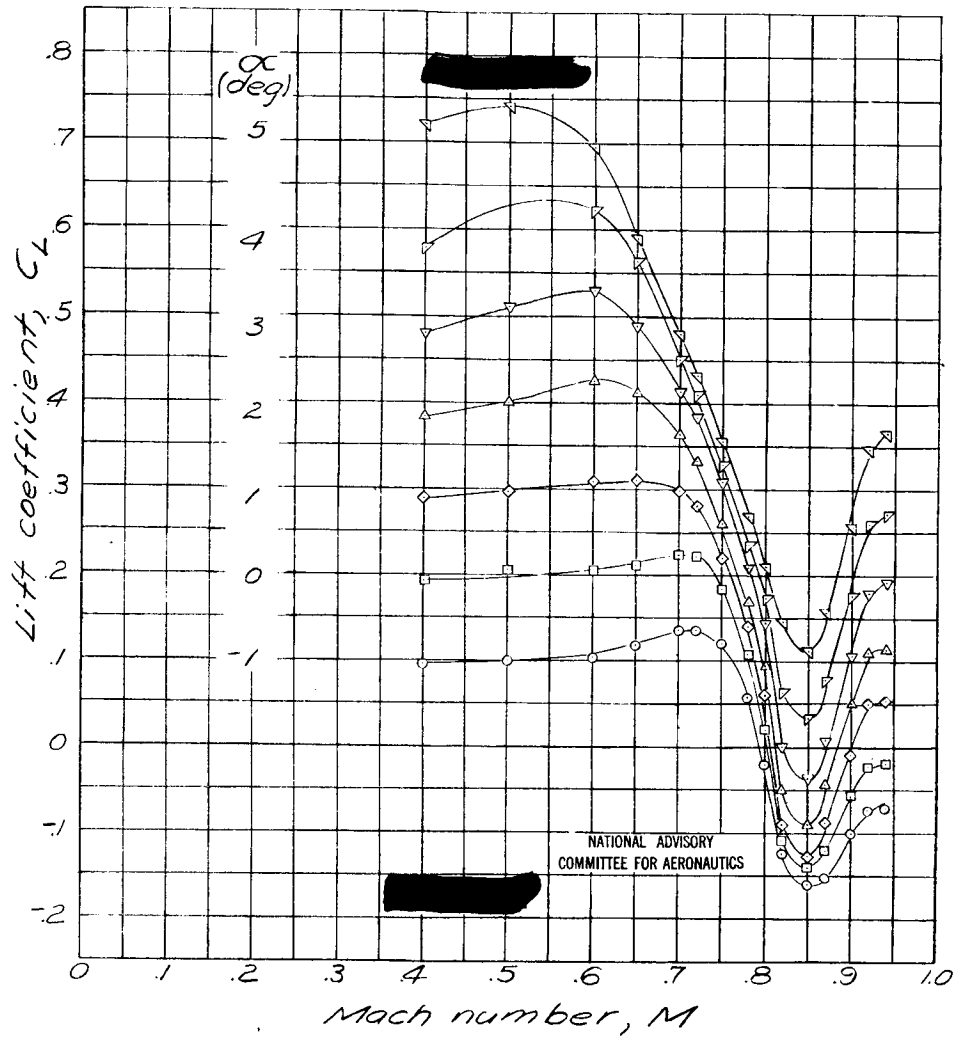
Figure 35.— Effect of compressibility on the aerodynamic characteristics of the NACA 2315 airfoil.
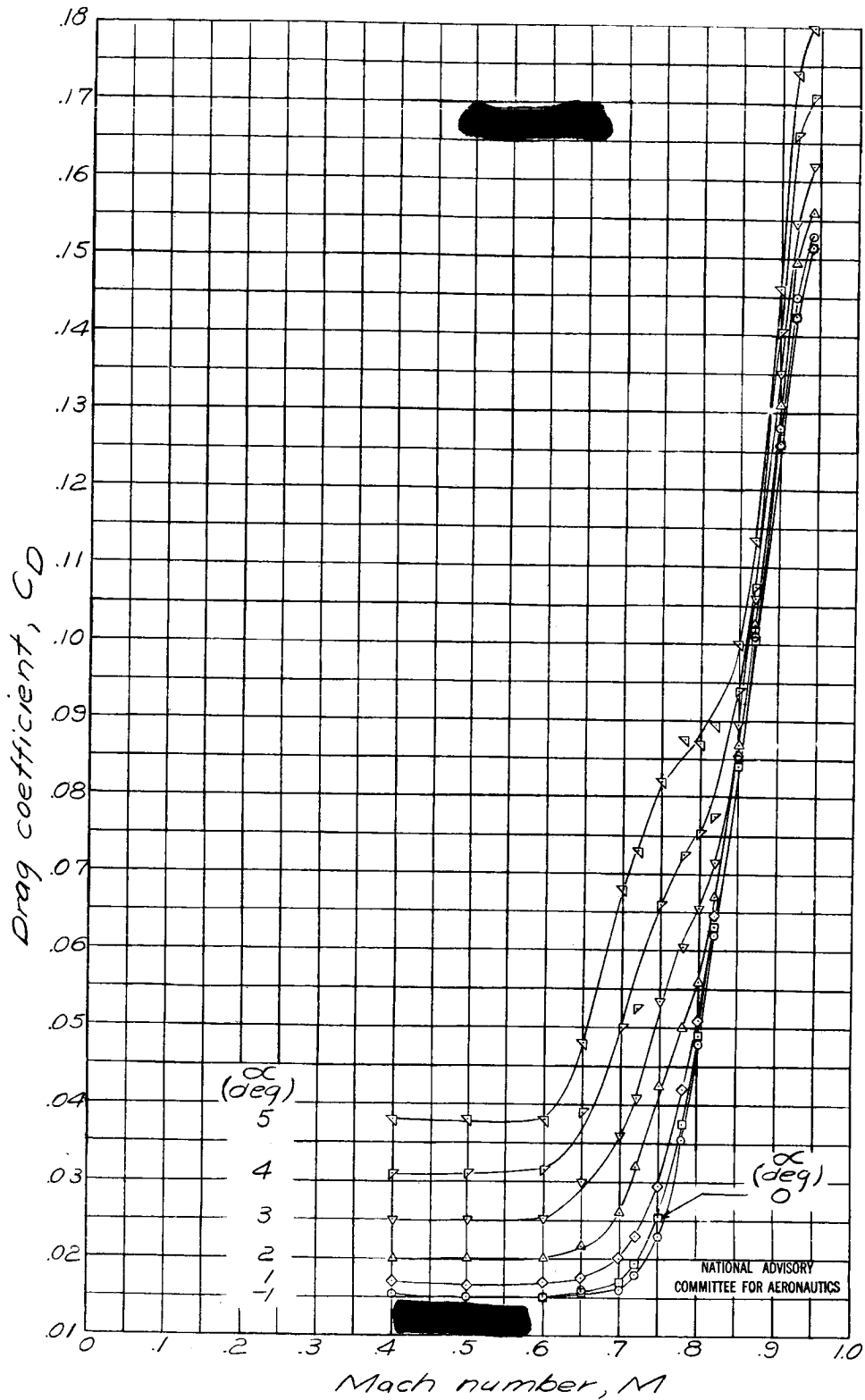
Figure 35.— Continued.
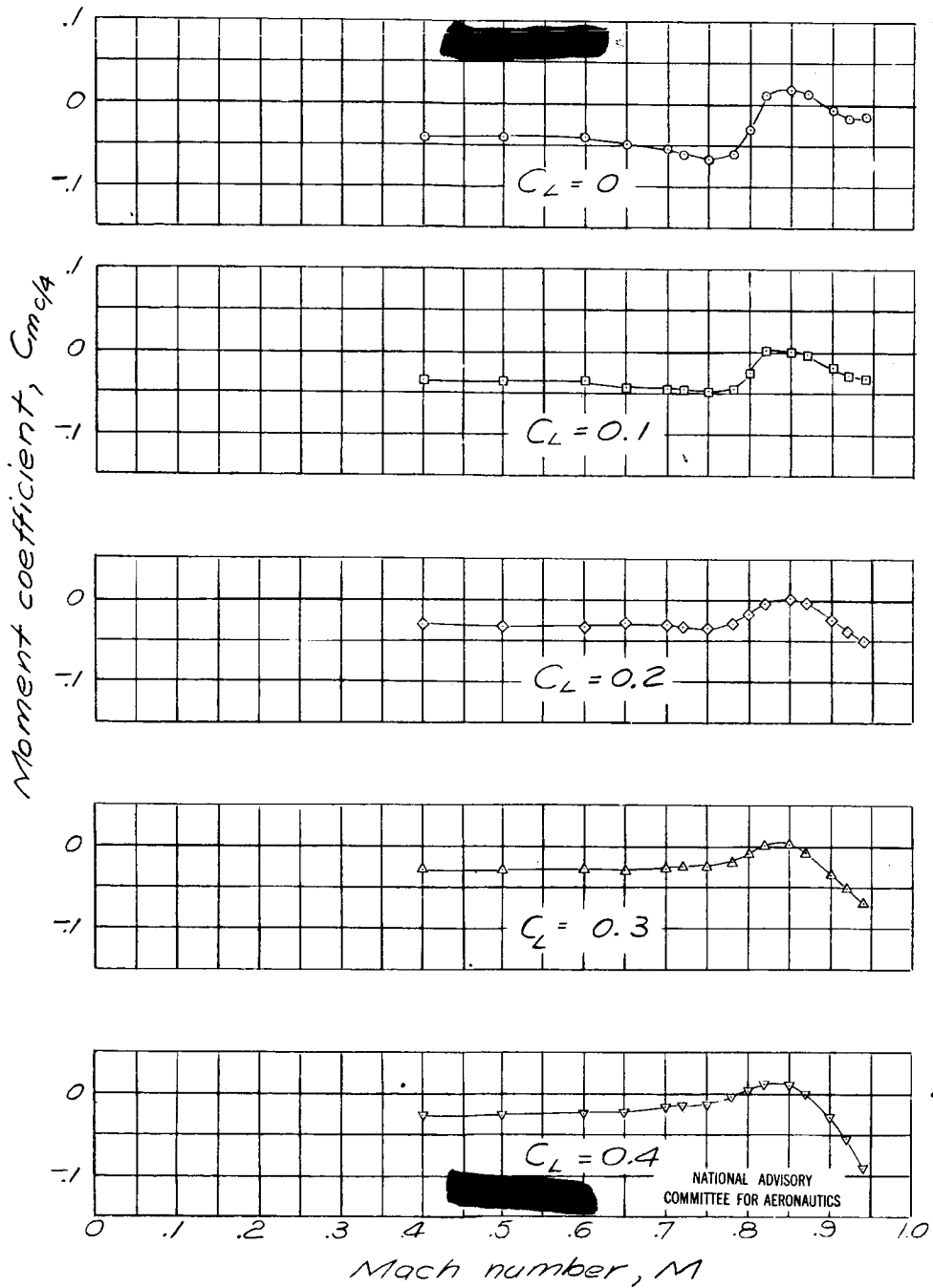
Figure 35.— Concluded.
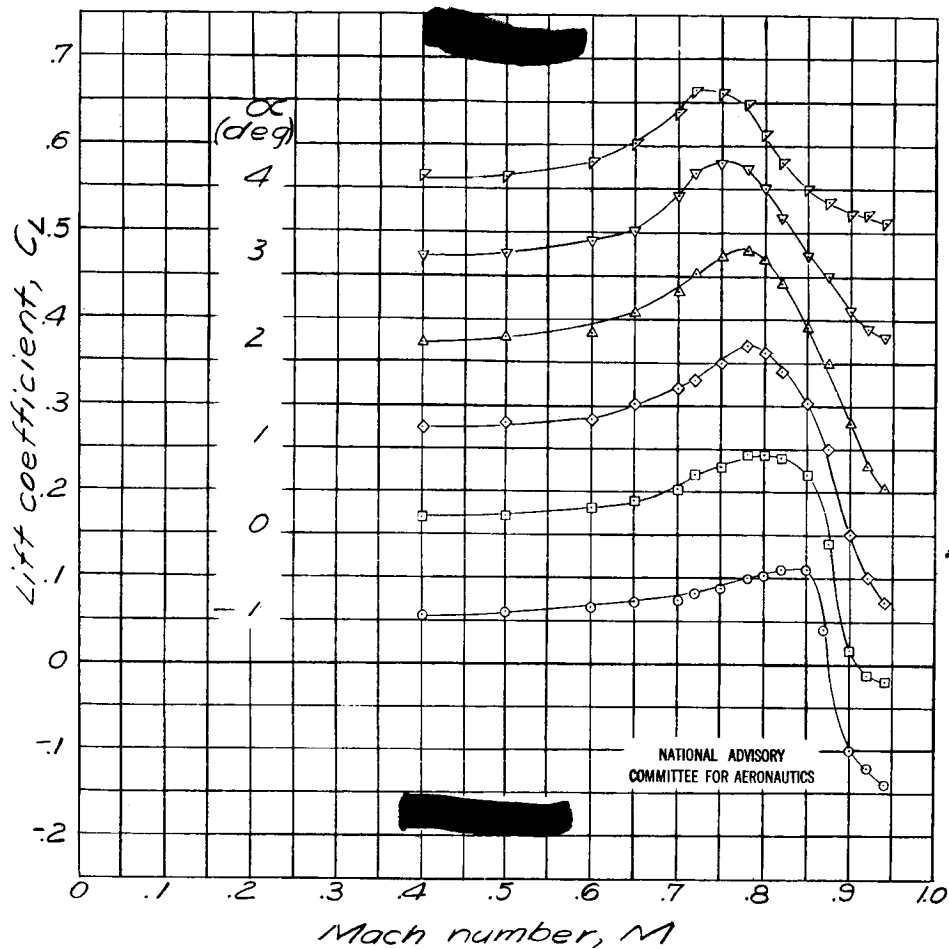
Figure 36.— Effect of compressibility on the
aerodynamic characteristics of the
NACA 2406 airfoil.
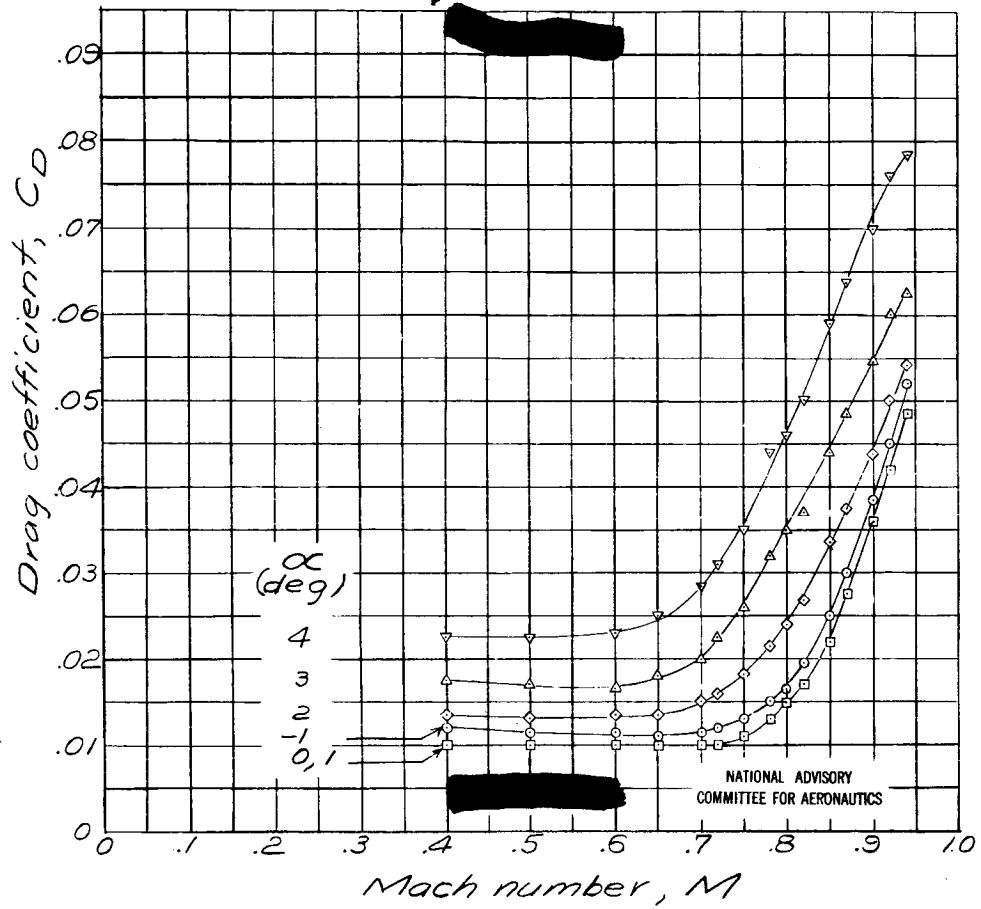
Figure 36.— Continued.
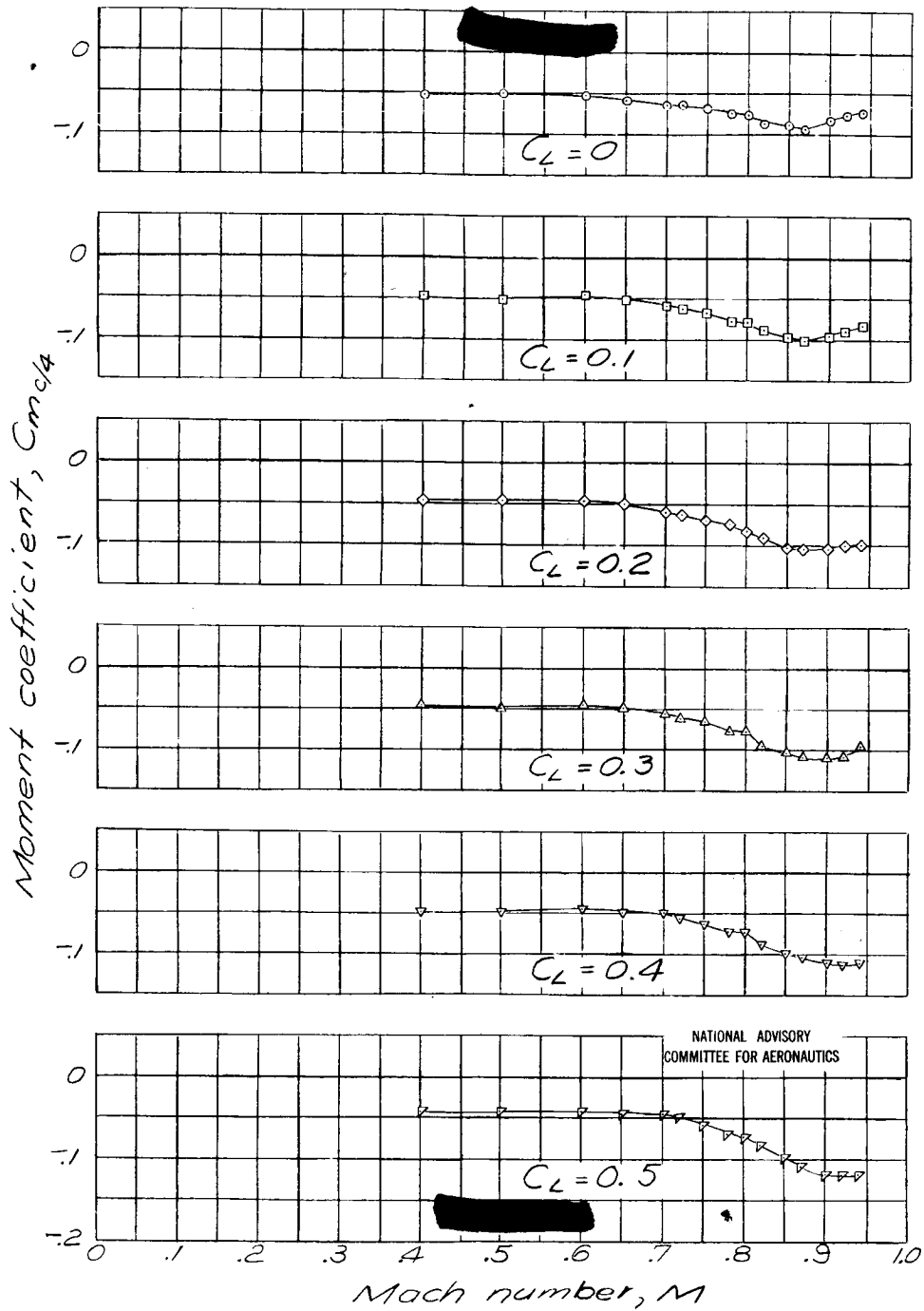
Figure 36.— Concluded.
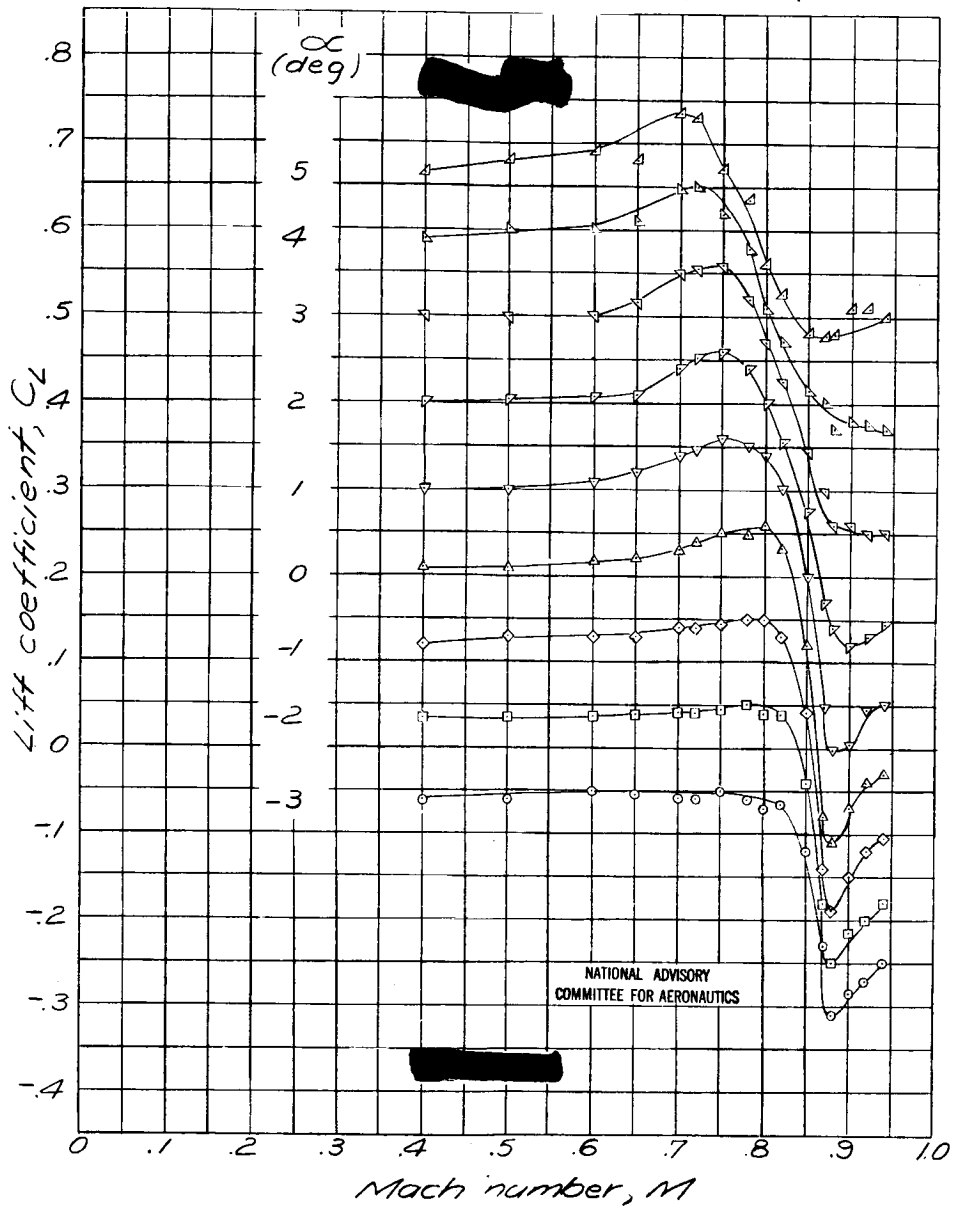
Figure 37.— Effect of compressibility on the aerodynamic characteristics of the NACA 2409 airfoil.
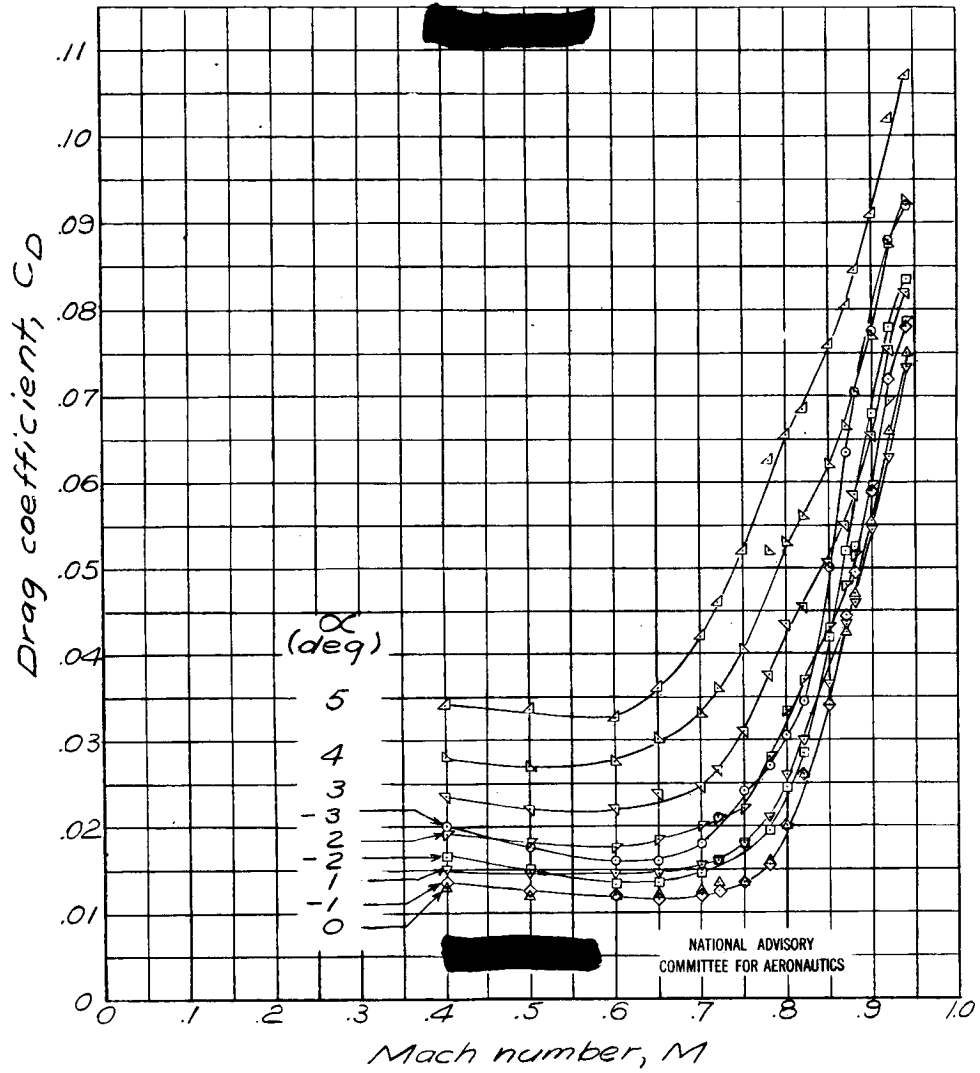
Figure 37 .— Continued.
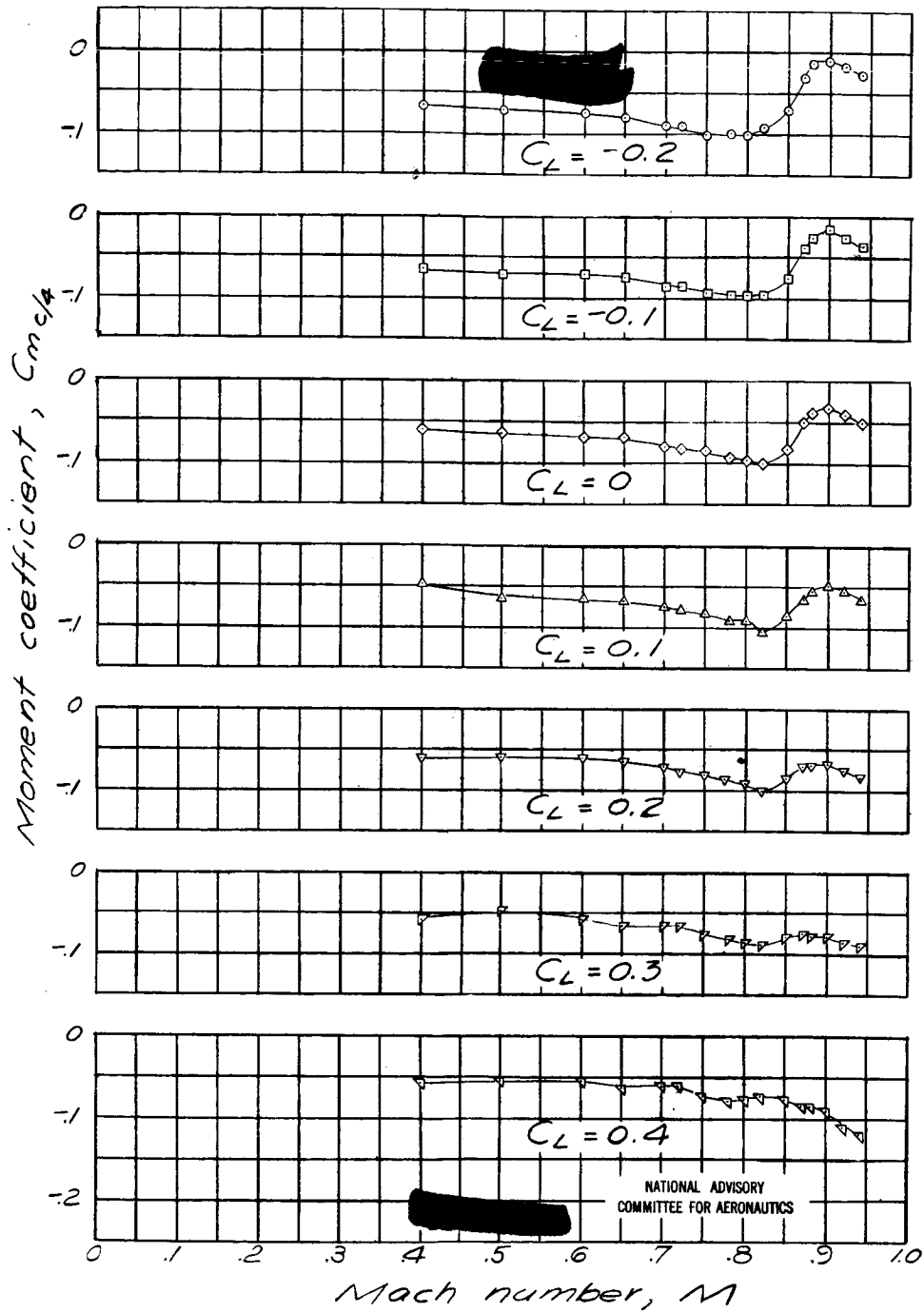
Figure 37 .— Concluded.
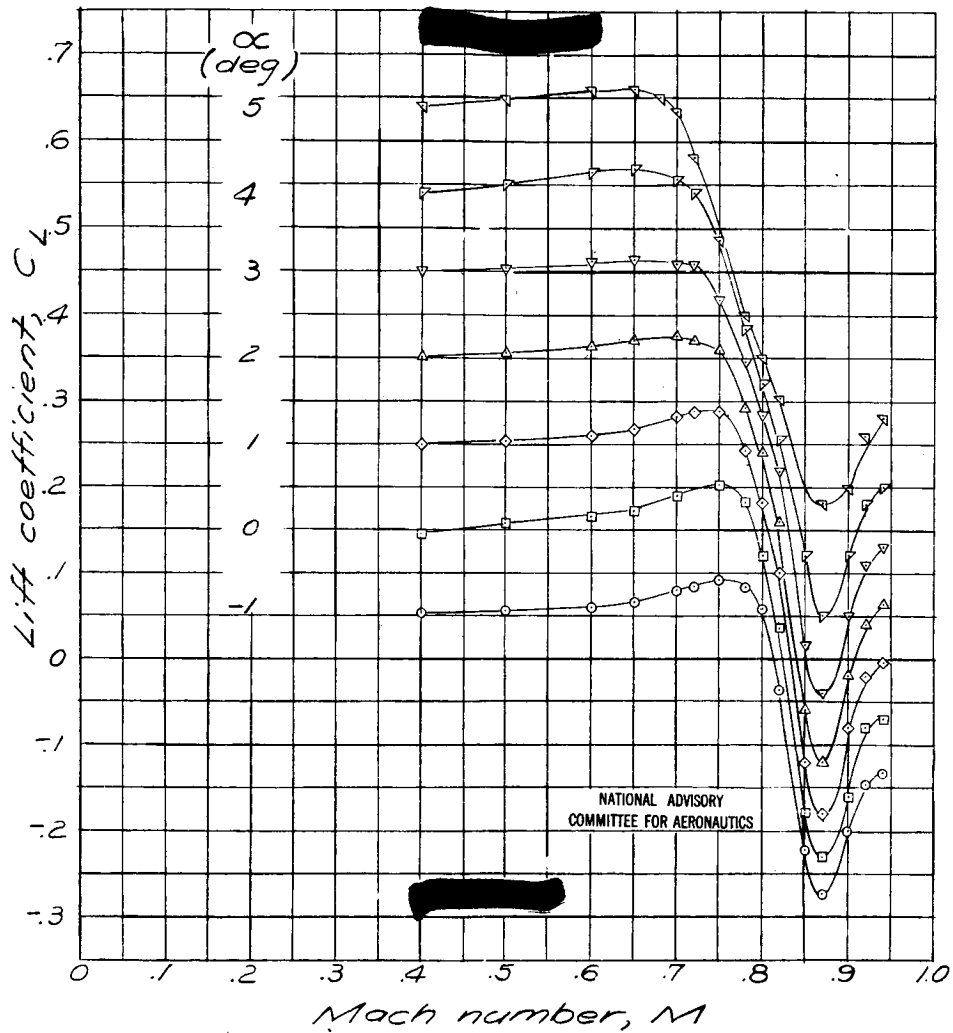
Figure 38.— Effect of compressibility on the aerodynamic characteristics of the NACA 2412 airfoil.
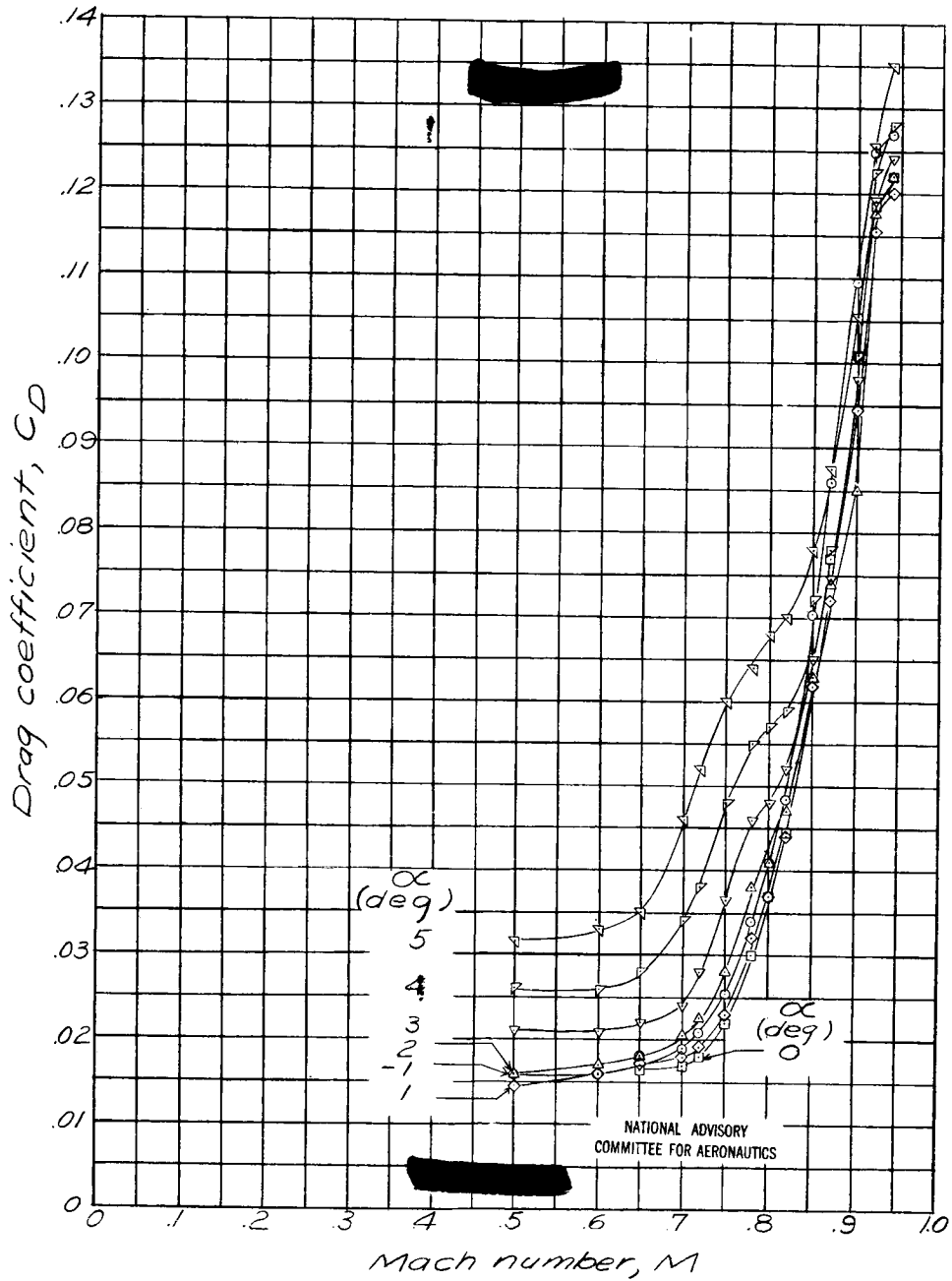
Figure 38 . — Continued.
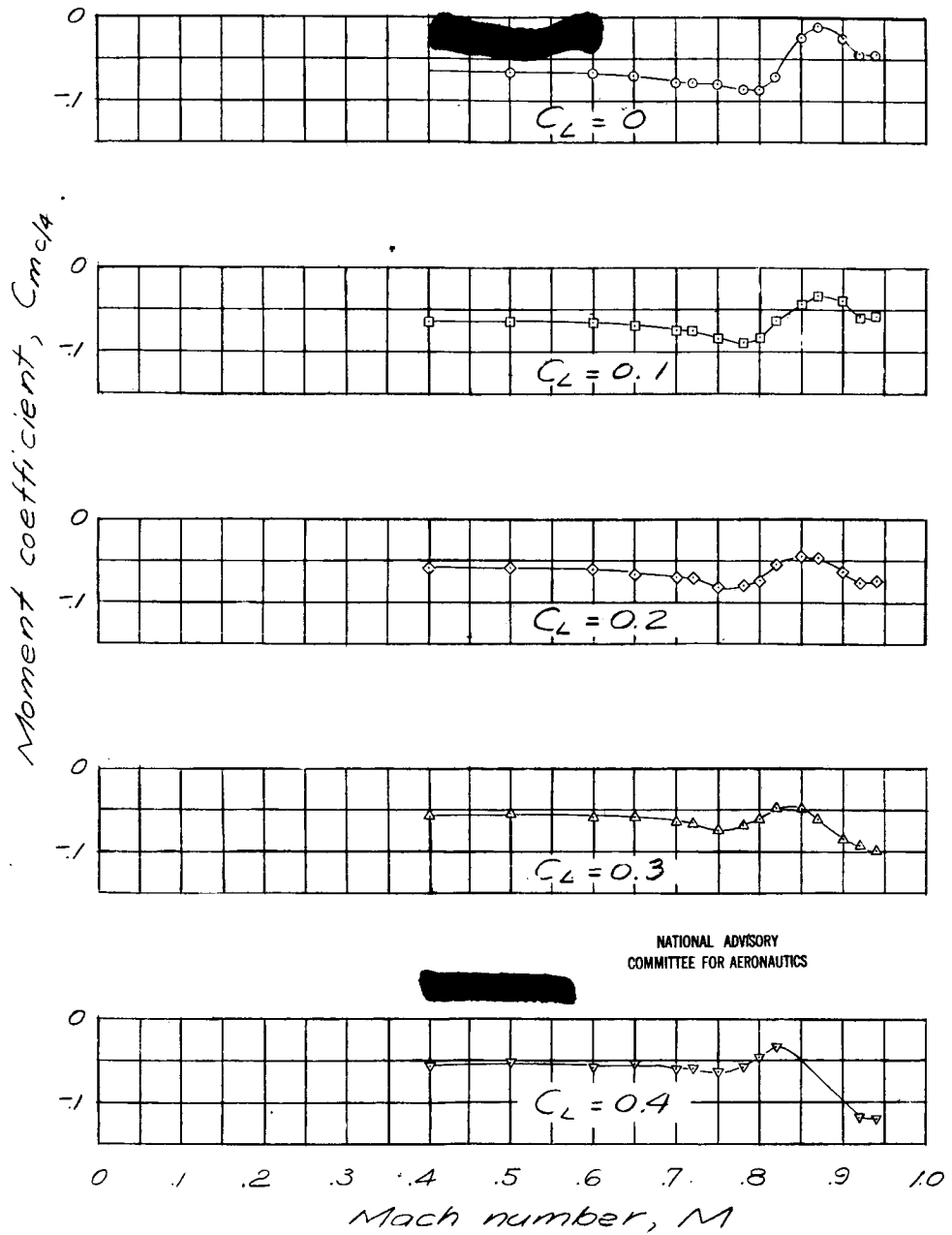
Figure 38 .— Concluded.
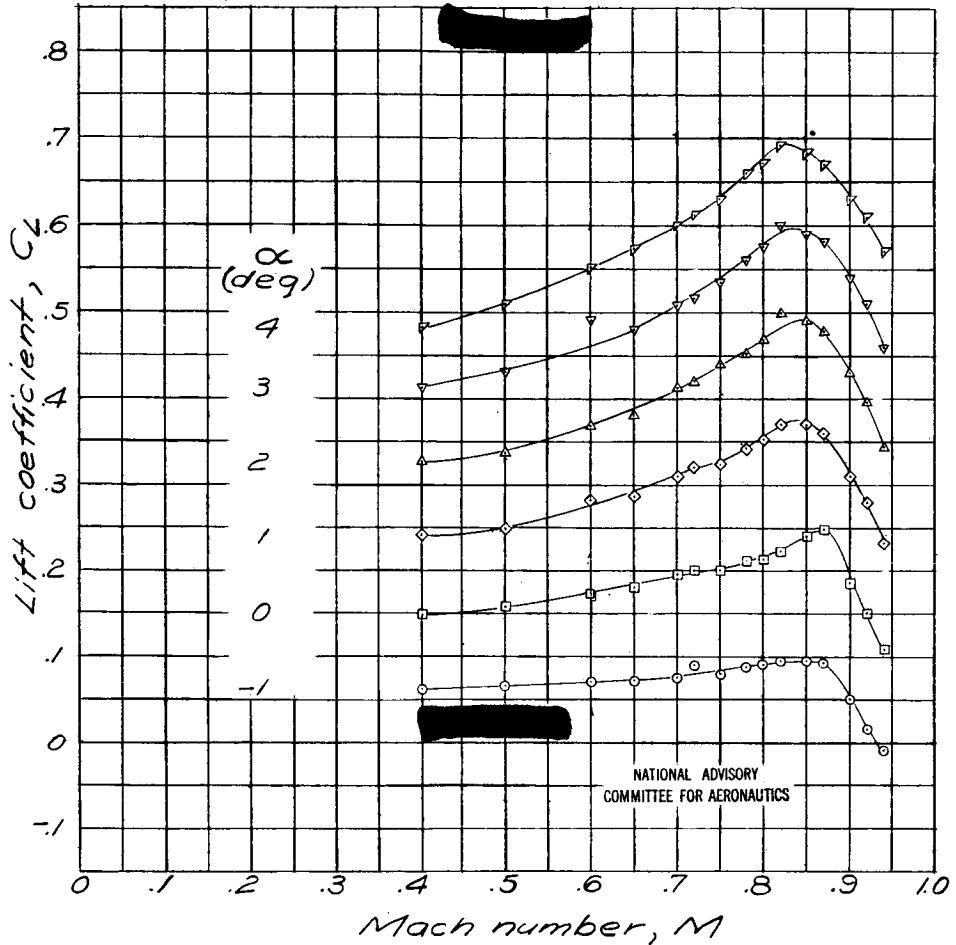
Figure 39 .— Effect of compressibility on the aerodynamic characteristics of the U.S.N.P.S. 1 airfoil, 4 percent thick.
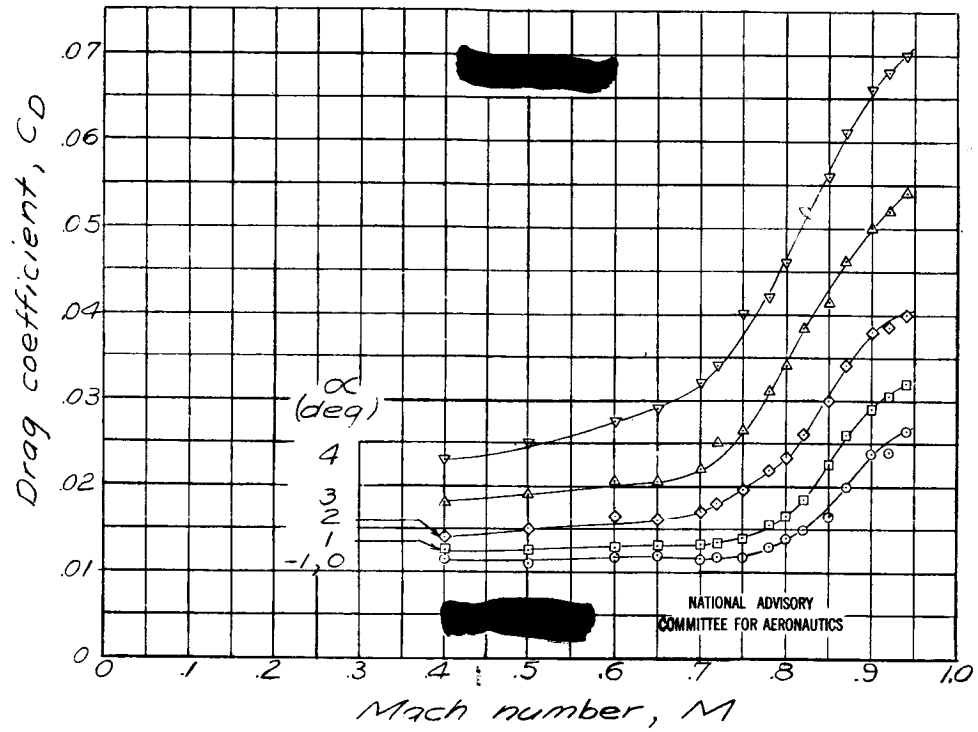
Figure 39.— Continued.
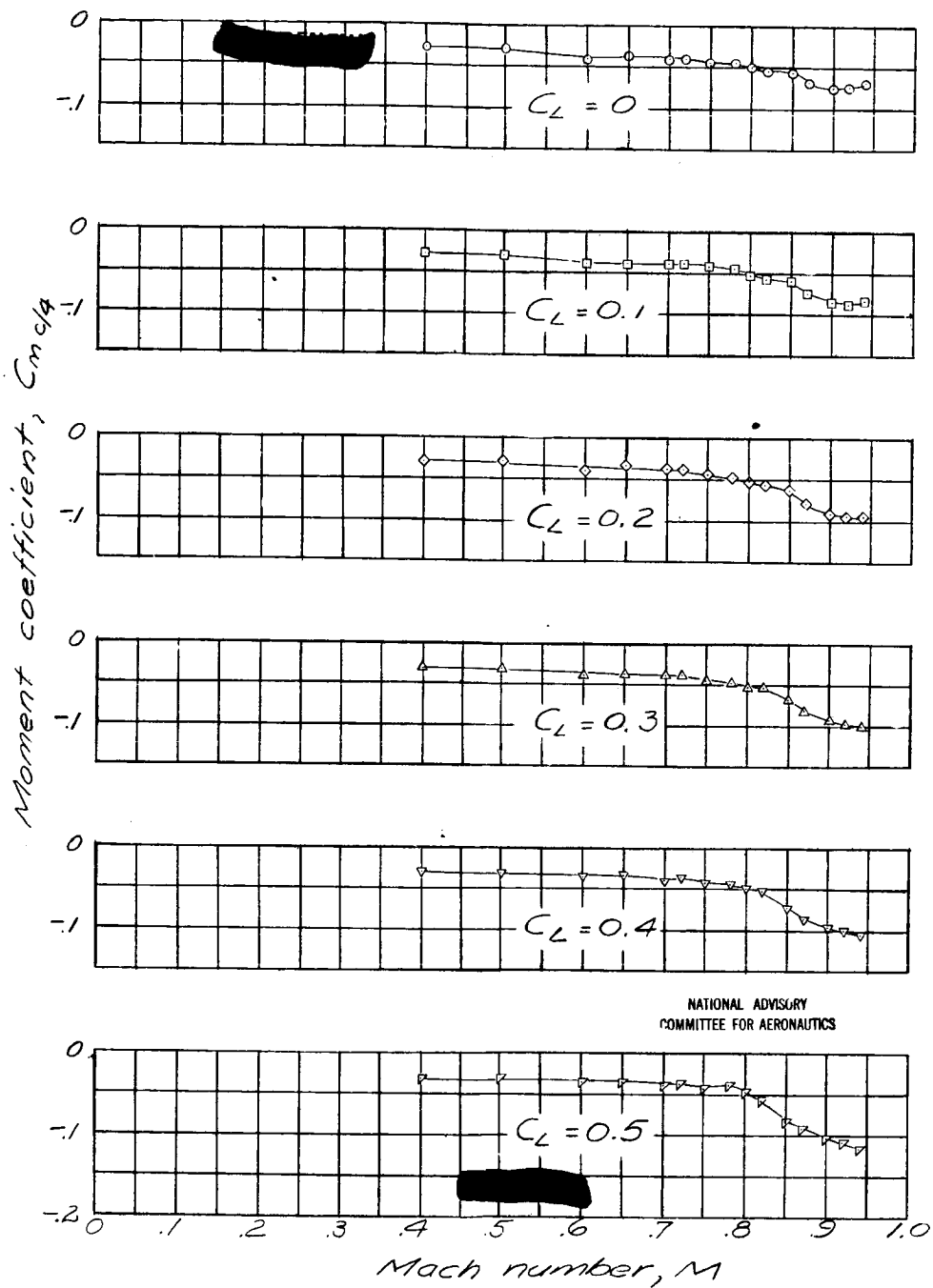
Figure 39.— Concluded.
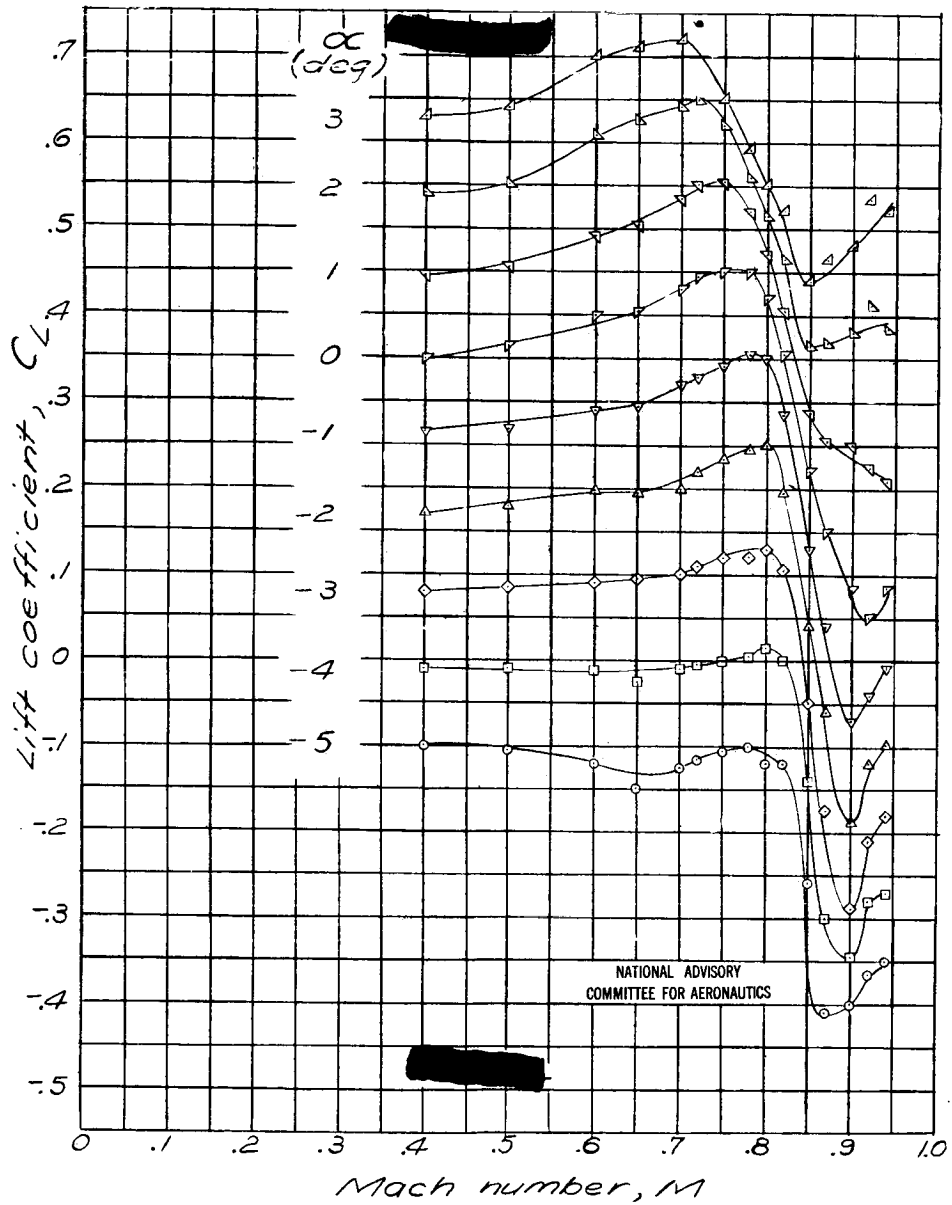
Figure 40. — Effect of compressibility on the aerodynamic characteristics of the U.S.N.P.S. 2 airfoil, 8 percent thick.
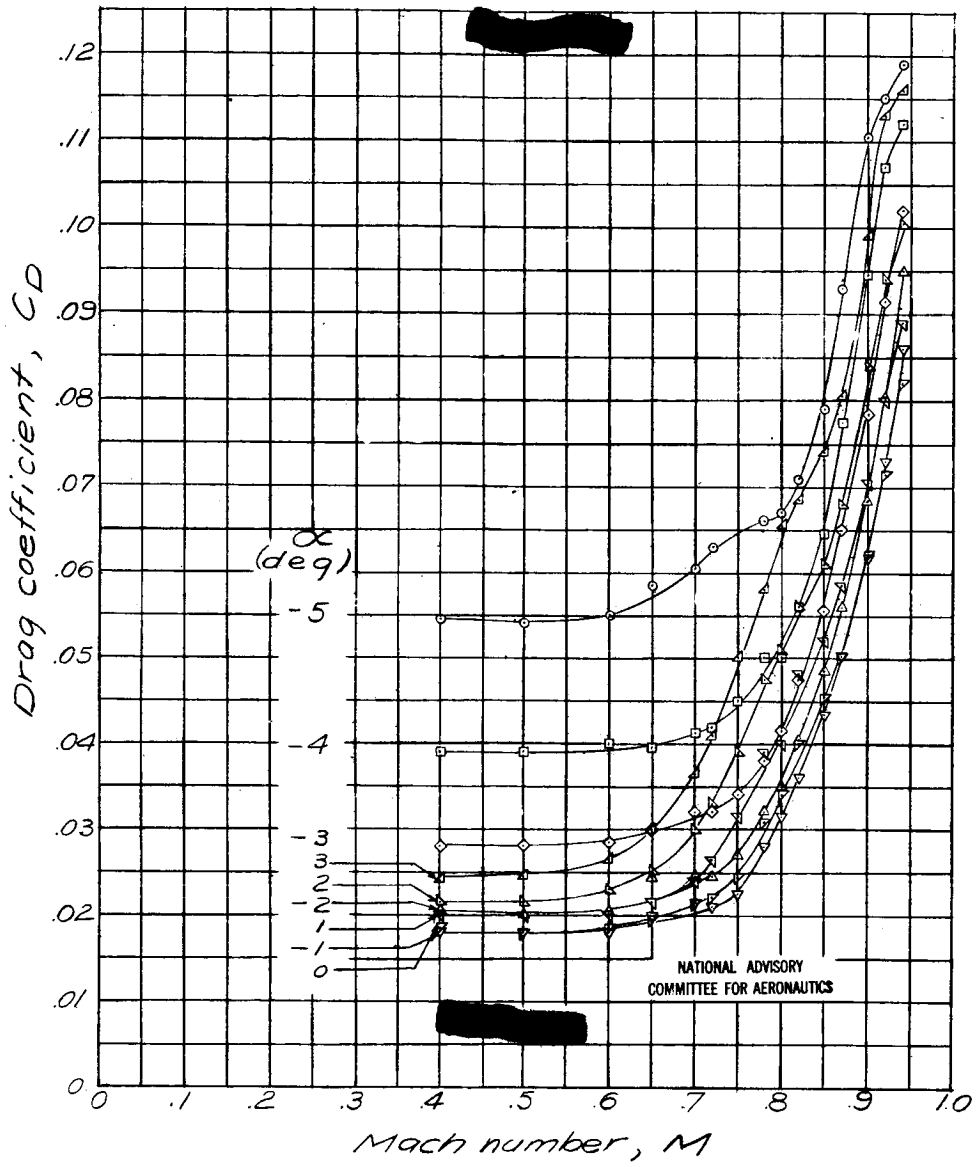
Figure 40.— Continued.
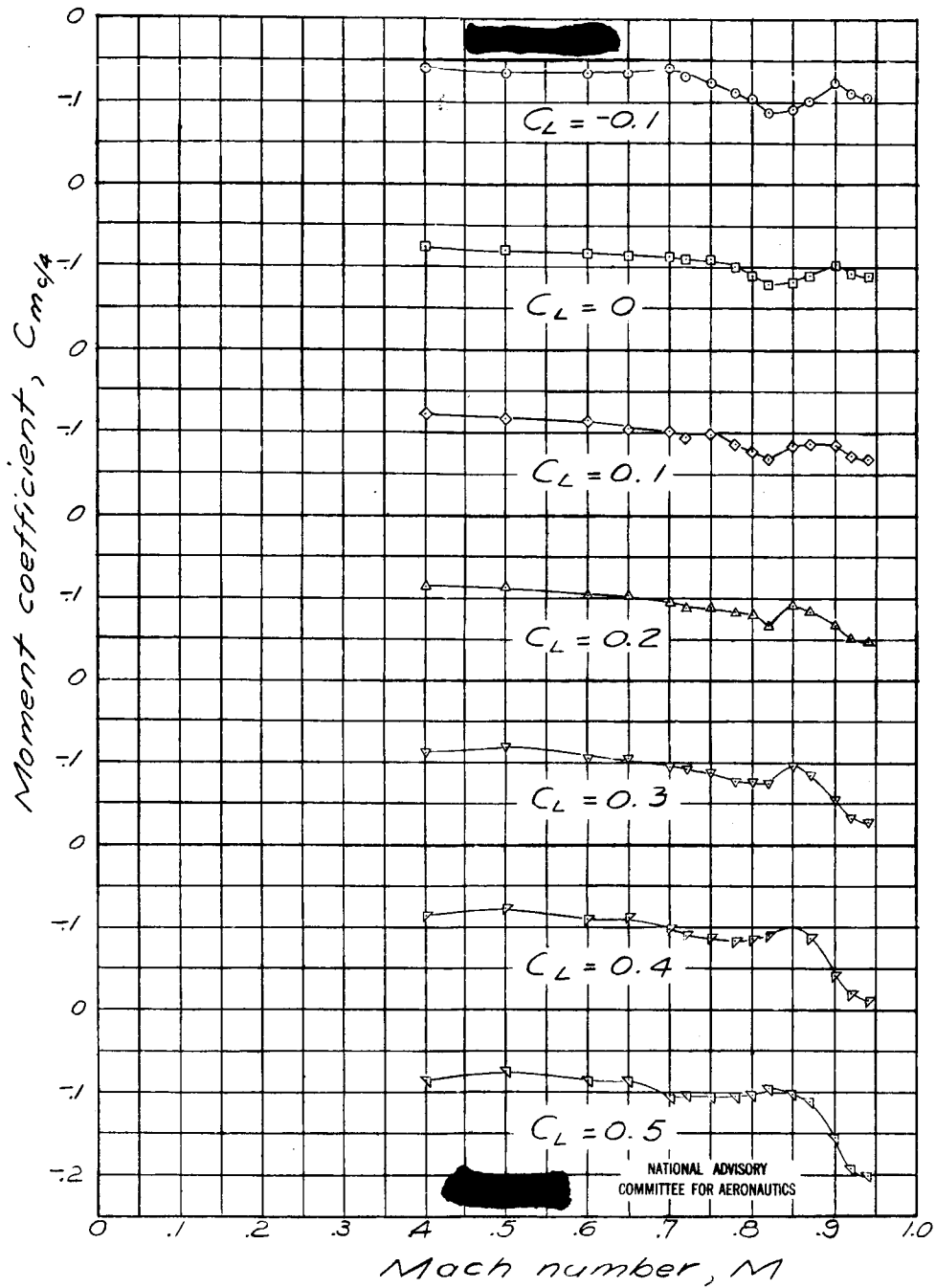
Figure 40.— Concluded.
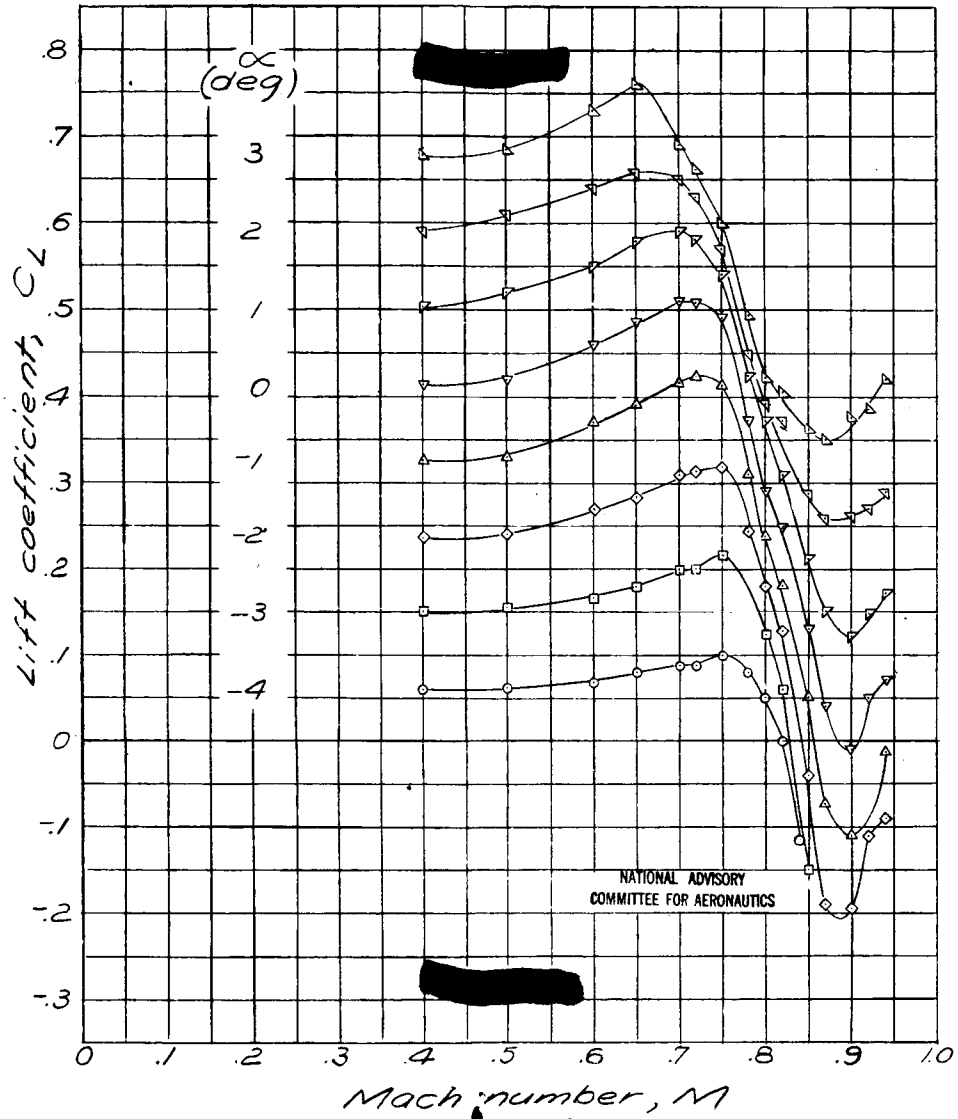
Figure 41. — Effect of compressibility on the
aerodynamic characteristics of the
U.S.N.P.S. 3 airfoil, 10 percent thick.
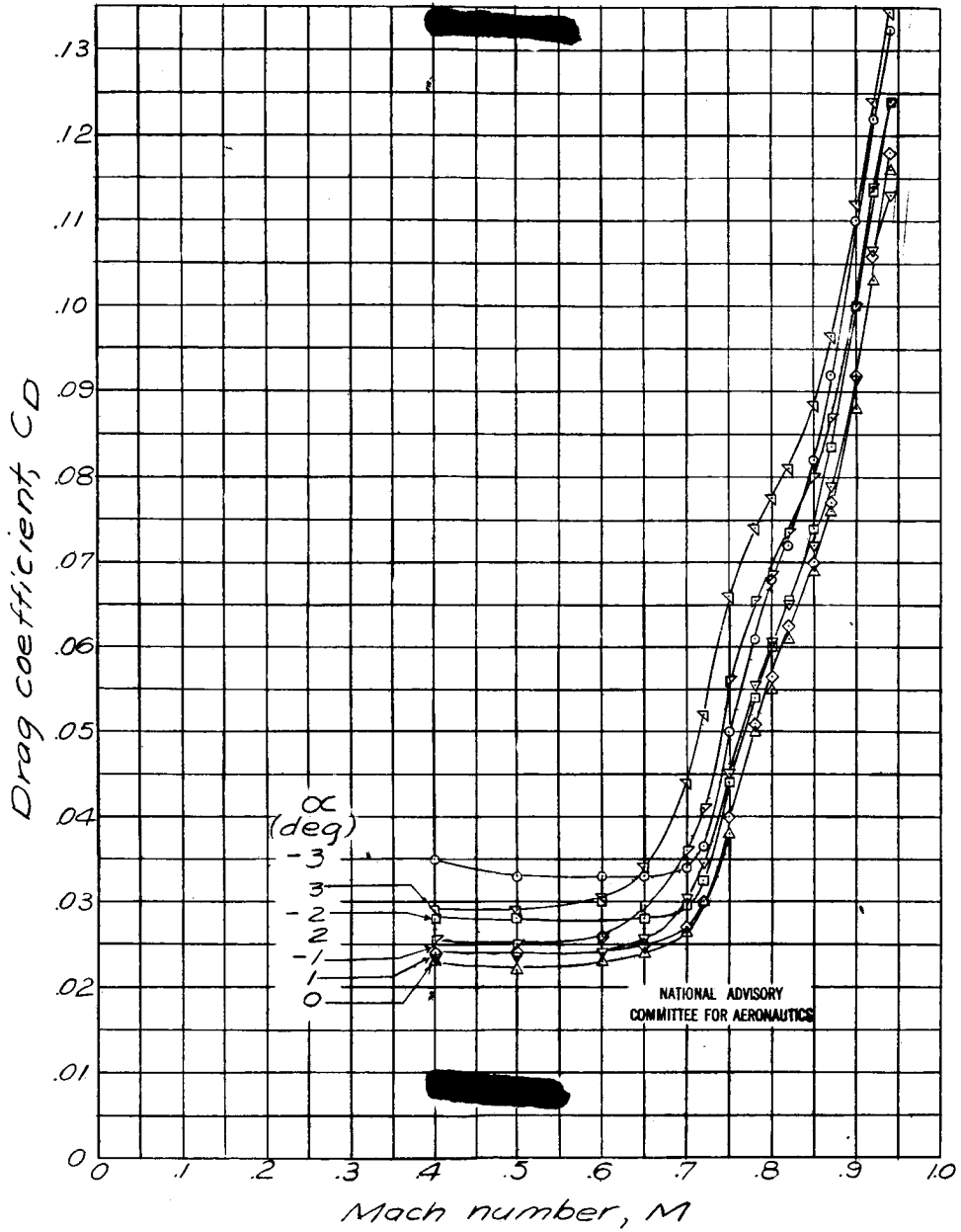
Figure 41.— Continued.
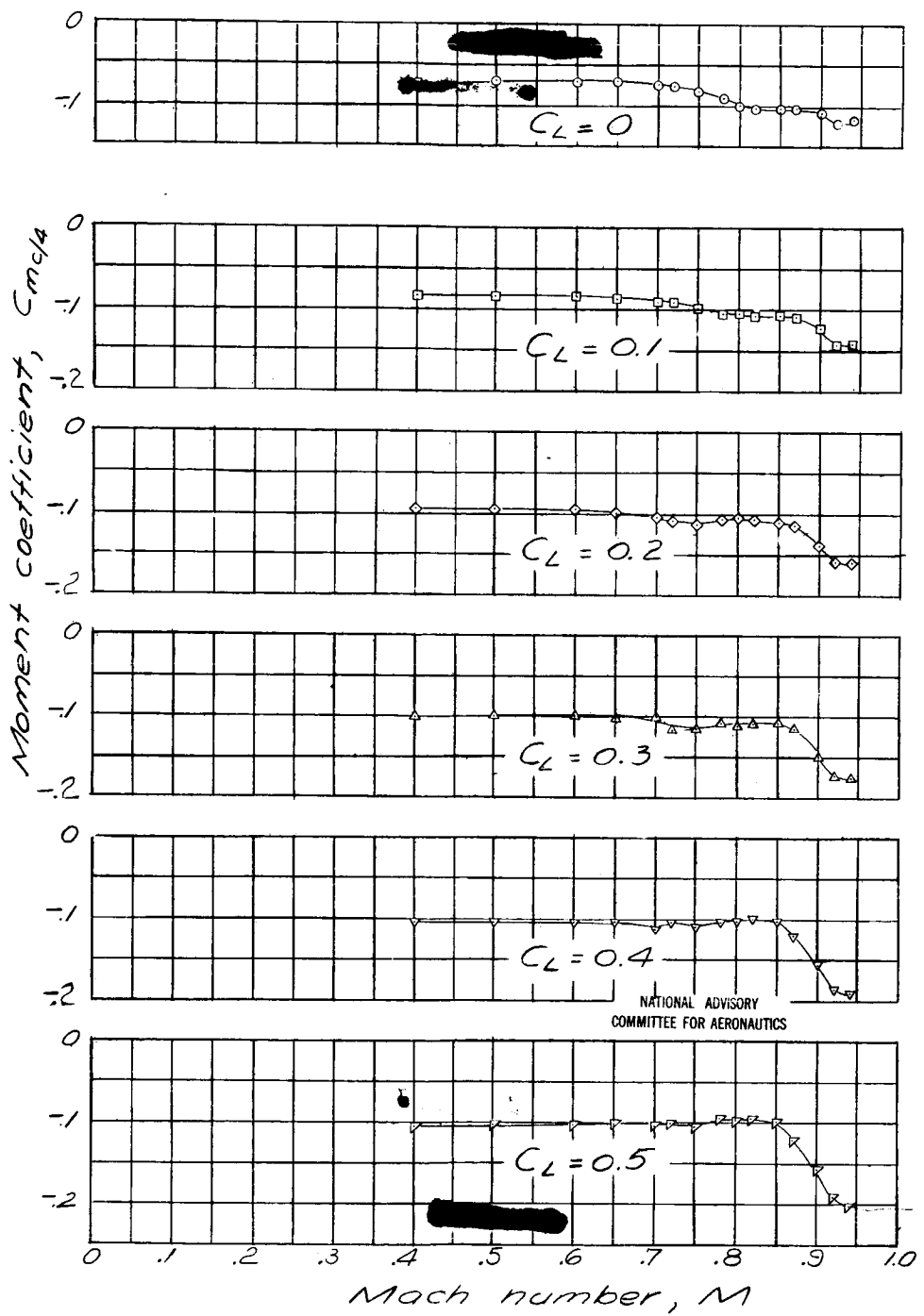
Figure 41.—Concluded.
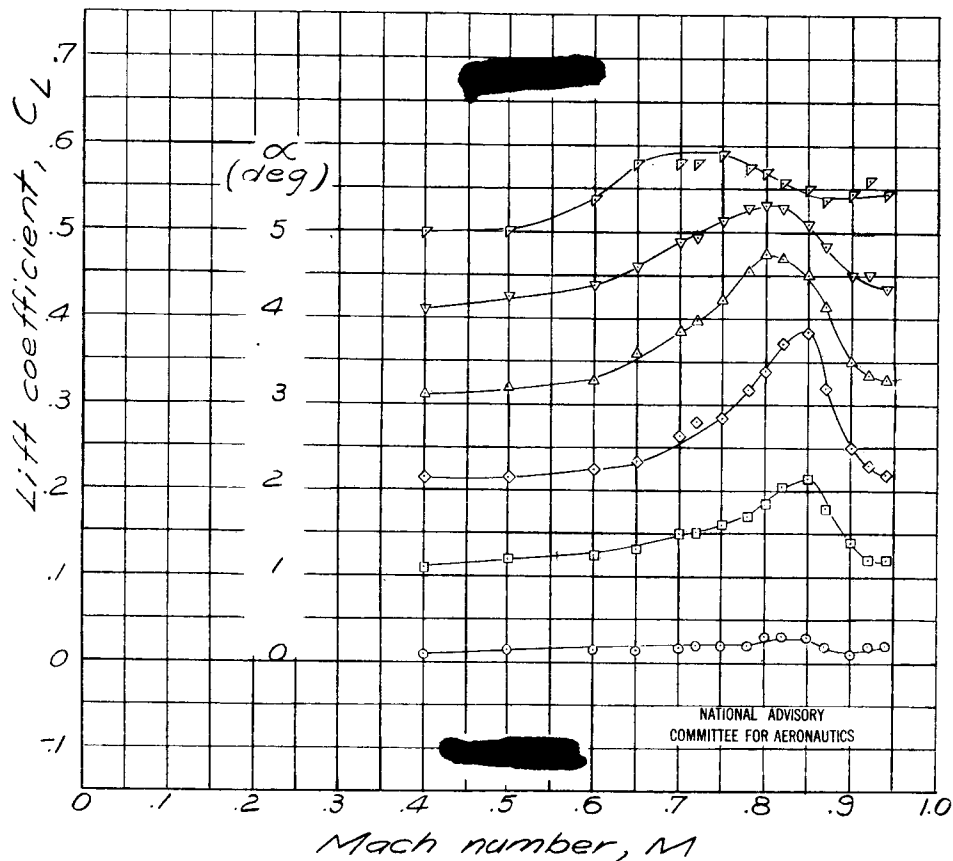
Figure 42 .— Effect of compressibility on the aerodynamic characteristics of the M1 airfoil.
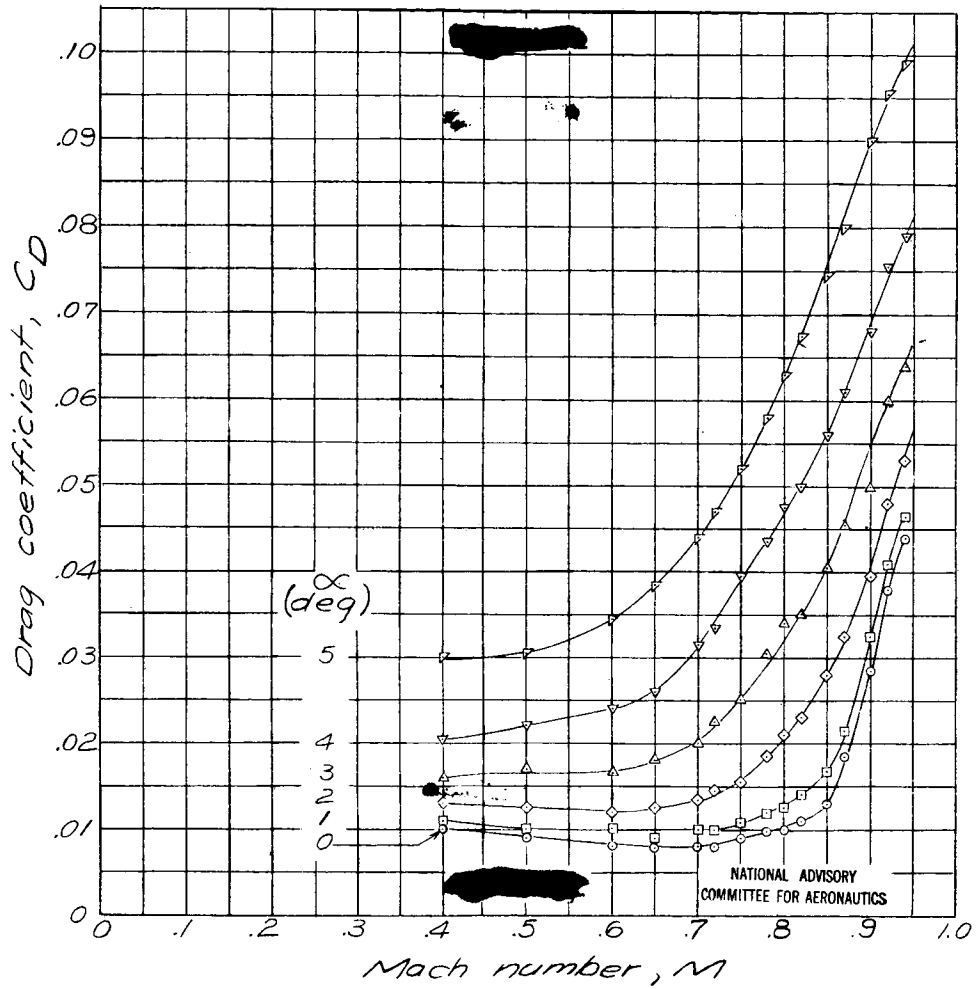
Figure 42.— Continued.
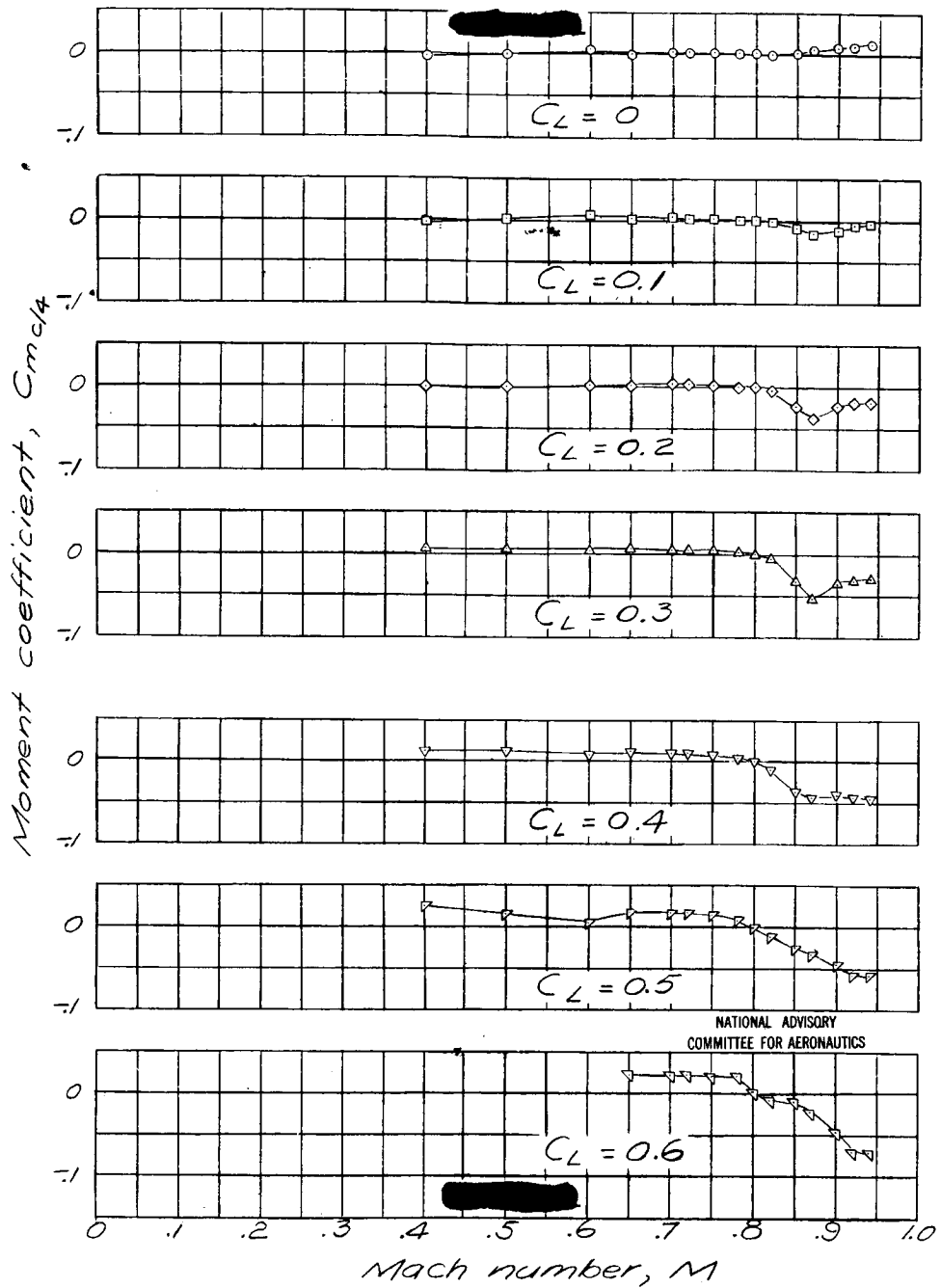
Figure 42, — Concluded.
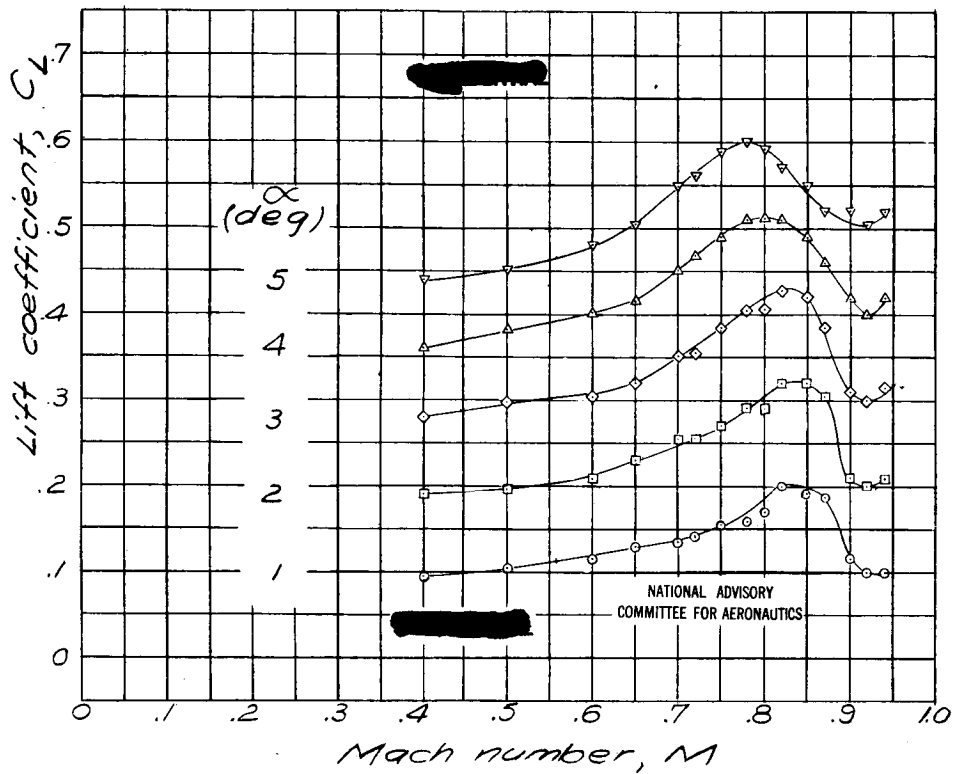
Figure 43.— Effect of compressibility on the aerodynamic characteristics of the 0006 airfoil.
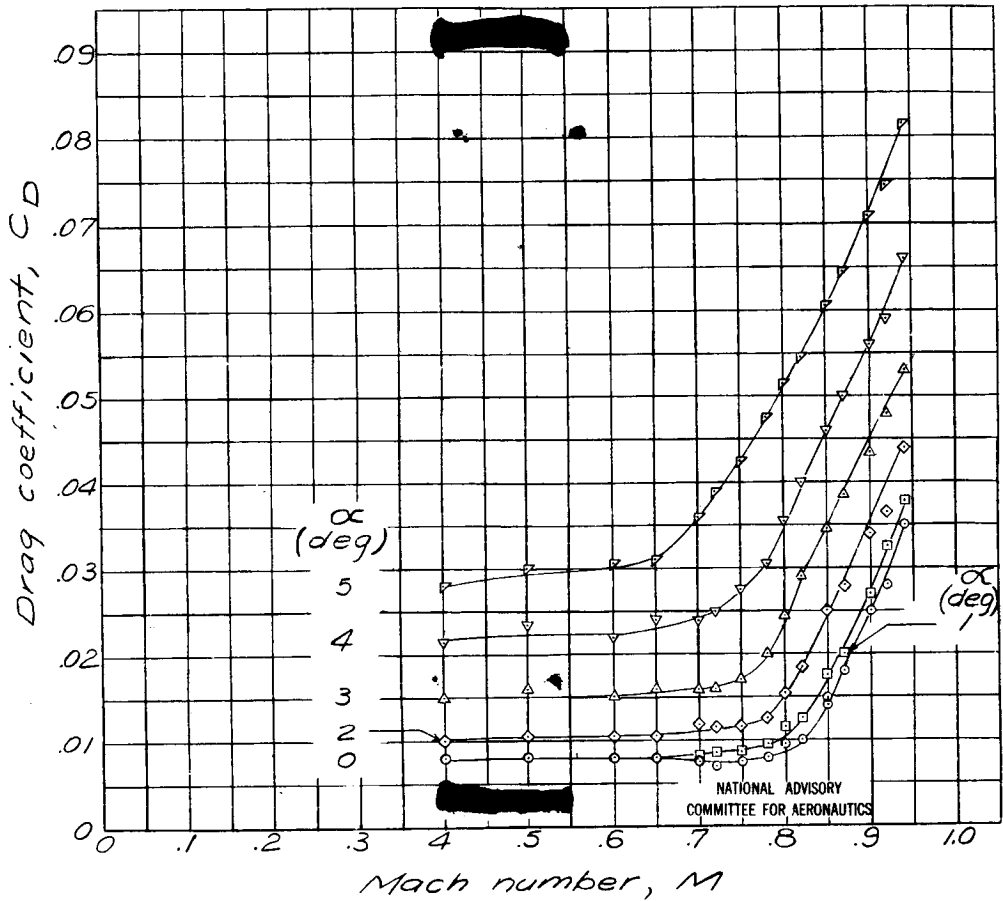
Figure 43 .— Continued.
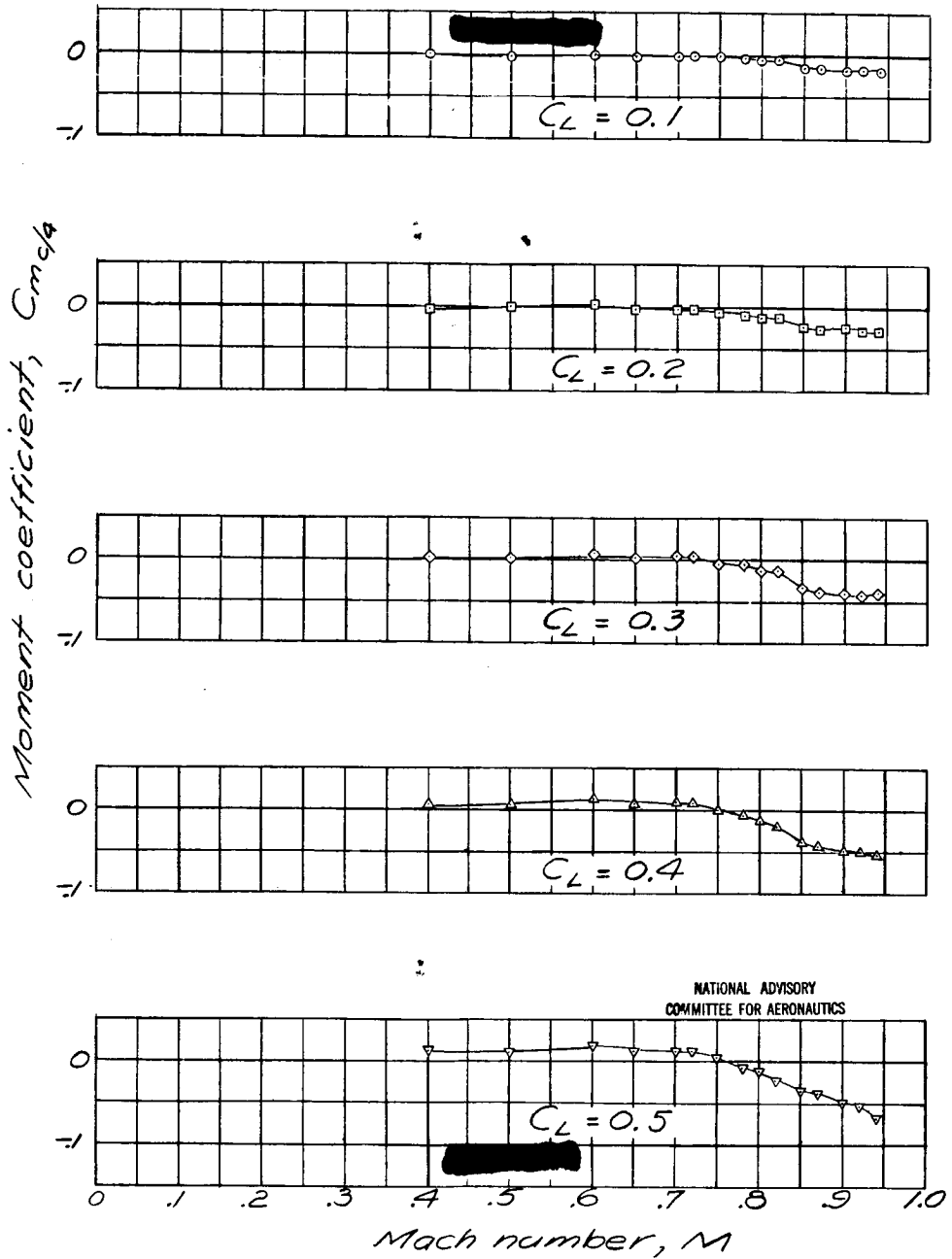
Figure 43. — Concluded.
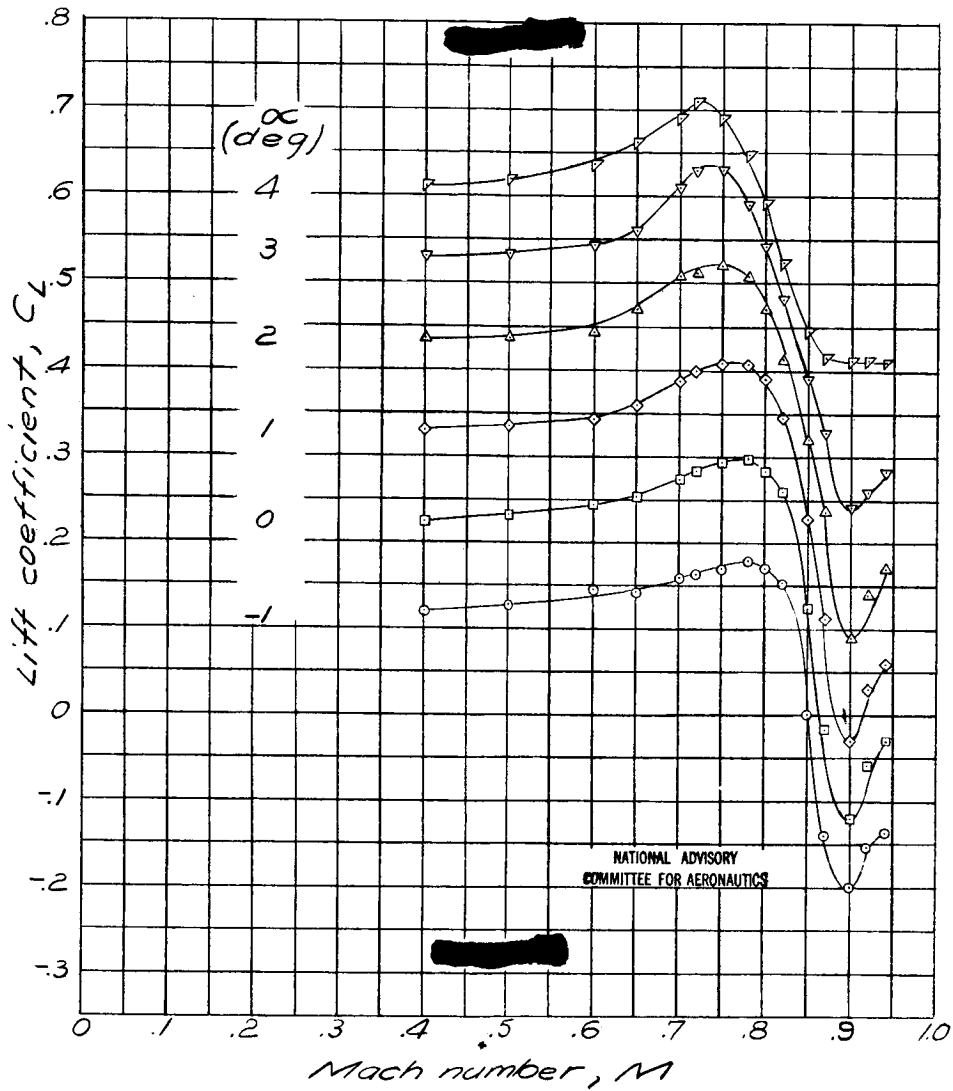
Figure 44.— Effect of compressibility on the aerodynamic characteristics of the NACA 2509 airfoil.
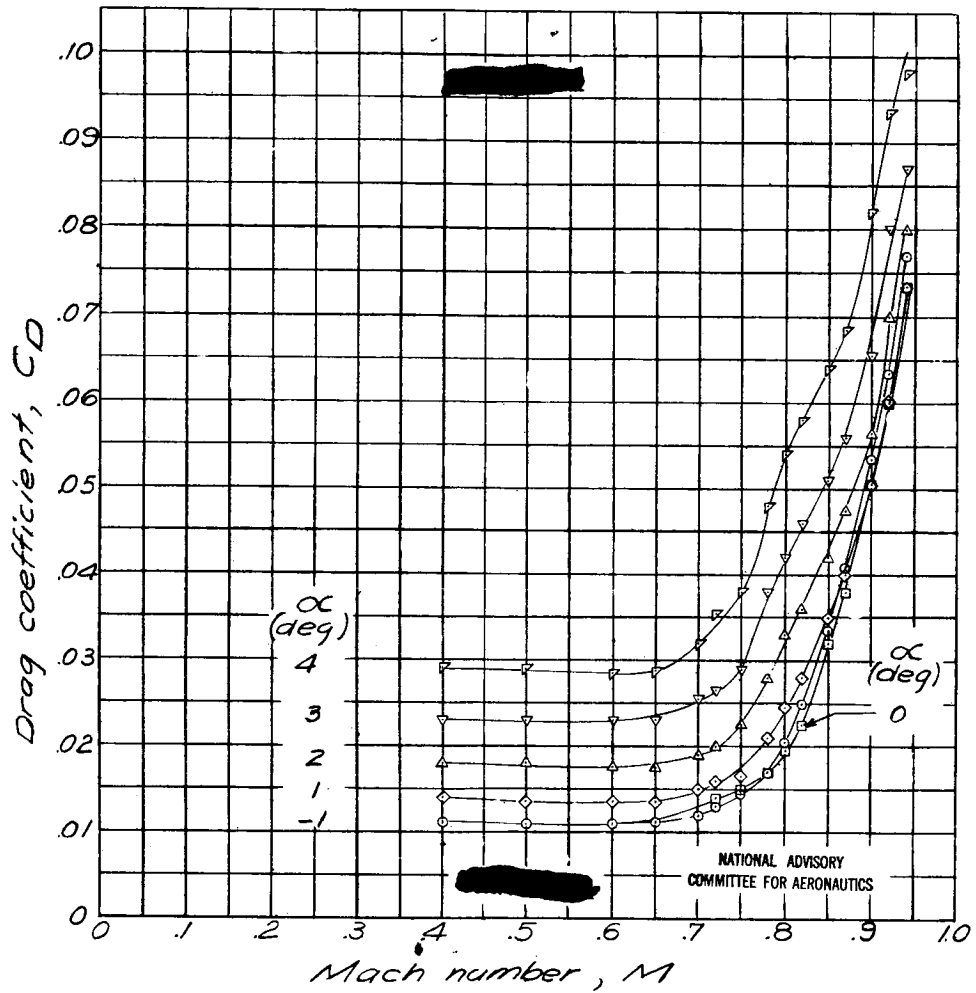
Figure 44. - Continued.
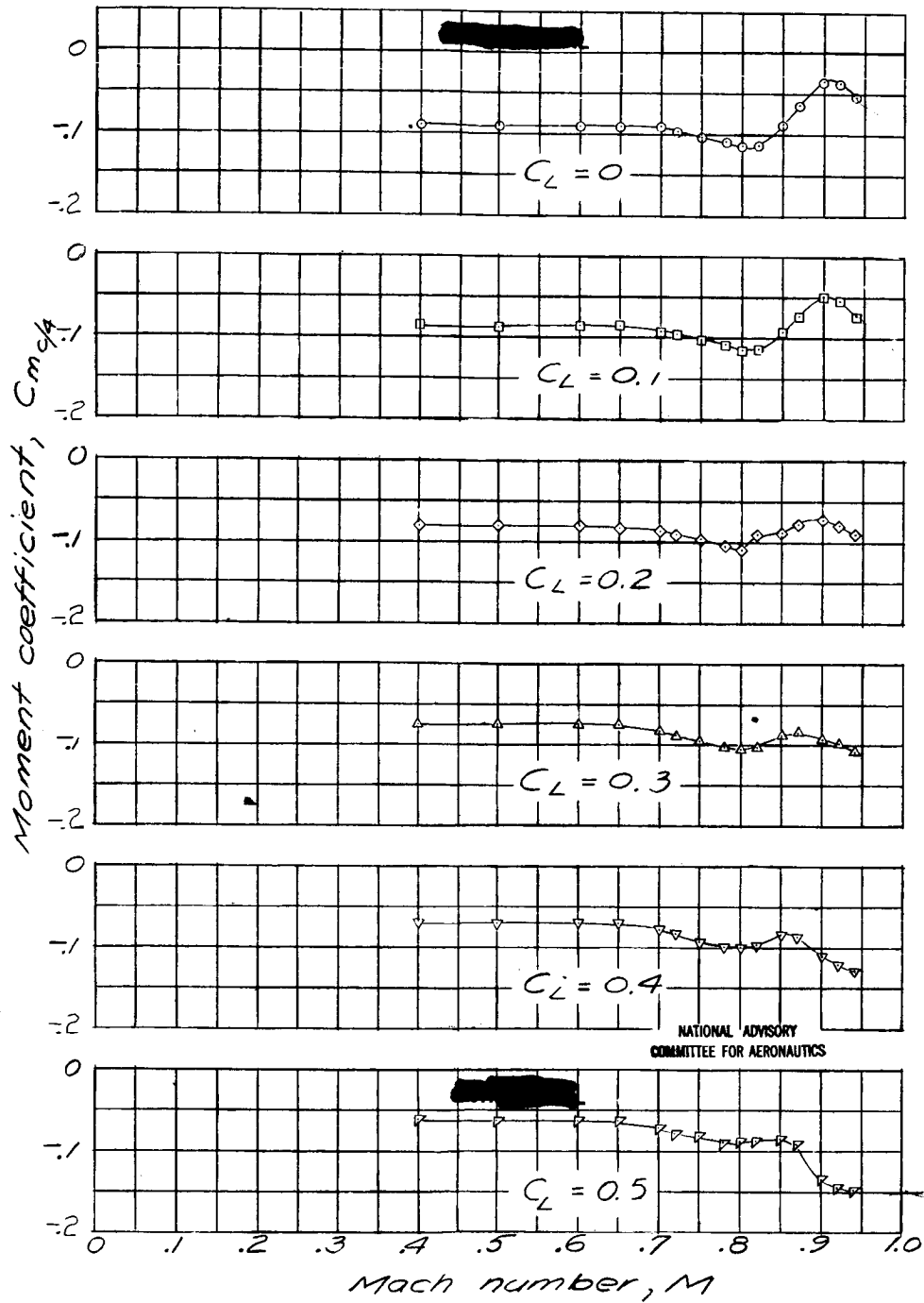
Figure 44 . — Concluded.
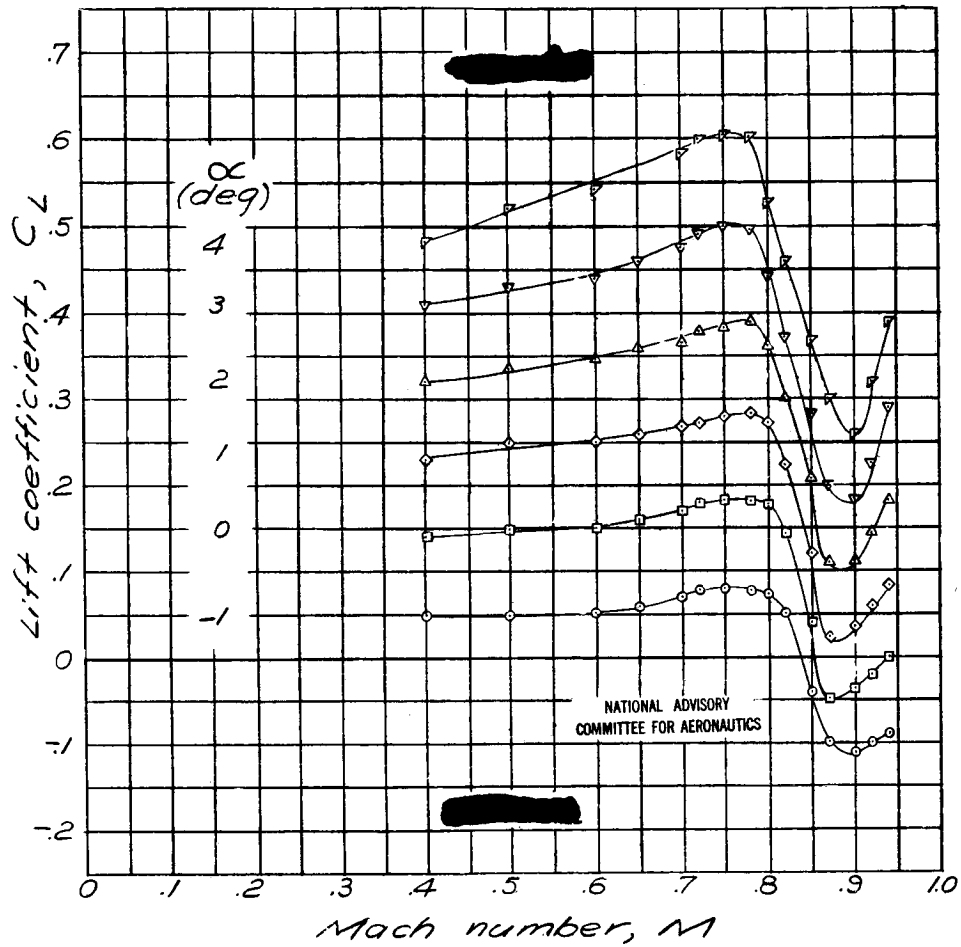
Figure 45 .— Effect of compressibility on the aerodynamic characteristics of the Davis 9-percent-thick airfoil.
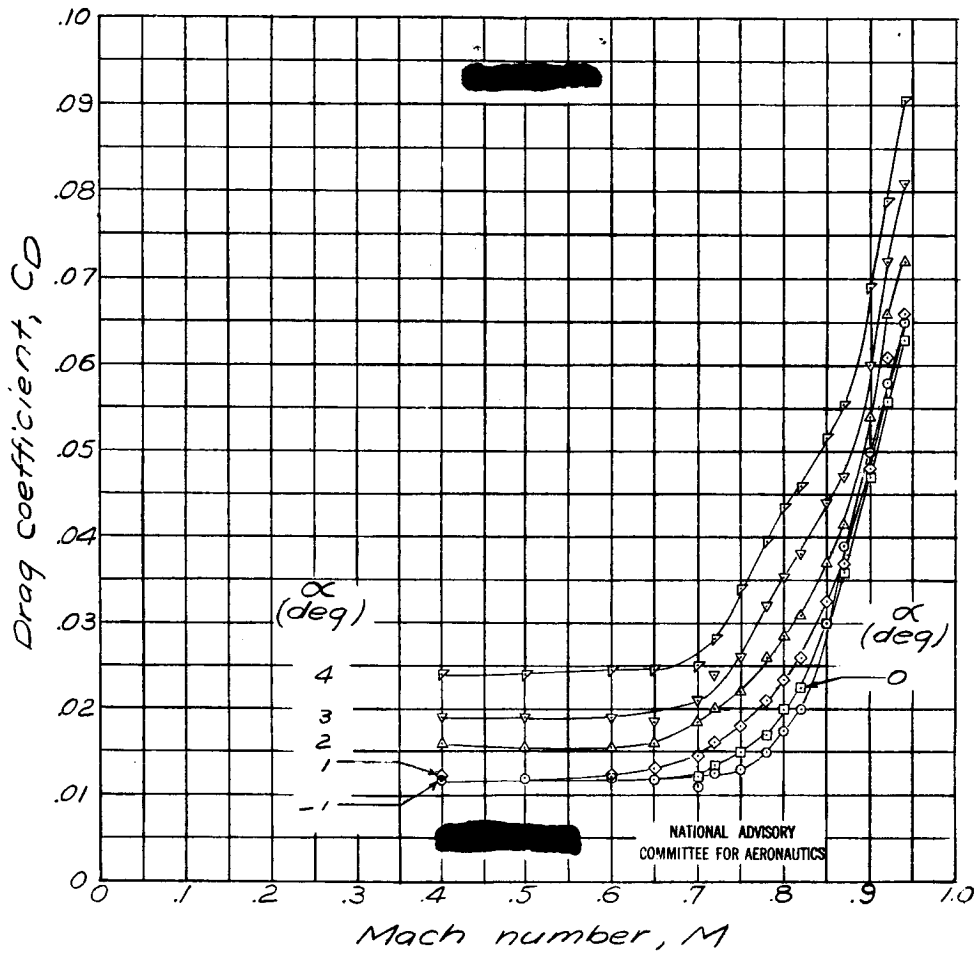
Figure 45. — Continued.
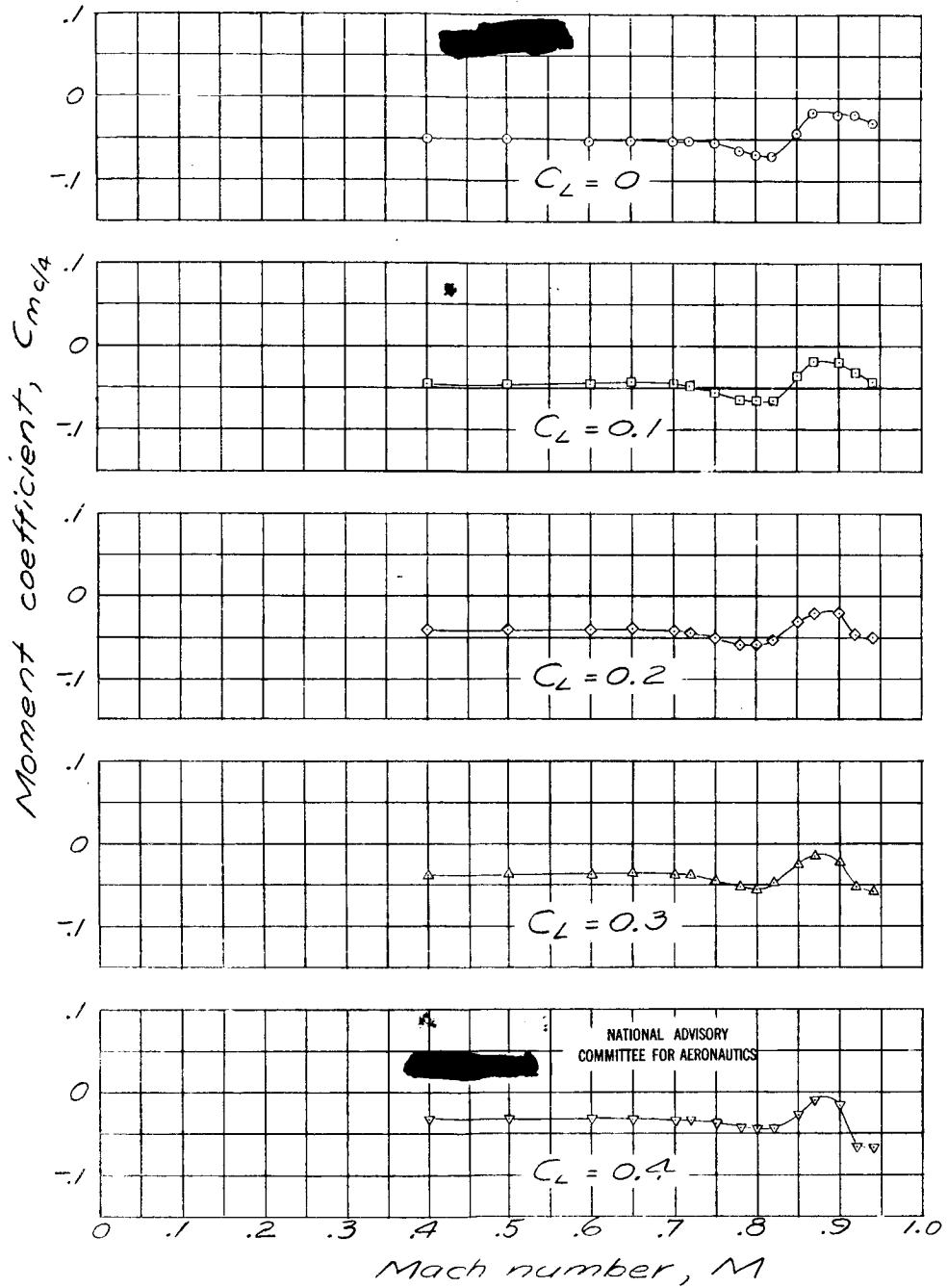
Figure 45.— Concluded.
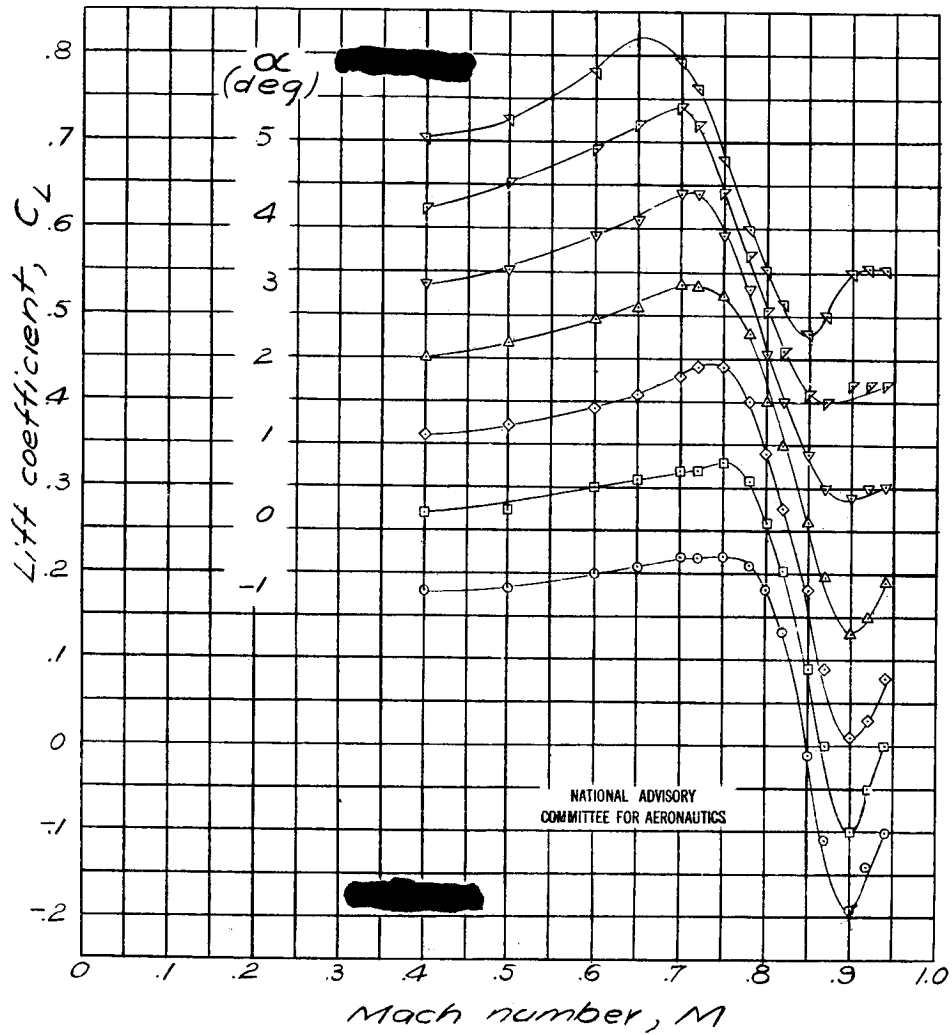
Figure 46. — Effect of compressibility on the aerodynamic characteristics of the ETH 3609 airfoil.
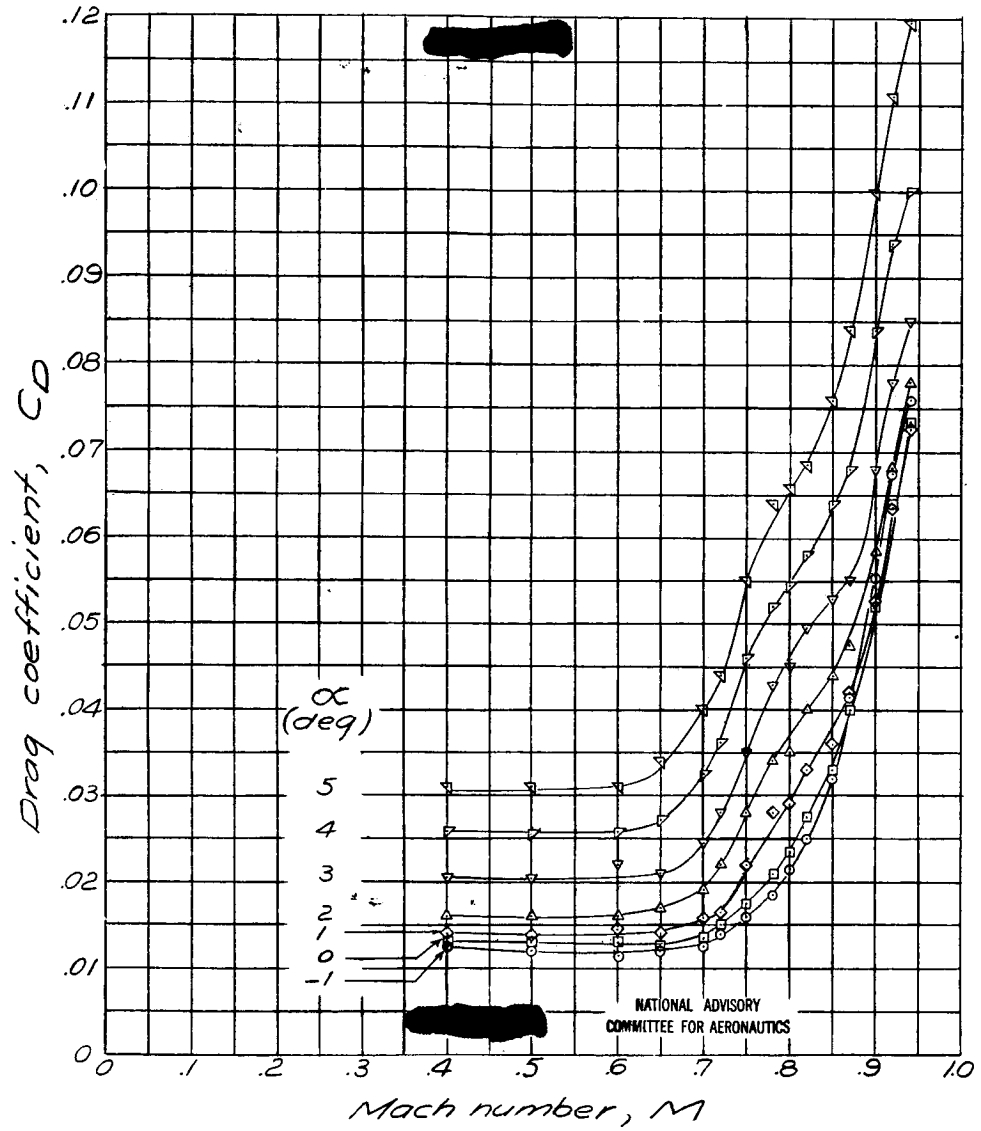
Figure 46. – Continued.
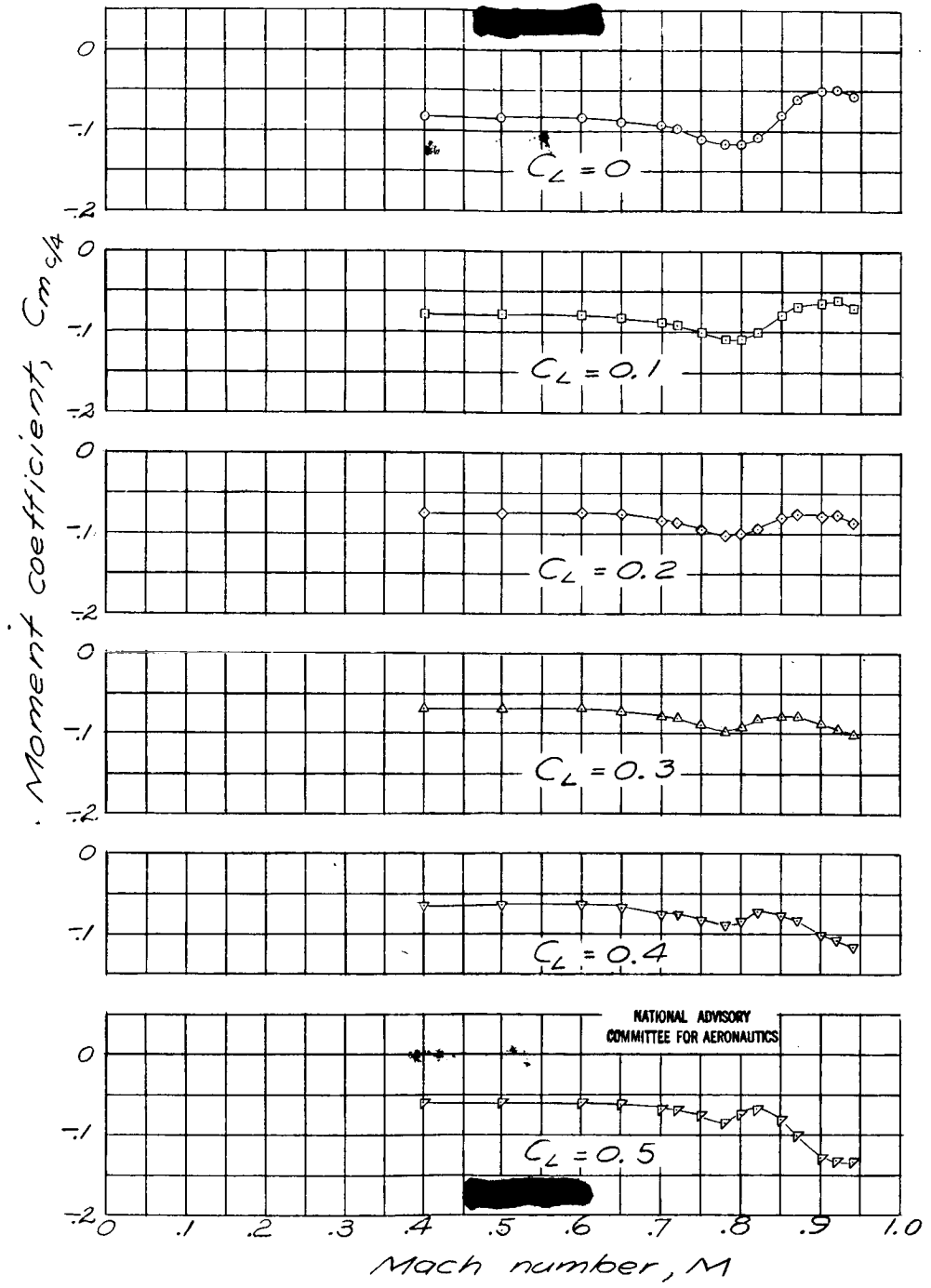
Figure 46.- Concluded.
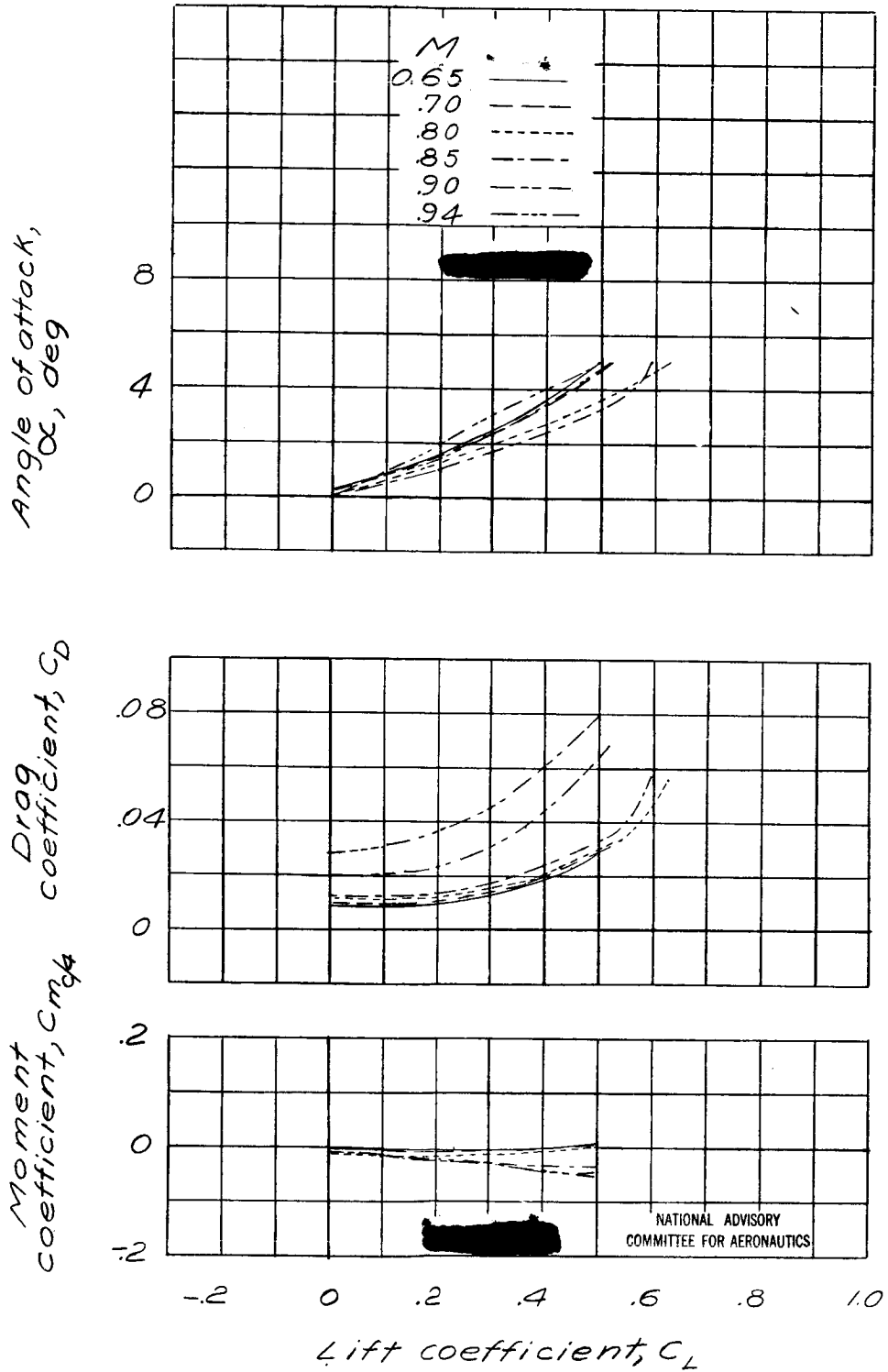
Figure 47.— Aerodynamic characteristics
of the NACA 0006-64 airfoil.
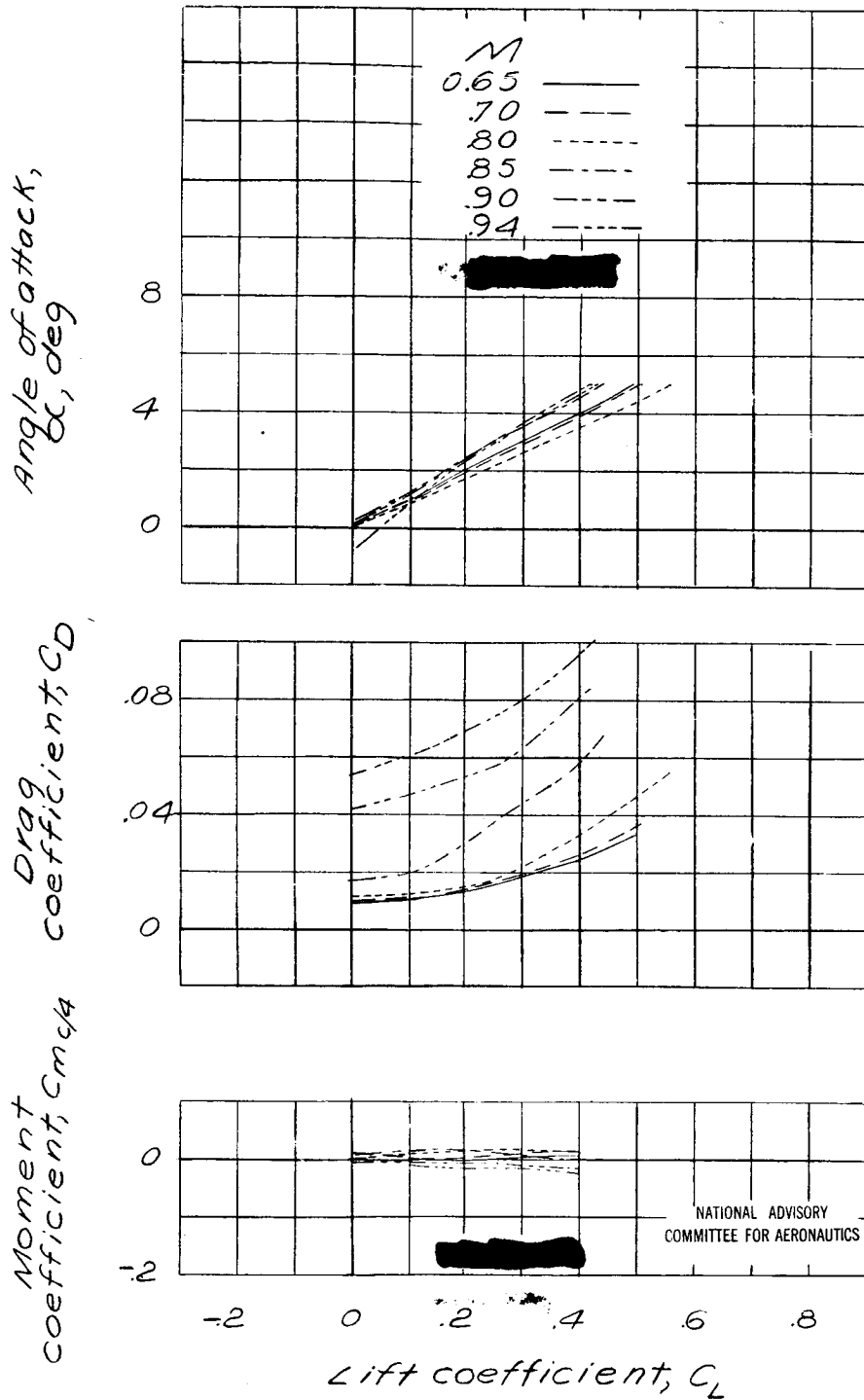
Figure 48.- Aerodynamic characteristics of the NACA 0009-64 airfoil.
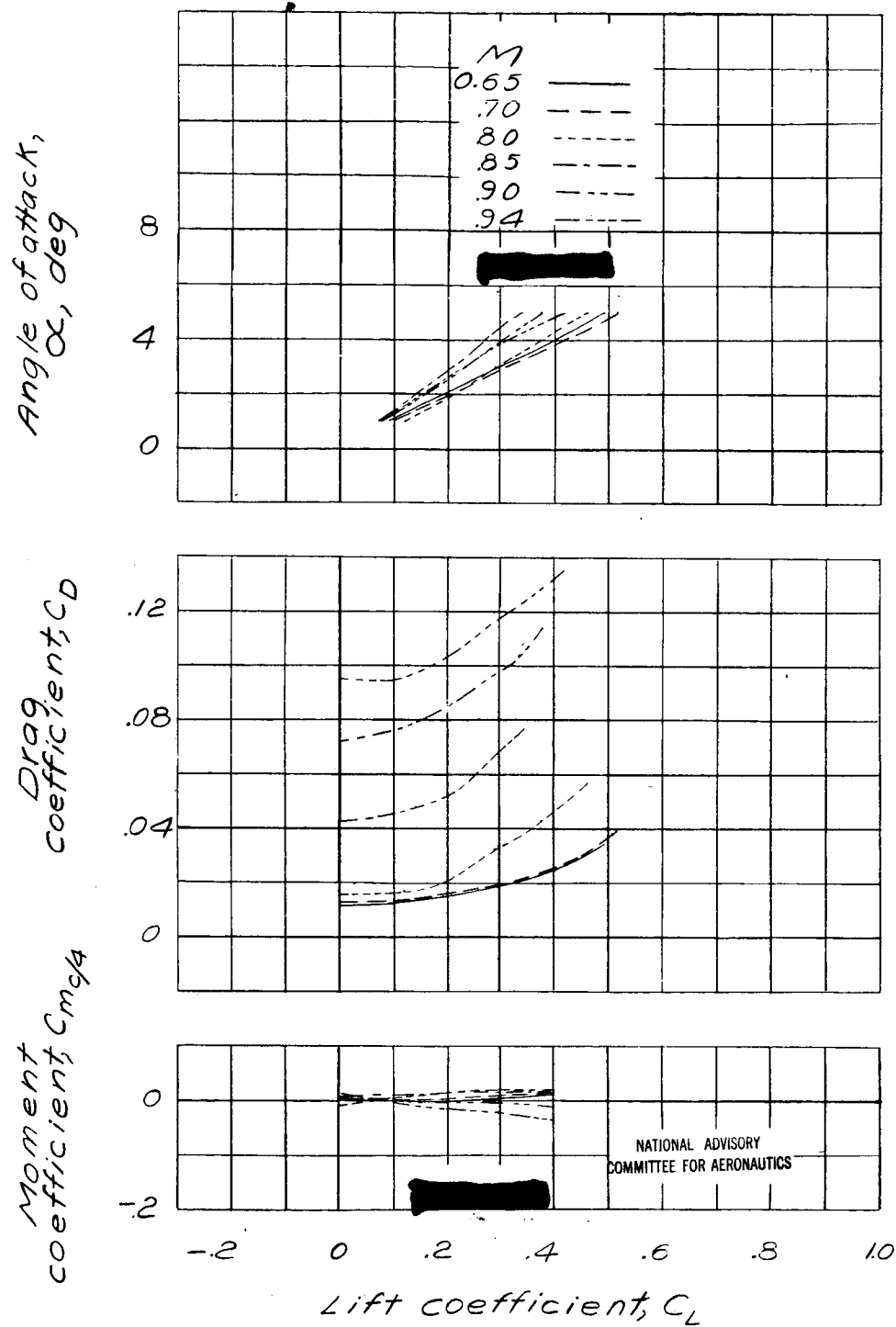
Figure 49.— Aerodynamic characteristics of the NACA 0012-64 airfoil.
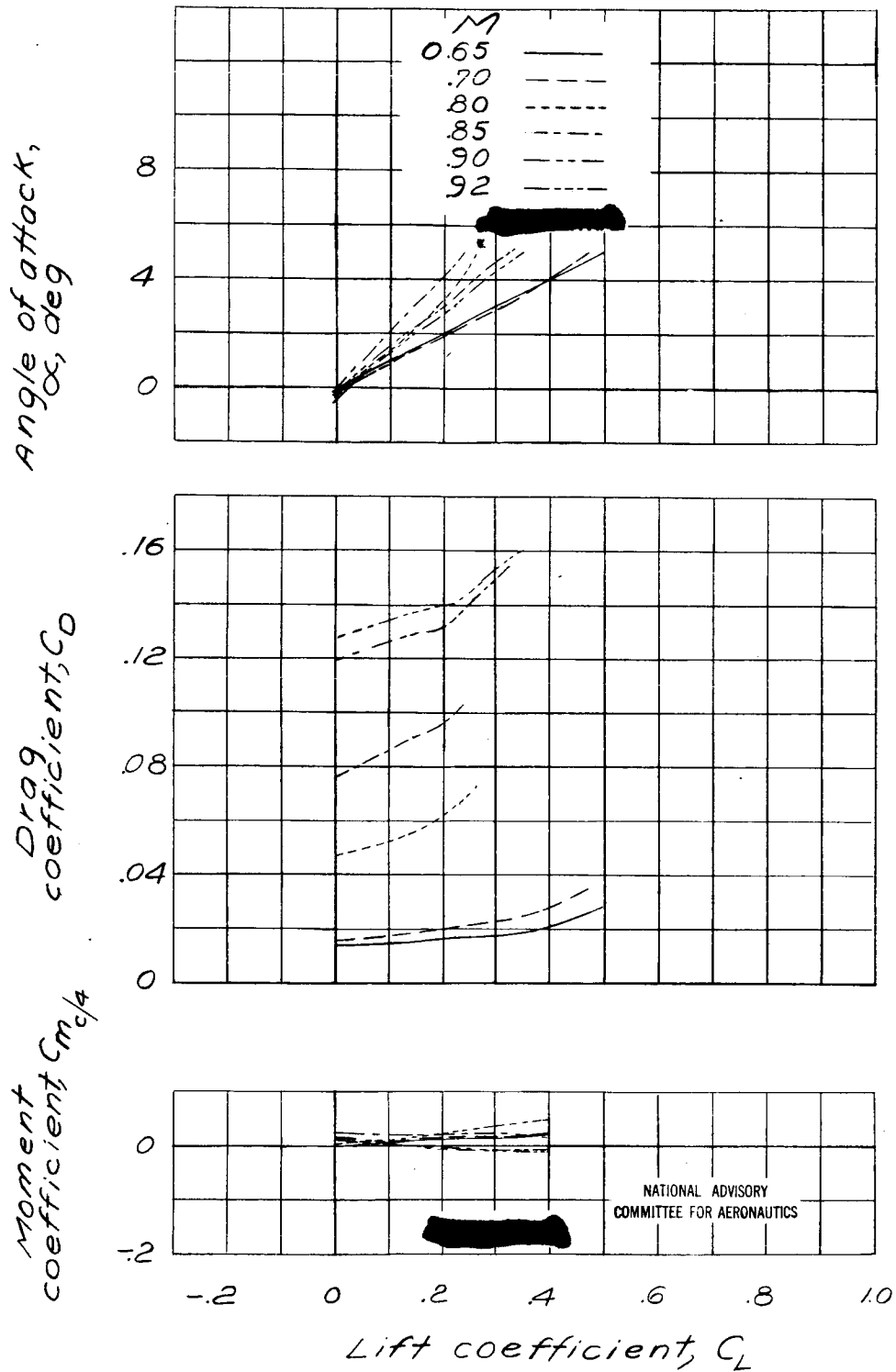
Figure 50 .- Aerodynamic characteristics of the NACA 0015-64 airfoil.
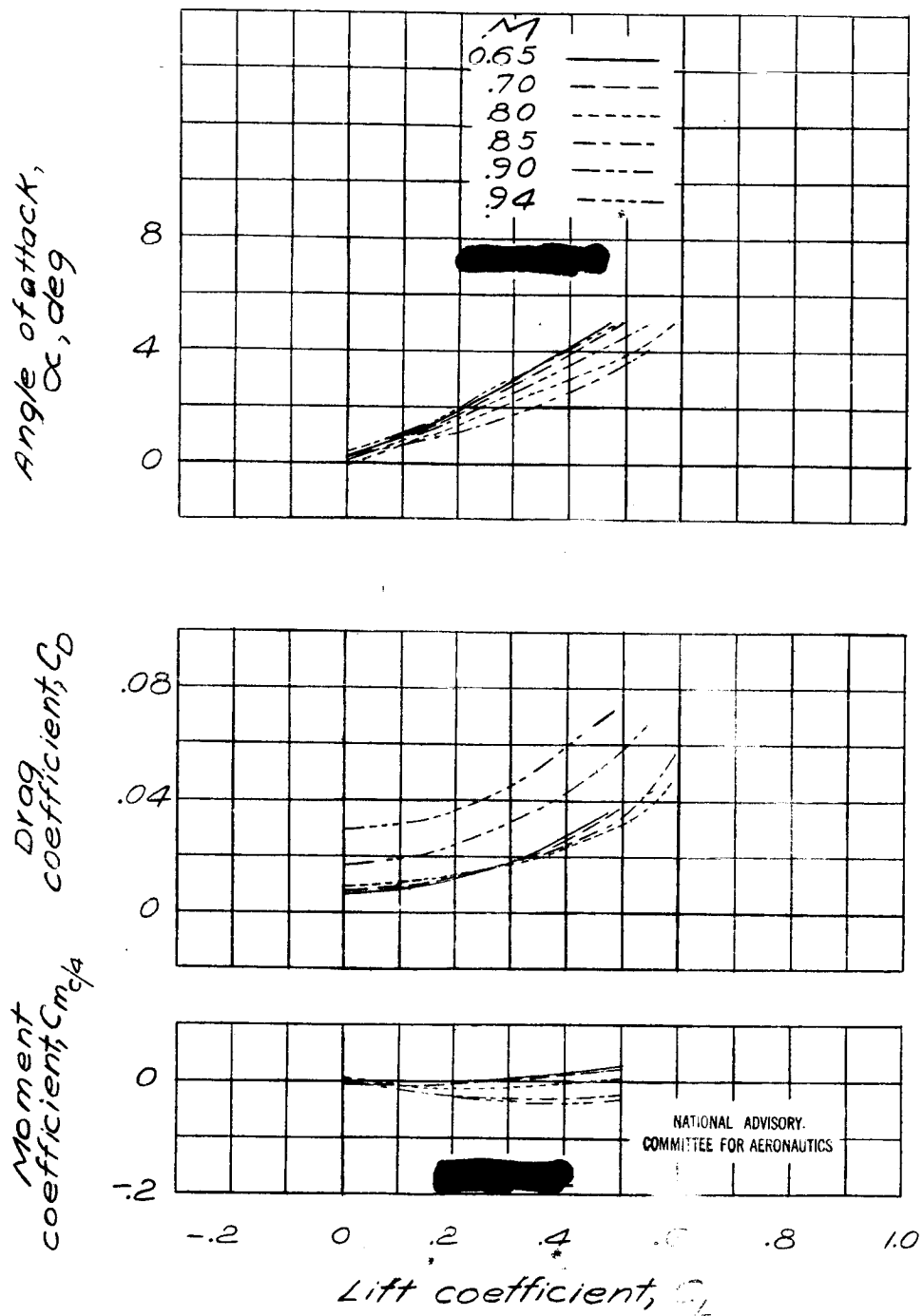
Figure 51.— Aerodynamic characteristics
of the NACA 0006-34 airfoil.
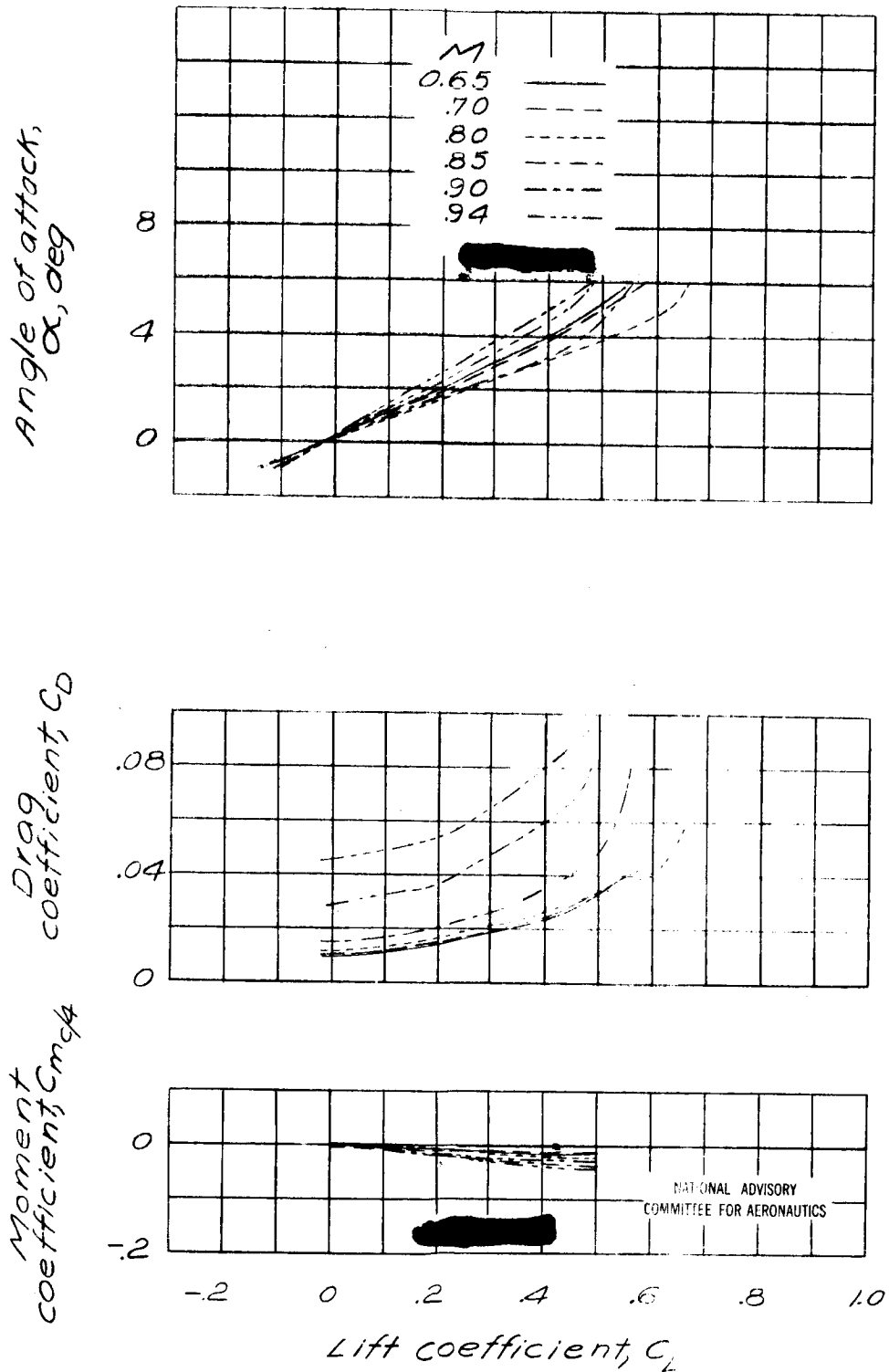
Figure 52.— Aerodynamic characteristics of the NACA 0008-34 airfoil.
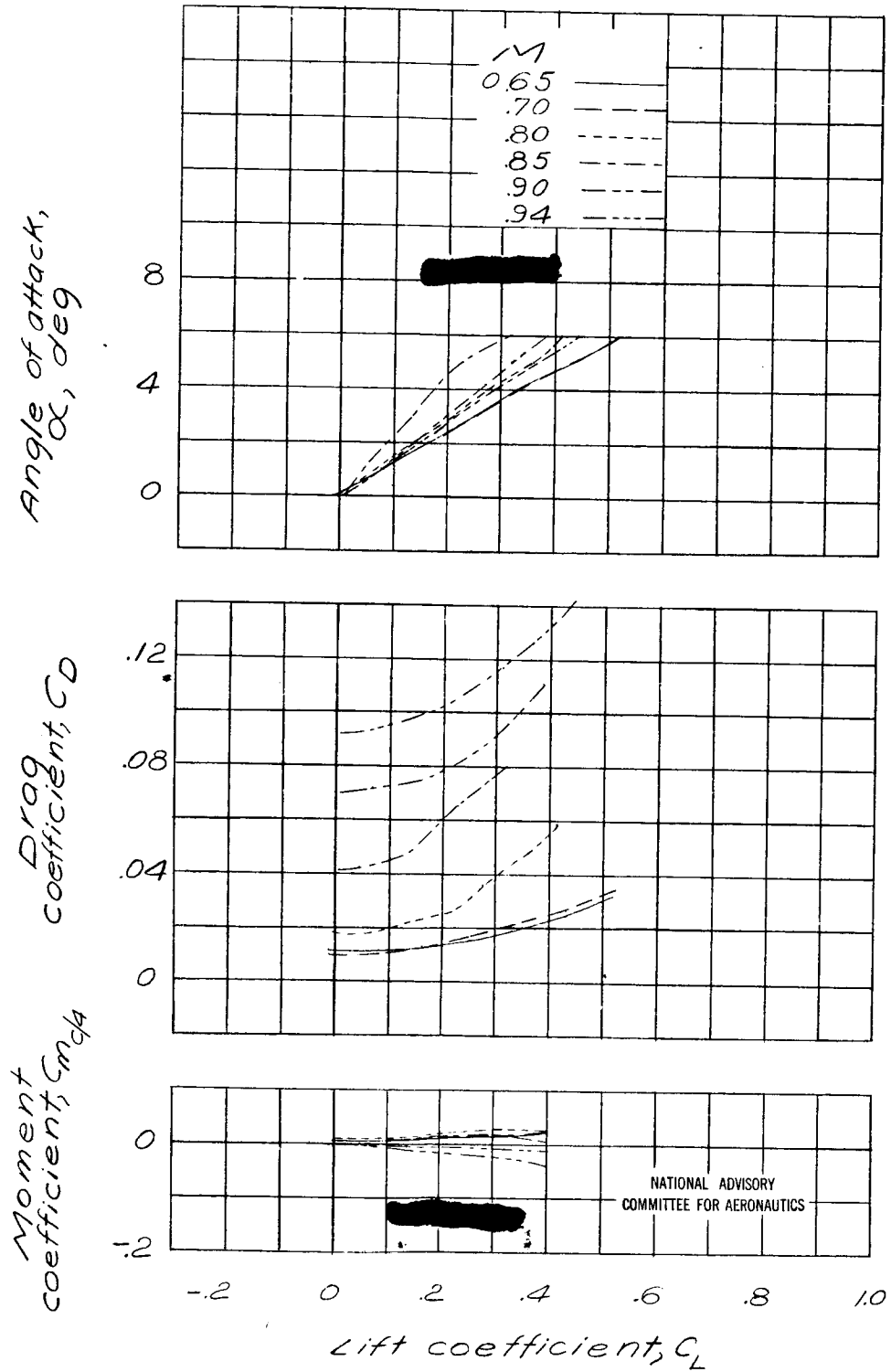
Figure 53.— Aerodynamic characteristics of the NACA 0012-34 airfoil.
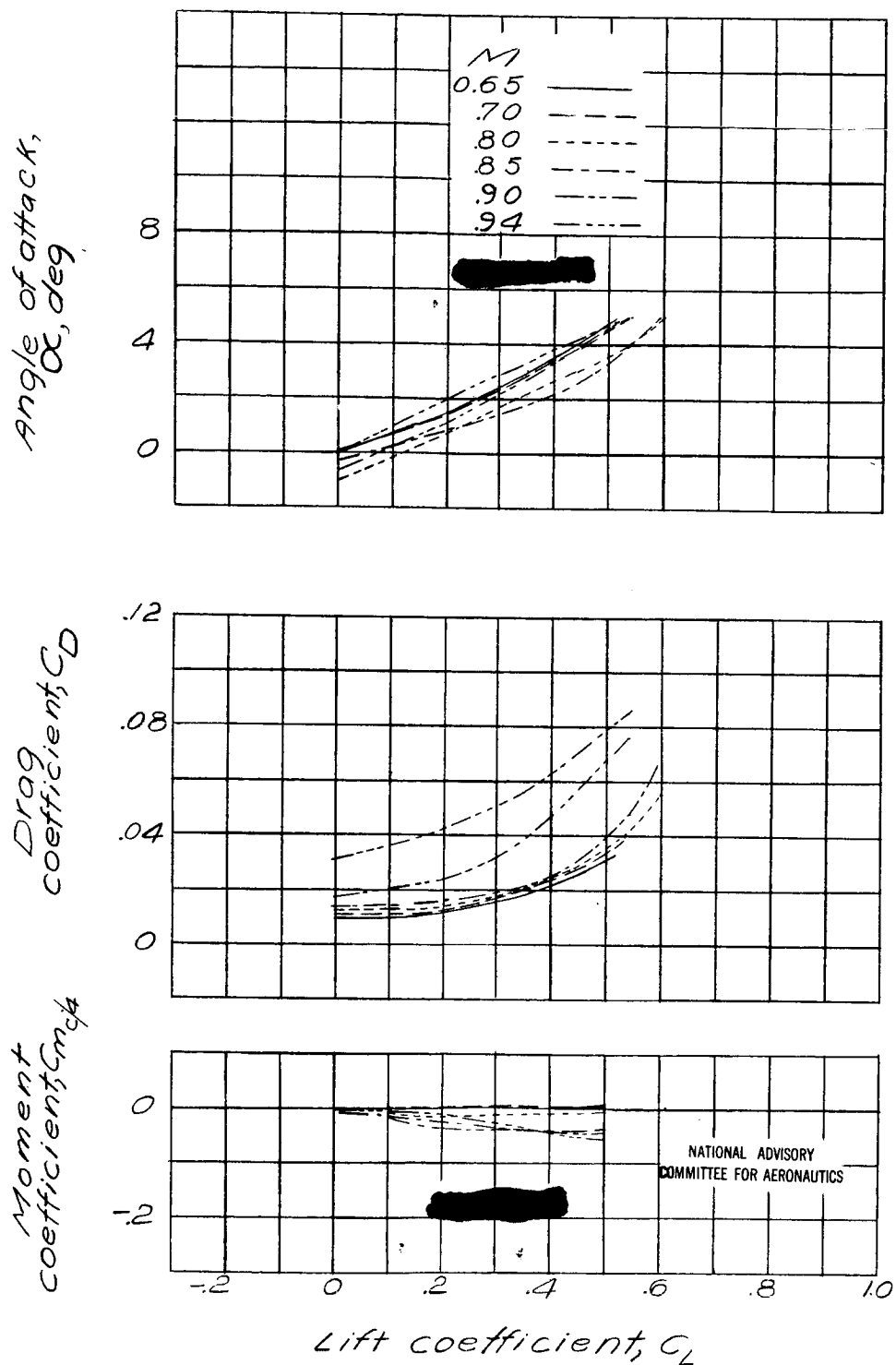
Figure 54 .— Aerodynamic characteristics
of the NACA 0006-63 airfoil.
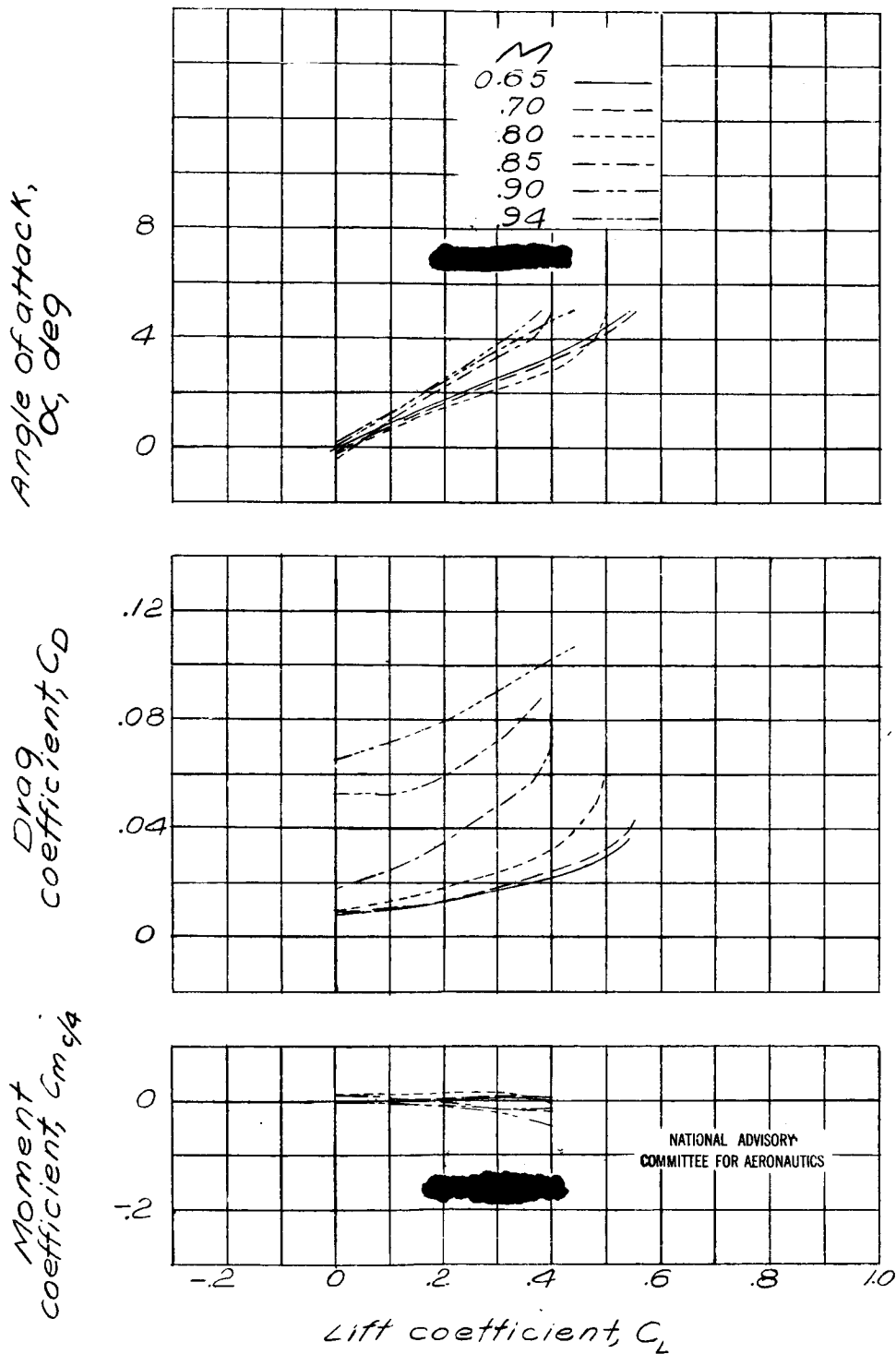
Figure 55 .— Aerodynamic characteristics
of the NACA 0009-63 airfoil.
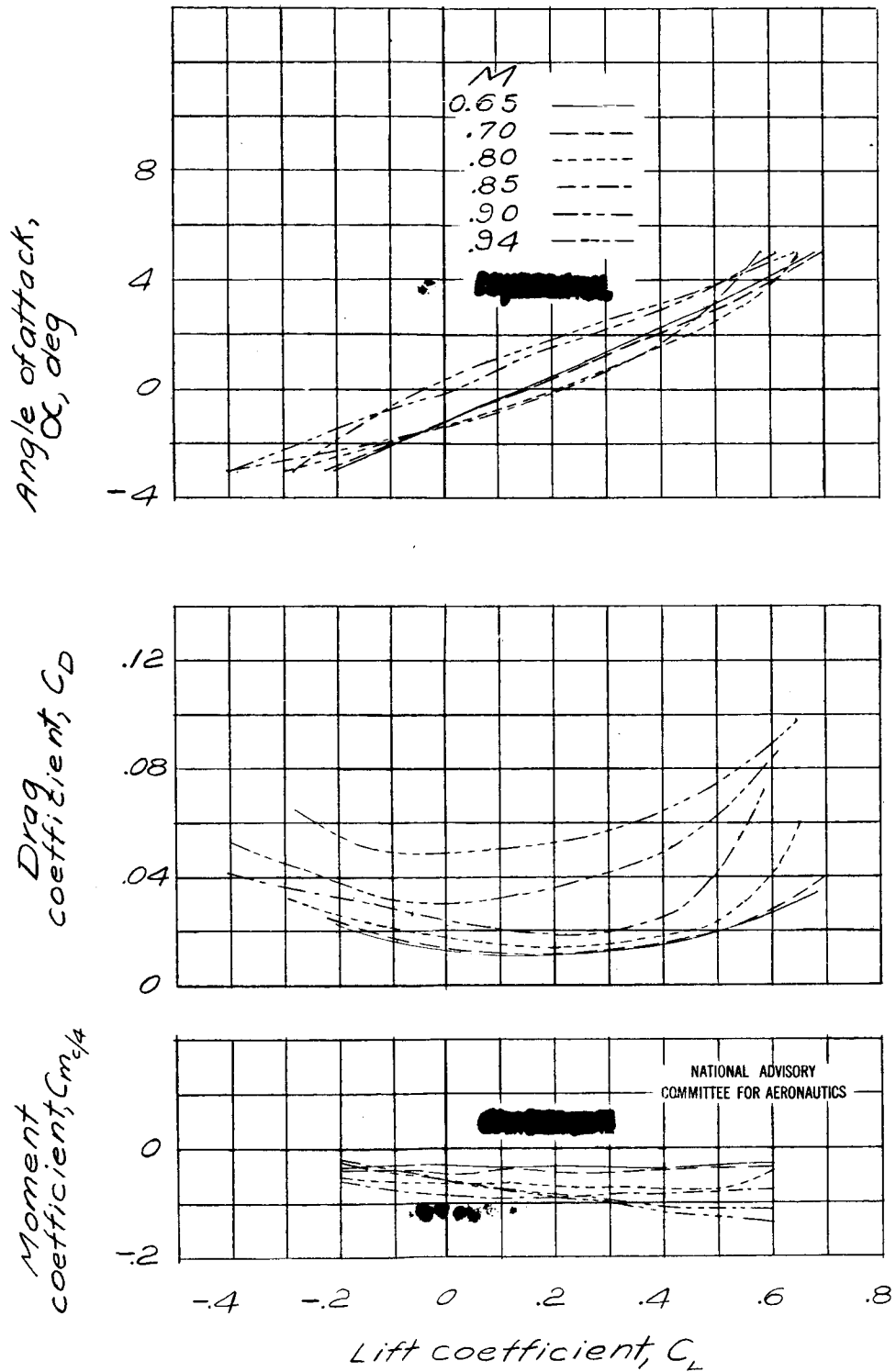
Figure 56 .—Aerodynamic characteristics
of the NACA 2306 airfoil.
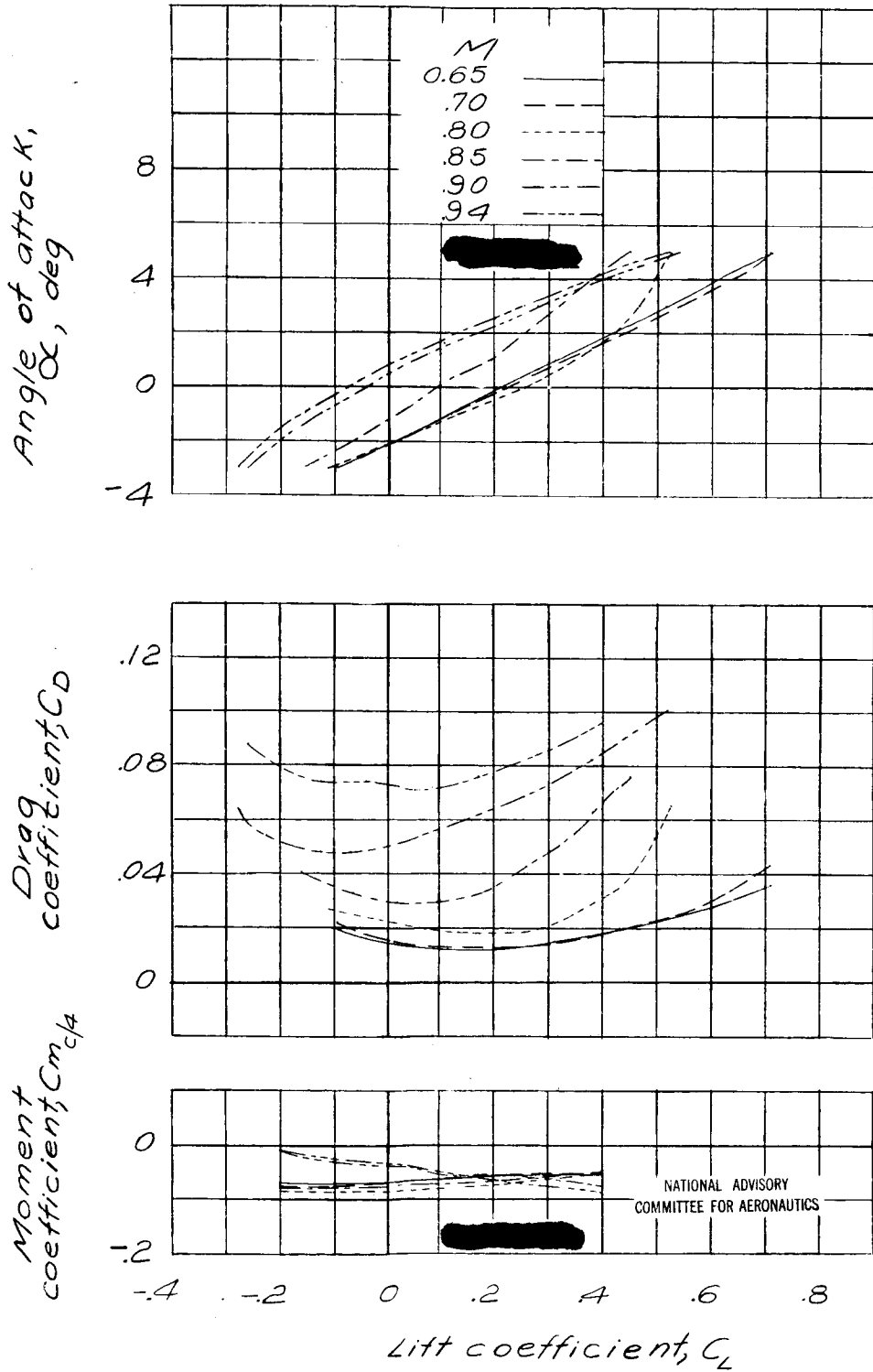
Figure 57.— Aerodynamic characteristics
of the NACA 2309 airfoil.
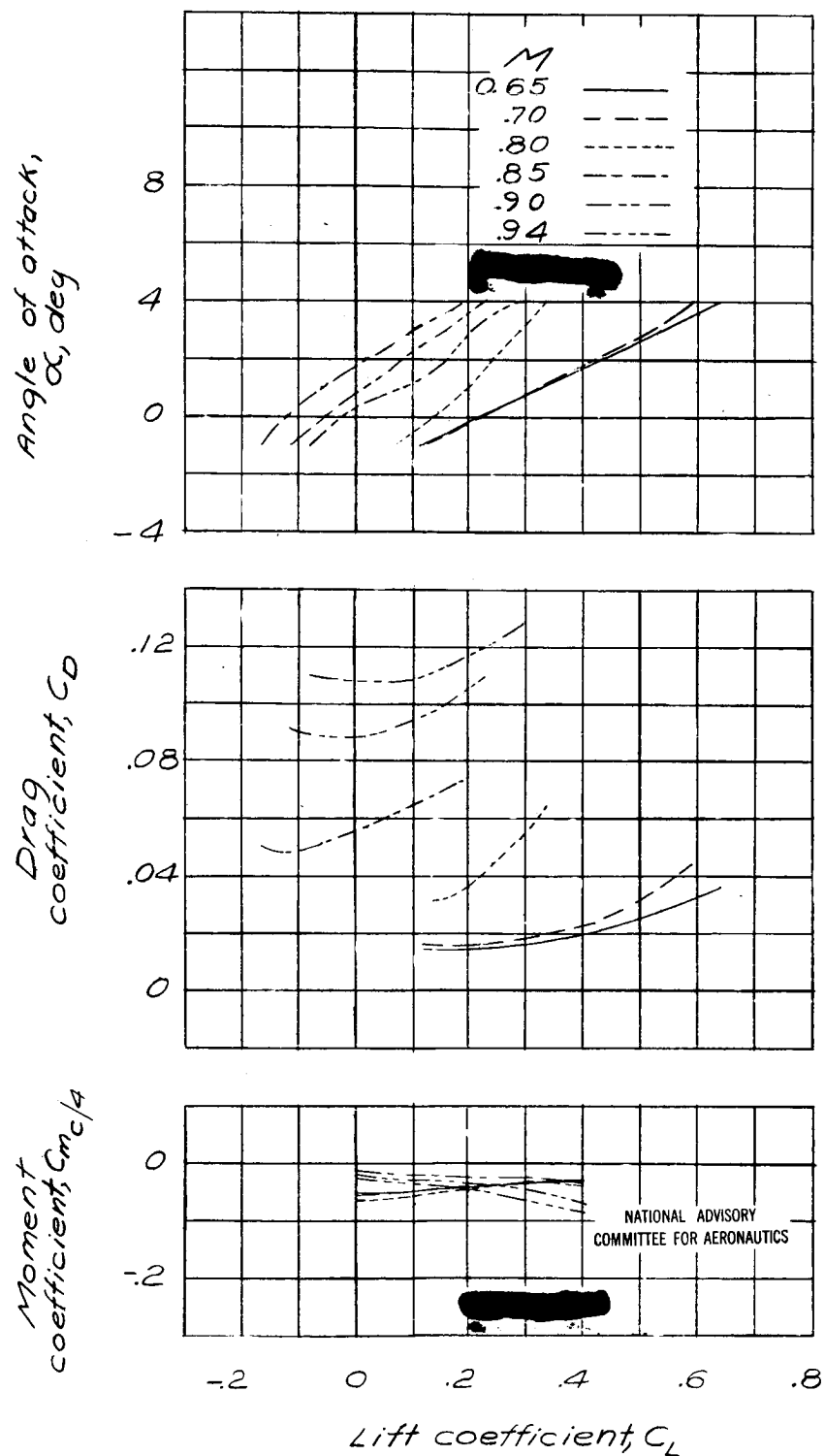
Figure 58.— Aerodynamic characteristics of the NACA 2312 airfoil.
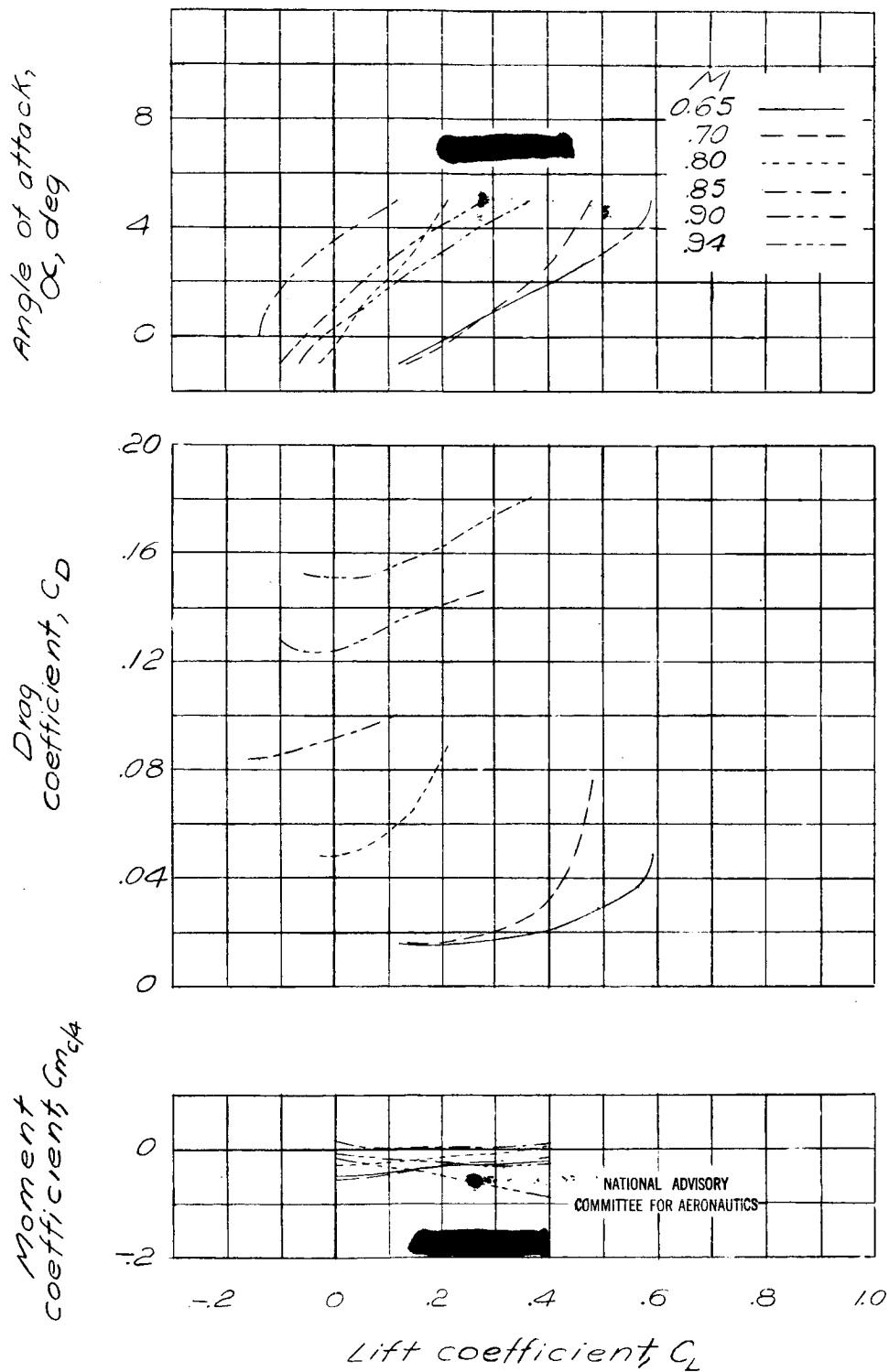
Figure 59.— Aerodynamic characteristics of the NACA 2315 airfoil.
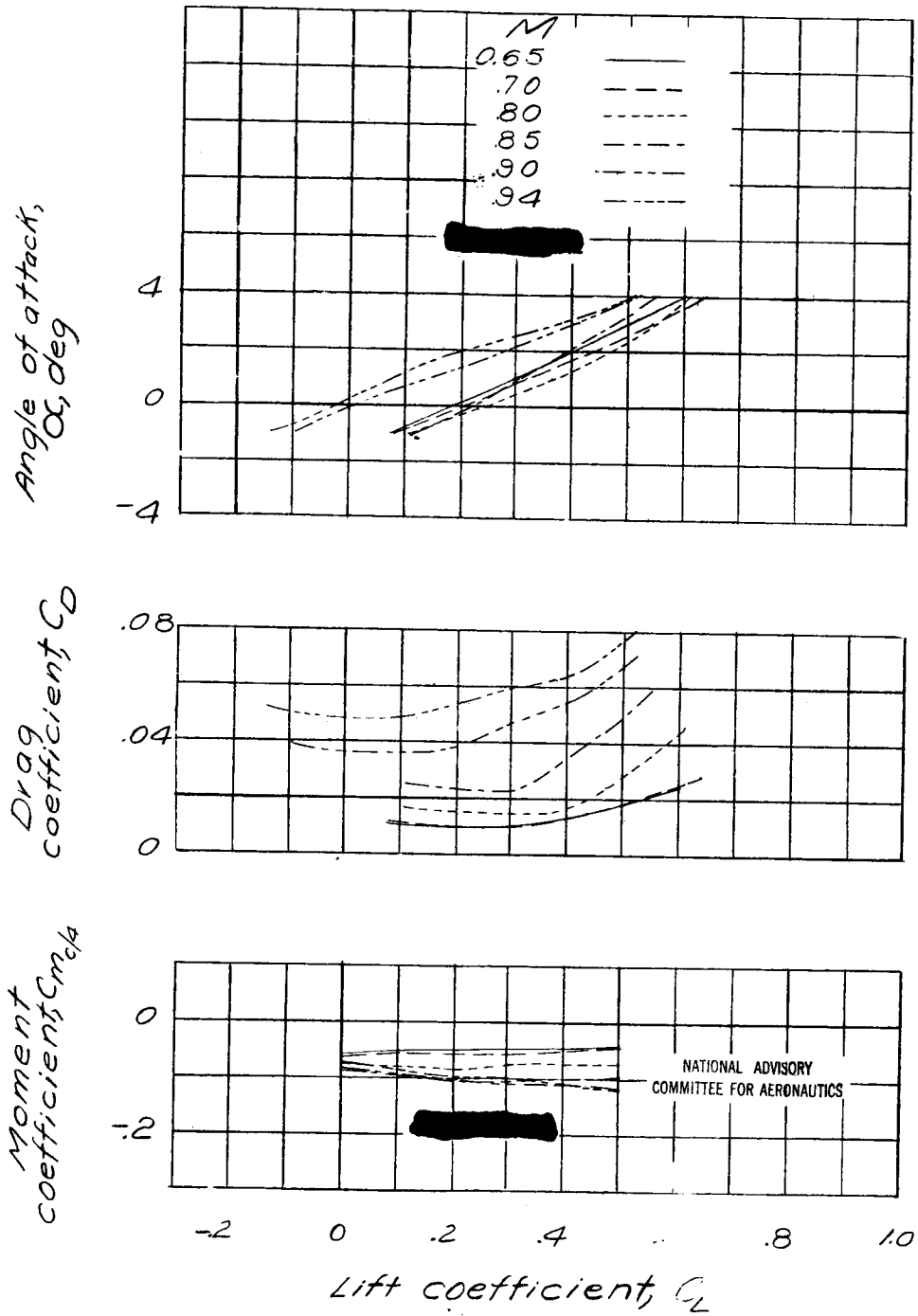
Figure 60 .— Aerodynamic characteristics of the NACA 2406 airfoil.
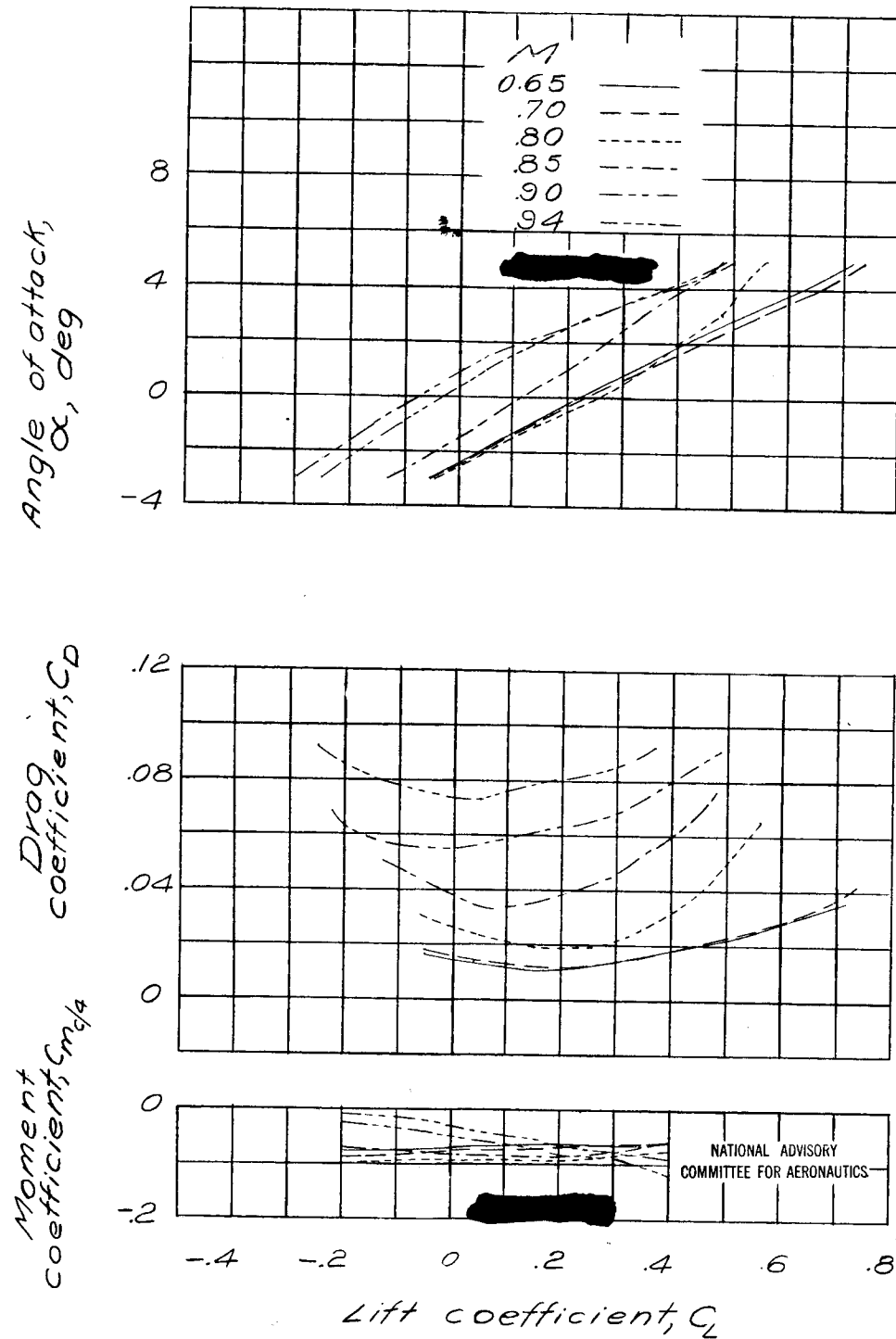
Figure 61 .— Aerodynamic characteristics
of the NACA 2409 airfoil.
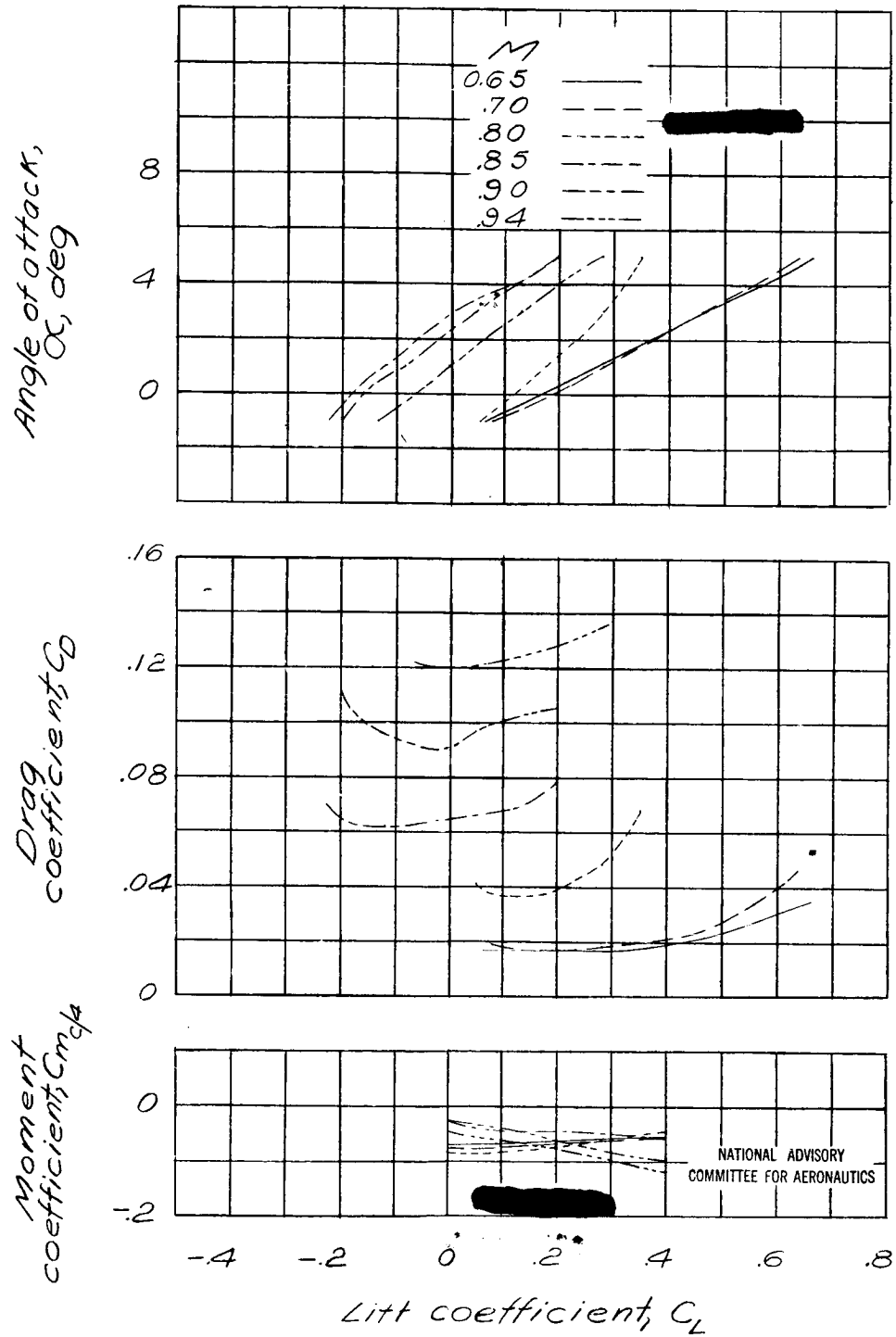
Figure 62.— Aerodynamic characteristics
of the NACA 2412 airfoil.
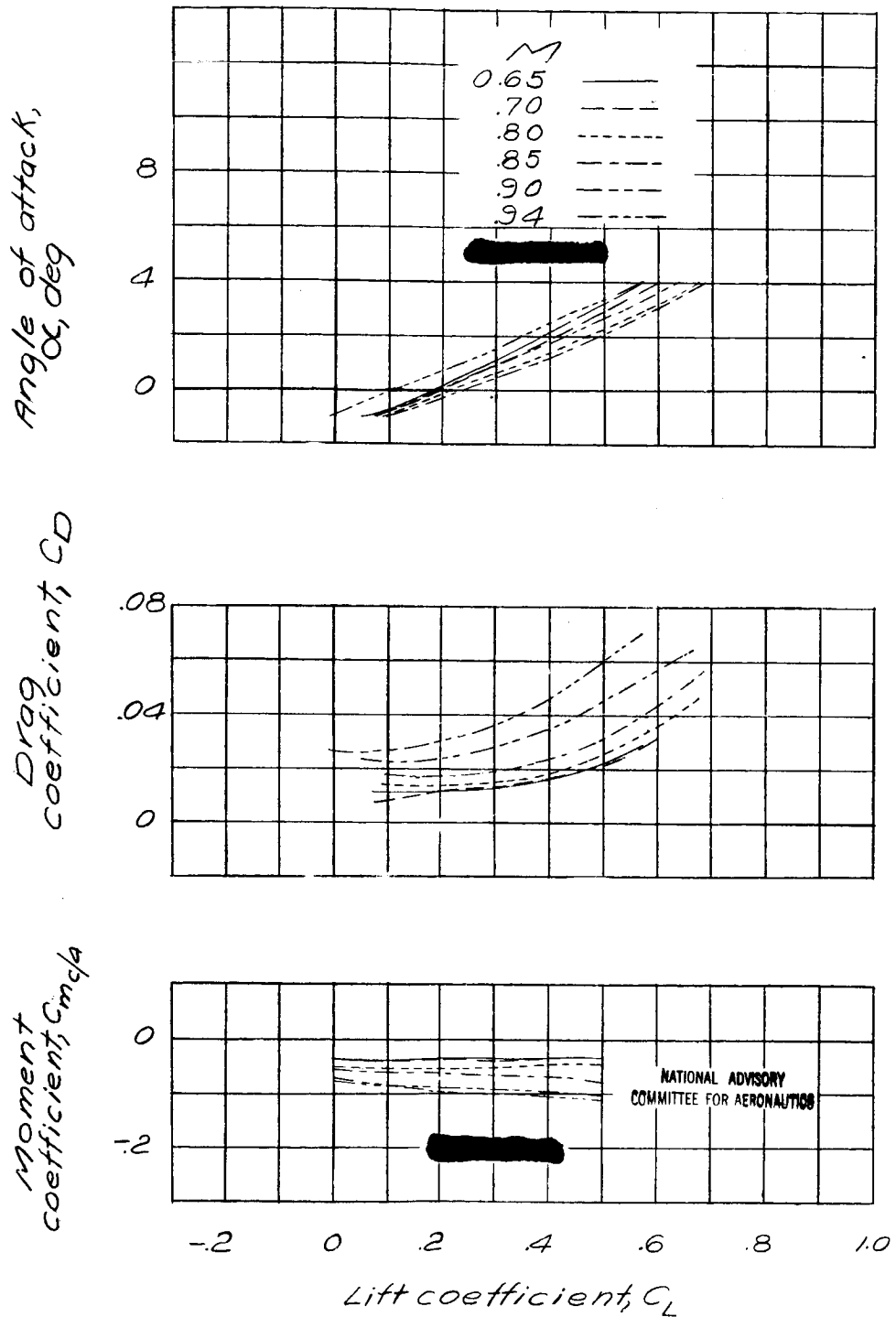
Figure 63.— Aerodynamic characteristics of the U.S.N.P.S. 1 airfoil.
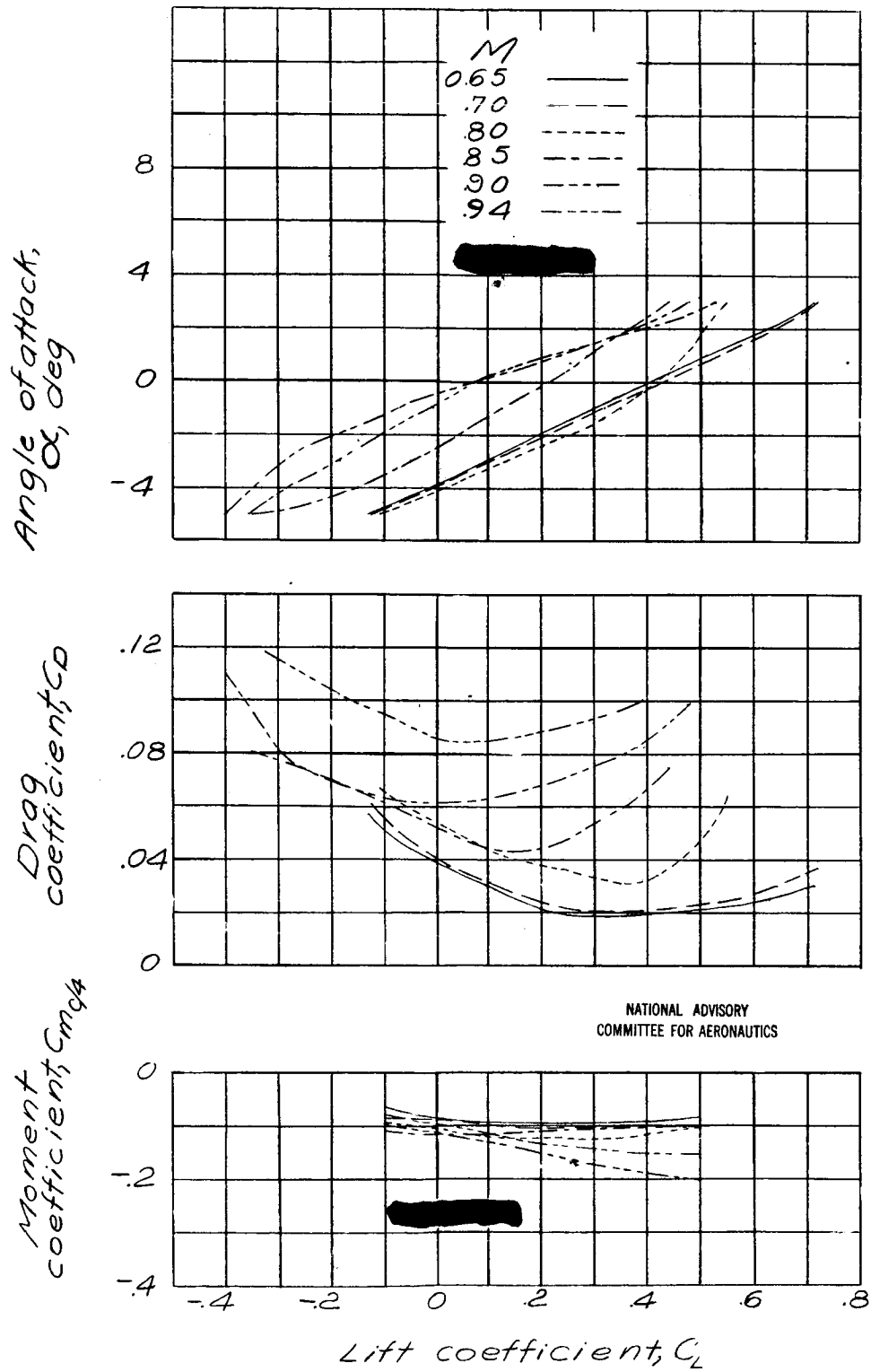
Figure 64.— Aerodynamic characteristics
of the U.S.N.P.S. 2 airfoil.
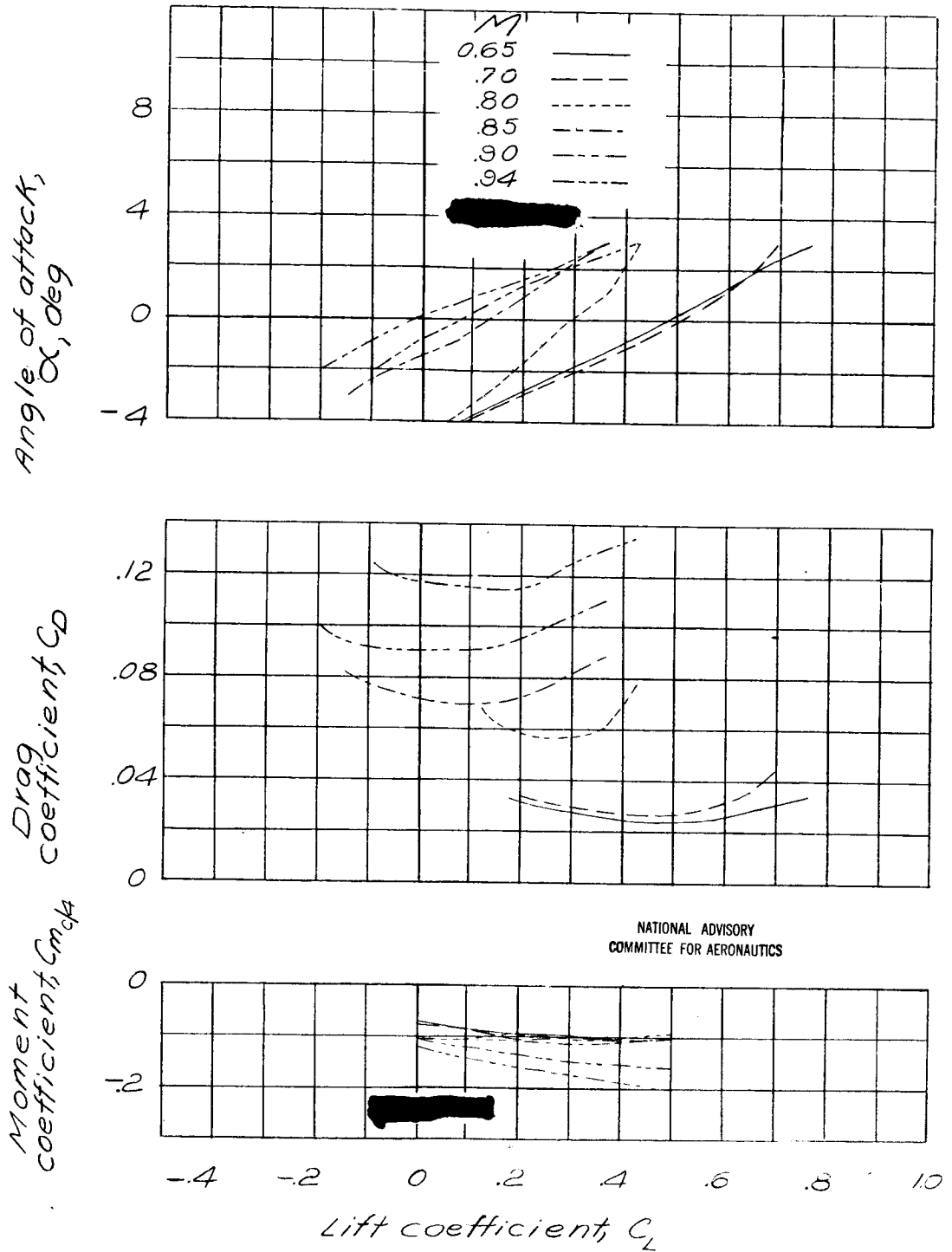
Figure 65.— Aerodynamic characteristics
of the U.S.N.P.S. 3 airfoil.
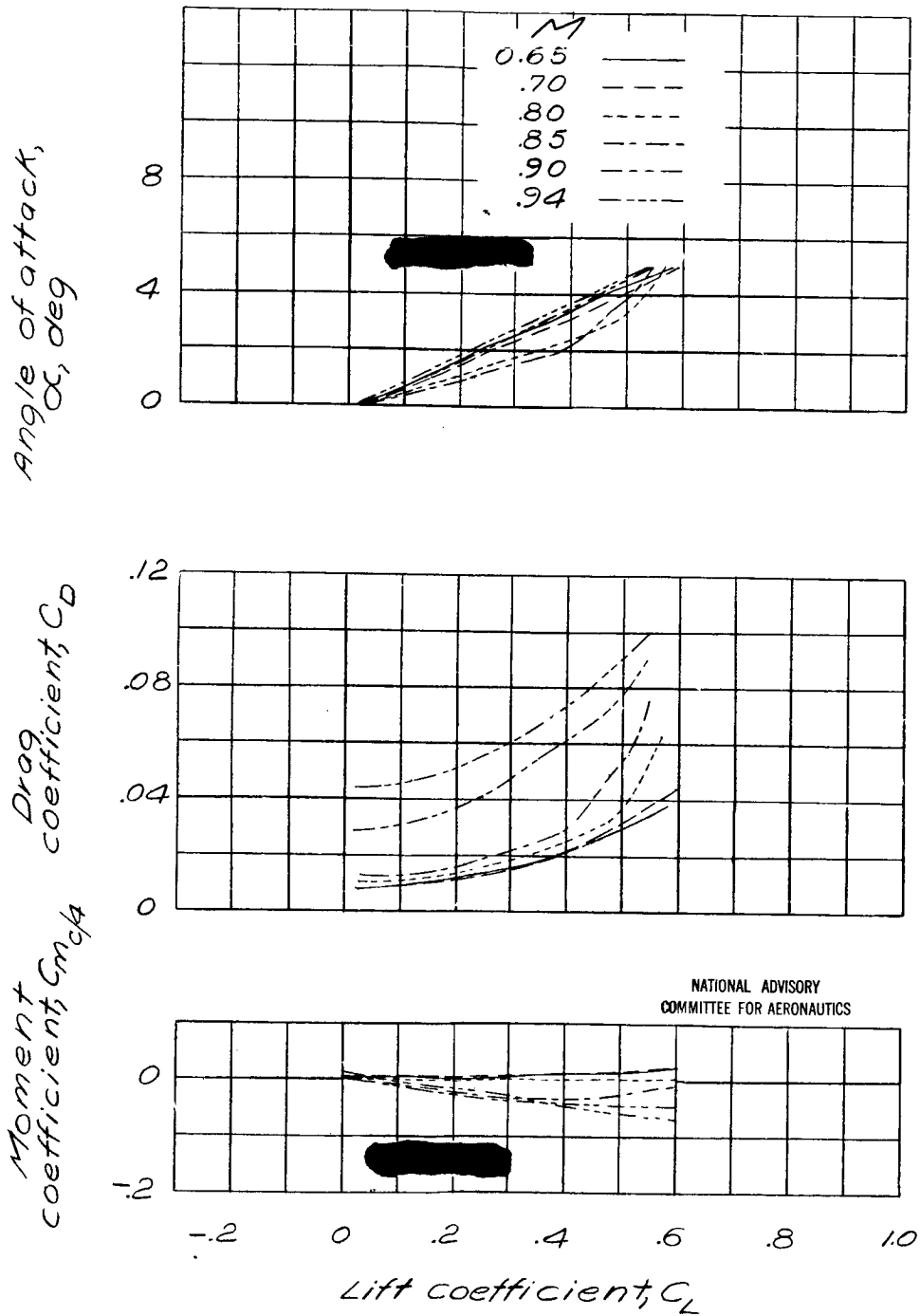
Figure 66.— Aerodynamic characteristics of the M1 airfoil.
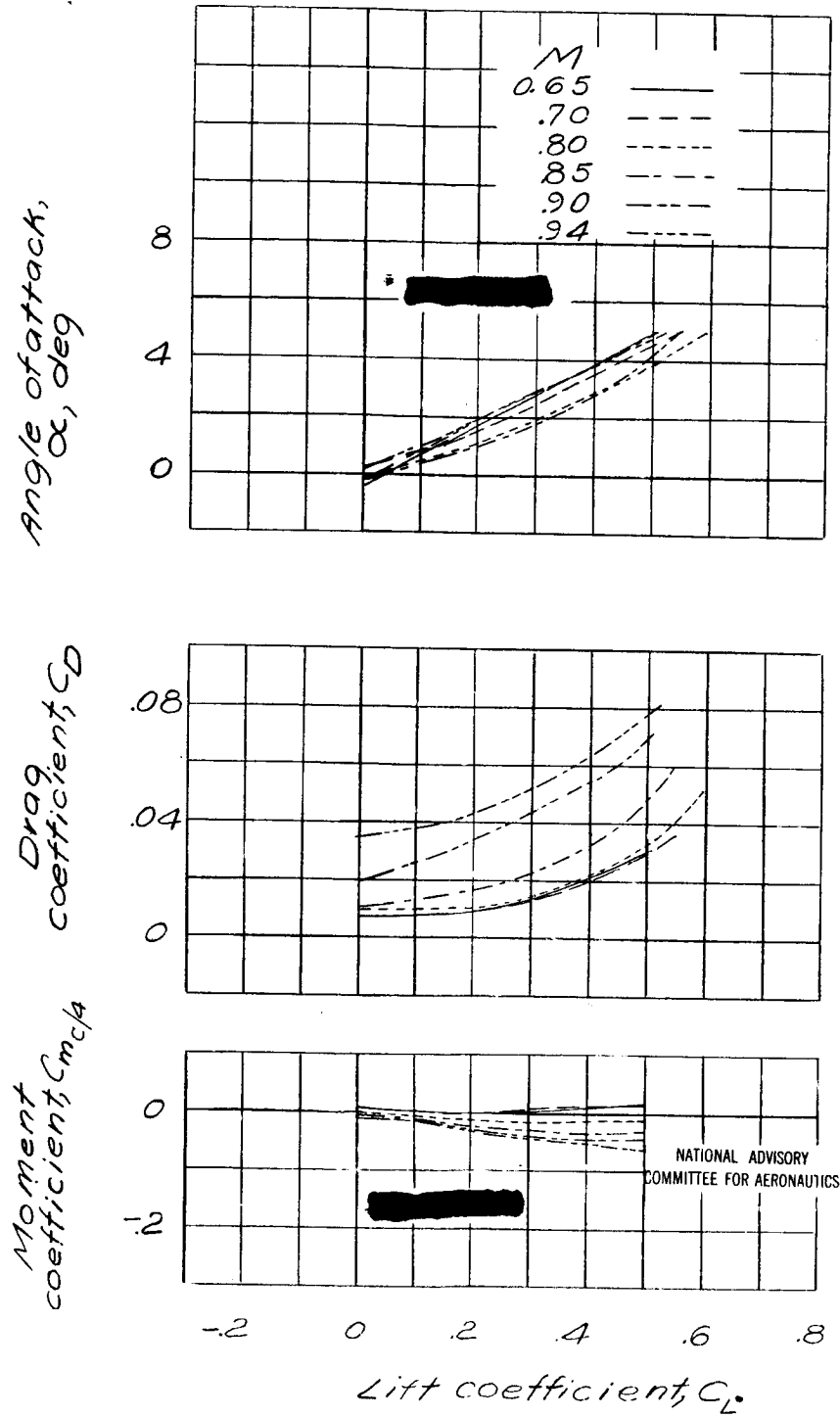
Figure 67.— Aerodynamic characteristics
of the NACA 0006 T airfoil.
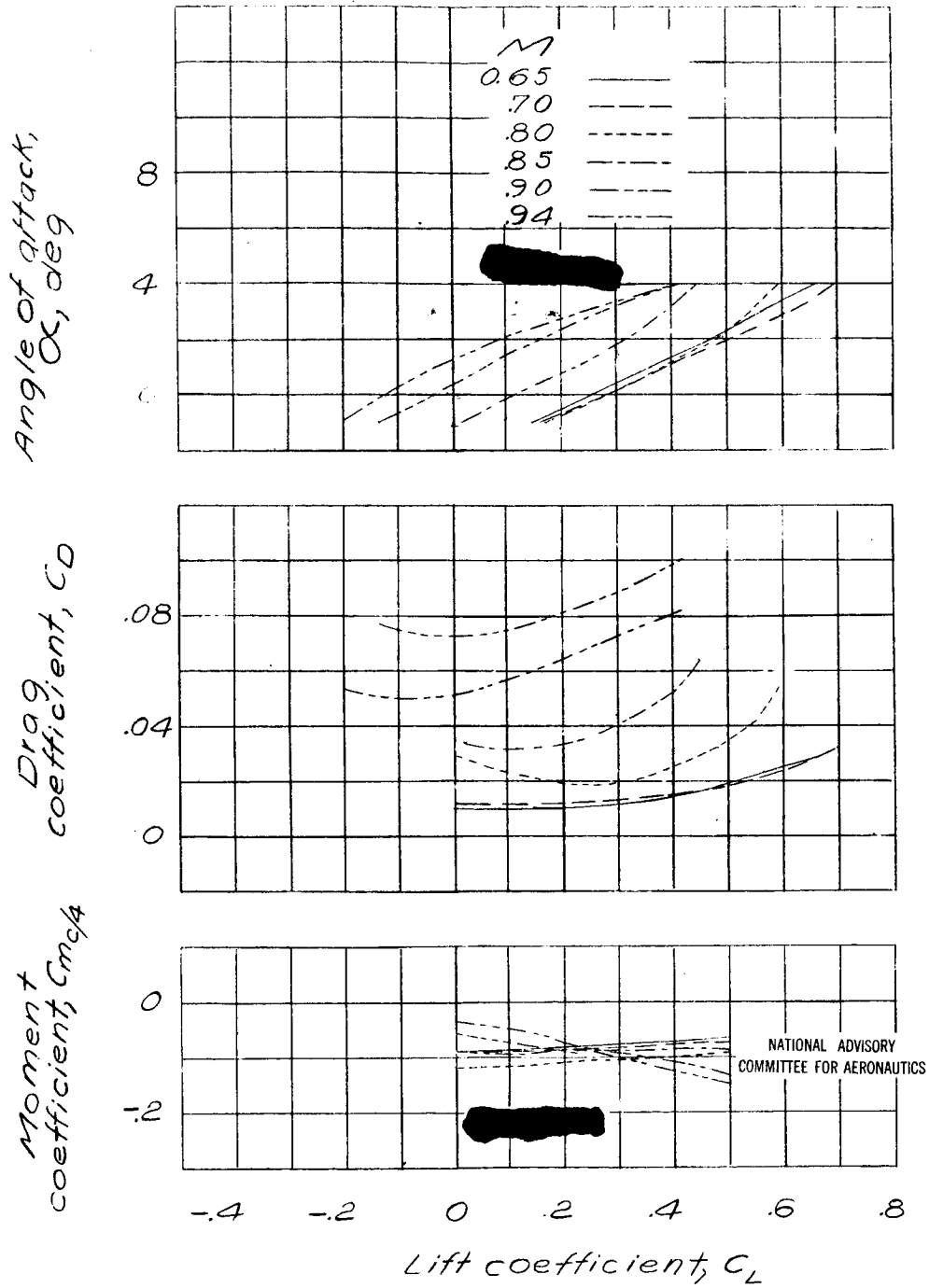
Figure 68.— Aerodynamic characteristics
of the NACA 2509 airfoil.
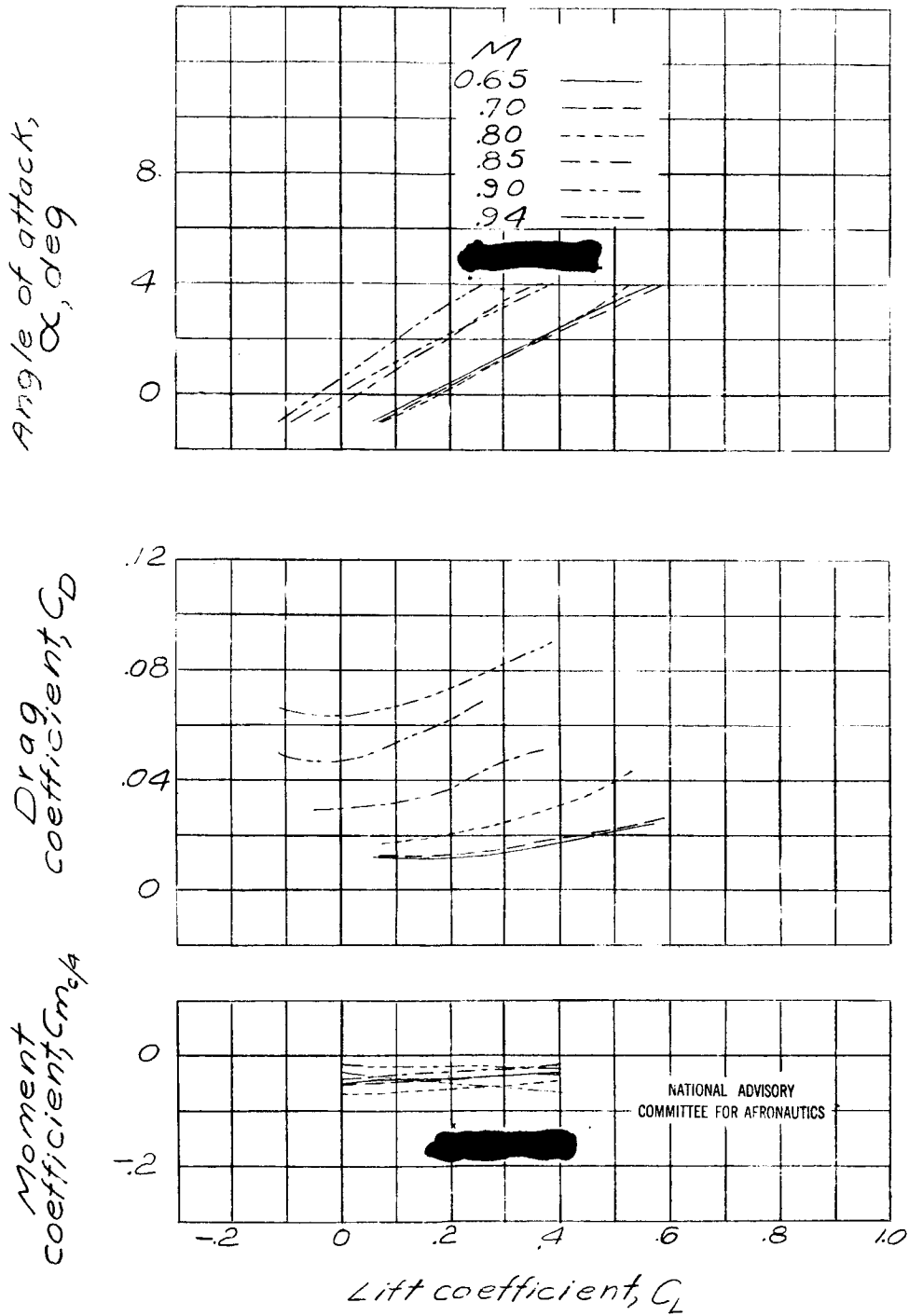
Figure 69.— Aerodynamic characteristics of the Davis 9-percent-thick airfoil.

Angle of attack, $\alpha$, deg

Drag coefficient, $C_D$

Moment coefficient, $C_{m_{c/4}}$

M
0.65
.70
.80
.85
.90
.94

NATIONAL ADVISORY
COMMITTEE FOR AERONAUTICS

8

4

0

.12

.08

.04

0

0

-.2

-.2        0        .2        .4        .6        .8        1.0

Lift coefficient, $C_L$
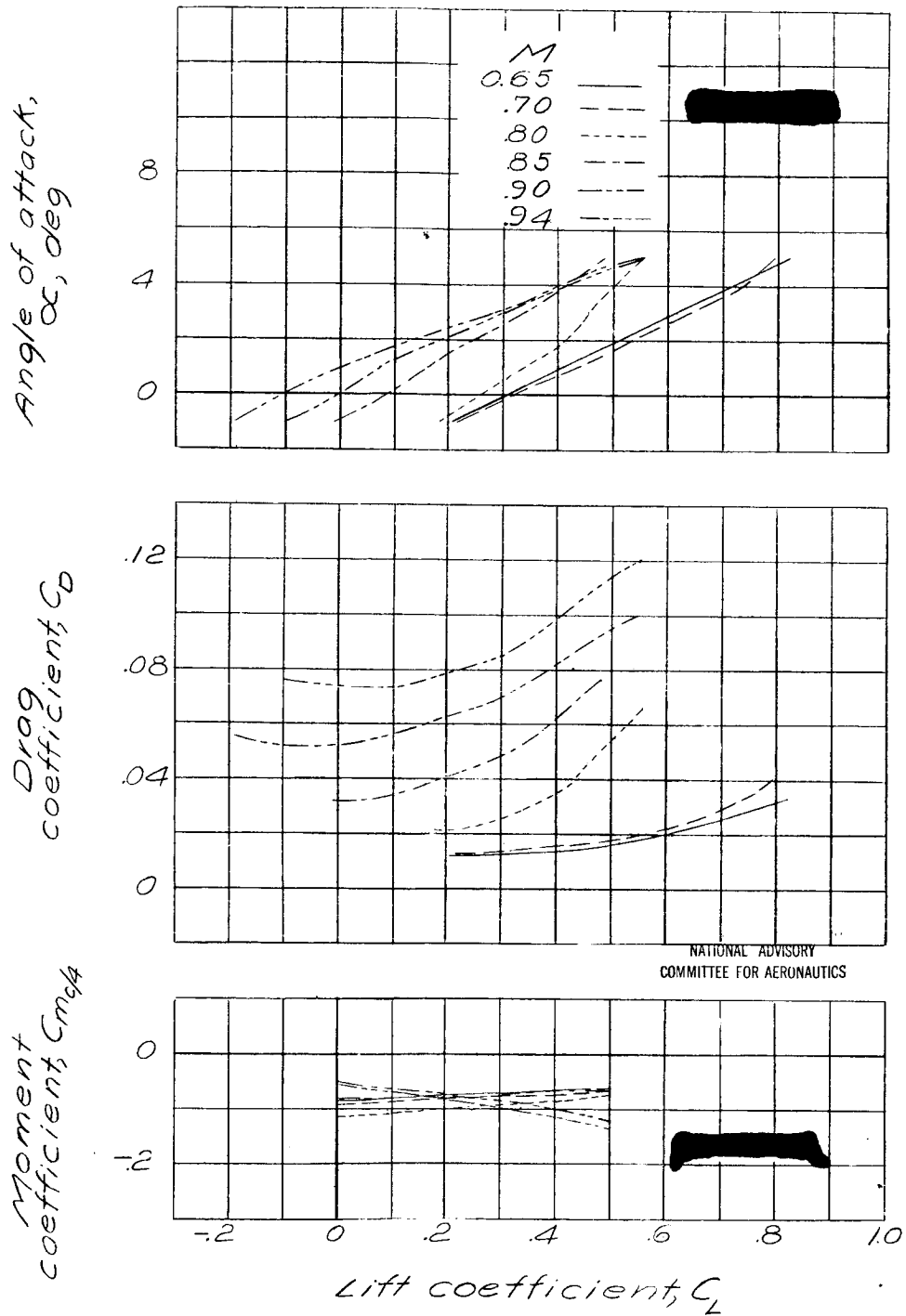
Figure 70.- Aerodynamic characteristics
of the ETH 3609 airfoil.

(a) NACA 2306 airfoil.

(b) NACA 2309 airfoil.

NATIONAL ADVISORY
COMMITTEE FOR AERONAUTICS

(c) NACA 2312 airfoil.

(d) NACA 2315 airfoil.

Angle of zero lift, $\alpha_{l_0}$
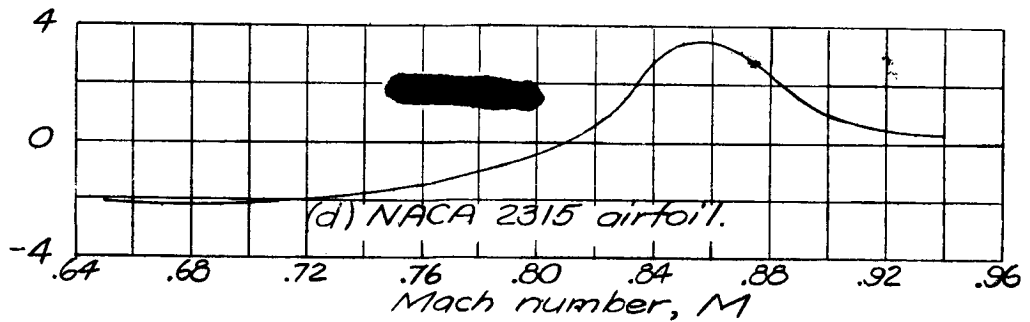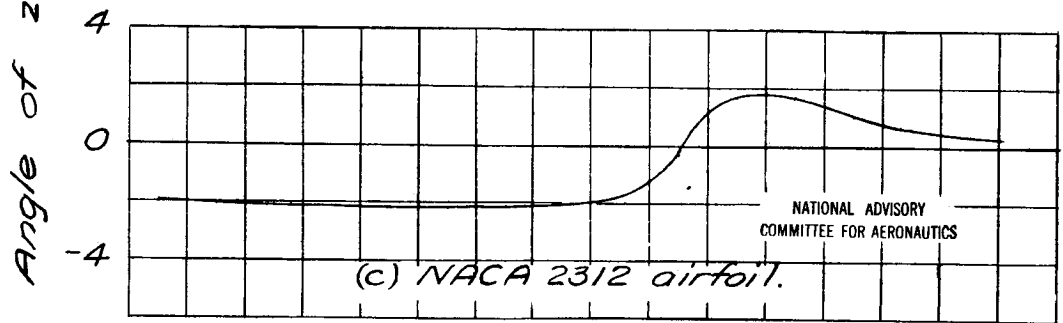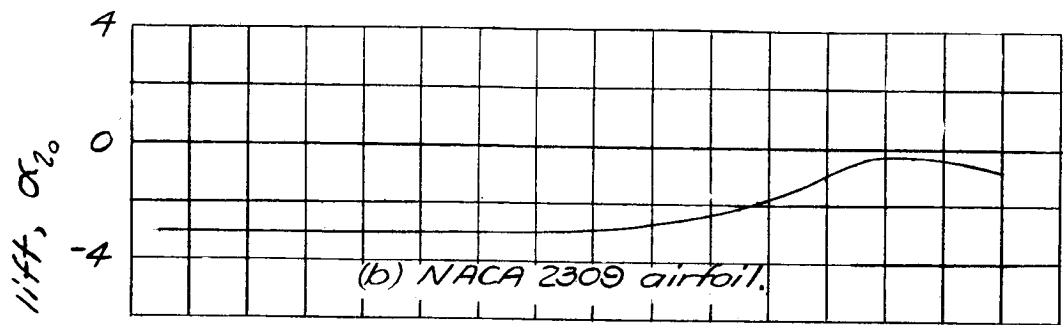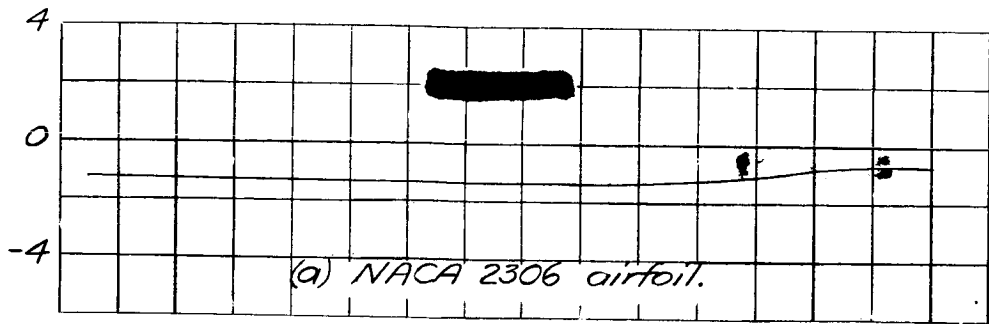
Mach number, M

Figure 71.- Variation of angle of zero
lift with Mach number.

(e) NACA 2406 airfoil.

(f) NACA 2409 airfoil.

NATIONAL ADVISORY
COMMITTEE FOR AERONAUTICS

(g) NACA 2412 airfoil.

Mach number, M

Angle of zero lift, $\alpha_{z_0}$

Figure 71 .— Continued.

Angle of zero lift, $\alpha_{l_0}$

(h) U.S.N.P.S. 1 airfoil,
4 percent thick.

(i) U.S.N.P.S. 2 airfoil,
8 percent thick.

NATIONAL ADVISORY
COMMITTEE FOR AERONAUTICS

(j) U.S.N.P.S. 3 airfoil,
10 percent thick.

Mach number, M

Figure 71.— Continued.

(k) NACA 2509 airfoil.

(l) Davis 9-percent-thick airfoil.

(m) ETH 3609 airfoil.

Angle of zero lift, $\alpha_{z_o}$

Mach number, M

NATIONAL ADVISORY
COMMITTEE FOR AERONAUTICS
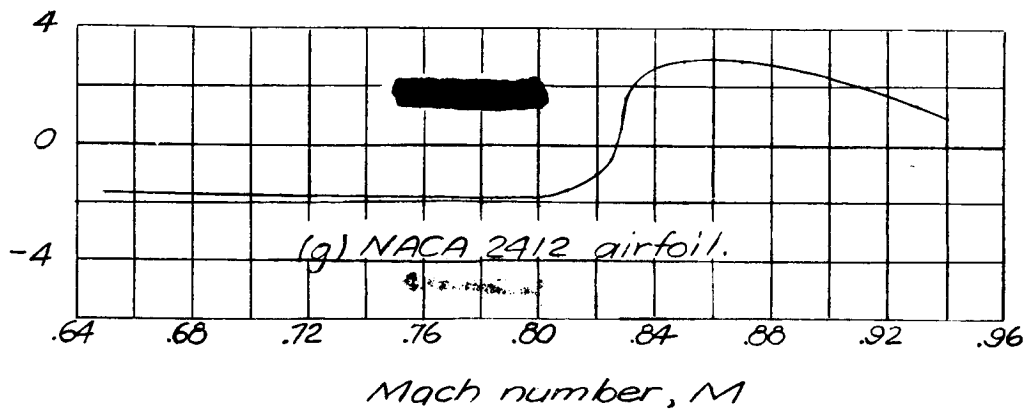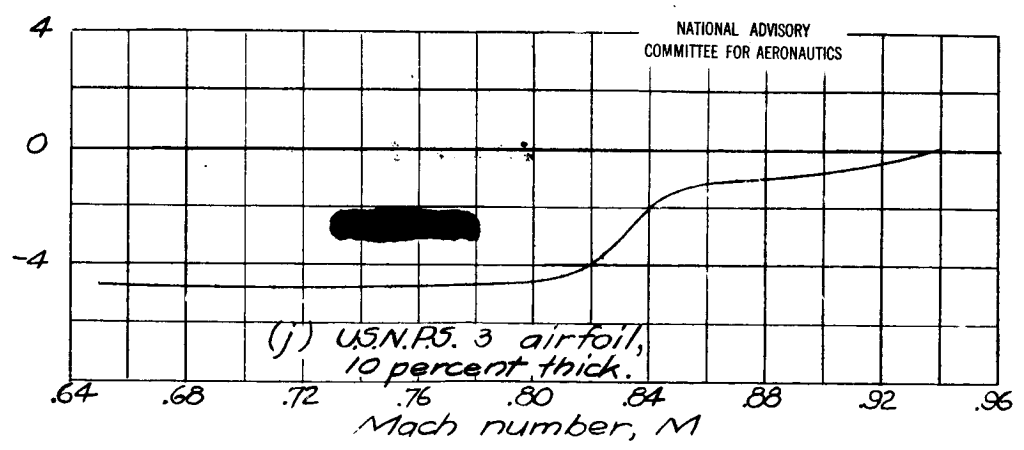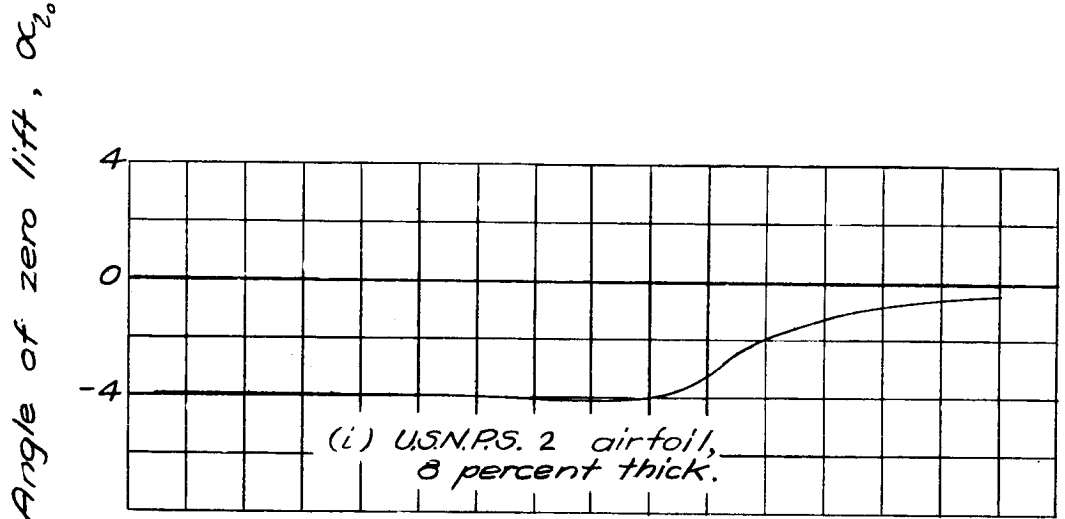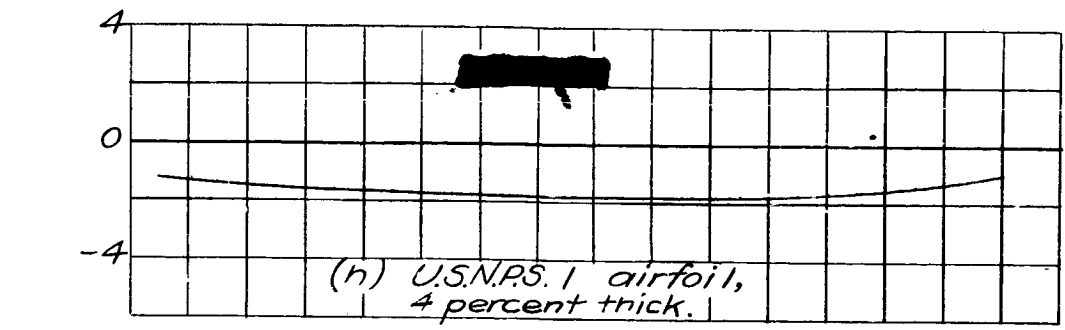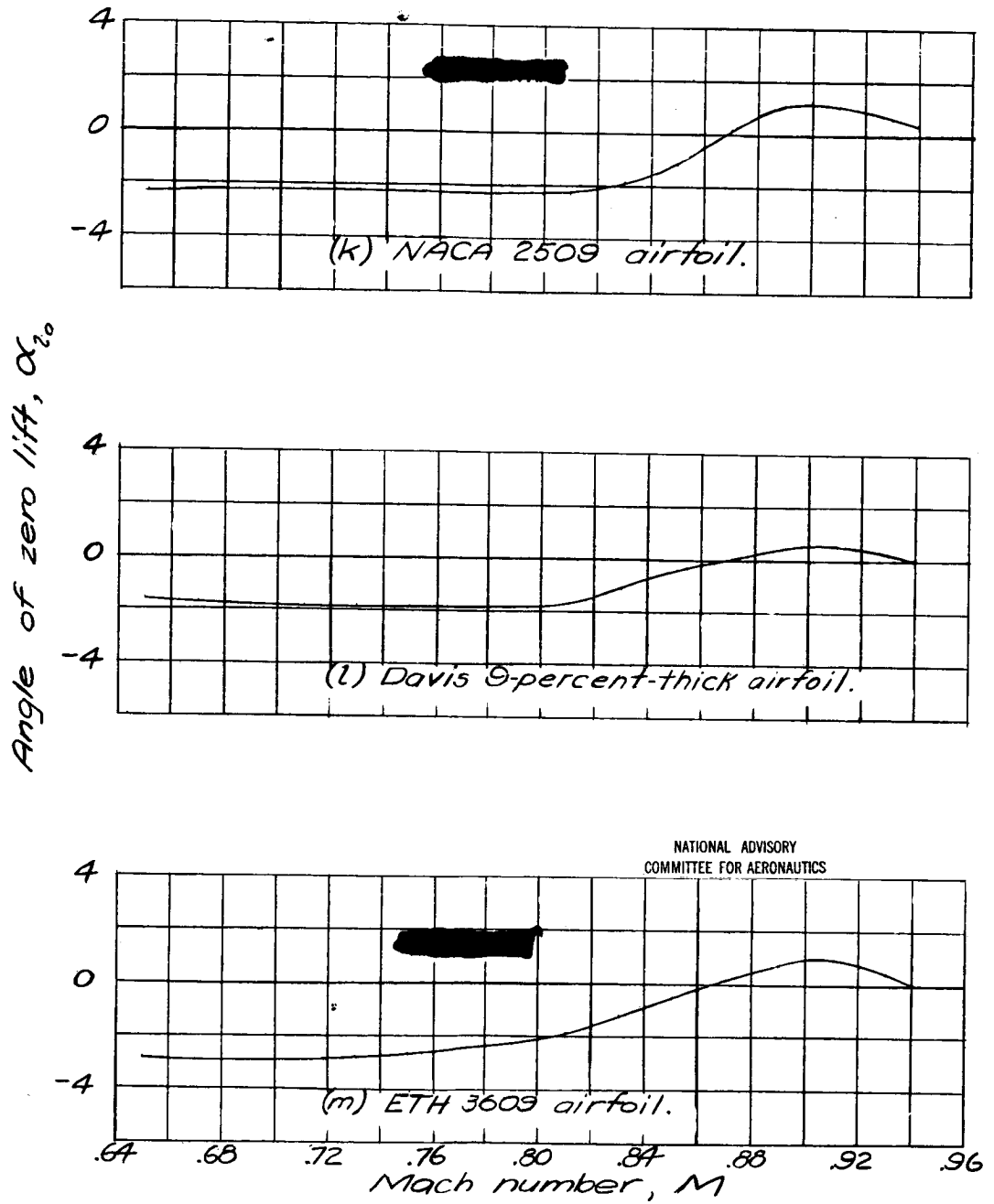
Figure 71.— Concluded.
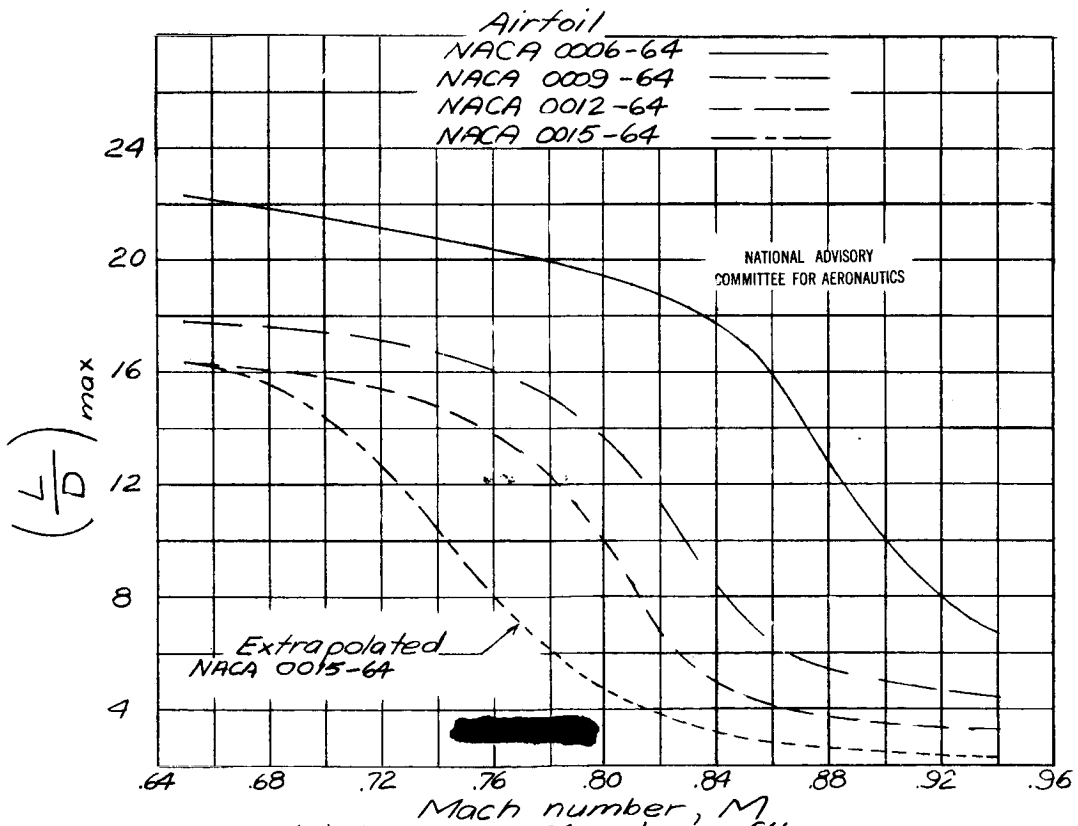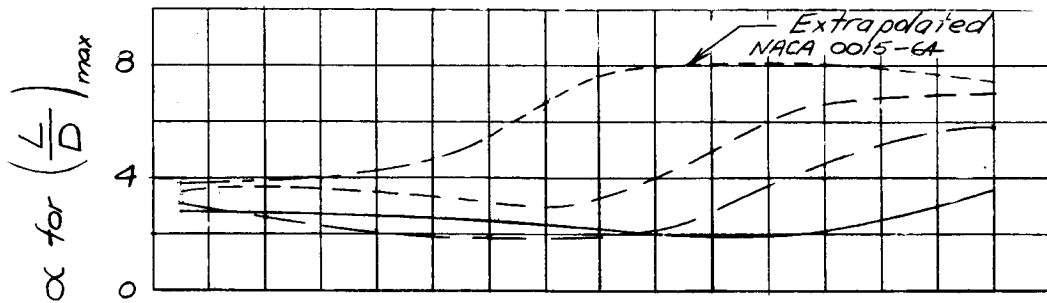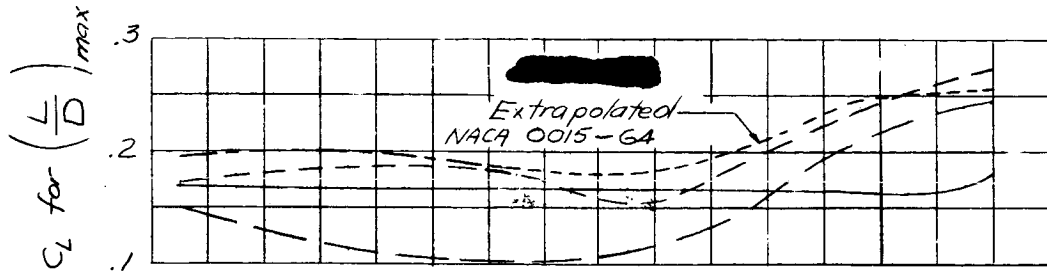
(a) NACA 0000-64 series airfoils.

Figure 72. — Variation of $(L/D)_{max}$ and of the lift coefficient and angle of attack corresponding to $(L/D)_{max}$ with Mach number.

(b) NACA 0000-34 series airfoils.
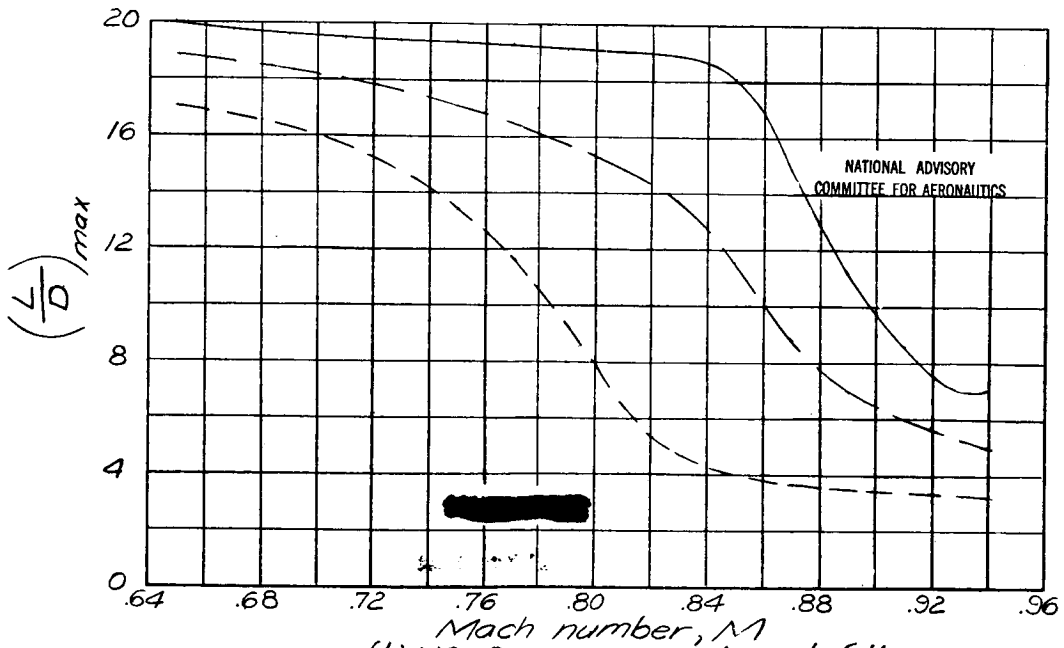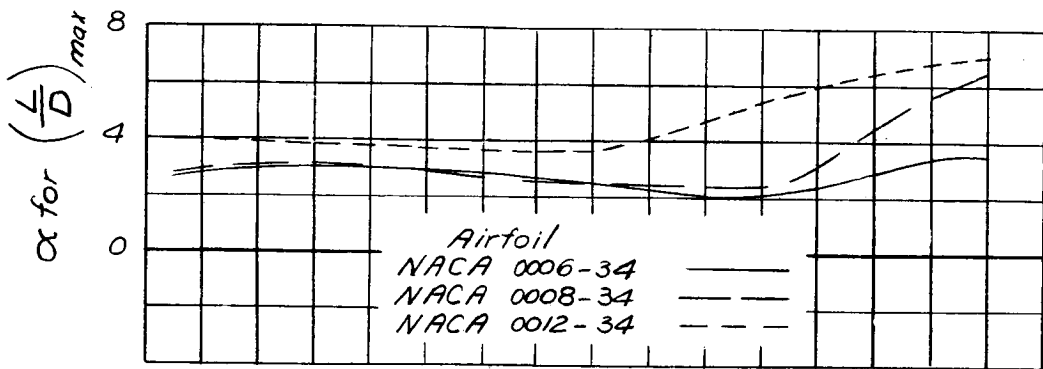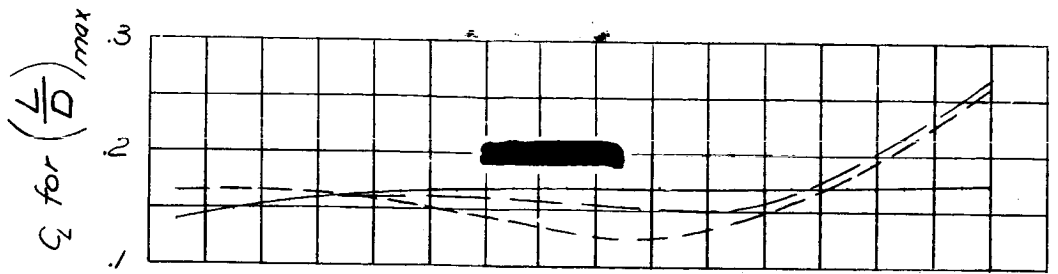
Figure 72. - Continued.

Airfoil
NACA 0006-63 ————
NACA 0009-63 —— ——
NACA M 1 ———
NACA 0006 T —·—·—
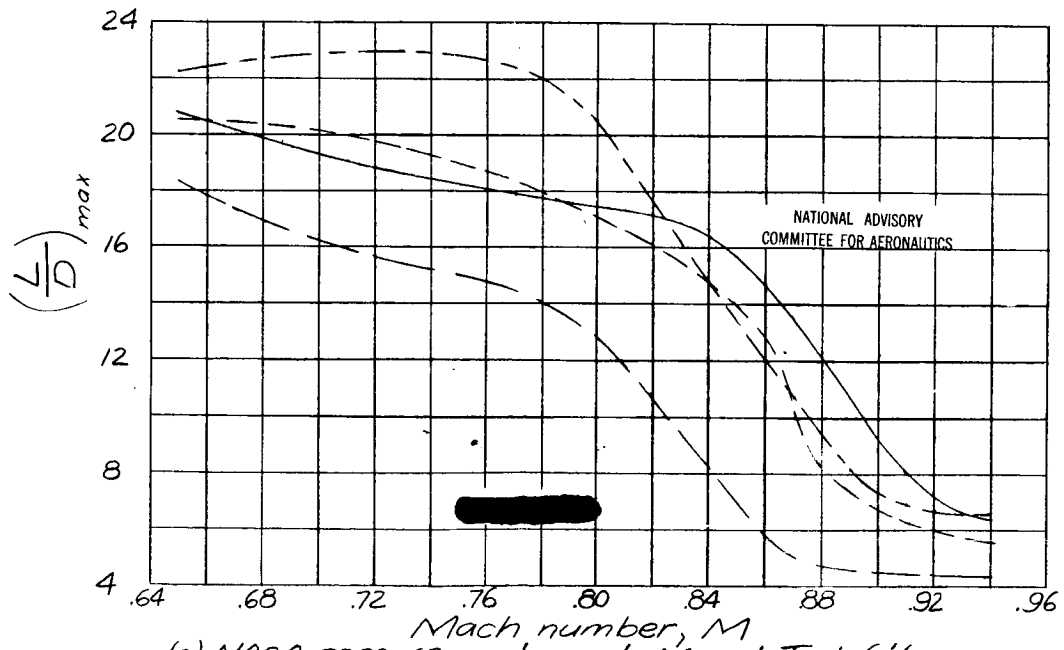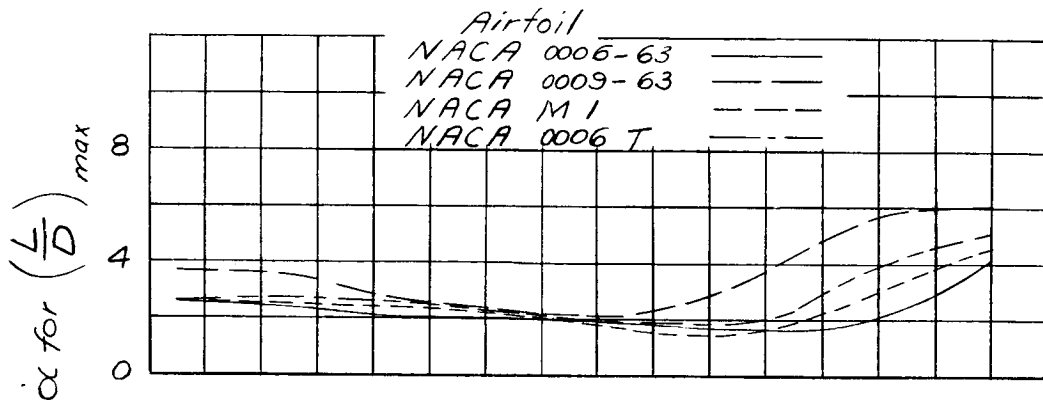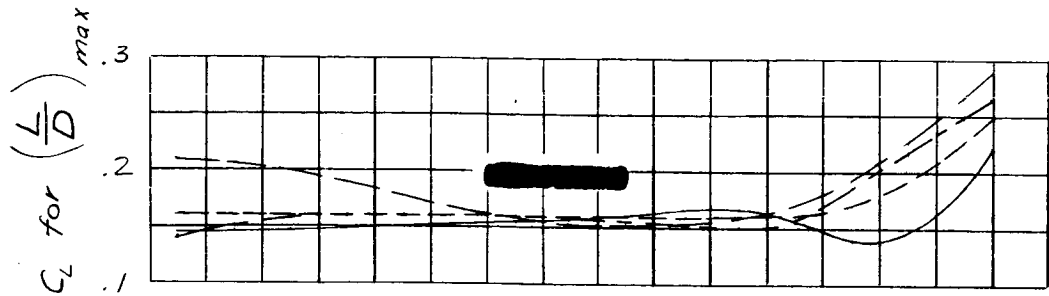
(c) NACA 0000-63 series and M and T airfoils.
Figure 72 .— Continued.

Airfoil
NACA 2306 ————
NACA 2309 ————
NACA 2312 — — —
NACA 2315 —·—·—

NATIONAL ADVISORY
COMMITTEE FOR AERONAUTICS
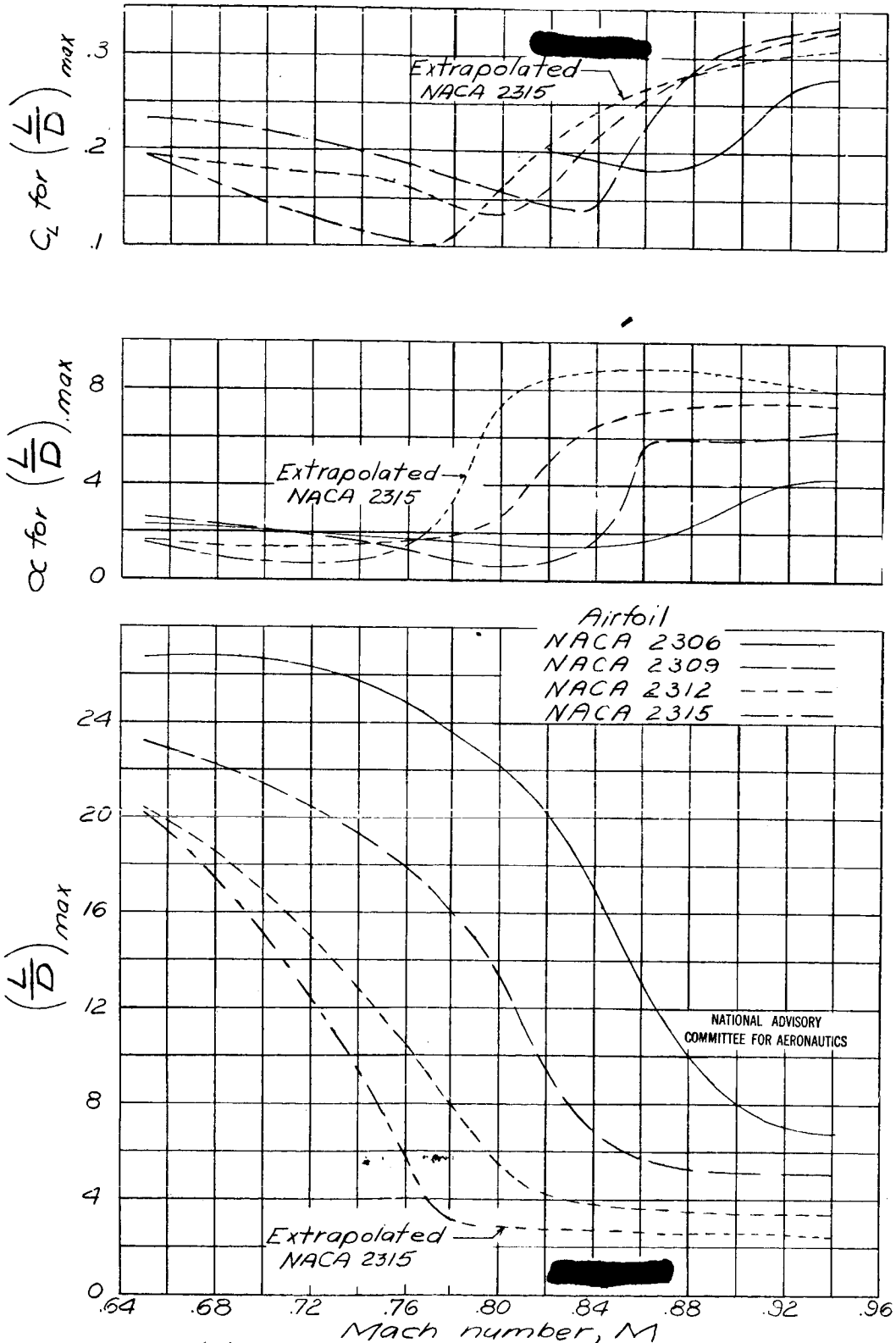
(d) NACA 2300 series airfoils.
Figure 72. — Continued.
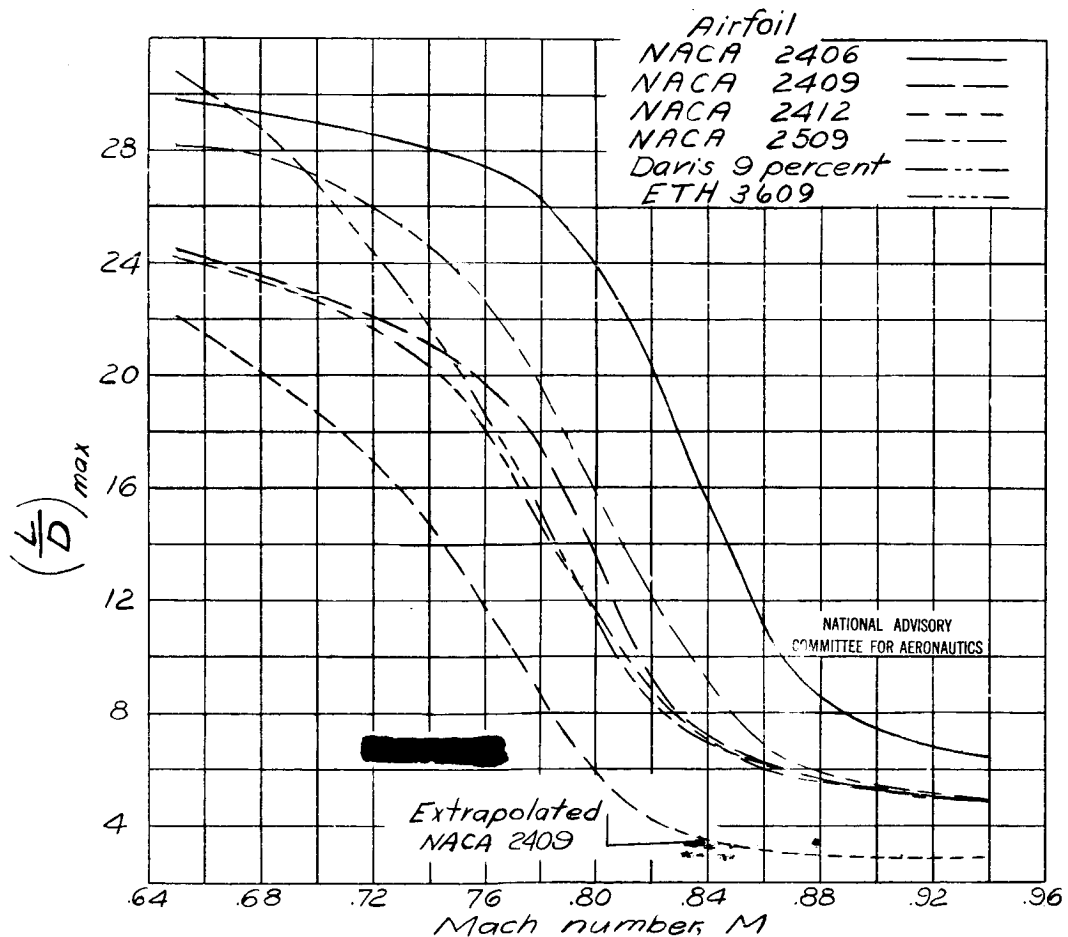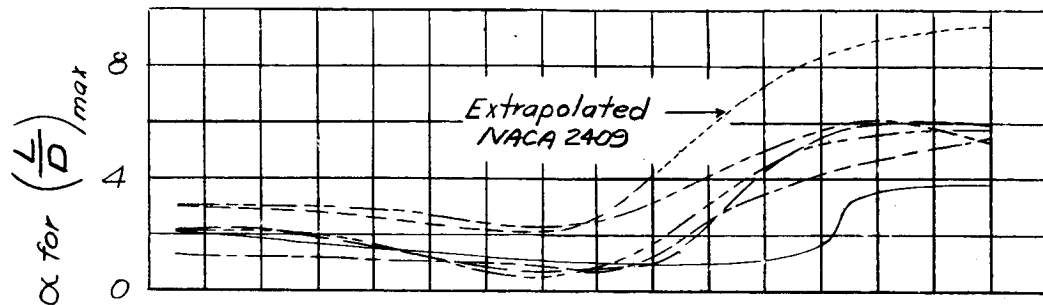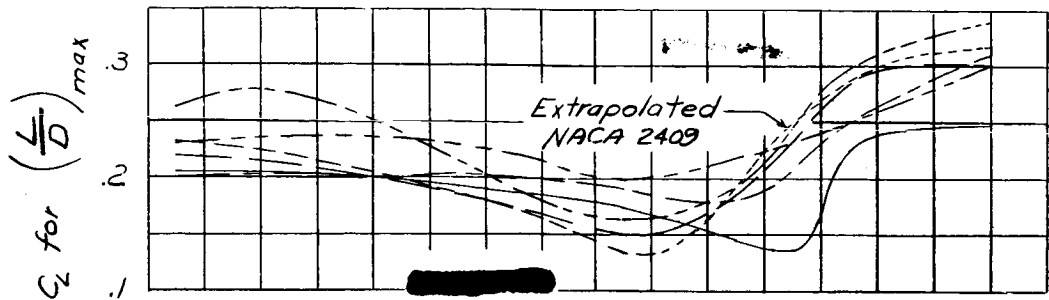
(e) NACA 24 and 25 series airfoils.

Figure 72.—Continued.

Airfoil
U.S.N.P.S. 1, 4 percent thick ————
U.S.N.P.S. 2, 8 percent thick —— ——
U.S.N.P.S. 3, 10 percent thick —————

(f) U.S.N.P.S. series airfoils.
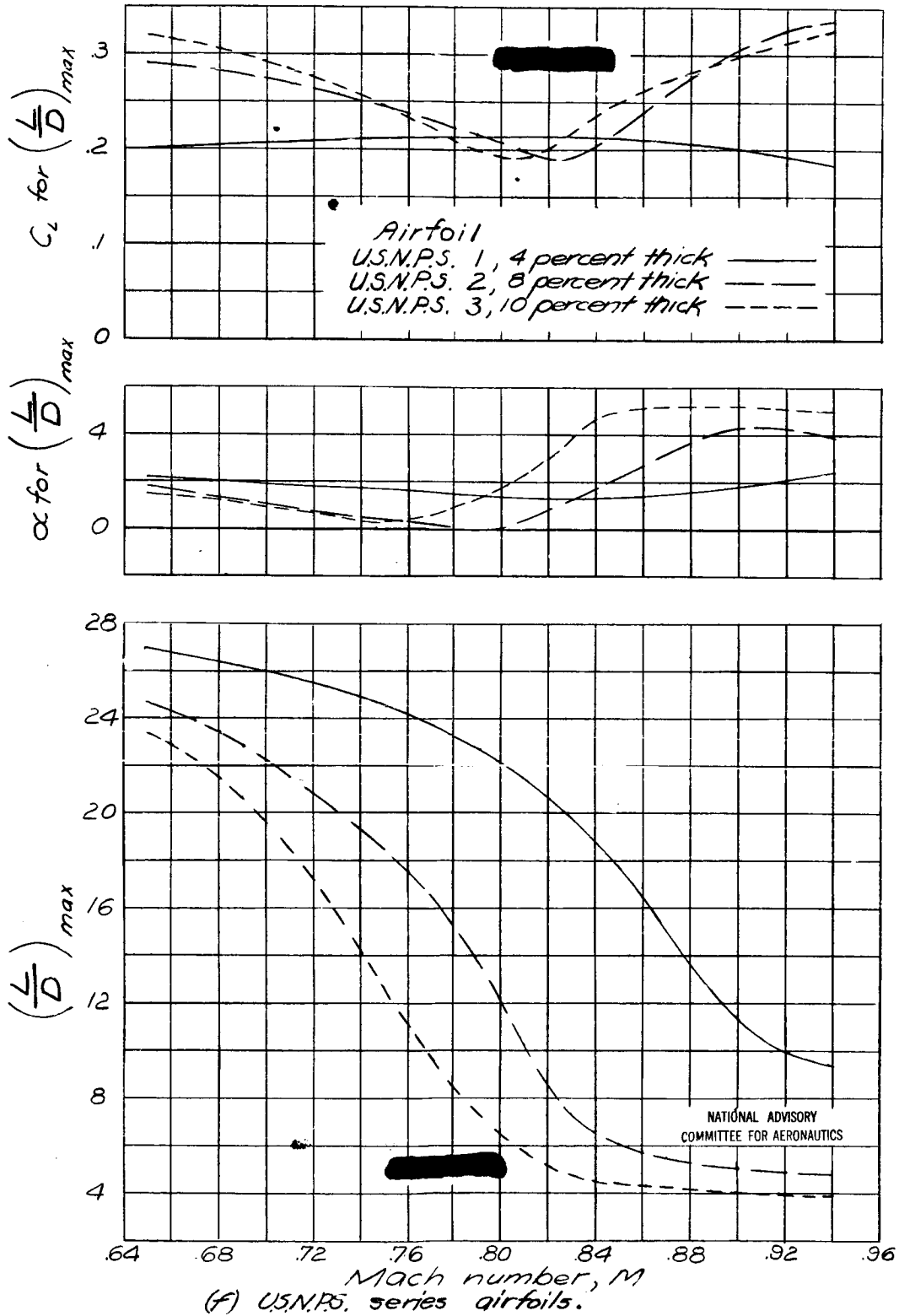
Figure 72. — Concluded.
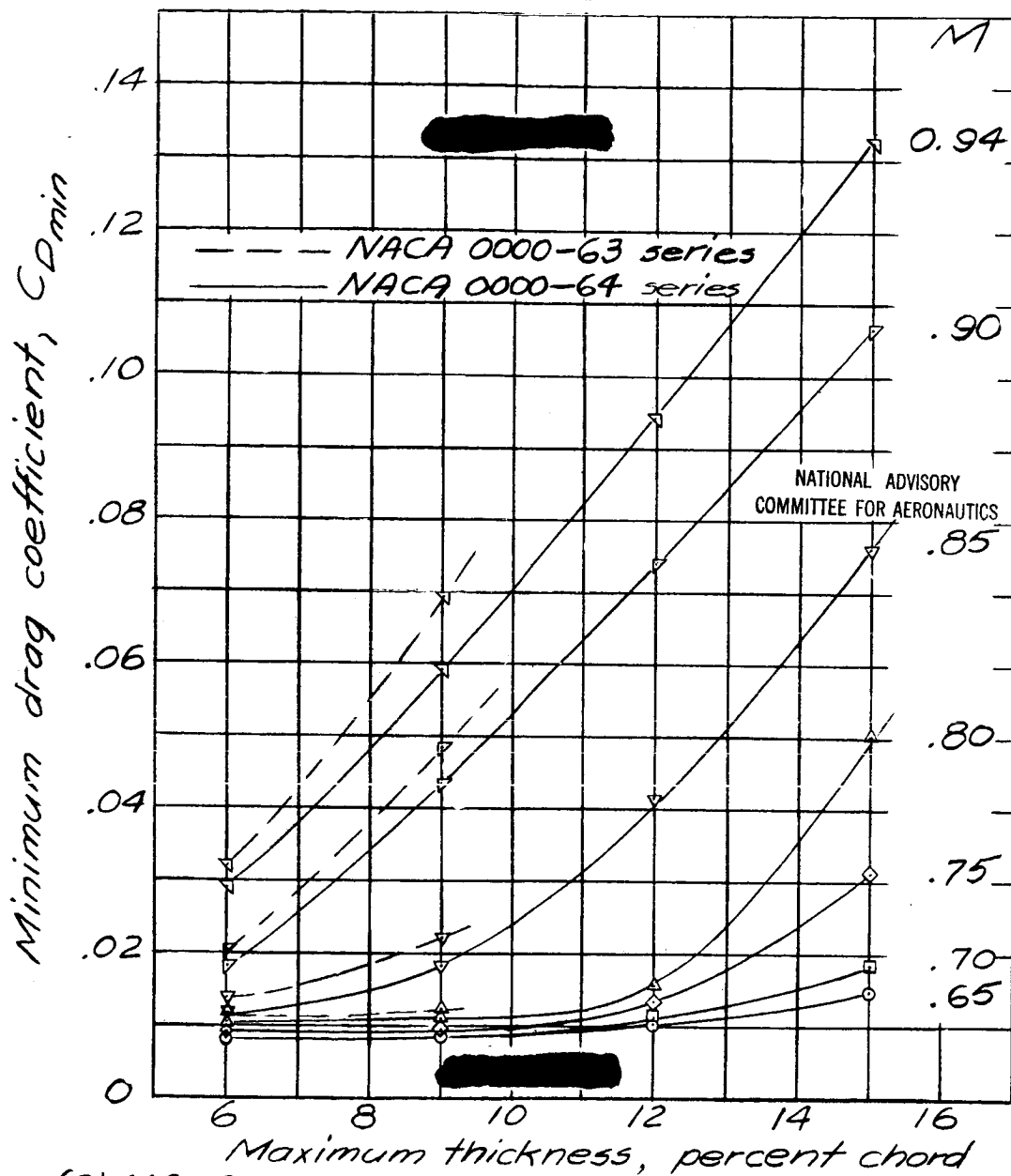
(a) NACA 0000-63 and 0000-64 series airfoils.
Figure 73.—Variation of minimum drag coefficient with maximum thickness for various Mach numbers.
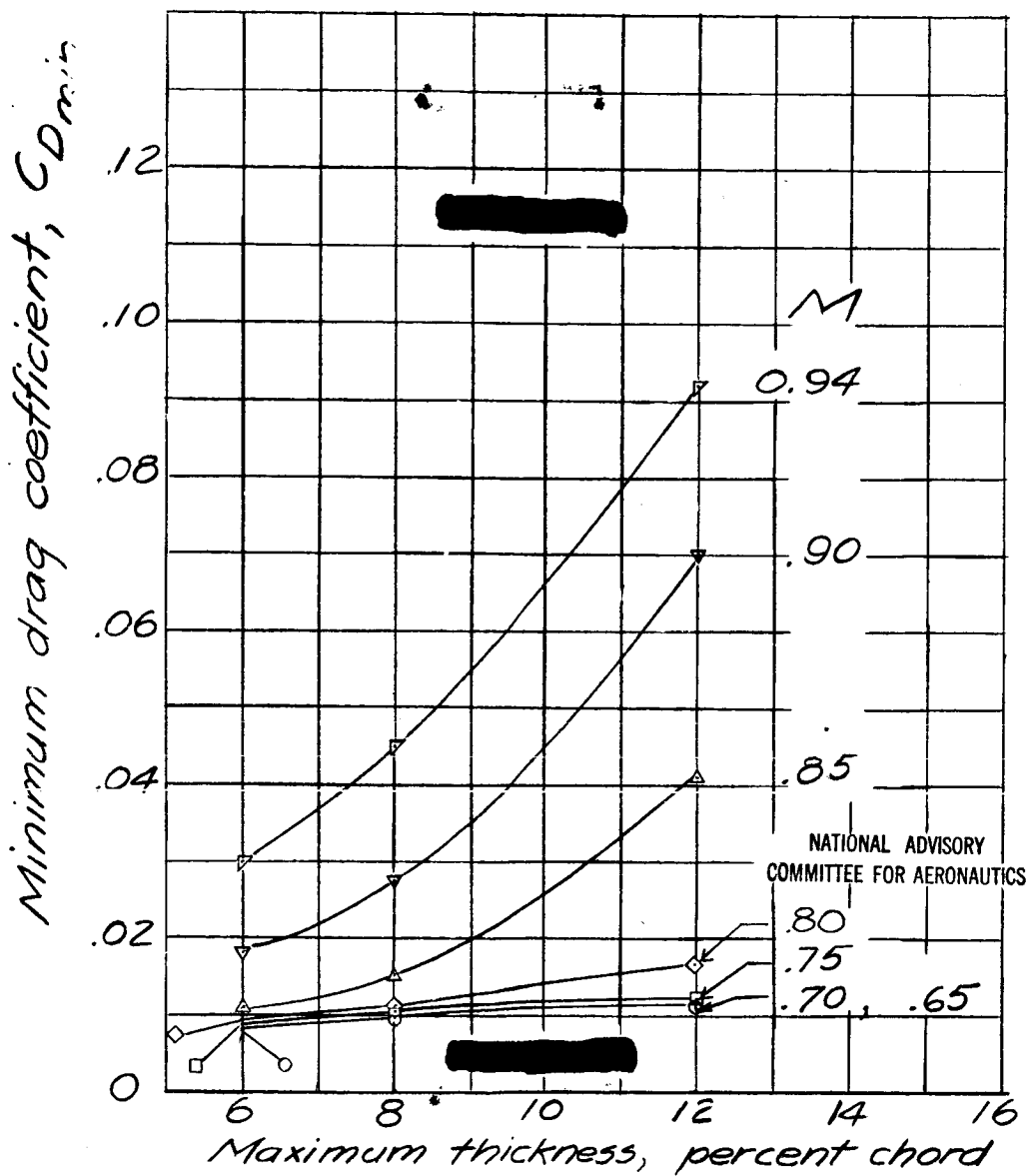
(b) NACA 0000-34 series airfoils.
Figure 73. — Continued.
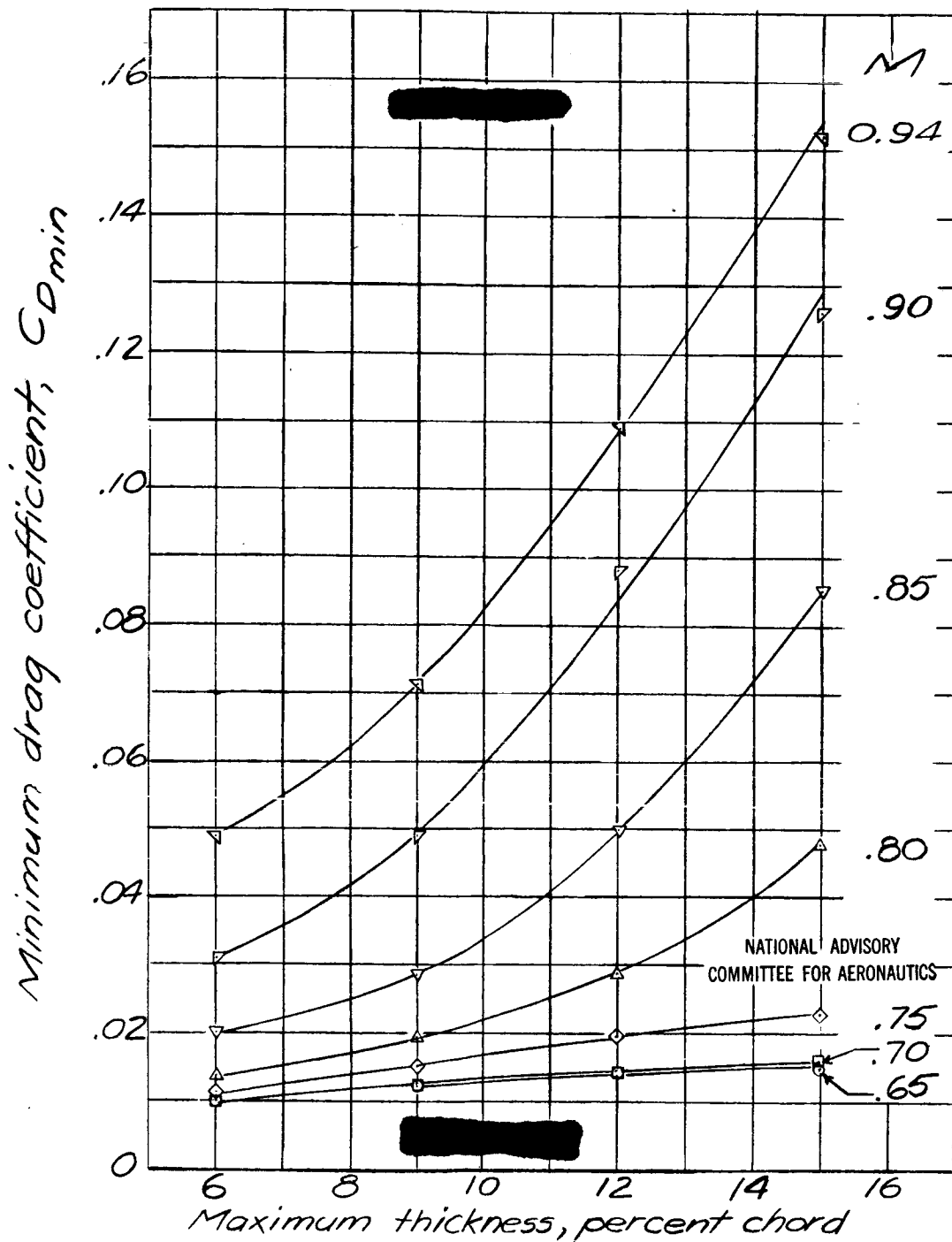
(C) NACA 2300 series airfoils.
Figure 73. — Continued.
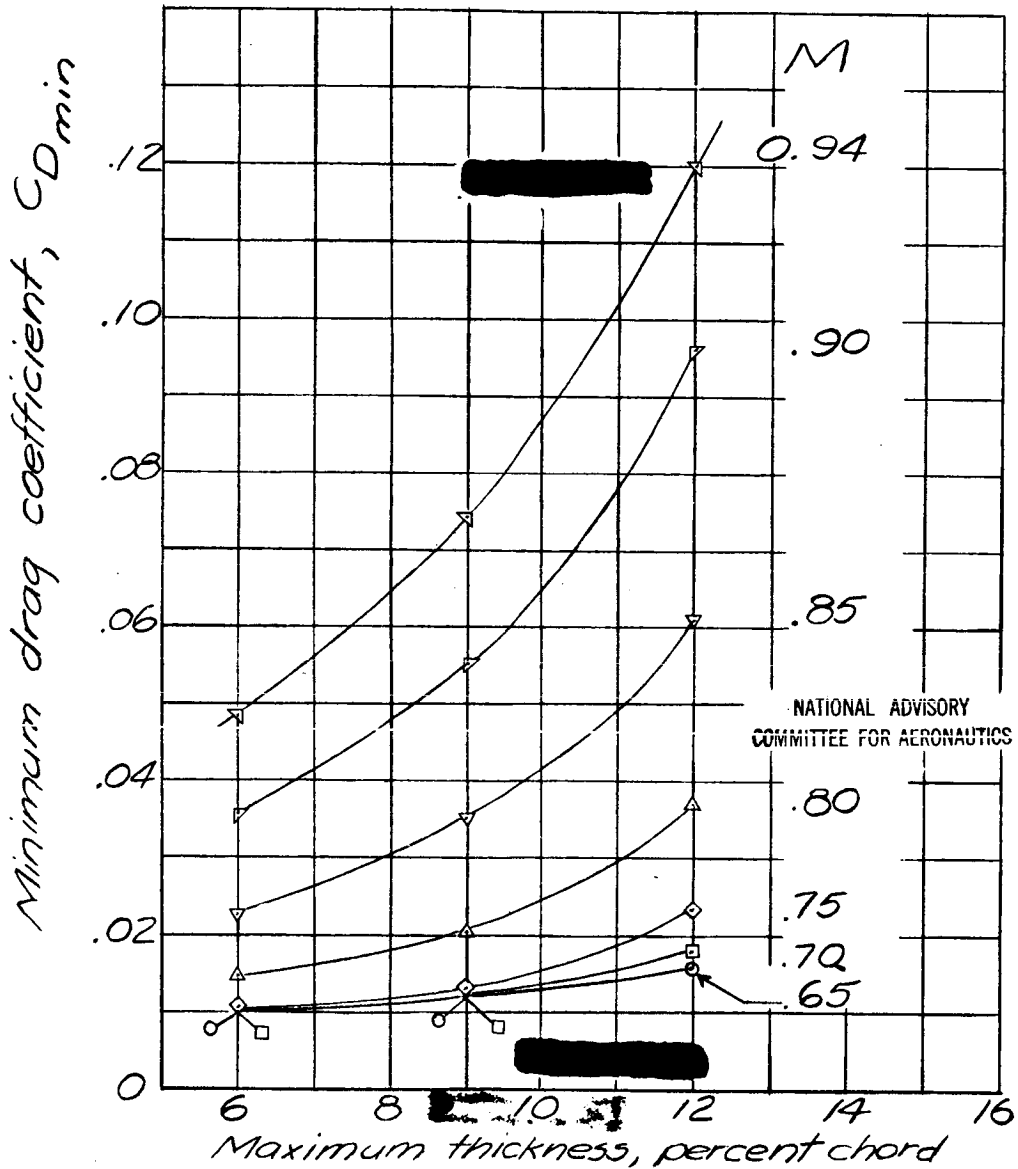
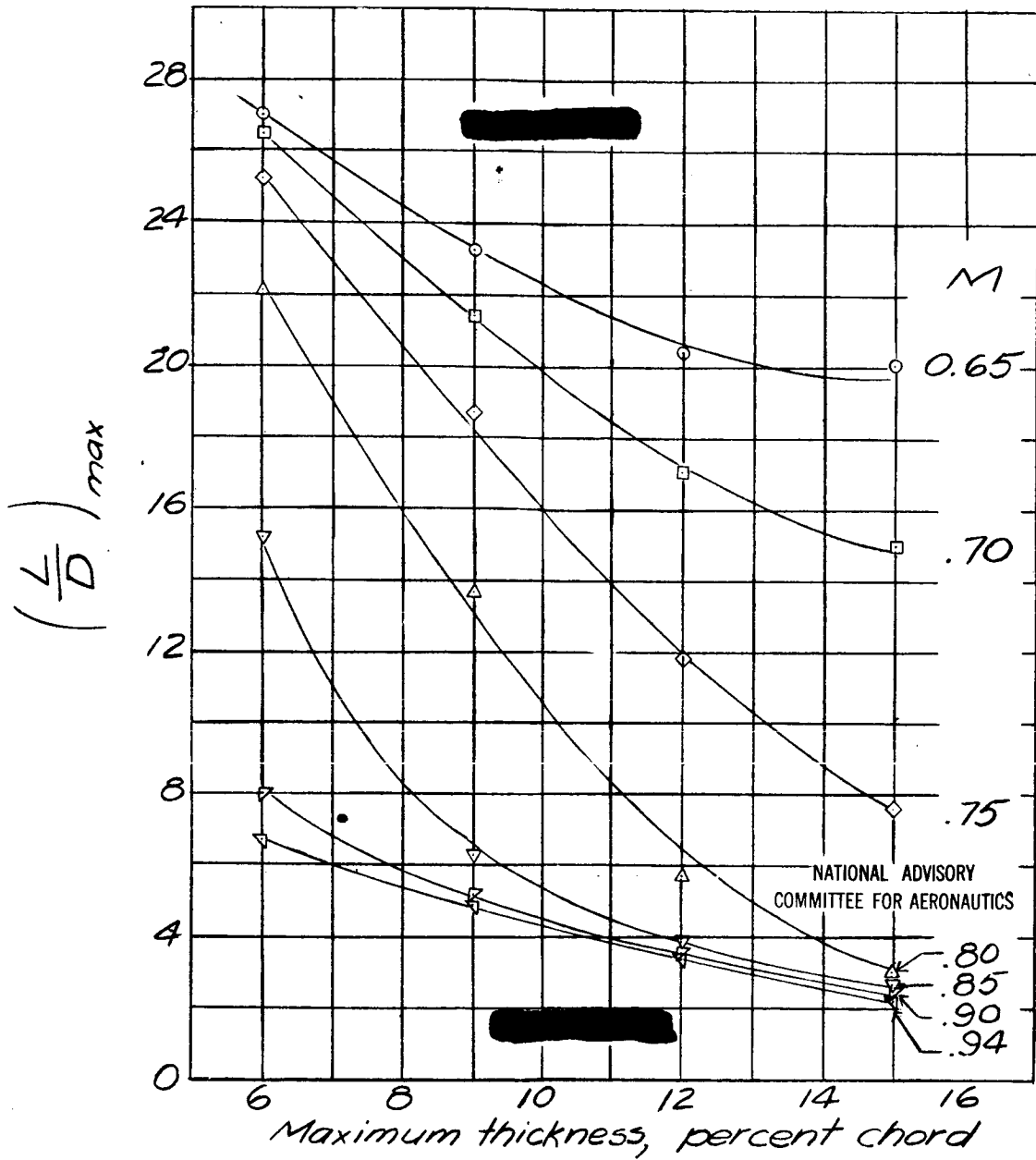(d) NACA 2400 series airfoils.
Figure 73. – Continued.
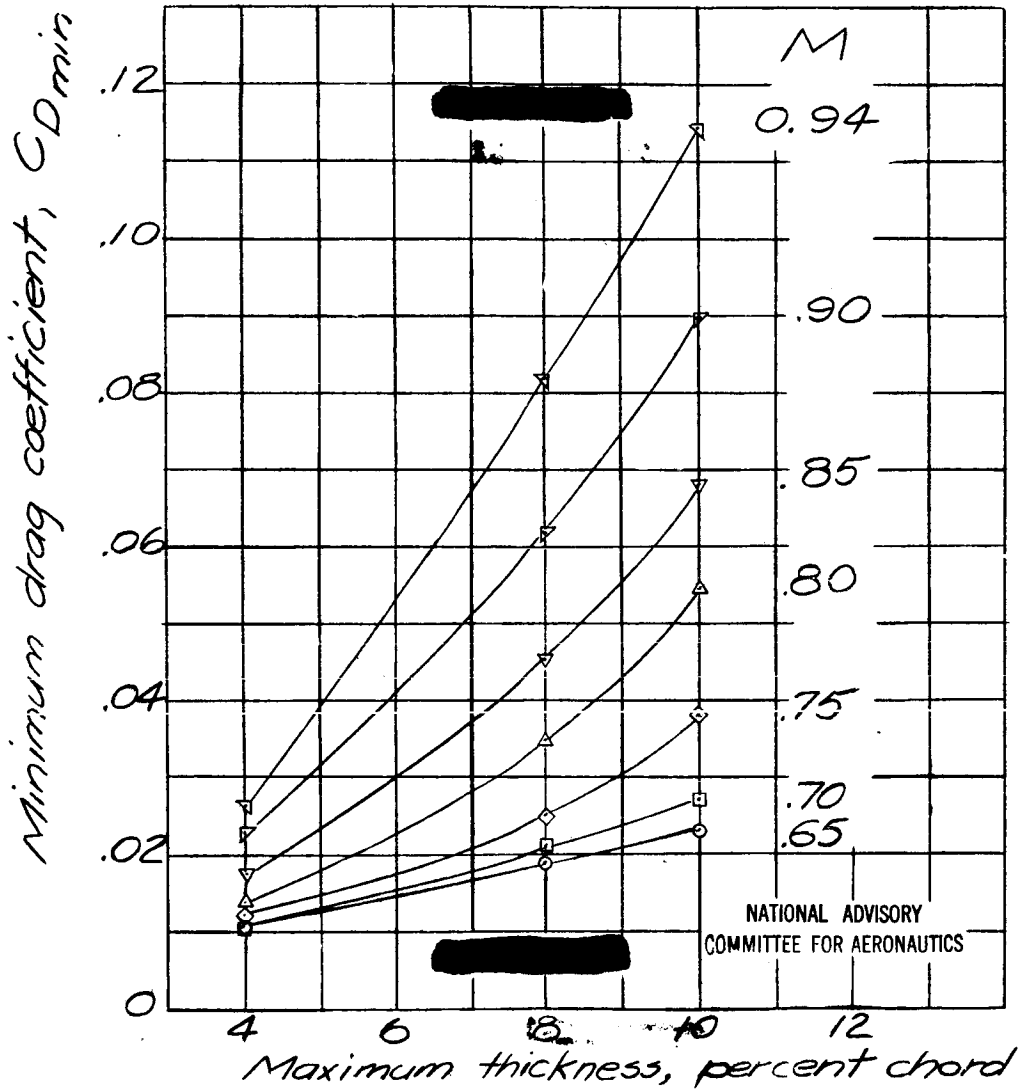
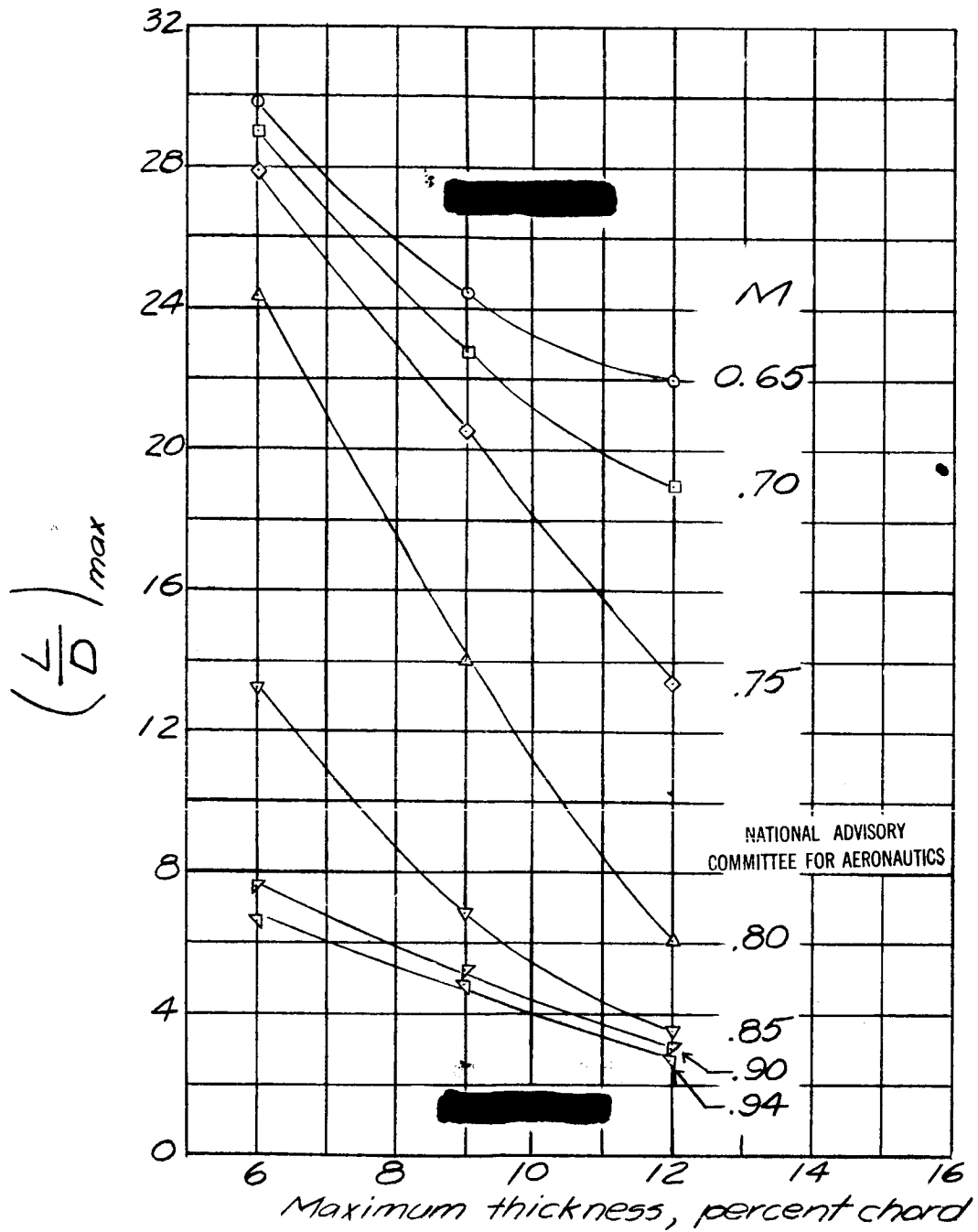(e) U.S.N.P.S. series airfoils.

Figure 73.— Concluded.
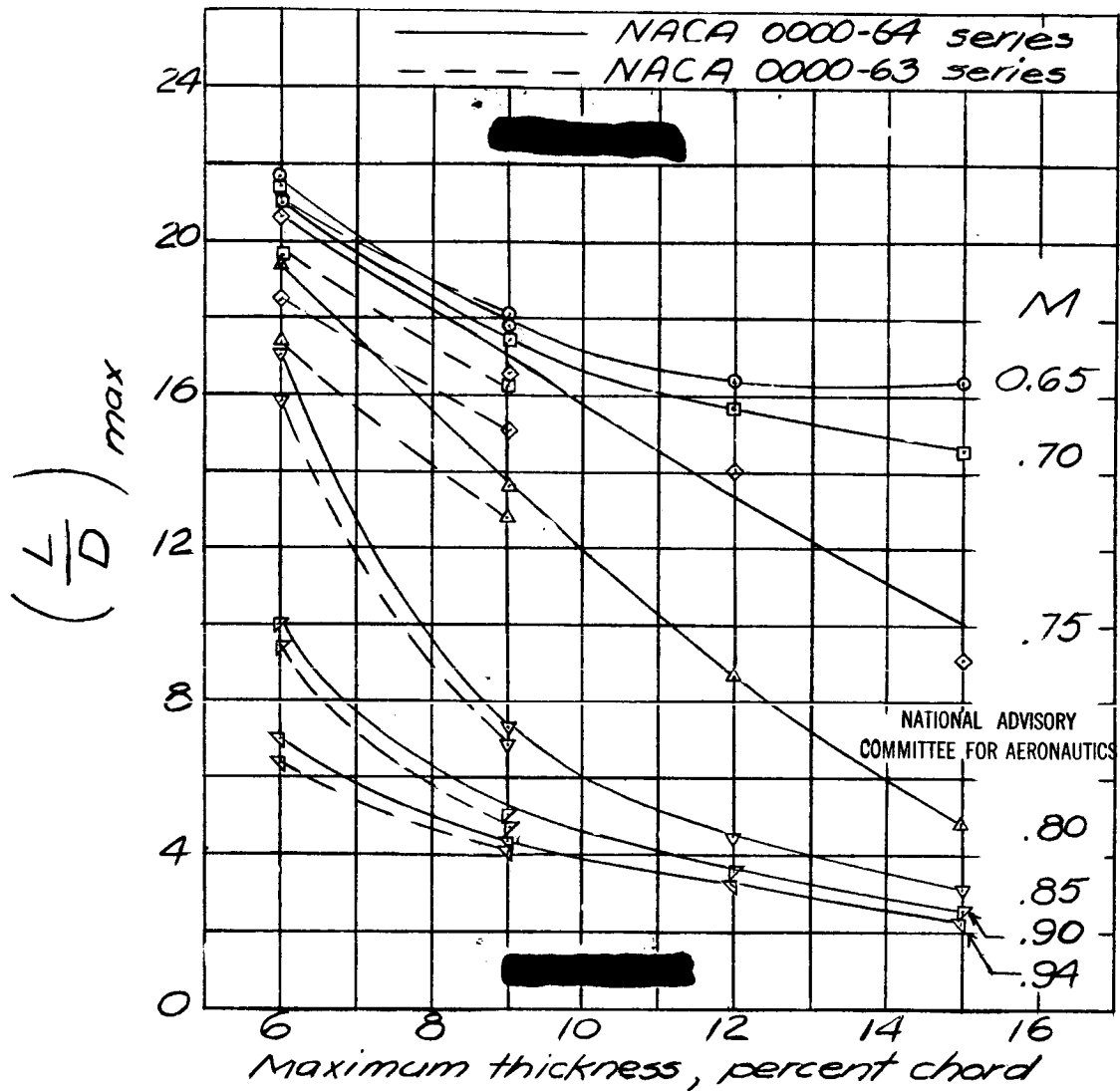
(a) NACA 0000-63 and 0000-64 series airfoils.

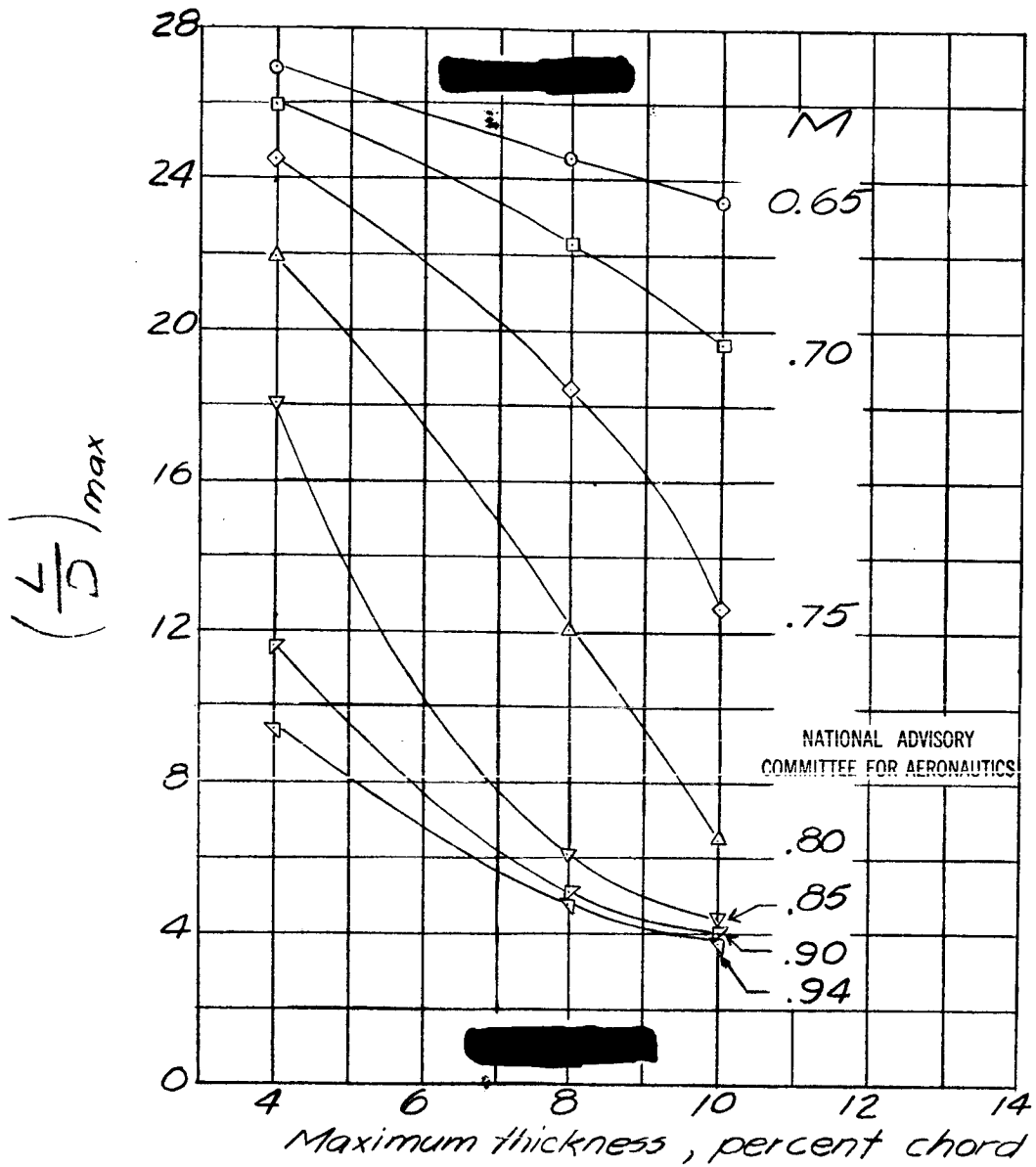Figure 74. — Variation of $(L/D)_{max}$ with maximum thickness for various Mach numbers.
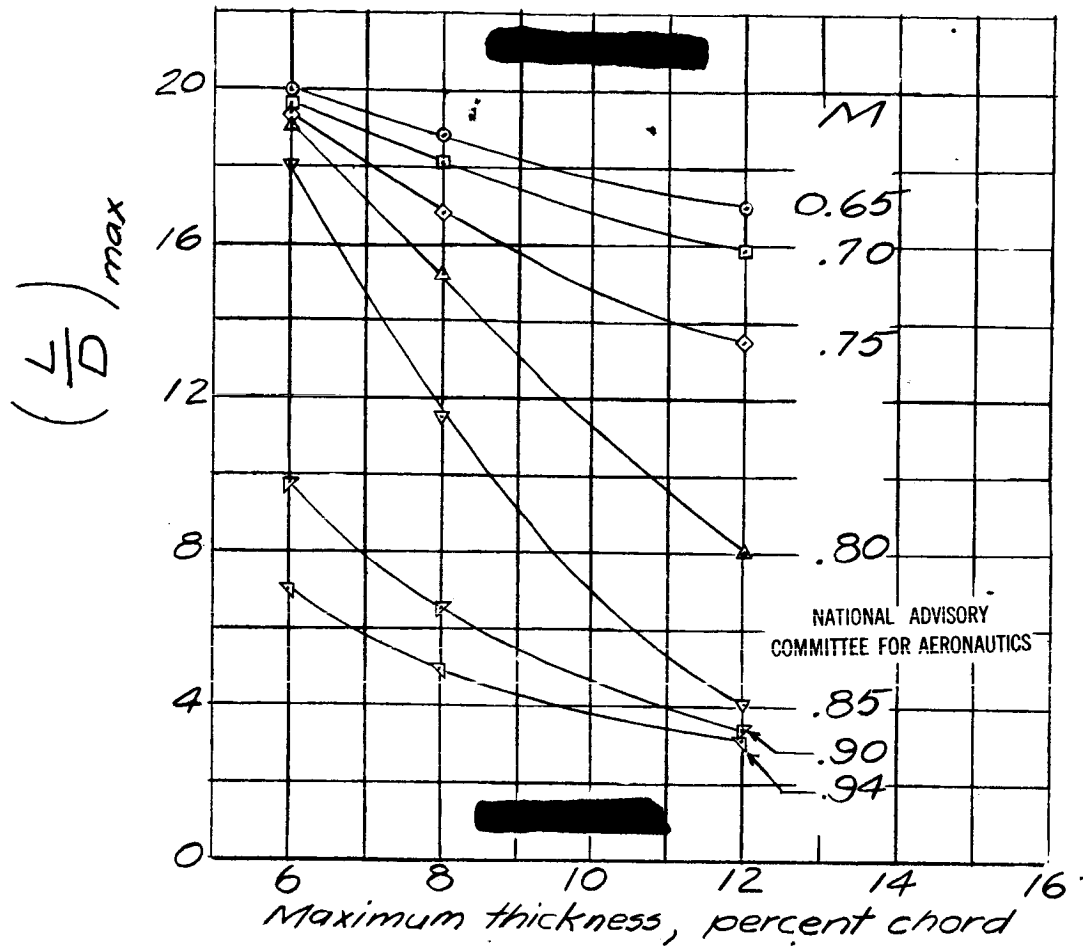
(b) NACA 0000-34 series airfoils.
Figure 74. — Continued.

(C) NACA 2300 series airfoils.
Figure 74. - Continued.

(d) NACA 2400 series airfoils.
Figure 74. — Continued.
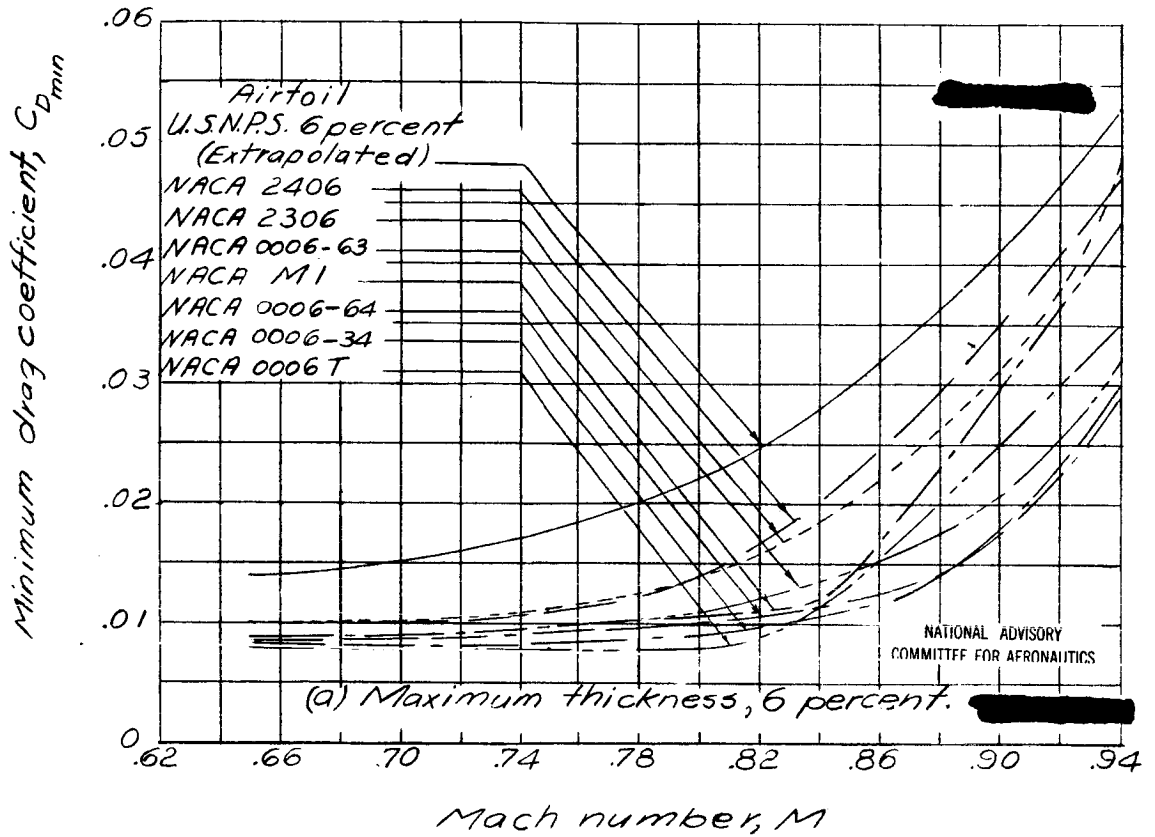
(e) U.S.N.P.S. series airfoils.

Figure 74.— Concluded.

Minimum drag coefficient, $C_{D_{min}}$

Airtoil
U.S.N.P.S. 6 percent
(Extrapolated)
NACA 2406
NACA 2306
NACA 0006-63
NACA M1
NACA 0006-64
NACA 0006-34
NACA 0006 T

.06

.05

.04

.03

.02

.01

0

NATIONAL ADVISORY
COMMITTEE FOR AERONAUTICS

(a) Maximum thickness, 6 percent.

.62    .66    .70    .74    .78    .82    .86    .90    .94

Mach number, M

Figure 15.— Variation of minimum drag coefficient
with Mach number for several airfoils having
the same maximum thickness.

Figure 15.  — Continued.

Airfoil

NACA 2412
NACA 2312
NACA 0012-64
NACA 0012-34

NATIONAL ADVISORY
COMMITTEE FOR AERONAUTICS

(c) Maximum thickness, 12 percent.

Mach number, M
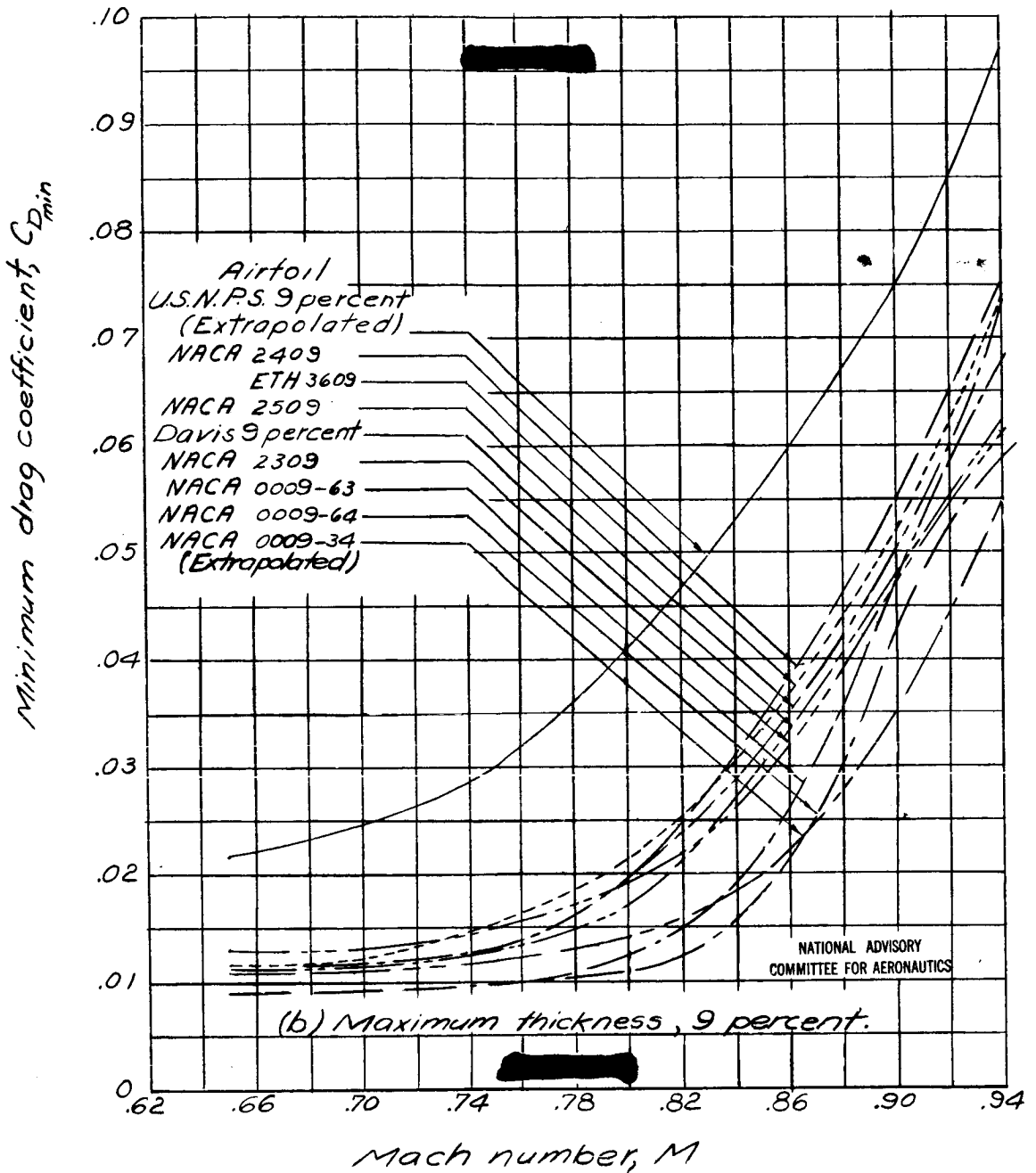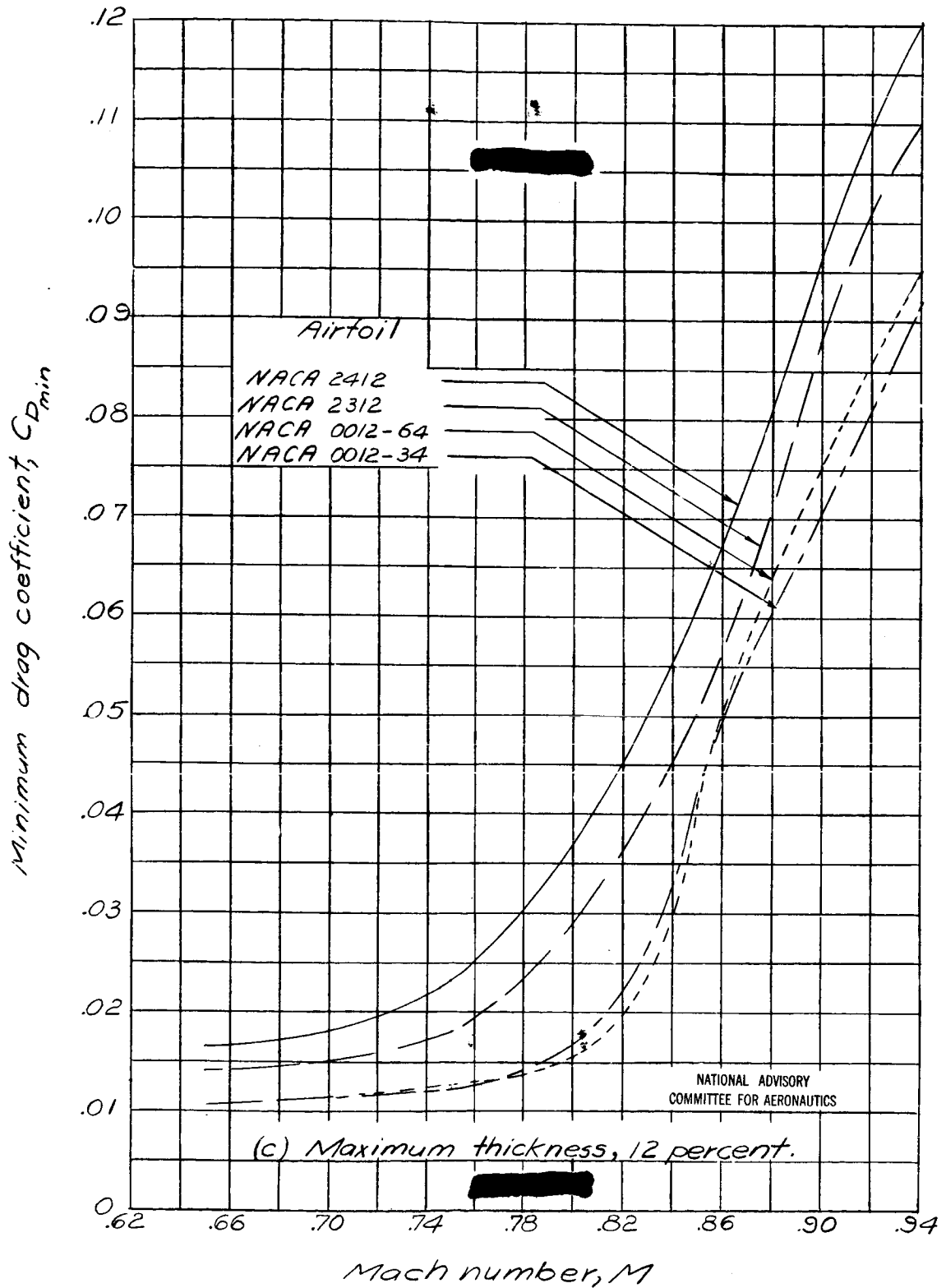
Figure 75.- Concluded.
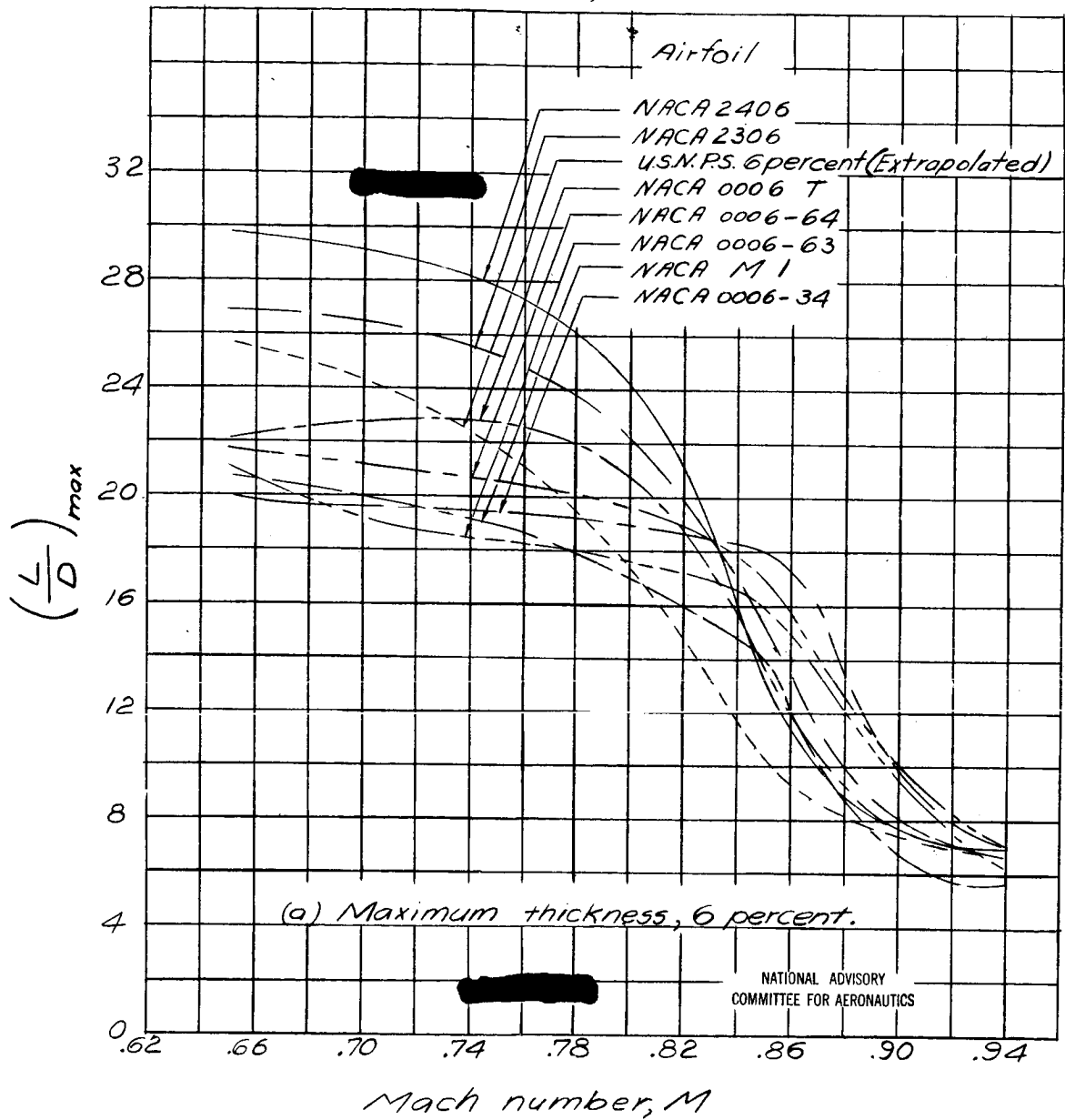
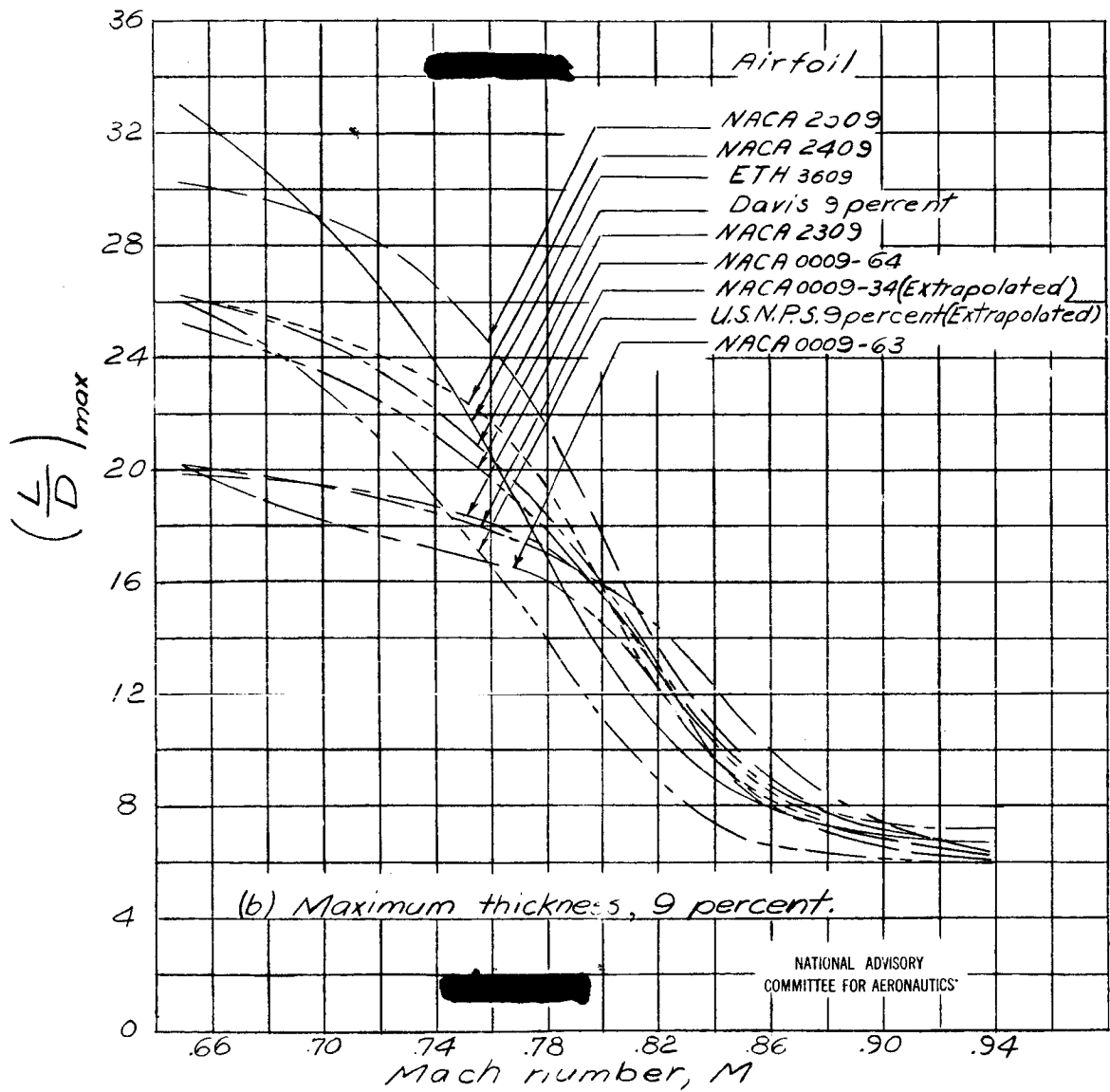Figure 76 .— Variation of $(L/D)_{max}$ with Mach number for several airfoils having the same maximum thickness.
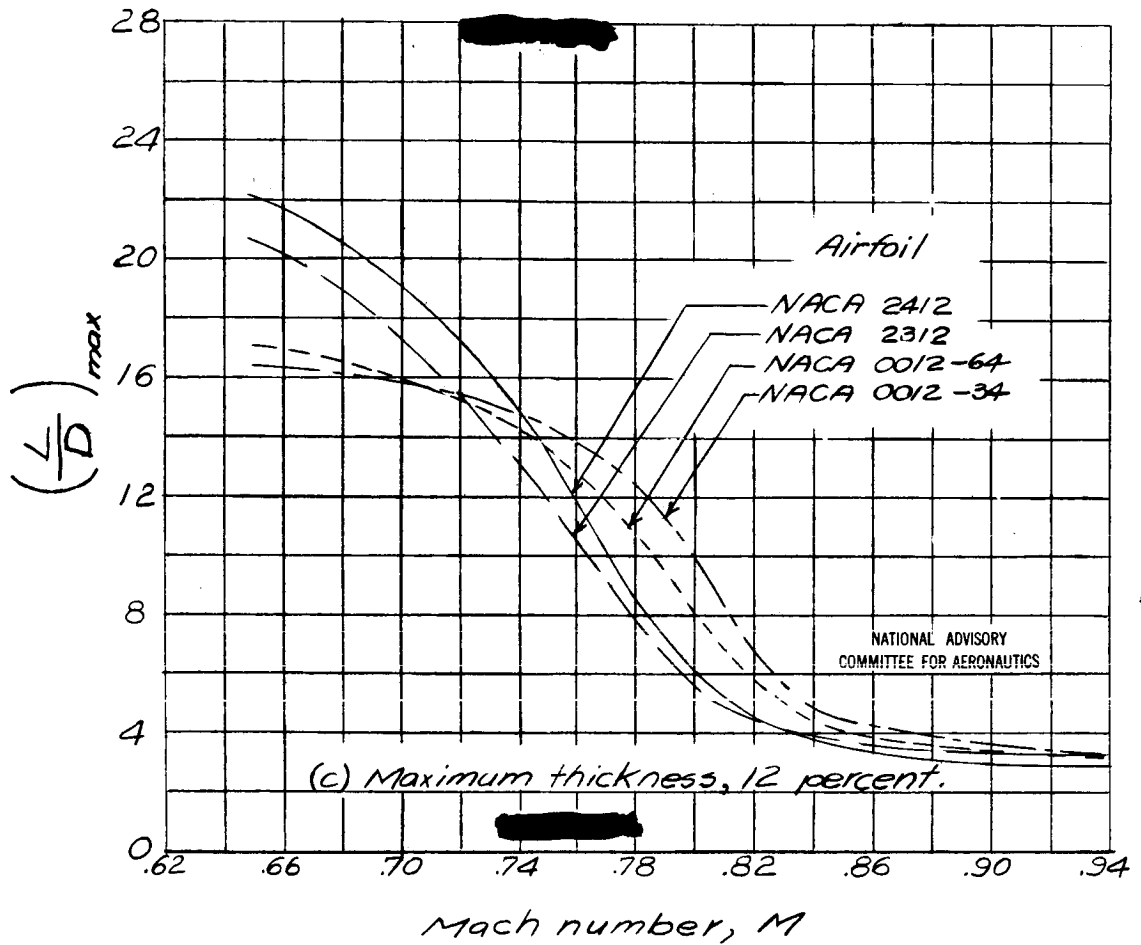
Figure 76 .— Continued.

(c) Maximum thickness, 12 percent.

Mach number, M

Figure 76.- Concluded.